



Resistance of cold-formed L-columns made of high strength steel

Author: Jakub Doležal, Maksym Podgayskyy

Supervisor: Anh Tuan Tran

Examiner: Prof. Milan Veljkovic

University: Luleå University of Technology



Date: 15.01.2014

PREFACE

It has been a chance being too tempting to refuse. Studying a brand new master program, that connects six technical universities together. SUSCOS created a huge opportunity to meet and learn a lot from European most recognized steel experts. Getting access to endless space of information regarding research, experiences and future demands connected with steel structures, all that was available to every student attending this course.

Our journey started in Coimbra University (Portugal), where our knowledge got significantly improved by Professor Luis Simoes da Silva and that was just the beginning. After half year we moved to Prague to the Czech Technical University, where our experiences with steel structures got expanded by Professor František Wald. Of course, not only those two Professors helped us, there were more and it will take a lot of time to thank each of them personally.

Now here we are in Lulea Technical University at our final stage of master degree, under supervision of Professor Milan Veljkovic, working on topic, that offers so much new to learn. Behaviour of high-strength steel is still a big mystery in many cases and it is a big privilege to be a part of research focused on material, which will be used all around the world.

And again our most sincere thanks to everyone, who enabled this journey.

ABSTRACT

Steel is a material with constant development and recent years showed, that by changing the initial mixture of minerals and alloys, the strength of the material can be significantly improved. New generation is called high-strength steel (HSS) and in many cases the value of yield or ultimate strength is nearly doubled compared to the steel products used nowadays.

Designers across Europe can therefore design less massive or much bigger structures than ever before. Great help for every designer is Eurocode and for steel structures it is namely part 3 (EN-1993-1-3). Unfortunately the majority of formulas, buckling curves, tables and all other recommendations were created according to the tests on steel with strength ranging from 235-460 MPa.

Higher strength classes (till 700 MPa) were briefly described in Eurocode EN1993-1-12 from February 2007 and in most of the cases it is recommended to use similar procedure as for steel S460, which is a part of traditional Eurocode. Question of designing high-strength steels according seems to be understood, however it isn't.

It is year 2013 and six years in development means a lot of time to improve or totally change the behaviour of high-strength steels. It can be assumed, that using traditional parts of Eurocode in combination with EN1993-1-12 is safe and the designed structure will sustain all design loads.

Yet, designers are no more focused just on reliability of structure, but also on its economic and environmental part. Usage of current Eurocode, which is more than 6 years old and doesn't reflect improvements of modern steel, can easily lead to very conservative design, which can increase the price of final structure and also use of more material, than it is actually necessary.

This thesis is focused on high strength steel cold-formed equal-leg angles with different angles of folding. This topic includes combination of research questions connected with high strength steel and cold-forming.

Peculiarities of this type of cross-sections will be studied through investigation of its resistance. Due to the press-braking it is expected that the corner area has changed its material properties. Moreover, changes of design resistance will differ according to change of angle of folding. Therefore, the optimum angle will be searched for economical design. Furthermore, the influence of material thickness will also be investigated as the fact which influences on resistance.

It is expected that the current design according to Eurocode is conservative in terms of predicting the design resistance for high strength steel. Moreover, it is expected that classification of considered specimens might not be fully applicable.

First part of this thesis is dedicated to theoretical background and evaluating geometrical properties of cross-section, followed by calculation of critical forces for each element.

To check results of mathematical evaluation of this thesis, in next part finite element analysis is used, both linear and nonlinear. Each specimen will be modelled and its behaviour estimated during compression. The influence of initial imperfections and boundary conditions on the model will be studied.

Next step will include laboratory test, where all specimens will be tested in compression.

After performed procedures comparison of obtained results will be held. Therefore, there will be three steps of research: design according EN, FEM analysis and experimental investigation. This type of research method gives possibility to obtain validated results and to make conclusions which will be safe.

As the outcome of the research it is expected to find answer if current Eurocode produces economical predictions, or there is a need for further testing and change of current design rules and recommendations.

Keywords: High-strength steel, compression, buckling, local buckling, cold-forming, Eurocode



NOTATIONS & SYMBOLS

All notations and symbols used in this thesis are given below in alphabetical order.

Latin letters:

A_{eff}	-	Cross-section effective area
A_g	-	Cross-section gross area
b	-	Width of specimen
b_p	-	Notional width
c.o.g.	-	Centre of gravity of cross-section
d_y, d_z	-	Distance between SC and c.o.g of the section in y and z direction
e	-	Eccentricity
E	-	Modulus of elasticity
ε	-	Strain
$\varepsilon_1, \varepsilon_2, \varepsilon_3$	-	Strain values BSK 99
e_N	-	Shift of the centroid
$\varepsilon_{pl.true}$	-	True plastic strain
ε_{true}	-	True strain
ε_u	-	True strain
f_u	-	Ultimate strength
f_y	-	Yield strength
f_{ya}	-	Average yield strength
f_{yb}	-	Basic yield strength
G	-	Shear elastic modulus
h	-	Height of specimen
i_c	-	Radius of polar gyration
I_t	-	Torsional moment
$I_{t,eff}$	-	Effective torsional moment
I_w	-	Warping constant
$I_{w,eff}$	-	Effective warping constant

I_y, I_z	-	Moment of inertia
i_y, i_z	-	Radius of gyration
$I_{y,eff}, I_{z,eff}$	-	Effective moment of inertia
k	-	Parameter depending on support conditions
k_σ	-	Buckling factor
L	-	Length of member
$\bar{\lambda}$	-	Non-dimensional slenderness
L_e	-	Effective length
L_{ET}	-	Effective torsional or warping length
L_{ex}	-	Effective length for major axis (flexural buckling)
L_{ey}	-	Effective length for minor axis (flexural buckling)
L_{ez}	-	Effective length for torsional buckling
$M_{b,Rd}$	-	design buckling resistance moment
M_{Ed}	-	Design value of bending moment
N	-	Axial force
n	-	Number of 90° bends
$N_{b,Rd}$	-	Design buckling resistance of the compressed member
N_{cr}	-	Critical flexural load
$N_{cr,TF}$	-	Critical flexural-torsional buckling load
$N_{cr,loc}$	-	Critical local buckling load
$N_{cr,t}$	-	Critical torsional buckling load
$N_{cr,y}, N_{cr,z}$	-	Critical flexural load in y and z direction
N_{Ed}	-	Design value of the compression force,
P	-	Axial load
P_{cr}	-	Critical axial load
P_{EN}	-	Predicted member strength according to Eurocode
P_{FEA}	-	Predicted member strength from Finite Element Analysis
P_{test}	-	Maximum strength of a member obtained in test
P_u	-	Ultimate load

r	-	Radius
r_0	-	Polar radius of gyration
SC	-	Shear centre
t	-	Thickness of specimen
t_{cor}	-	Thickness of core
W	-	Section modulus
W_{eff}	-	Effective section modulus
x_0	-	Distance from the centroid to shear centre
y	-	Principal major axis; axis of symmetry
z	-	Principal minor axis

Greek letters

α	-	Imperfection factor
β	-	Factor
λ_1	-	Slenderness coefficient
ν	-	Poisson's coefficient
π	-	Ludolph's van Ceulen number
ρ	-	Reduction factor
γ_{M0}	-	Partial safety factor for resistance of cross-section
γ_{M1}	-	Partial safety factor for resistance of members to instability
φ	-	Angle of rotation
χ	-	Buckling reduction factor
χ_{LT}	-	Reduction factor for lateral-torsional buckling
ψ	-	Stress ratio
$\bar{\lambda}_p$	-	Plate slenderness
σ_{cr}	-	Critical elastic buckling stress
$\sigma_{cr,t}$	-	Critical elastic torsional buckling stress
σ_{true}	-	True stress
σ_u	-	Ultimate stress
σ_{test}	-	Maximum stress of a member obtained in test

TABLE OF CONTENTS

PREFACE	2
ABSTRACT	3
NOTATIONS & SYMBOLS	6
1 INTRODUCTION	14
1.1 Problems, aim, method	14
1.2 Research questions.....	15
1.3 Limitations	15
1.3.1 Scope limitation.....	15
1.3.2 Work limitation	16
1.4 Structure of the work	16
1.5 Separation of the work.....	18
2 HIGH STRENGTH STEEL.....	19
2.1 Material overview.....	19
2.2 Eurocode for HSS (EN 1993-1-1 and 1993-1-12)	22
2.3 HSS by Ruukki	22
3 REVIEW OF PERFORMED RESEARCHES	24
4 PROPERTIES OF CROSS-SECTIONS	33
4.1 Tested specimens	33
4.2 Expected versus real shape	34
4.3 Cold forming and change of material properties	35
4.4 Influence of rounded corners.....	37
4.5 Geometrical proportions	41
4.6 Classification of cross-sections	43
4.7 Determination of cross-section effective area.....	44
4.8 Determination of cross-section geometrical properties.....	46
5 ELASTIC CRITICAL LOAD.....	49
5.1 General	49
5.2 Flexural buckling (theory) and boundary conditions	49
5.3 Torsional and flexural-torsional buckling (theory).....	53
5.4 Elastic critical load for local buckling (theory).....	56
5.5 Peculiarities of buckling modes for L-shape cross-section.....	57

5.6	Elastic critical load evaluation	59
6	IMPERFECTIONS AND DESIGN ACCORDING EN	61
6.1	Imperfections in columns (theory)	61
6.1.1	Initial imperfection / out of straightness	61
6.1.2	Eccentricity of applied load	64
6.1.3	Residual stresses in cross-section	65
6.2	Current design according Eurocode	68
6.2.1	General	68
6.2.2	Compression.....	68
6.2.3	Bending.....	71
6.2.4	Combined compression and bending	73
6.3	Buckling resistance evaluation	74
7	FINITE ELEMENT MODELLING	75
7.1	Introduction	75
7.2	General	75
7.3	Finite element type and mesh.....	75
7.4	Boundary conditions and load application.....	76
7.5	Material modelling	80
7.6	Modelling of imperfection.....	82
7.8	Tracking of shear centre movement	83
7.9	Modelling output.....	85
7.9.1	General	85
7.9.2	Tracking of shear centre movement	85
7.9.3	Failure modes	86
8	EXPERIMENTAL INVESTIGATION	93
8.1	Experimental evaluation of imperfections	93
8.1.1	Introduction.....	93
8.1.2	Scanning methodology.....	93
8.1.3	Evaluation of measured imperfections	101
8.2	Compression test.....	102
8.2.1	Specimen labelling.....	102
8.2.2	Test rig and operation	102
8.2.3	Test results	105

9	OUTPUT COMPARISON	111
9.1	Summary of calculation according to EN.....	111
9.2	Comparison of elastic critical load according to hand calculations and FEA	111
9.3	Sensitivity analysis. Comparing design strength according to EN, FEA and tests ...	115
9.4	Force-displacement curve analysis for EN, FEA and tests	117
9.5	Buckling curves - parametric study	121
10	DISCUSSIONS AND SUGGESTIONS.....	128
10.1	Factors which influence results of tests and FEA	128
10.1.1	The inaccuracy of using S4R shell element	128
10.1.2	Eccentricity of applied load	130
10.1.3	Flexibility of the setup	131
10.2	Suitability of classification according EN 1993-1-1.....	134
10.2.1	1st approach.....	135
10.2.2	2nd approach	140
10.2.3	Conclusion	144
10.3	Influence of angle of folding and thickness of material on resistance	145
10.3.1	Influence of folding angle on resistance	145
10.3.2	Influence of material thickness on resistance.....	145
10.4	Suggestions	146
10.4.1	Proposed changes in design procedure for cross-sections with fixed BC.....	146
10.4.2	Suggestions for further research.....	152
11	CONCLUSIONS	154
12	ATTACHMENTS	156
	Attachment 1 – Determination of average yield strength.....	157
	Attachment 2 – Classification of cross-sections.....	158
	Attachment 3 – Determination of effective width for Class 4 cross-sections	159
	Attachment 4 – Determination of geometrical properties and elastic critical force (fixed BC)	160
	Attachment 4a– Determination of geometrical properties and elastic critical force - fixed BC (neglecting rounded corners)	162
	Attachment 4b – Elastic critical force for local buckling.....	164
	Attachment 5 – Determination of flexural buckling resistance (fixed BC)	165
	Attachment 6 – Determination of torsional buckling resistance (fixed BC)	166
	Attachment 7 – Determination of torsional buckling resistance (fixed BC)	167

Attachment 8 – Determination of moment buckling resistance for Class 4 cross-sections for bending about weak axis	168
Attachment 9 – Determination of member resistance for combined compression and bending interaction (fixed BC)	169
Attachment 10 – Combined table of buckling resistance according to EN (fixed BC)	170
Attachment 11 – Combined table of buckling resistance according to EN for fixed BC (neglecting additional moment for Class 4 cross-sections)	171
Attachment 12 – Combined table of buckling resistance according to EN (pinned BC)....	172
Attachment 13 – Combined table of buckling resistance according to EN for pinned BC (neglecting additional moment for Class 4 cross-sections)	173
Attachment 14 – Calculation procedure according to EN for cross-sections P1-4 (Class 4) and P1-10 (Class 3)	174
Attachment 15 – Combined table of buckling resistance – fixed BC.....	189
Attachment 16 – Combined table of buckling resistance – pinned BC.....	192
Attachment 17 – Elastic critical loads curves	195
Attachment 18 – Buckling curves.....	204
Attachment 19 – Load-displacement curves (test results)	222
13 REFERENCES	229

1 INTRODUCTION

1.1 Problems, aim, method

Cold-formed structural members are becoming more and more used in the construction practice around the world. This happens due to the benefits which can provide this type of manufacturing: light weight and high strength. Using cold-forming manufacturing for high strength steel increases design strength even more with bigger reduction in weight.

This thesis is focused on high strength steel cold-formed equal-leg angles with different angles of folding. Analysis of this type of cross-section can be beneficial in different ways. Firstly, the effect of cold-forming for different angles on the basis of equal-leg angles can be used for other structures with cold-forming manufacturing process (e.g. polygonal sections of tubular wind towers, polygonal chords of trusses). Secondly, they can be used as structural members of lattice towers and trusses. Moreover, angles are widely used in construction because of their simple geometry and ease of connection.

The research performed previously is mostly connected with the angles which have 90° angle of folding. Moreover, most of research about cold-formed equal-leg angles is mostly made in the frame of American and Australian/New Zealand design codes. Therefore, this research is innovative and interesting due to the fact that it will study angles with different angles of folding, thicknesses with regard to EN standards.

Despite the fact that considered cross-sections are simple structural members their design is quite complicated and has to be analysed thoroughly. The problems connected with considered specimens are described below.

As stated in previous paragraph, there is a doubt, whether current design standards in Europe fully reflect behaviour of modern high strength steels. The issue of full utilization of HSS benefits is currently very important. Moreover, it is vital to assess if the current design codes provide procedures where excessive resistance is used. Furthermore, it is necessary to study if improvements can be implemented in EN standards in order to provide more economical and safe design.

Moreover, it has not been studied yet how much the resistance of equal-leg angles is affected by combination of different angles of folding and thicknesses of material.

Furthermore, classification in case of cold-formed members is not an issue in most cases because usually they are produced from very thin profiles and can be classified as Class 4. However, considered specimens have thickness up to 20 mm. Therefore, verification of classification according to EN is needed.

One of the problems of equal-leg angles is distinguishing between global and local buckling modes. Flexural, flexural-torsional, torsional and local buckling modes will be analysed for different length of considered cross-sections.

The method of research will be based on three steps: hand calculation, Finite Element Analysis and experimental investigation. This approach enables to validate FEA model with test result and to compare obtained results with predictions from EN. Combination of these three steps can be found in most of the research papers connected with this type of problem. Therefore, it can be stated that this method of research is reliable and does not require any alternatives. Brief description of methodology is given further.

Starting from very beginning, members will be studied on the basis of elastic stability theory. Furthermore, design resistance will be calculated according to EN. The next step is going to be finite element analysis (FEA) both linear and non-linear, trying furthermore to predict behaviour of compressed HSS steel elements. Additionally, experimental investigation of cross-sections using compression tests will be held. This will enable to validate FEA results and to perform parametric study for different lengths. Moreover, it will be possible to compare actual strength of specimen and the one predicted by EN.

The aim of this research is to answer research questions which will lead to possible improvements of design procedures.

1.2 Research questions

The research questions raised in this thesis can be listed as follows:

1. How accurately the ultimate resistance can be predicted for considered specimens?
2. How big is the influence of different thicknesses and angles of folding on resistance of considered specimens?
3. Is classification of the cross-sections according to EN 1993-1-1 suitable for considered specimens?

1.3 Limitations

1.3.1 Scope limitation

The scope of this thesis is limited as follows:

1. Review of classic theory of elastic stability.
2. Predicting results of experiments according Eurocode for all studied cross-sections.
3. Performing of linear and nonlinear Finite Element Analysis for all studied cross-sections.
4. Performing of compression tests for cross-sections with thickness 4 mm and 6 mm.
5. Performing parametric study for different length of specimens.
6. Comparison of results according EN, FEA, test.

1.3.2 Work limitation

Following work limitations are observed regarding the topic of thesis.

Firstly, the design of the structures made of high strength steel is governed by EN 1993-1-12. However, this design standard is mostly based on EN 1993-1-1 and is limited in terms of utilization the properties of high strength steel. Therefore, this research is focused on comparing of results from EN, test and Finite Element Analysis in order to suggest improvements of design procedures.

Second limitation is connected with the range of specimens available for test. The length is limited with 600 mm and 300 mm. Therefore, it will not be possible to verify the results of EN and FEA with tests for big range of slenderness.

Third limitation is connected with initial imperfections and residual stresses. In this research experimental values of these factors will not be used. The initial imperfections were measured experimentally but analyzing of obtained data is not in the scope of this work. Therefore, it can be used for further investigation of this topic. The evaluation of effect of residual stresses will be studied analytically. The experimental measurement is not planned for this work. Moreover, according to research it is stated that the effect of residual stresses is negligible in case of considered specimens.

Fourth limitation is connected with the change of material properties in the corners of cross-sections due to press-braking. For investigation of influence of this change on member resistance it is required to determine experimentally properties of flat parts and corner parts. This has to be done through tensile tests. At this stage of work these results were unavailable and that is why Finite Element Model will be based on nominal material properties.

1.4 Structure of the work

This chapter will provide overview of the performed work in every chapter.

Chapter 2 “High strength steel” provides overview of high strength steel as a material. The grades of tested specimens are reviewed.

Chapter 3 “Review of performed researches” provides state-of-art review of literature. This chapter gives information on research previously made on high strength steel cold-formed equal-leg angles. The suggestions for improvement of design procedures are outlined in order to implement them in the thesis.

In **chapter 4 “Properties of cross-section”** the shape and geometrical properties of cross-sections are investigated. Moreover, influence of cold-forming according to EN 1993-1-3 and possibility of application of this standard are presented. Furthermore, classification of cross-sections, determination of effective area for Class 4 is made.

Chapter 5 “Elastic critical load” presents overview and determination of elastic critical load for flexural, torsional, flexural-torsional and local buckling. Moreover, peculiarities of elastic critical load determination are provided for considered specimens.

Chapter 6 “Imperfections and design according EN” provides overview of possible imperfections in columns. Calculation procedure of compressed members according EN is presented. Class 4 cross-sections are calculated for combined compression and bending moment (due to shift of centroid). Class 3 cross-sections are calculated for compression only.

Chapter 7 “Finite Element Modelling” presents linear and non-linear analysis using Finite Element Analysis. All investigated cross-sections are modelled with fixed-fixed and pinned-pinned boundary conditions. Sensitivity analysis is performed for different values of imperfection in RIKS analysis. Failure modes and tracking of shear centre movement are investigated.

Chapter 8 “Experimental investigation” provides review of experimental work performed. Firstly, review of the experimental evaluation of imperfections using 3D scanner is provided. Using of measurement results in FEA is not in the scope of this work. Secondly, review of compression tests on equal-leg angles is presented. Finally, test results are provided.

Chapter 9 “Output comparison” provides comparison of results obtained using EN, FEA and tests. Firstly, elastic critical load is compared according to elastic stability theory and linear FEM analysis. Secondly, ultimate resistance is compared for tested cross-sections of 600 mm according to EN, FEM and test. Moreover, force-displacement curves are analysed. Finally, parametric study is performed on the basis of FEA. Buckling curves are plotted for variable length of considered specimens with fixed supports. Conclusions are made on the basis of comparison.

Chapter 10 “Discussions and suggestions” gives overview of factors which influence the results of tests and FEA. Furthermore, suitability of classification according EN 1993-1-1 for considered specimens is investigated. Conclusion about influence of angle of folding and thickness on the resistance is made. Suggestions for changes in EN design procedure (for cross-sections with fixed supports) are provided together with suggestions for further research.

Chapter 11 “Conclusions” summarizes fulfilled objectives of the thesis.

Chapter 12 “Attachments” consists of attachments. The description of provided information is given in relevant chapter.

Chapter 13 “References” consists of used references.

1.5 Separation of the work

As long as this work has been done by two students the performance of work has been separated as follows:

No	Chapter	Performed by
1	INTRODUCTION	Maksym Podgayskyy
2	HIGH STRENGTH STEEL	Jakub Doležal
3	REVIEW OF PERFORMED RESEARCHES	Maksym Podgayskyy
4	PROPERTIES OF CROSS-SECTIONS	Jakub Doležal
5	ELASTIC CRITICAL LOAD	Maksym Podgayskyy
6	IMPERFECTIONS AND DESIGN ACCORDING EN	Jakub Doležal
7	FINITE ELEMENT MODELLING	Maksym Podgayskyy
8	EXPERIMENTAL INVESTIGATION	Jakub Doležal
9	OUTPUT COMPARISON	Maksym Podgayskyy
10	DISCUSSIONS AND SUGGESTIONS	Jakub Doležal
11	CONCLUSIONS	Maksym Podgayskyy and Jakub Doležal

Table 1.1: Separation of work.

2 HIGH STRENGTH STEEL

2.1 Material overview

In civil engineering steel is considered as very young material, since the mass production started around year 1800. Therefore it is difficult to give a proper label to high-strength steel (HSS), which is even younger. The main expansion of HSS is happening for last 10-15 years and it can be assumed, that this material is still under heavy development.

Nowadays, there is a high demand for HSS. Currently used steel grades all around the world are limiting engineers in their design and often result in very massive structures. Developing a better grade of steel with double or even three times higher ultimate strength will allow both architects and engineers to design and build slender and light structures, which weren't possible in past.

Long-term research showed, that to achieve high strength of steel, very low amount of carbon content must be kept with addition of alloying admixtures including copper, titanium, vanadium or zirconium. Main goal is to create a different microstructure than in case of "classic" carbon steel. Very fine dispersion of alloy carbides is the key element to achieve higher strengths.

Understanding of HSS structure may not seem relevant to civil engineer, but in fact it is. Change of internal arrangement of atoms results in different properties of steel, than designers are used to. Engineer unaware of this fact can easily create a structure, which will collapse or sustain heavy damage despite the fact, that on paper it worked.

Several differences between regular and high-strength steel can be observed in document published by German Institute of Steel Construction (Sedlacek & Müller). Steel with higher yield stress can deliver much thinner and lighter structures, difference between current European steel S235 and most modern S960 is almost 70% in terms of weight savings (Figure 2.1.1).

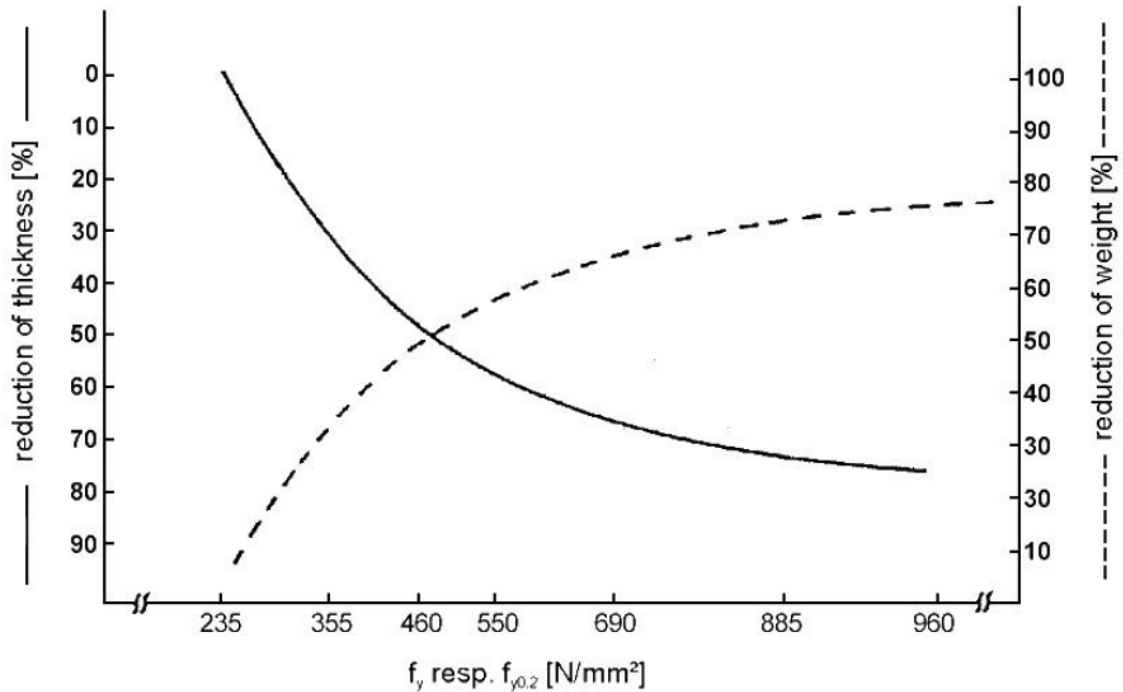


Figure 2.1.1: Reduction of wall thickness and weight according to steel grade
 Source: Institute of Steel Construction (Sedlacek & Müller)

In case of true stress- strain curve (not engineering ones provided by Eurocode) the HSS steel behaves similarly, only difference is by parallel of the curve by magnitude of yield strength (f_y). More can be seen in the Figure 2.1.2 below this paragraph.

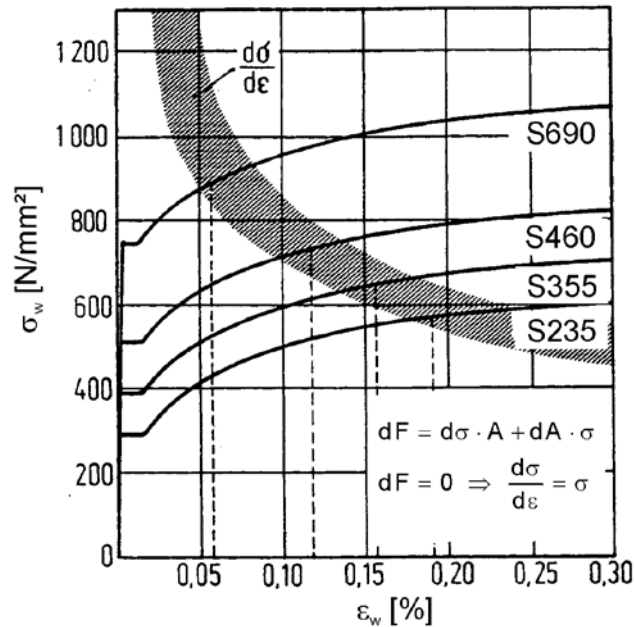


Figure 2.1.2: True stress strain curves according to steel grade
 Source: Institute of Steel Construction (Sedlacek & Müller)

So far HSS looks as better material in every direction, but in terms of ductility, there is a significant complication. From tests (Figure 2.1.3 and 2.1.4) it can be assumed, that the higher the ultimate strength (f_u), the lower is the true strain (ϵ_u). This fact makes usage of HSS more troublesome in case of structural detailing with high local ductility demand.

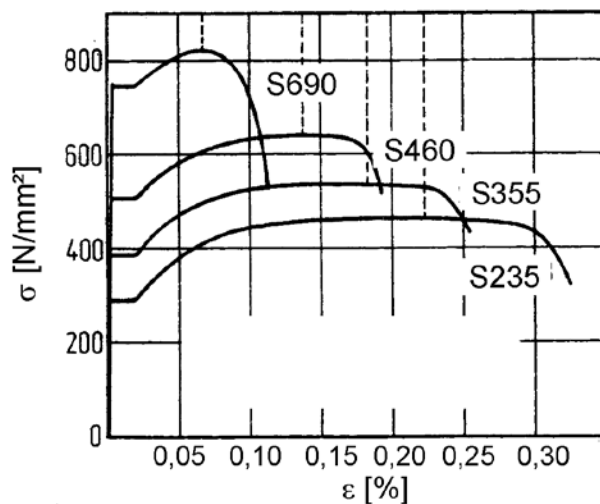


Figure 2.1.3: Load-deflection lines according to steel grade

Source: Institute of Steel Construction (Sedlacek & Müller)

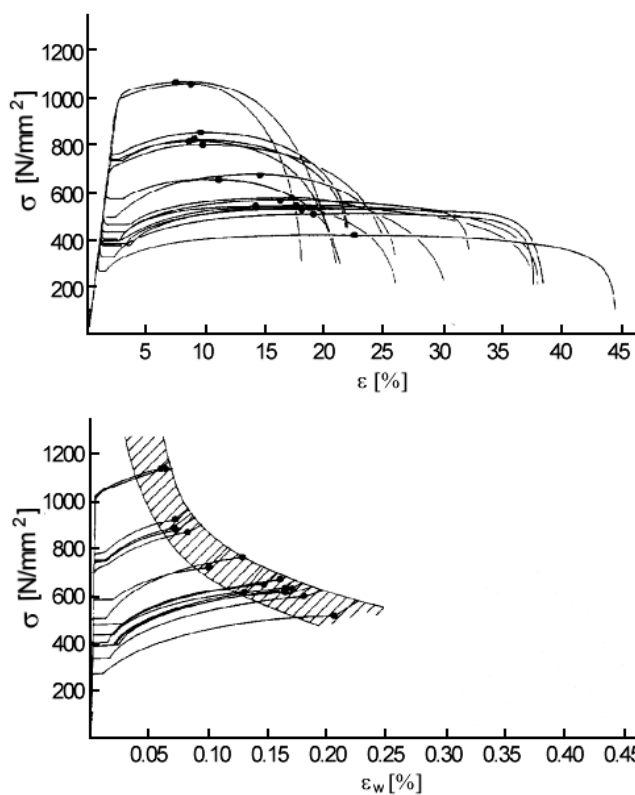


Figure 2.1.4: Stress strain and true stress strain curves according to steel grade

Source: Institute of Steel Construction (RWTH Aachen, Germany)

2.2 Eurocode for HSS (EN 1993-1-1 and 1993-1-12)

From previous paragraphs it can be assumed, that in case of HSS most of engineers lack experience and same issue corresponds to the Eurocode. Current version of EN 1993-1-1 (May 2005) is applicable to steels from S235 to S460. Two years after (February 2007) this problem was partly solved by EN 1993-1-12, which extends design rules up to steel grade S700. However all recommendations given in part 1-12 are simply saying, that use of 1-1 and following parts is safe.

Unfortunately “safe” isn’t always in balance with “effective” and therefore designed structure from HSS may have higher resistance than actually needed. This will lead to safe, but uneconomic design and waste of high-strength steel material. Part EN 1993-1-12 is also more than 6 years old and does not cover all improvement, that have been done till recent year (2013). There is also demand to increase the range to higher grades of steel (up to S960), but that won’t be covered in this thesis.

2.3 HSS by Ruukki

For the tests, that will follow later, steel producer (company Ruukki) provided different grades of high-strength steel. Several specimens created for two steel grades were obtained. Ruukki is branding them as 650MC and 500ML. Following information were taken from Ruukki leaflet. (Ruukki, 2013)

Optim 650 MC structural steel

Extra high-strength structural steel grade with improved bendability, weldability and cutting properties. Optim MC is thermo-mechanically rolled (M), cold formable (C) and according to producer, exceeds requirements of EN 10149-2.

Steel grade	Thickness [mm]	Yield strength [MPa]	Tensile strength [MPa]	Min. Elongation [%]
Optim 650 MC	2.5 – 10	650	700-870	15

Table 2.3.1: Properties of steel Optim 650 MC.

Steel grade	Max. C	Max. Si	Max. Mn	Max. P	Max. S	Min. Al
Optim 650 MC	0.10	0.20	2.00	0.020	0.010	0.015

Table 2.3.2: Chemical composition of steel Optim 650 MC.

Optim 550 ML structural steel

Structural steel with following properties: easy to weld, bend or generally process in workshops and building sites. Optim 550 ML is high strength, thermo-mechanically rolled (M) and low temperature tough (L) structural steel grade. There is no equivalence of Optim 550 ML to any structural steel standard.

Steel grade	Thickness [mm]	Yield strength [MPa]	Tensile strength [MPa]	Min. Elongation [%]
Optim 500 ML	8.0-16.0	500	570-720	16
	16.01-40.0	480	570-720	16
	40.01-60.00	470	560-710	16

Table 2.3.3: Properties of steel Optim 500 MC.

Steel grade	Max. C	Max. Si	Max. Mn	Max. P	Max. S	Min. Al
Optim 550 ML	0.18	0.50	1.70	0.020	0.015	0.020

Table 2.3.4: Chemical composition of steel Optim 550 ML.

3 REVIEW OF PERFORMED RESEARCHES

The research on behaviour of cold-formed equal-leg angles has attracted attention of significant number of authors. Most of the works are based on comparison of results obtained from hand calculations according to design standards, simulation using FEA and experimental investigations. In this chapter general overview of computed researches will be presented. Some of the author's conclusions will be described in details further in appropriate chapter. This will assist in understanding of the basis for further research of considered problem.

Popovic et al. (1999) "Axial Compression Tests of Cold-Formed Angles"

The aim of this work was to perform tests on cold-formed angles, compare results with Australian and American Specifications for cold-formed, hot-rolled structures and to propose appropriate changes in Standards.

Tests were performed on 12 fixed-ended and 18 pin-ended cold-formed, in-line galvanized DuraGal angles with yield strength 350 MPa. Sections were as follows: L50x50x2.5, L50x50x4.0, L50x50x5 mm with nominal thickness 2.4, 3.8 and 4.7 mm respectively. First cross-sections were classified as slender and the last was classified as non-slender. Material properties of flat and corner part, residual stresses and initial imperfections were determined experimentally.

Fixed boundary conditions were implemented by restricting warping, twisting rotations and rotations about weak and strong axis. This was achieved by applying at the end of cross-section steel box and a bearing plate inside it, which was free to move in direction of applied load. Moreover, eight high-strength steel bolts locked bearing plate and twist rotations were restricted by four end plates. Four stiff steel rods were used to mount this assembly to support frame. Pin-ended conditions were different from fixed-ended in the way that four rods were substituted with pin-ended bearing connected to a shaft which allowed rotation about vertical axis. The average measured initial imperfection for long columns at mid-length was $L/2310$. Cross-sections with pinned boundary conditions were tested with minimal eccentricity of $L/1000$ which was applied about weak axis.

It was concluded that for stub columns the design strength predicted by AS 4100 and AS 4600 is higher than experimental capacity by values between 15 and 40 %. Additionally, it was concluded that additional moment causing compression in the tips of angle legs (according to AS 4600) equal to $N \cdot L/1000$ should be applied about minor axis only to slender sections. Moreover, additional moment due to shift of centroid should not be included for slender angles due to too conservative results. The current (1998) methods of distinguishing between slender and non-slender sections in AS 4100 were too conservative and needed amendments. This was due to the fact that although cross-section L50x50x4.0 was classified as slender it behaved as non-slender by failing in a purely flexural mode.

From conclusions it can be stated that it is necessary to study the influence of additional moment due to shift of centroid in slender angles. The slender cross-sections studied in thesis

should be designed with and without effect of shift of centroid due to local buckling and appropriate conclusion should be done. According to EN 1993-1-1 it is required to account for it but the results might be too conservative as it has been shown on the basis of American and Australian codes in work by Popovic et al. (1999).

Popovic et al. (2001) "Compression Tests of DuraGal Angles Loaded Parallel With a Leg"

The purpose of this work was to perform tests on cold-formed angles, compare results with predictions by Australian and American design rules and suggest improvements in design procedures.

Test program consisted of experiments on 11 cold-formed DuraGal slender angle sections with cross-section L50x50x2.5 and yield strength 400 MPa. Initial imperfections, material properties of flat and corner part were measured. Residual stresses were taken from test by Popovic et al. (1999). The average imperfections were reported as follows: L/1168 for tips of legs and L/2955 for corner. The specimens were loaded eccentrically what caused bending parallel with a leg at the ends of cross-section.

Compression tests were performed on pinned columns what was achieved by restraining perpendicular rotation and twist rotation at the ends, while rotation about axis parallel with a leg was free. Implementing of these boundary conditions was achieved by welding of 20 mm steel plates to each end of specimen. Afterwards, through holes in the corners of the plates they were bolted to bearing. Bearing was installed on the shaft allowing rotation about vertical axis and consisted of thick steel plate. One leg of the cross-section was parallel with axis of support rotation, which made specimen to bend in horizontal non-principal plane.

Test results have been compared with the design provisions by AS/NZS 4600-1996, AS 4100-1998, AISI-1997, ASCE-1991, AISC-1993. It has been shown that AS/NZS 4600-1996, AS 4100-1998, AISI-1997 predict very conservative design strength (in case of AS/NZS 4600-1996, AS 4100-1998 the difference 108% to 186% higher than test results; in case of AISI-1997 – 41% to 110 %). The changes proposed to design rules consisted of ignoring flexural-torsional critical load and calculation design strength based only on minor flexural mode. This approach does not neglect torsion because it is already accounted for in calculation of effective area of cross-section due to local buckling and local buckling is identical to torsional at vanishing lengths. ASCE rules are reported to be in good agreement with tested results. AISC rules are conservative at short and intermediate length.

The proposed approach of improving design standards AS/NZS 4600-1996 and AS 4100-1998 can be applied to the rules given in EN 1993-1-3 in case of very conservative results (ignoring flexural-torsional critical load and calculation design strength based only on minor flexural mode). Study of buckling curves based on this approach will be required to compare tests results, FEA predictions and hand calculations.

Young B. (2004) "Tests and Design of Fixed-Ended Cold-Formed Steel Plain Angle Columns"

The main objective of this work was to carry out experimental research of cold-formed angles and to compare results with design standards (AISI 1996 and AS/NZS 1996).

Test program was computed on slender brake-pressed plain angles with fixed boundary conditions. Angles were produced from high strength zinc-coated structural steel with nominal yield strength 500 and 450 MPa. Core thicknesses of plates were 1.2, 1.5 and 1.9 mm with the flange width 70 mm. Tested specimens had various lengths: 250, 1000, 1500, 2000, 2500, 3000 and 3500 mm. Material properties have been determined by coupon tests with coupons taken from the centre of the flange.

Implementing of fixed boundary conditions in compression test included following measures: welding of two steel end plates to the ends of specimen; connecting of top and bottom end plates of specimen to rigid flat bearing plates with bolts; restraining end plates against twist rotations, warping rotations, weaker and stronger axis rotation. The load was applied using displacement control procedure through lower end. The initial geometric imperfections have been measured and maximum global imperfections at mid-length were $L/1970$, $L/2150$, $L/2950$ for specimens with thicknesses 1.9, 1.5, 1.2 mm respectively.

The test results have shown that at all specimen's length failure is caused by interaction of flexural and flexural-torsional modes. However, this is not the case for stub columns with length 250 mm where failure is by local buckling and for length 1000 mm with thickness 1.9 mm where failure mode is flexural-torsional.

Experimental results have been compared with the design strength according to American Iron and Steel Institute (AISI 1996) Specification and Australian/New Zealand Standard (AS/NZS 1996) for cold-formed structures. Author also included in calculation specimens from Popovic et al. (1999) – L50x50x2.5, L50x50x4.0, L50x50x5 mm. It has been concluded that these standards provide very conservative results. Therefore, modifications for current design methods were considered. Firstly, author does not include recommendation of Popovic et al. (1999) to include additional moment for design of concentrically loaded columns. The reason for this is that ultimate loads without additional moment appear to be already lower than experimental results. Secondly, author uses recommendation proposed by Popovic et al. (2001) and calculates design strengths for slender and non-slender angles based only on flexural elastic critical load by ignoring torsional and torsional-flexural modes. It is shown that this method provides conservative results for non-slender section and unsafe for slender. Therefore, author proposed small modifications to AISI equations for calculation of critical inelastic and elastic buckling stresses. Furthermore, reliability analysis has been held and it has shown that this design rules provide reliable results for fixed slender and non-slender angles.

Ellobody E. and Young B. (2005) "Behaviour of Cold-Formed Steel Plain Angle Columns"

The purpose of this work was to simulate behaviour of cold-formed angles using FEM, perform parametric study and compare output with test results by Young (2004) and design standards.

The simulation was based on the specimens which were tested by Young (2004). Initial local imperfections, residual stresses and corner material properties were experimentally investigated and used as the input data for model in FEA. The magnitude of local imperfections was reported as 0.14% of plate thickness. From tensile coupon tests it has been noticed that ductility of flat part is much higher than in corner part. Moreover, static 0.2% proof stress of flat part is 15% lower than in corner part.

The Finite Element Model has been verified with experimental results and it has been shown that good agreement has been achieved with maximum difference of 15%. It has been noticed that residual stresses have negligible effect on the behaviour of cold-formed angles. More details on this are given in relevant chapter of this work.

Furthermore, parametric study on 35 angles has been performed using validated Finite Element Model. The results from FEA have been compared with design equations proposed by Young (2004) and design standards AISI 1996 and AS/NZS 1996. It has shown that American and Australian/New Zealand Standards were conservative for ratios b/t equal to 85, 65, 25 and they overestimated design strengths for ratios b/t equal to 15 and 5. Design strengths calculated using just flexural elastic critical buckling showed overestimated results for all columns. However, design equation proposed by Young (2004) showed good agreement with FEM parametric study results.

It can be summarized from works by Young (2004, 2005) that AISI 1996 and AS/NZS 1996 provide conservative results for calculation of design resistance of cold-formed concentrically loaded angles what can be also seen in case of results according to EN 1993-1-3. Therefore, the adjustments to calculation procedure proposed by author can also be applied and studied for making results less conservative (using minor flexural critical mode in calculations of design strengths; ignore additional moments in slender cross-sections; change in coefficients might be required). Parametric study will help to develop understanding of behaviour of cross-section with different slenderness.

Rasmussen, K. (2003, 2005). "Design of Angle Columns with Locally Unstable Legs."

The main aim of this work was to investigate the behaviour of slender cold-formed equal angles and to propose improvements to current design rules. The paper is mainly concerned about pin-ended columns. However, design proposals are also made for fix-ended specimens.

The author states that for slender angles local buckling mode is identical to torsional mode. This fact is described in more details in appropriate chapter of this thesis. As a result, the design provisions take torsional mode twice into account: through effective width and elastic

critical load, what leads to conservative results. Moreover, it is stated that in case of pinned angles the shift of centroid due to local buckling induces overall failure of the column what is not the case for fixed-ended angles. It is stated that slender equal-angle columns should inevitably be designed as beam-columns by introducing additional moment due to shift of centroid. This statement contradicts with the proposals made by Young (2004) who ignored any additional moments in design of fixed-ended concentrically loaded slender equal-leg angles.

The conclusion has been made that design methods provided by NAS Specification and AS/NZS 4600 are conservative. Therefore, following proposals were made to implement in design rules as a general design approach:

1. Use only minor flexural elastic critical load in calculation of design strength by ignoring torsional (local) buckling mode (this statement is in line with proposals by Popovic (2001) and Young (2004)).
2. Use changed design equations for calculation of effective width of legs;
3. Use proposed design equation in calculation of shift of effective centroid.

This design method is based on the slender equal-leg angles with the load applied through gross cross-section or with small eccentricity. This approach has shown good agreement for pin-ended and fixed-ended columns, except short length for fixed-ended columns where results become too conservative.

Moreover, simple design method has been proposed for calculation of angles with equal and unequal angles. This approach doesn't use bending capacity and compression-bending interaction equation.

Following statements can be concluded on the basis of work by Rasmussen (2003, 2005). It can be seen that approach proposed by Rasmussen (2003, 2005) requires design of slender angles as beam-columns what is not in line with the method proposed by Young (2004) for fixed-ended columns. Moreover, it can be seen that the approach of using flexural critical load by ignoring torsional critical mode in calculation of elastic critical load is similar for Rasmussen (2003, 2005), Young (2004) and Popovic et al. (2001).

Rasmussen (2006). "Design of Slender Angle Section Beam-Columns by the Direct Strength Method"

This work was aimed to propose approach to calculation of cold-formed slender equal-leg angles according to Direct Strength Method.

Continuing the work represented in Rasmussen (2003, 2005) author calculates slender equal-leg angles using beam-column approach. DSM (Direct Strength Method) is different from the existing approaches in design rules. In latter compression and bending strength are determined separately and combined using interaction formula. While using DSM elastic local buckling stress is determined for the actual stress distribution due to combined acting of compression and bending, and then this stress is used in direct strength equation for

beam-columns. DSM is proposed as an alternative which would help to omit complex calculations of effective width.

In the paper it is stressed that design of equal-leg angles needs special attention due to the fact that torsional mode is equal to local mode at short column lengths. Therefore, in line with the conclusions made in Rasmussen (2003, 2005) author ignores torsional critical load in determination of design strength using DSM. Moreover, additional loading eccentricity is used to account for shift of effective centroid which is determined using actual stress distribution. Finally, paper proposes the summarized procedure with given equations for using of Design Strength Method for slender equal-leg angles.

Design strengths obtained using DSM are compared with test results Willhoite et al. (1984) and Popovic et al. (1999). It is shown that DSM provides conservative results: for Popovic et al. (1999) mean value equal to 1.14 for ratio test strength/design strength; for Willhoite et al. (1984) mean value is 1.40. It can also be seen that compared to experiments DSM provides good prediction for variation in strength due to change of applied eccentricity.

This paper shows different approach for solution of the problem using Direct Strength Method. This might be the solution for the complex problem of equal-leg angles but the approach provided by Rasmussen (2006) provides fairly conservative results.

Shi, G., Liu, Z., and Chung, K. F. (2009). "Numerical study on the local buckling of 420MPa steel equal angle columns under axial compression."

The main aim of this paper was to investigate behaviour of hot-rolled equal-leg angle cross-section with yield strength of 420 MPa. This included determination of design strength according to ANSI/AISC 360-05 and Eurocode 3; performing of tests and Finite Element Analysis. Despite the fact that this paper is concerned only about hot-rolled profile, the investigation of local buckling in equal-leg angles and comparison with results from Eurocode 3 is of particular interest.

Test program consisted of stub compression tests with 5 sections: L125x8, L140x10, L160x10, L180x12 and L200x14. Each section had 3 specimens and 15 specimens were tested in total. The global buckling behaviour was excluded by limiting slenderness ratio of the cross-sections.

The specimens were tested as pin-ended. These boundary conditions were implemented by flattening of the end plane and using 4 ear plates welded to bearing plate. These plates restrained the horizontal displacement of the stub column, while the specimen was free to deform.

Material properties of flat part, initial geometric imperfections have been measured experimentally.

It has been concluded that local buckling is significant for high-strength steel columns with small slenderness and it governs the evaluation of design strength. After comparison of experimental results with design strengths according to ANSI/AISC 360-05 (2005) and

Eurocode 3 (EN 1993-1-1 2005, EN 1993-1-5 2006) it has been seen that these design rules predicted conservative results with an average excess of 18 % and 27 % respectively. It is also noticed that excess increases when width-to-thickness ratio of specimen gets bigger. After parametric study performed on the basis of FEA it has been concluded that Eurocode and ANSI/AISC 360-05 predict conservative results. However, Eurocode results are noticed to be more conservative.

From this paper it can be seen that Eurocode predictions for slender equal-leg angles predict conservative results. However, comparing with the results presented by other researchers about cold-formed angles bigger discrepancy in results of tests and hand calculations according to AISI has been observed. Moreover, it cannot be seen if shift of effective centroid has been incorporated in design strength evaluation by author. Therefore, it is hard to judge the approach used for calculations according to EN.

Silvestre, N., Dinis, P., and Camotim, D. (2013). "Developments on the Design of Cold-Formed Steel Angles."

The aim of this paper was to develop the method for design of fixed and pin-ended equal-leg angles for short-to-intermediate lengths on the basis of Direct Strength Method.

In the work author makes extensive research of the previously done investigations on equal-leg angles. This leads to gathering of large column ultimate strength data which was taken as experimental results from literature and results from performed Finite Element Analysis.

Author reports that despite the fact that it is hard to distinguish between local and torsional buckling, it is necessary to separate these two modes. This is due to different postcritical strength capacities of two modes. On the basis of review of works by Dinis et al. (2010a, 2011, 2012a, b) and Dinis and Camotim (2011) it is stated that pin-ended and fixed-ended short-to-intermediate columns have different behaviour and design strength. Moreover, flexural displacements of the corner part play key role in separating these behaviours. Therefore, flexural component cannot be omitted in calculations and local buckling cannot be viewed as only torsional mode. DSM has been incorporated in the most recent standards AISI (2007), SA/NZS 2005 and some of cold-formed shapes (Z-sections, lipped channels, rack sections) are already pre-qualified for implementation of DSM in design strength evaluation. However, this is not the case for equal-leg angles yet. It is also stated that despite the researches which have been done in the field of Direct Strength Method by Rasmussen (2005) and Chodraui et al. (2006) the application cannot be widely considered due to significant number of poor strength predictions.

Newly proposed design procedure combines equations suggested by Young (2004) with modified Direct Strength Method equations. Different DSM curves are used for design for fixed and pin-ended columns. Newly proposed design method leads to better results than those proposed by Rasmussen (2005). This approach has shown good results compared with the test results and methods proposed in literature, while keeping simple provisions of Design Strength Method. However, it is stressed that currently available methods don't

provide as good ultimate strength predictions as for more complex cross-sections (plain or lipped channels).

It can be summarized that author presents the new DSM-based approach and stresses the importance of distinguishing between local and torsional modes. However, most of the previous researches were based on the fact stated by Popovic et al. that local mode is equal to torsional at vanishing lengths.

Conclusion

From the available researches it can be seen that development of the design of cold-formed equal-leg angles is mostly studied in the frames of American and Australian/New Zealand design codes. The only research which compared predictions by Eurocode was done by Shi G. et al (2009) but this work was concerned only about hot-rolled high strength steel profiles. Unfortunately, detailed description of applied EN procedures cannot be seen in the work and that is why it is hard to compare results with the results from other researchers. Moreover, none of the suggestions for improvements of results have been proposed. Therefore, the results of the research on cold-formed equal-leg angles in the frame of Eurocode design rules will be of major interest to scientific society.

Moreover, it can be seen that the method used in the current thesis is in line with the methods implemented by most of the researches: comparison of design rules outputs, FEA parametric study and experimental results.

Despite the fact that most of works in the field of cold-formed equal angles is done in the frame of American and Australian/New Zealand design codes, the outcomes might be applied to the research with basis on EN. The steps taken by researchers described above might be applied and studied. The main applicable steps will be summarized further.

According to Popovic et al. (1999) it was proposed to disregard additional moment due to shift of centroid but to include additional moment for slender angles equal to $N \cdot L / 1000$ (latter might be applicable only for American and Australian Specifications). According to Popovic et al. (2001) flexural-torsional critical load should be ignored and calculation of design strength should be based only on minor flexural mode; local mode is identical to torsional at short lengths. According to Young (2004), Ellobody E. and Young B. (2005) for fixed-ended equal-leg angles should be used minor flexural critical mode in calculations of design strengths (incorporated from Popovic et al. (2001); ignored additional moments in slender cross-sections; change in coefficients of strength calculation might be required. The way proposed by Rasmussen K. (2003, 2005) is different from previous author and it suggests design of slender cold-formed angles as beam-columns accounting for additional moment due to shift of effective centroid. Moreover, only flexural critical load is used for determination of design strength what is in line with Popovic et al. (2001) and Young (2004). According to Rasmussen K. (2006) previously described suggestions are incorporated but calculation is performed using proposed Design Strength Method procedure which has different approach compared to design strength provisions of design codes. Silvestre N.

(2013) suggested distinguishing between torsional and local mode; using DSM-based approach (equations proposed by Young (2004) with local strength DSM-curves).

It can be stated that the development of Direct Strength Method is currently the main approach which is being developed in order to achieve the most accurate predictions of ultimate strength for cold-formed angles. This approach might also be considered for using in EN in case of conservative results. However, current design methods studied by mentioned researchers cannot yet provide as good predictions of ultimate strength as for more complex cross-sections, as plain or lipped channels.

4 PROPERTIES OF CROSS-SECTIONS

4.1 Tested specimens

Steel producer delivered for tests several specimens from two steel grades 650MC and 550ML, which were described in detail in previous paragraphs. All profiles have same length 600 mm and are separated in six groups according to their internal angle, which varies from 90° to 170°. Each group also includes variation of thickness, ranging from 4 mm to 20 mm. More information can be obtained from the Table 4.1.1 below this paragraph.

Group	Codename	Steel grade	b [mm]	h [mm]	t [mm]	Angle [°]
P1	P1-4	650MC	60	60	4	90
	P1-6	650MC	60	60	6	90
	P1-10	650MC	60	60	10	90
	P1-16	500ML	60	60	16	90
	P1-20	500ML	60	60	20	90
P2	P2-4	650MC	60	60	4	100
	P2-6	650MC	60	60	6	100
	P2-10	650MC	60	60	10	100
	P2-16	500ML	60	60	16	100
	P2-20	500ML	60	60	20	100
P3	P3-4	650MC	60	60	4	120
	P3-6	650MC	60	60	6	120
	P3-10	650MC	60	60	10	120
	P3-16	500ML	60	60	16	120
	P3-20	500ML	60	60	20	120
P4	P4-4	650MC	60	60	4	140
	P4-6	650MC	60	60	6	140
	P4-10	650MC	60	60	10	140
	P4-16	500ML	60	60	16	140
	P4-20	500ML	60	60	20	140
P5	P5-4	650MC	60	60	4	160
	P5-6	650MC	60	60	6	160
	P5-10	650MC	60	60	10	160
	P5-16	500ML	60	60	16	160
	P5-20	500ML	60	60	20	160
P6	P6-4	650MC	60	60	4	170
	P6-6	650MC	60	60	6	170
	P6-10	650MC	60	60	10	170
	P6-16	500ML	60	60	16	170
	P6-20	500ML	60	60	20	170

Table 4.1.1: Basic geometry of tested specimens

4.2 Expected versus real shape

All elements for testing had specified geometry and AutoCAD drawings were prepared by Lulea Technical University, later sent to the manufacturer. Unfortunately during initial check of delivered specimens it had been discovered, that expected and real shape is slightly different. From the photo below (Figure 4.2.1), it is visible, that almost none of checked specimen fit to designed cross-section.

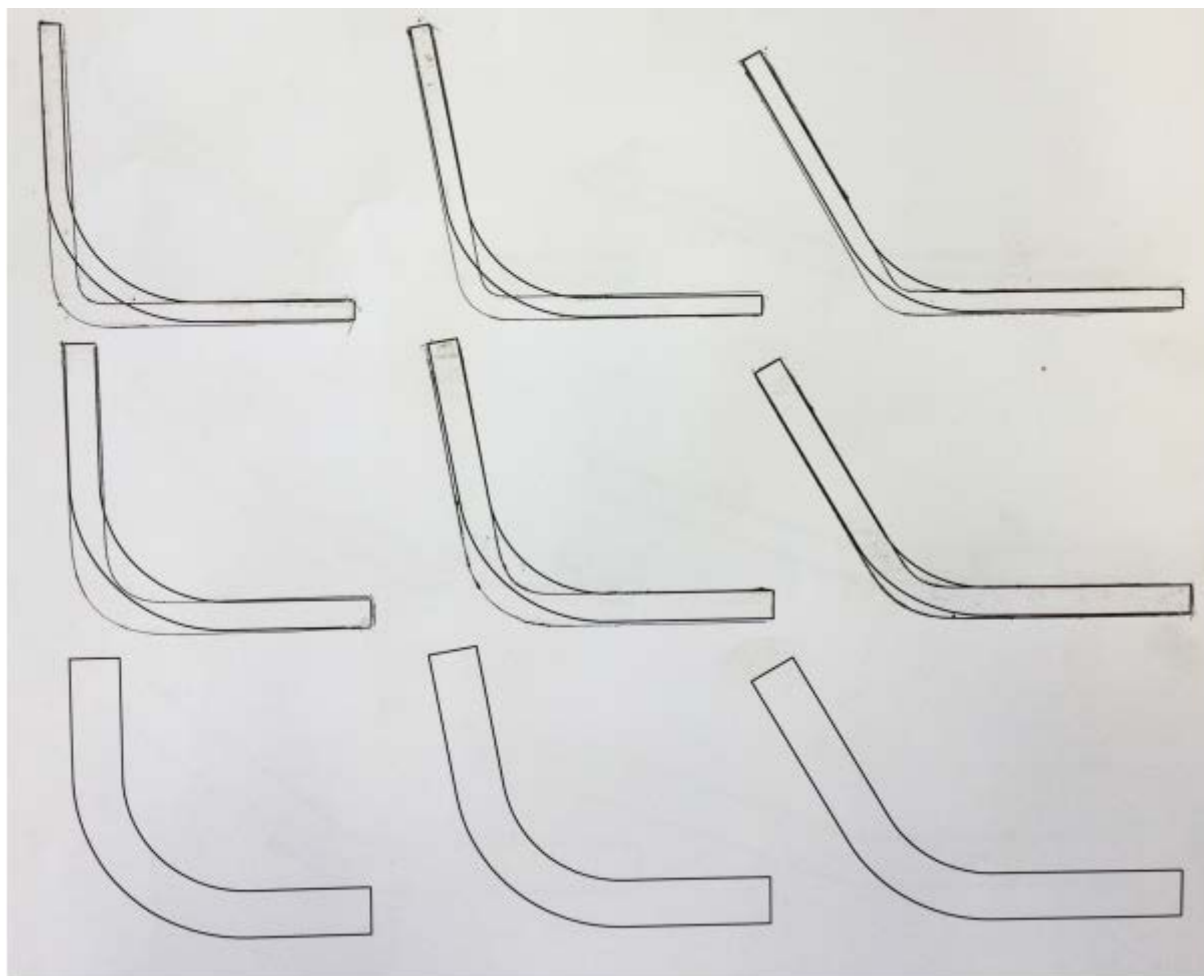


Figure 4.2.1: Expected shape (thinner line) versus real shape (thicker line)

Therefore, it was decided to create new AutoCAD design, which will fit cold-formed specimens. After several trials it has been discovered, that internal radius of 1.5 times the thickness is the closest to real shape. Unfortunately there is still a slight inaccuracy for some elements, since it is not possible to bend all elements exactly to given angle (Figure 4.2.2).

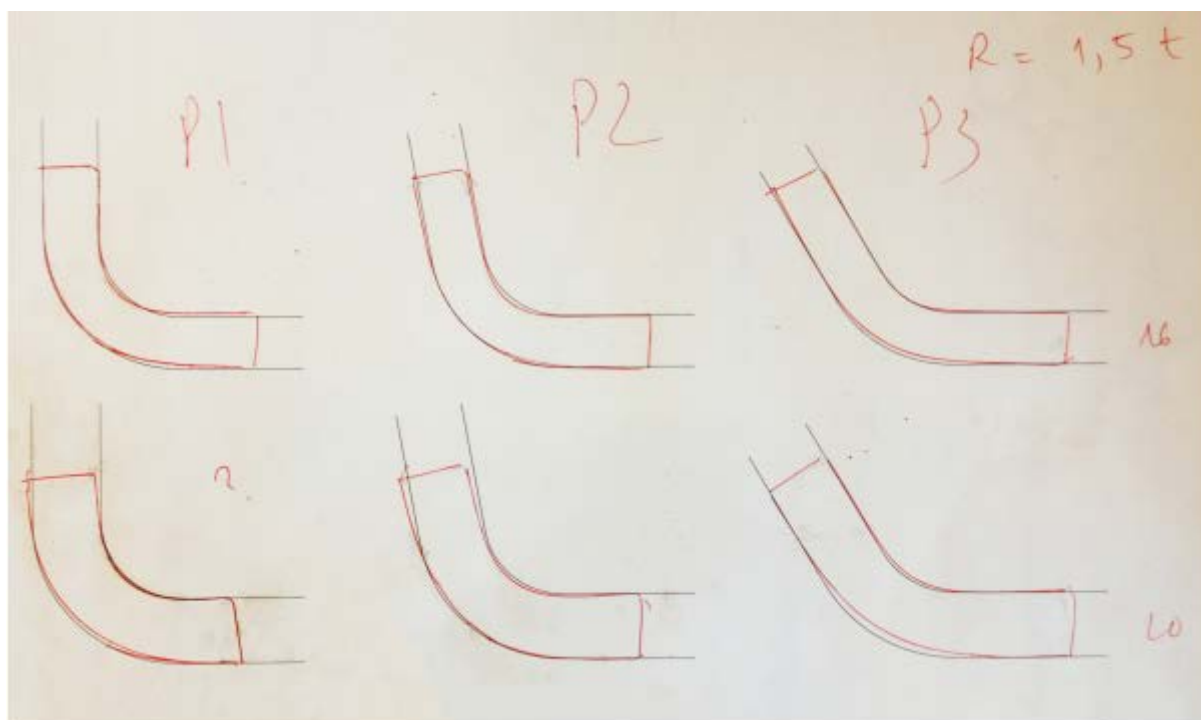


Figure 4.2.2: Internal radius $1.5t$ (black line) matches most of the profiles (red line)

Conclusion for design of cold formed elements in general is therefore to contact producer and discuss limits in production of final steel cross-sections. It can be easily discovered, that ideal shape developed by designer can't be produced in practice.

4.3 Cold forming and change of material properties

In steel industry two main ways are recognized, in terms of shaping of raw steel to its final shape. First is hot-rolling method, but this won't be part of this thesis, since elements delivered by company Ruukki were shaped by the second method, cold forming. More specifically by method called press-braking, which is nowadays quite popular.

It is known, that the manufacturing process plays a governing role for some material characteristics and in this case can influence the buckling behaviour of profiles (see Table 4.3.1). Cold forming leads to a modification of the stress-strain curve of the steel. With respect to the virgin (original) material, cold-forming can increase the yield and ultimate strength. Effected area with increased resistance depends on type of cold-forming, in our case the press-braking influences corner area, while leaving the straight parts almost unchanged.

Forming method		Hot rolling	Cold forming	
			Cold rolling	Press braking
Yield strength	Corner	-	high	high
	Flange	-	moderate	-
Ultimate strength	Corner	-	high	high
	Flange	-	moderate	-

Table 4.3.1: Influence of manufacturing process on the basic strength of hot and cold-formed profiles. (Dubina, Ungureanu, & Landolfo, 2013)

Eurocode provides straightforward method for evaluation of increased resistance in part EN1993-1-3. Increased resistance can be applied on cold formed structures, if they fulfil following conditions:

- In case of axially loaded members in which the effective area of cross-sections A_{eff} equal the gross area A_g (in case of Class 4, ρ must be equal to 1.0)
- In determining the A_{eff} the yield strength f_y should be taken as the basic yield strength f_{yb}

Generally the average yield strength f_{ya} of a cross-section member formed by cold-forming method should be evaluated according formula:

$$f_{ya} = f_{yb} + (f_u - f_{yb}) \frac{knt^2}{A_g} \quad \text{but} \quad f_{ya} \leq \frac{(f_u + f_{yb})}{2} \quad (\text{ref. EN 1993-1-3, ch. 3.2.2(3)})$$

Where:

A_g is the gross cross-sectional area;

k is a numerical coefficient that depends on the type of forming as follows:

(a) $k = 7$ for roll forming;

(b) $k = 5$ for other methods of forming;

n is the number of 90° bends in the cross-section with an internal radius $r \leq 5t$ (fractions of 90° bends should be counted as fractions of n);

t is the design core thickness of the steel material before cold-forming, exclusive of metal and organic coatings.

The average yield strength f_{ya} may be utilized while determining:

- Cross-section resistance of an axially loaded tension member;
- Cross-section resistance and the buckling resistance of an axially loaded compression member with a fully effective cross-section;
- Moment resistance of a cross-section with fully effective flanges.

In the following calculations where the yield strength is specified using the symbol f_y the average yield strength f_{ya} will be used. This will be done if previously mentioned conditions apply. In other cases the basic yield strength f_{yb} will be used. Where the yield strength is specified using the symbol f_{yb} the basic yield strength f_{yb} will be used.

However, according to EN 1993-1-3, chapter 3.2.4(1) the provisions for design by calculation given in Part 1-3 of EN1993 may be used for steel within given ranges of core thickness t_{cor} . The following values are recommended:

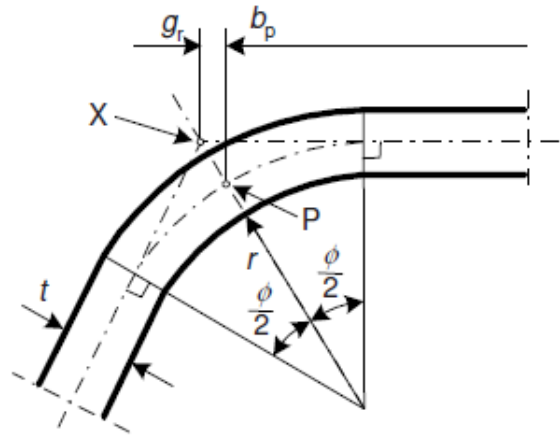
- For sheeting and members: $0.45 \text{ mm} < t_{cor} < 15 \text{ mm}$
- For connections: $0.45 \text{ mm} < t_{cor} < 4 \text{ mm}$

Thicker or thinner material may also be used, provided the load bearing resistance is determined by design assisted by testing.

The results are presented in **Attachment 1 – Determination of average yield strength**.

4.4 Influence of rounded corners

As a result of manufacturing process (press-braking), cold formed steel sections have rounded corners. Value of internal radius of rounded corners in provided specimens is dependent on the thickness of the specimens ($r = 1.5t$). According to Eurocode EN 1993-1-3, chapter 5.1(1) the notional flat widths of the plane elements shall be measure from the midpoints of the adjacent corner elements as indicated in Figure 4.4.1 (EN 1993-1-3:2006).



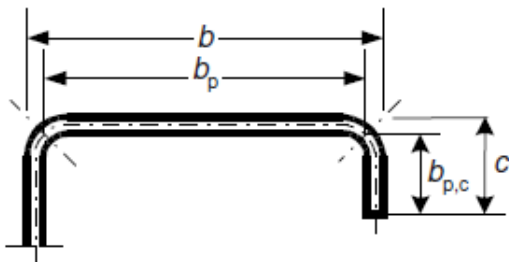
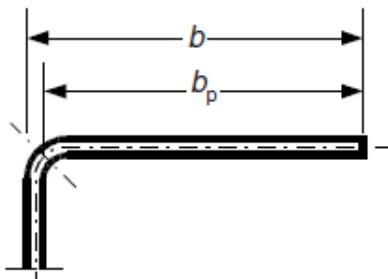
(a) midpoint of corner or bend

X is intersection of midlines

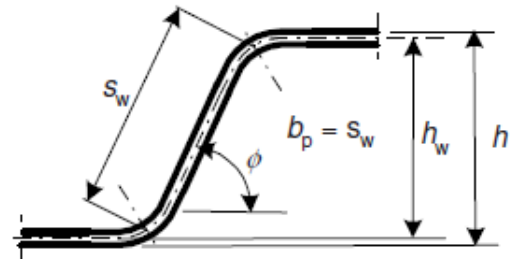
P is midpoint of corner

$$r_m = r + t/2$$

$$g_r = r_m \left(\tan\left(\frac{\phi}{2}\right) - \sin\left(\frac{\phi}{2}\right) \right)$$

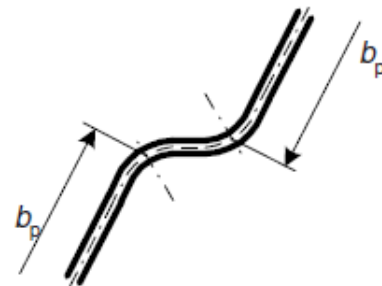


(b) notional flat width b_p of plane parts of flanges

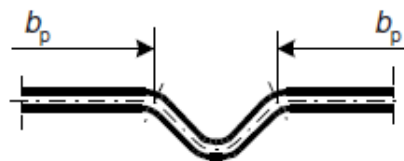


(c) notional flat width b_p for a web

($b_p = \text{slant height } s_w$)



(d) notional flat width b_p of plane parts adjacent to web stiffener



(e) notional flat width b_p of flat parts adjacent to flange stiffener

Figure 4.4.1: Notional widths of plane cross section parts b_p allowing for corner radii.

According to EN 1993-1-3, chapter 5.1(3) the influence of rounded corners on cross-section resistance may be neglected if the internal radius $r \leq 5t$ and $r \leq 0.10b_p$ and the cross-section may be assumed to consist of plane elements with sharp corners. Calculation of this limitation is presented in Table 4.4.1 and 4.4.2.

Group	Profile number	t [mm]	r [mm]		5t	Verification
P1	P1-4	4	6,00	<	20	OK
	P1-6	6	9,00	<	30	OK
	P1-10	10	15,00	<	50	OK
	P1-16	16	24,00	<	80	OK
	P1-20	20	30,00	<	100	OK
P2	P2-4	4	6,00	<	20	OK
	P2-6	6	9,00	<	30	OK
	P2-10	10	15,00	<	50	OK
	P2-16	16	24,00	<	80	OK
	P2-20	20	30,00	<	100	OK
P3	P3-4	4	6,00	<	20	OK
	P3-6	6	9,00	<	30	OK
	P3-10	10	15,00	<	50	OK
	P3-16	16	24,00	<	80	OK
	P3-20	20	30,00	<	100	OK
P4	P4-4	4	6,00	<	20	OK
	P4-6	6	9,00	<	30	OK
	P4-10	10	15,00	<	50	OK
	P4-16	16	24,00	<	80	OK
	P4-20	20	30,00	<	100	OK
P5	P5-4	4	6,00	<	20	OK
	P5-6	6	9,00	<	30	OK
	P5-10	10	15,00	<	50	OK
	P5-16	16	24,00	<	80	OK
	P5-20	20	30,00	<	100	OK
P6	P6-4	4	6,00	<	20	OK
	P6-6	6	9,00	<	30	OK
	P6-10	10	15,00	<	50	OK
	P6-16	16	24,00	<	80	OK
	P6-20	20	30,00	<	100	OK

Table 4.4.1: Verification of limits for neglecting of rounded corners.

Group	Profile number	t [mm]	b _p [mm]	r [mm]		0.10*b _p	Verification
P1	P1-4	4	55.66	6.00	>	5.566	NOT OK
	P1-6	6	53.49	9.00	>	5.349	NOT OK
	P1-10	10	49.14	15.00	>	4.914	NOT OK
	P1-16	16	42.63	24.00	>	4.263	NOT OK
	P1-20	20	38.28	30.00	>	3.828	NOT OK
P2	P2-4	4	56.75	6.00	>	5.675	NOT OK
	P2-6	6	55.13	9.00	>	5.513	NOT OK
	P2-10	10	51.88	15.00	>	5.188	NOT OK
	P2-16	16	47.01	24.00	>	4.701	NOT OK
	P2-20	20	43.76	30.00	>	4.376	NOT OK
P3	P3-4	4	58.23	6.00	>	5.823	NOT OK
	P3-6	6	57.34	9.00	>	5.734	NOT OK
	P3-10	10	55.57	15.00	>	5.557	NOT OK
	P3-16	16	52.91	24.00	>	5.291	NOT OK
	P3-20	20	51.13	30.00	>	5.113	NOT OK
P4	P4-4	4	59.1	6.00	>	5.91	NOT OK
	P4-6	6	58.64	9.00	>	5.864	NOT OK
	P4-10	10	57.74	15.00	>	5.774	NOT OK
	P4-16	16	56.39	24.00	>	5.639	NOT OK
	P4-20	20	55.48	30.00	>	5.548	NOT OK
P5	P5-4	4	59.63	6.00	>	5.963	NOT OK
	P5-6	6	59.44	9.00	>	5.944	NOT OK
	P5-10	10	59.06	15.00	>	5.906	NOT OK
	P5-16	16	58.5	24.00	>	5.85	NOT OK
	P5-20	20	58.13	30.00	>	5.813	NOT OK
P6	P6-4	4	59.82	6.00	>	5.982	NOT OK
	P6-6	6	59.73	9.00	>	5.973	NOT OK
	P6-10	10	59.56	15.00	>	5.956	NOT OK
	P6-16	16	59.29	24.00	>	5.929	NOT OK
	P6-20	20	59.11	30.00	>	5.911	NOT OK

Table 4.4.2: Verification of limits for neglecting of rounded corners.

According to verifications provided in tables, influence of rounded corners cannot be neglected in specimens P1-P6. As a result, the calculation of section properties should be based upon the nominal geometry of the cross-section. Notional width has to be calculated according to EN 1993-1-3.

4.5 Geometrical proportions

As stated in EN 1993-1-3, chapter 5.2(1) the provisions for design by calculation given in this part 1-3 of EN 1993 should not be applied to cross-sections outside the range of width-to-thickness ratios b/t , h/t , c/t and d/t give in Figure 4.5.1.


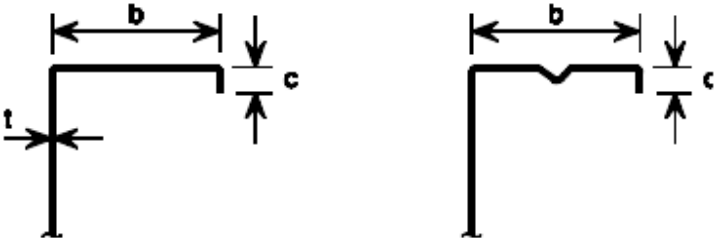
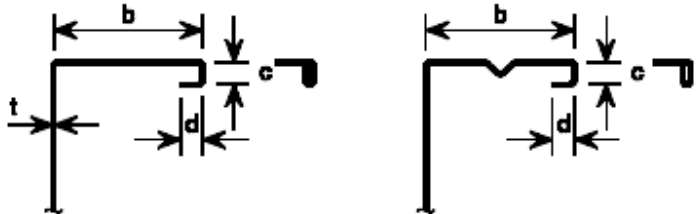
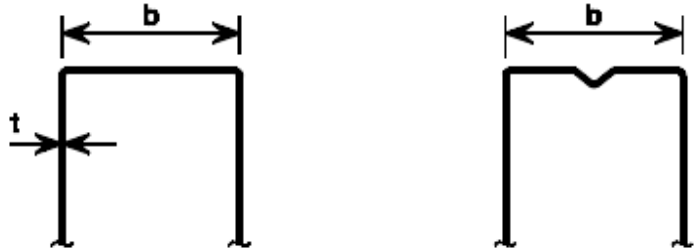

Element of cross-section	Maximum value
	$b/t \leq 50$
	$b/t \leq 60$ $c/t \leq 50$
	$b/t \leq 90$ $c/t \leq 60$ $d/t \leq 50$
	$b/t \leq 500$
	$45^\circ \leq \phi \leq 90^\circ$ $h/t \leq 500 \sin \phi$

Figure 4.5.1: Maximum width-to-thickness ratios (EN 1993-1-3, Table 5.1)

Verification of tested specimens according given limits is provided in Table 4.5.1 on the next page.

Group	Profile number	b [mm]	t [mm]	b/t		Limit	Verification
P1	P1-4	60	4	15.00	<	50	OK
	P1-6		6	10.00	<	50	OK
	P1-10		10	6.00	<	50	OK
	P1-16		16	3.75	<	50	OK
	P1-20		20	3.00	<	50	OK
P2	P2-4		4	15.00	<	50	OK
	P2-6		6	10.00	<	50	OK
	P2-10		10	6.00	<	50	OK
	P2-16		16	3.75	<	50	OK
	P2-20		20	3.00	<	50	OK
P3	P3-4		4	15.00	<	50	OK
	P3-6		6	10.00	<	50	OK
	P3-10		10	6.00	<	50	OK
	P3-16		16	3.75	<	50	OK
	P3-20		20	3.00	<	50	OK
P4	P4-4		4	15.00	<	50	OK
	P4-6		6	10.00	<	50	OK
	P4-10		10	6.00	<	50	OK
	P4-16		16	3.75	<	50	OK
	P4-20		20	3.00	<	50	OK
P5	P5-4		4	15.00	<	50	OK
	P5-6		6	10.00	<	50	OK
	P5-10		10	6.00	<	50	OK
	P5-16		16	3.75	<	50	OK
	P5-20		20	3.00	<	50	OK
P6	P6-4		4	15.00	<	50	OK
	P6-6		6	10.00	<	50	OK
	P6-10		10	6.00	<	50	OK
	P6-16		16	3.75	<	50	OK
	P6-20		20	3.00	<	50	OK

Table 4.5.1: Verification of geometrical properties for cold-formed sections.

4.6 Classification of cross-sections

Classification of all cross-sections has been performed on the basis of EN 1993-1-1 considering the yield strength of high-strength steel. Details regarding steel properties were given in 2.3 HSS by Ruukki. Main task is to recognize Class 4 cross-section, which is susceptible to local buckling phenomena and therefore full cross-section area and other geometrical properties can't be used.

According to EN 1993-1-1, ch. 5.5.2 classification of cross-sections is given as follows: Class 1 cross-sections are those which can form a plastic hinge with the rotation capacity required from plastic analysis without reduction of the resistance. Class 2 cross-sections are those which can develop their plastic moment resistance, but have limited rotation capacity because of local buckling. Class 3 cross-sections are those in which the stress in the extreme compression fibre of the steel member assuming an elastic distribution of stresses can reach the yield strength, but local buckling is liable to prevent development of the plastic moment resistance. Class 4 cross-sections are those in which local buckling will occur before the attainment of yield stress in one or more parts of the cross-section.

Eurocode provides detailed setup of evaluating class of cross-section (Figure 4.6.1), however in case of angles is used hot-rolled profile with straight corner. Therefore modification was needed and dimensions (h, b) were taken as a distance from the edge of profile to the midpoint of the outer corner.

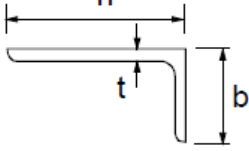
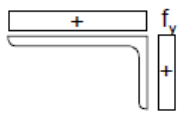
<p>Refer also to "Outstand flanges" (see sheet 2 of 3)</p>		<p>Angles</p> 	<p>Does not apply to angles in continuous contact with other components</p>
Class	Section in compression		
Stress distribution across section (compression positive)			
3	$\boxed{AC_2} \quad h / t \leq 15\epsilon \quad \text{and} \quad \frac{b+h}{2t} \leq 11,5\epsilon \quad \boxed{AC_2}$		

Figure 4.6.1: Classification of angle cross-section

Classification of the cross-sections can be found in **Attachment 2 – Classification of cross-sections**.

4.7 Determination of cross-section effective area

With respect to previously performed classification of cross-sections it was determined that cross-sections in groups P1-P6 with thicknesses 4 and 6 mm are Class 4. Therefore it is necessary to evaluate their effective properties. This procedure will be done according to EN 1993-1-3, chapter 5.5.2 as for plane elements without stiffeners.

All specimens are subjected to uniform compression. Effective width of outstand compression elements is evaluated according to Figure 4.7.1 (EN 1993-1-5, Table 4.2).

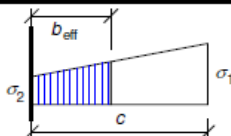
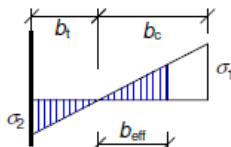
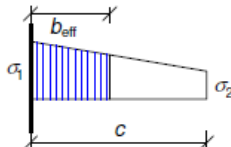
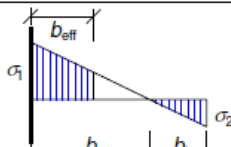
Stress distribution (compression positive)		Effective ^p width b_{eff}			
		$1 > \psi > 0:$ $b_{eff} = \rho c$			
		$\psi < 0:$ $b_{eff} = \rho b_c = \rho c / (1-\psi)$			
$\psi = \sigma_2/\sigma_1$	1	0	-1	$1 \geq \psi \geq -3$	
Buckling factor k_σ	0,43	0,57	0,85	$0,57 - 0,21\psi + 0,07\psi^2$	
		$1 > \psi \geq 0:$ $b_{eff} = \rho c$			
		$\psi < 0:$ $b_{eff} = \rho b_c = \rho c / (1-\psi)$			
$\psi = \sigma_2/\sigma_1$	1	$1 > \psi > 0$	0	$0 > \psi > -1$	-1
Buckling factor k_σ	0,43	$0,578 / (\psi + 0,34)$	1,70	$1,7 - 5\psi + 17,1\psi^2$	
				23,8	

Figure 4.7.1: Outstand compression elements (EN 1993-1-5, Table 4.2)

The reduction factor ρ is taken as follows:

$$\rho = 1 \quad \text{for } \bar{\lambda}_p \leq 0.748$$

(ref. EN 1993-1-5, ch.4.4(2))

$$\rho = \frac{\bar{\lambda}_p - 0.188}{\bar{\lambda}_p^2} \quad \text{for } \bar{\lambda}_p > 0.748$$

Where:

$$\bar{\lambda}_p = \frac{b_p/t}{28.4\epsilon\sqrt{k_\sigma}}$$

ψ is the stress ratio,

b_p is the notional width taken according to EN 1993-1-3, ch. 5.5.2.

k_σ is the buckling factor corresponding to the stress ratio ψ and boundary conditions;

t is the thickness;

$$\varepsilon = \sqrt{\frac{235}{f_y \left[\frac{N}{mm^2} \right]}}$$

Numerical evaluation of effective cross-section properties can be found in **Attachment 3 – Determination of effective width for Class 4 cross-sections.**

4.8 Determination of cross-section geometrical properties

To correctly evaluate resistance of each cross-section, it is needed to determine its geometrical properties first. In case of double-symmetrical cross-section (I profile, H profile, etc.) the evaluation is simple and fast, but unfortunately for L shaped profile it is much more complicated. Angles are symmetric only about one axis and therefore centre of gravity and shear centre are not in the same position. For the analysis was used mostly computer and appropriate software, however some values were checked by hand calculations.

Evaluated geometrical properties:

A / A_{eff}	Area / Effective Area	$[\text{mm}^2]$
$I_y, I_z / I_{y.\text{eff}}, I_{z.\text{eff}}$	Moment of inertia / Effective value	$[\text{mm}^4]$
i_y, i_z	Radius of gyration	$[\text{mm}]$
d_y, d_z	Distance between c.o.g and shear centre	$[\text{mm}]$
$I_t / I_{t.\text{eff}}$	Torsional moment / Effective value	$[\text{mm}^4]$
$I_w / I_{w.\text{eff}}$	Warping constant / Effective value	$[\text{mm}^6]$

First part of determination consisted of drawing all cross-sections in AutoCAD 2014 (Autodesk) by polyline and creating an independent region from each L shaped element. This software has ability to calculate several geometrical properties, but as was discovered its capabilities are limited and not suitable for purposes of this thesis. Current version can calculate centre of gravity and after moving UCS (user coordinate system) to object's c.o.g (centre of gravity) it will evaluate its moments of inertia (Figure 4.8.1).

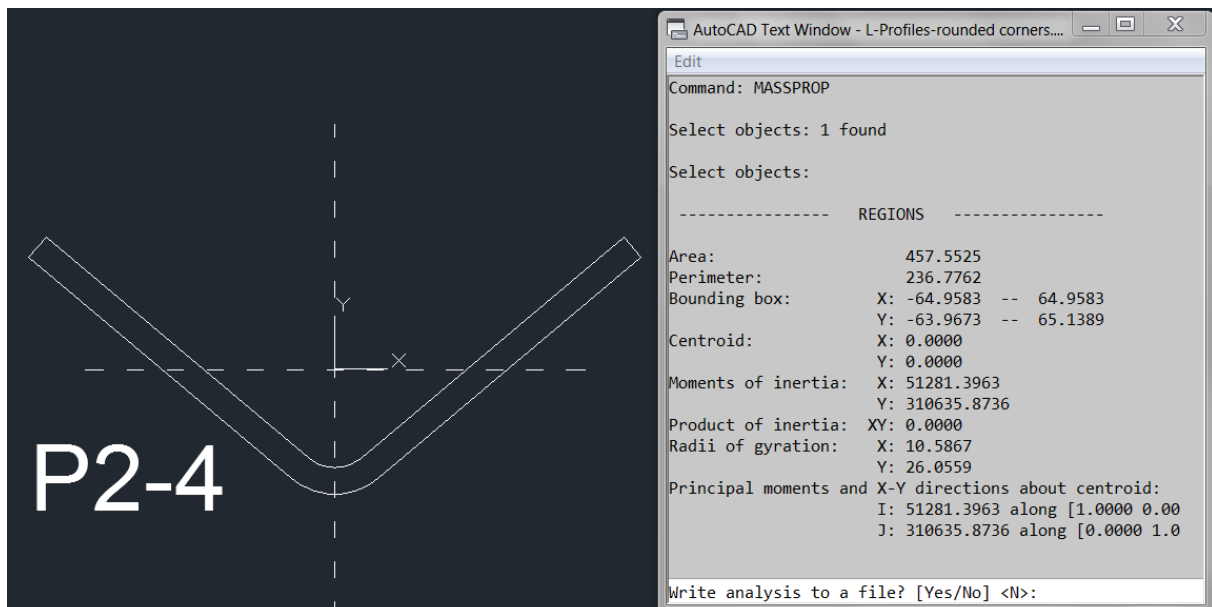


Figure 4.8.1: AutoCAD provides limited list of geometrical properties

More cross-sectional properties like Torsional moment or Warping constant are not available, therefore another software called Robot Structural Analysis Professional (Autodesk) was considered. Function of creating new cross-section may help evaluate all properties, but import of drawings from AutoCAD 2014 was very complicated and not working properly.

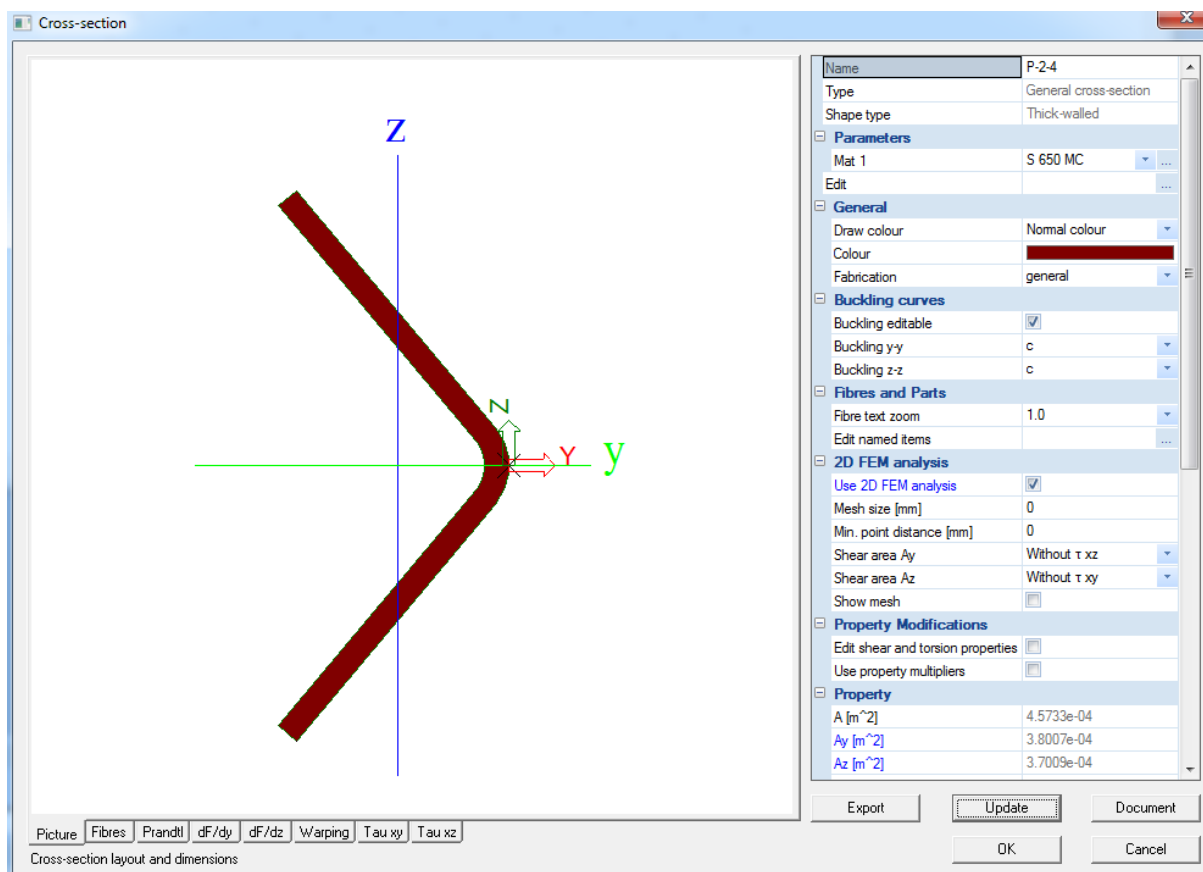


Figure 4.8.2: SCIA Engineer provides complete cross-section analysis

Finally software SCIA Engineer 2013.0 (Nemetschek, 2013) was used. Its graphical interface provides easy and fast evaluation of all needed properties (Figure 4.8.2). Import of cross-section from AutoCAD was used to preserve accurate shape. All values obtained from this software are calculated with respect to the principal axis of the angle, therefore it was necessary to rotate the section axis according the main axis in the software (y – principal major axis; z – principal minor axis). Output in form of notepad was imported to the Microsoft Excel 2013 and after conversion to appropriate units the elastic critical load, torsional buckling critical load and torsional-flexural buckling critical load were evaluated.

All geometrical properties will be presented with following orientation of axis (Figure 4.8.3):

- y – principal major axis; axis of symmetry;
- z – principal minor axis.

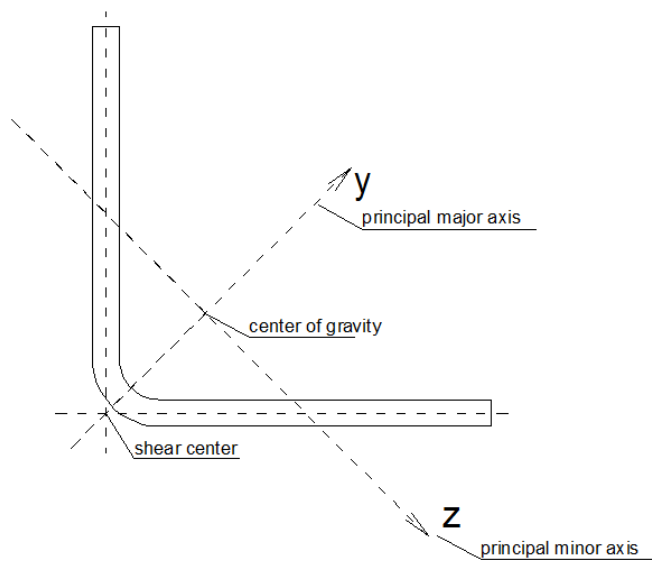


Figure 4.8.3: Orientation of principal axis of cross-section.

For the table with geometrical properties of cross-sections and critical loads see **Attachment 4 – Determination of geometrical properties and elastic critical force (fixed BC).**

5 ELASTIC CRITICAL LOAD

5.1 General

Tested steel elements can be considered as compressed bars and therefore significant part of their resistance is ability to resist buckling. Centrally loaded equal-leg angles can buckle in one of the following modes (Galambos, 1998):

- flexural buckling about the minor principal axis,
- torsional-flexural buckling.

The description of failure modes for equal-leg angles is presented further.

5.2 Flexural buckling (theory) and boundary conditions

A flexural buckling phenomenon was well described by Leonhard Paul Euler (1744). There is certain magnitude of an applied force, after which the bar loses its stability and buckles. Euler named this magnitude as “Critical load” and for a column it is the most basic force to calculate.

Before we start to evaluate the “Critical load” we need to make several assumptions (Narayanan, et al., 1999):

1. Strut is perfectly straight without any imperfection.
2. End supports are pinned, strut can rotate in all directions, but can't translate.
3. Strut is from homogenous material, which behaves in elastic range (Hooke's law is valid).
4. Load is applied at COG on both ends, no eccentricity and moment is produced.

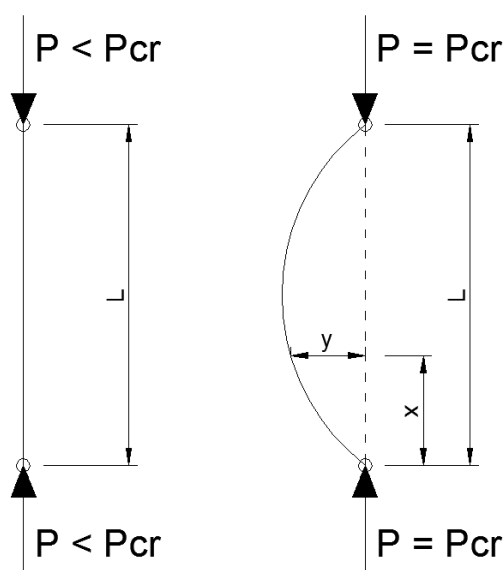


Figure 5.2.1: Ideal strut in compression

To simplify the problem from 3D to 2D, it is assumed that strut can bend (buckle) only in one plane (around one axis) as shown in Figure 5.2.1. Strut remains straight (stable) during loading as long as loading force P is smaller than P_{cr} . When $P = P_{cr}$ strut buckles (becomes instable). To express this behaviour in terms of differential equation, we need to consider deformation y at random distance x from the lower support B.

The bending moment is then given by equation:

$$M = P_{cr} \cdot y$$

Buckling deformation in terms of differential equation:

$$-E \cdot I \cdot \frac{d^2 \cdot y}{d \cdot x^2} = P_{cr} \cdot y$$

General solution can be expressed as follows:

$$y = A_1 \cdot \cos x \cdot \sqrt{\frac{P_{cr}}{EI}} + B_1 \cdot \sin x \cdot \sqrt{\frac{P_{cr}}{EI}}$$

Where:

A_1, A_2 – are constants

Now the expression will be observed, in order to see its behaviour under several conditions:

- 1) When $y = 0$, then $x = 0$ and consequently $\cos x \Rightarrow \cos 0 = 1$, therefore $A_1 = 0$
- 2) When $x = L$, then $y = 0$

From, which can be concluded:

$$B_1 \cdot \sin L \cdot \sqrt{\frac{P_{cr}}{EI}} = 0$$

and therefore:

$$B_1 = 0 \quad \text{or} \quad \sin L \cdot \sqrt{\frac{P_{cr}}{EI}} = 0$$

When $B_1 = 0$, then $y = 0$ for all values of x (column remains straight / stable), but more convenient is to focus on solution of the remaining part of the equation:

$$\sin L \cdot \sqrt{\frac{P_{cr}}{EI}} = 0$$

To satisfy given condition that left part of the equation is equal to the right, there is a need for series of numbers, where value of sinus is 0 and that is true only when:

$$\text{Argument } L \cdot \sqrt{\frac{P_{cr}}{EI}} = 0, \pi, 2\pi, 3\pi, 4\pi, 5\pi, \dots$$

By knowing this fact, P_{cr} can be extracted on the left side of the equation in following way

$$L \cdot \sqrt{\frac{P_{cr}}{EI}} = \pi \quad /^2$$

$$L^2 \cdot \frac{P_{cr}}{EI} = \pi^2 \quad / L^2$$

$$\frac{P_{cr}}{EI} = \frac{\pi^2}{L^2} \quad /. EI$$

$$P_{cr} = \frac{\pi^2 \cdot EI}{L^2} \quad \text{Final form of the equation}$$

According to previous sequence of numbers (0, π , 2π , 3π , 4π , 5π ...) it can be stated, that:

$$P_{cr} = \frac{\pi^2 \cdot EI}{L^2}, \frac{4 \cdot \pi^2 \cdot EI}{L^2}, \frac{9 \cdot \pi^2 \cdot EI}{L^2}, \frac{16 \cdot \pi^2 \cdot EI}{L^2}, \dots, \frac{n^2 \cdot \pi^2 \cdot EI}{L^2}$$

Where “n” can be substituted for any integer (n = 1, 2, 3, 4, 5 ...)

This statement is valid only in mathematical terms, because in real world the load is increasing continuously, so “n” can’t jump directly from value 1 to value 2. Therefore after reaching $n = 1$ the system becomes unstable.

Therefore the only stable buckling mode is the lowest, where $n = 1$.

Final form of buckling mode is then given by:
$$P_{cr} = \frac{\pi^2 \cdot EI}{L^2}$$

The critical load can be evaluated by using the described differential equation of the deflection curve. For simplicity slightly different form will be used, which is known for several decades by engineers all around the world. Formula for flexural elastic critical load is following:

$$N_{CR} = \frac{\pi^2 \cdot E \cdot I}{L^2}$$

Where:

π – mathematical constant defined by Ludolph van Ceulen

E – modulus of elasticity of steel (considered value: 210 000 MPa)

I – moment of inertia of given cross-section (preferably to the weaker axis)

L – length of specimen (considered value: 600 mm)

Unfortunately this basic formula doesn't take into account all possible support conditions and so there is a need to extend it by another parameter. Let's call this parameter as "k". Its main purpose will be to reduce or extend length of ideal member according to the distance of inflexion points (Figure 5.2.2). Finally, improved formula is covering all necessary aspects:

$$N_{CR} = \frac{\pi^2 EI}{kL^2}$$

Where:

k – parameter depending on support conditions

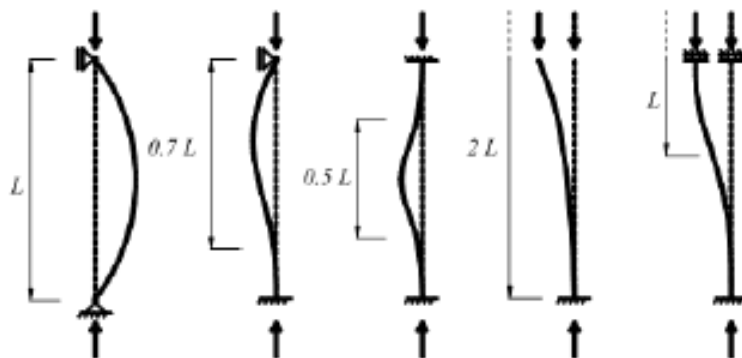


Figure 5.2.2: effective length according support conditions

Calculations were performed on the basis of two models: 1. fixed-ended at both ends, 2. pin-ended at both ends. This was required to see which output will be closer to the test results. Therefore, it will be possible to justify the boundary conditions implemented in the test.

The effective lengths for major (L_{ex}) and minor (L_{ey}) axis flexural buckling as well as torsional buckling (L_{ez}) are assumed equal to one half of the column length (L) for the fixed ended

columns ($L_e = L_{ex} = L_{ey} = L_{ez} = L/2$). For pin-ended supports these lengths were equalised to actual length of specimen.

5.3 Torsional and flexural-torsional buckling (theory)

L-profile has open mono-symmetric cross-section and centre of gravity does not coincide with shear centre. This results in low torsional stiffness and therefore this type of elements is susceptible to other instability phenomena: torsional and flexural-torsional buckling. Torsional buckling can be described as rotation of cross-section around longitudinal axis of the member (axis that is defined by the shear centre of the cross section). The flexural-torsional buckling is the instability mode when cross section undergoes combined twisting about shear centre and a translation of the shear centre. However, torsional mode is considered to be a theoretical one and mostly important as a component of naturally coupled flexural-torsional mode.

These buckling phenomena are illustrated in the following figures 5.3.1 and 5.3.2, where C – centre of gravity of cross-section, SC – shear centre, axis y – major principal axis, axis z – minor principal axis, ϕ – angle of rotation, y_c – distance between shear centre and centre of gravity in y-direction, z_c – distance between shear centre and centre of gravity in z-direction ($z_c=0$ in case of angle), u – displacement of cross-section in z-direction, v – displacement of cross-section in y-direction, C' – changed position of centre of gravity, SC' – changed position of shear centre, axis y' – changed position of major principal axis, axis z' – changed position of minor principal axis.

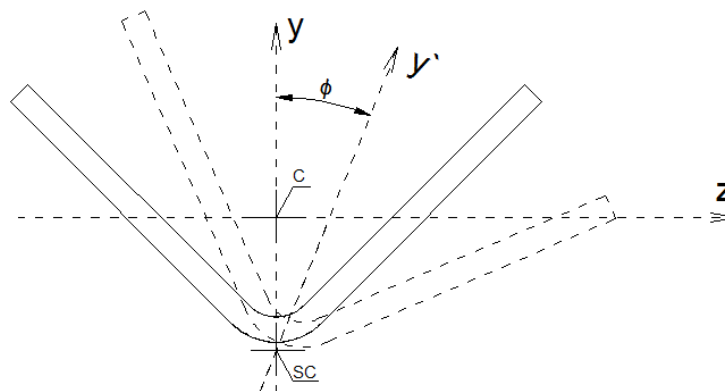


Figure 5.3.1: Torsional buckling

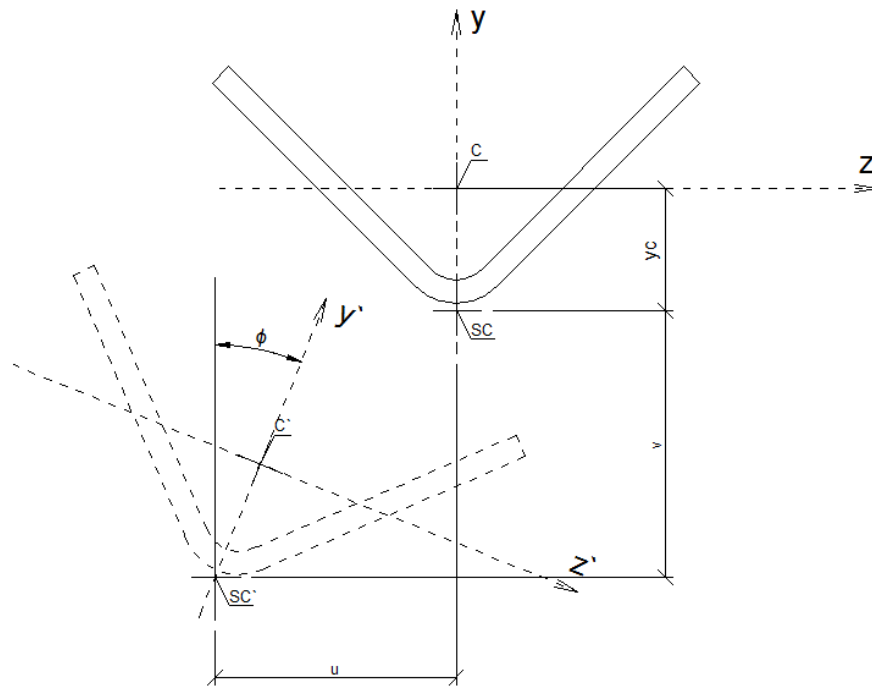


Figure 5.3.2: Flexural-torsional buckling

Theories for mentioned instability phenomena have been represented by many researchers. Determination of elastic critical loads presented by (Timoshenko & Gere, 1963), (Galambos, 1998), (Narayanan, et al., 1999) is based on calculation of the lowest root of cubic equation, created on the basis of the classic theory of elastic stability.

Described approach has been created assuming pinned boundary conditions. Figure 2 represents the notations used in the following equation.

Cubic equation is represented as follows:

$$(N_{cr,z} - N_{cr})(N_{cr,y} - N_{cr})(N_{cr,T} - N_{cr}) - (N_{cr,z} - N_{cr}) \frac{N_{cr}^2 y_c^2}{i_c^2} - (N_{cr,y} - N_{cr}) \frac{N_{cr}^2 z_c^2}{i_c^2} = 0$$

Where:

- | | |
|-------------------------------------|---|
| y_c, z_c | -the distance between shear centre and centre of gravity of the section in y and z direction. |
| $N_{cr,y} = \frac{\pi^2 EI_y}{L^2}$ | - representation of flexural buckling about y axis(major axis). |
| $N_{cr,z} = \frac{\pi^2 EI_z}{L^2}$ | - representation of flexural buckling about z axis (weaker axis). |

$$N_{cr,T} = \frac{1}{i_c^2} \left(GI_T + \frac{\pi^2 EI_w}{L^2} \right) \quad \text{- representation of torsional buckling load.}$$

i_c – the radius of polar gyration ($i_c^2 = y_c^2 + (I_y + I_z)/A$)
 L – length of the column.
 I_y, I_z – moments of inertia of the cross-section
 A – gross area of cross-section
 G – shear modulus of steel (considered value: 80 700 MPa)
 I_T – the torsional constant of the cross-section
 I_w – the warping constant of the cross-section

Studied angles are symmetric about y axis and shear centre is situated on this axis. Therefore, $z_c=0$. As a result, solution of cubic equation can be reduced to

$$N_{cr} = \min(N_{cr,z}, N_{cr,TF})$$

Where:

$N_{cr,z}$ – flexural buckling load about z axis (minor axis);

$N_{cr,TF}$ – flexural-torsional buckling load which is obtained from following equation:

$$(N_{cr,y} - N_{cr})(N_{cr,T} - N_{cr}) - \frac{N_{cr}^2 y_c^2}{i_c^2} = 0$$

This equation of second order has got two values for critical load, one of which is smaller and the other is larger than flexural and torsional critical loads. The smaller root is the torsional-flexural critical load. It is important to note that for small ratio $N_{cr,T}/N_{cr,y}$ critical load $N_{cr,TF}$ is very close to $N_{cr,T}$ and buckling is essentially torsional. For large values of $N_{cr,T}/N_{cr,y}$ critical load $N_{cr,TF}$ tends to $N_{cr,y}$ and buckling is flexural.

Solving above equation flexural-torsional critical load is obtained:

$$N_{CR,T} = \frac{1}{2\beta} \left[(N_{CR,y} + N_{CR,T}) - \sqrt{(N_{CR,y} + N_{CR,T})^2 - 4\beta N_{CR,y} N_{CR,T}} \right]$$

Where:

L_{ET} – length depending on the restrictions to torsion and warping at the end cross-sections

β – factor given by equation ($\beta = 1 - (y_c/i_c)^2$)

For other boundary conditions, different from pinned, value L (column length) will be substituted with effective length. In case of torsional critical load it will depend on the

restrictions to torsion and warping at the end sections. The procedure of obtaining effective length has been described previously.

5.4 Elastic critical load for local buckling (theory)

Local buckling phenomenon occurs when individual components of members buckle at stress levels which are less than yield point when subjected to compression, shear, bending or bearing. Normally local buckling does not result in failure of the section because it is characterized by post-buckling strength. Therefore, it limits the compression resistance of axially loaded members. Local buckling depends on width-to-thickness ratio of individual components of member and local buckling critical stress becomes lower when this ratio increases. Moreover, in “local” type of buckling length of buckles is comparable with the element width.

As it has been mentioned before all cross sections P1-P6 with thicknesses 4 mm and 6 mm are Class 4 according to EN 1993-1-1. Due to sectional instability of this class of cross-sections it is required to estimate elastic critical buckling load for local buckling mode. According to (Beg, Kuhlmann, Davaine, & Braun, 2012) for unstiffened plate it is given as follows:

$$\sigma_{cr} = \frac{k_{\sigma} \pi^2 E}{12 \cdot (1 - \nu^2)} \cdot \left(\frac{t}{b}\right)^2$$

Where:

b – appropriate width of the leg (taken as a notional width according to EN 1993-1-5),

t – plate thickness,

E – elastic modulus of steel,

ν – Poisson coefficient of steel,

k_{σ} – plate buckling coefficient (for outstand compression element is considered equal to 0.43).

Determination of critical force is calculated as follows:

$$N_{cr,loc} = \sigma_{cr} \cdot A$$

Where:

σ_{cr} – elastic critical load for local buckling,

A – gross area of the cross section.

Assessment of elastic critical loads for local buckling can be found in **Attachment 4b – Critical buckling load for local buckling**.

5.5 Peculiarities of buckling modes for L-shape cross-section

The geometry of angle cross section provides some peculiarities to their behaviour.

1. Similarity of torsional and local buckling modes.

According to (Rasmussen K. J., 2003) for 90° angles at short and intermediate length typical global buckling mode is flexural-torsional mode. At intermediate and long lengths of specimens it might change to a weak axis flexural mode. Typical behaviour of short specimens is that the flexural-torsional buckling load approaches torsional buckling load, which in case of slender equal angles is identical to local buckling mode. Moreover, it has already been stated on the basis of review of (Timoshenko & Gere, 1963) that for small ratio $N_{cr,T}/N_{cr,Y}$ critical load $N_{cr,TF}$ is very close to $N_{cr,T}$ and buckling is essentially torsional.

The fact that local buckling is identical to torsional buckling in case of short lengths can be confirmed by following procedure described in the work presented by Rasmussen (2003).

As it has already been said, elastic critical load for torsional buckling mode is calculated as follows:

$$N_{CR.T} = \frac{1}{i_c^2} (GI_T + \frac{\pi^2 EI_w}{L_{ET}^2})$$

This load can be presented as a torsional buckling stress:

$$\sigma_{CR.T} = \frac{1}{A(r_0^2 + x_0^2)} (GI_T + \frac{\pi^2 EI_w}{L_{ET}^2})$$

Where:

A – area of cross-section,

x_0 – distance from the centroid to shear centre as shown in Figure 5.5.1,

r_0 – polar radius of gyration.

The warping constant I_w is negligible for angles. Therefore, it can be stated that $I_w \approx 0$. As a result, torsional elastic critical buckling stress reduces to:

$$\sigma_{CR.T} = \frac{1}{A(r_0^2 + x_0^2)} (GI_T)$$

For simplification it is used an angle with sharp corners which is presented in Figure 5.5.1.

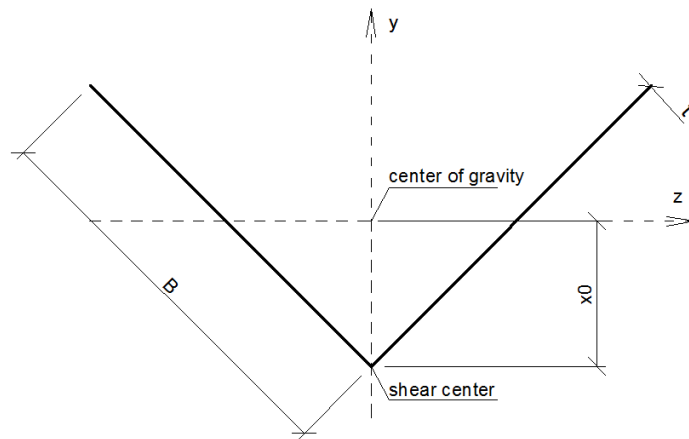


Figure 5.5.1: Simplification of cold-formed angle.

Following equations apply for this geometry:

$$r_0^2 = \frac{5}{24} B^2 \quad x_0^2 = \frac{1}{8} B^2 \quad I_T = \frac{2}{3} B t^3 \quad G = \frac{E}{2(1 + \nu)}$$

Therefore, the evaluation of elastic critical stress simplifies to

$$\sigma_{CR.T} = \frac{E}{2(1 + \nu)} \left(\frac{t}{B} \right)^2$$

As it has already been described, the local buckling stress is calculated as follows:

$$\sigma_{cr} = \frac{k_\sigma \pi^2 E}{12 \cdot (1 - \nu^2)} \cdot \left(\frac{t}{b} \right)^2$$

For finite aspect ratios, the plate buckling coefficient can be evaluated by (Bulson, 1969)

$$k = \frac{6(1 - \nu)}{\pi^2} + \frac{1}{\varphi^2}$$

The presented expression converges to asymptotic value $(6(1-\nu)/\pi^2)$ and therefore it can be stated that torsional buckling stress is equal to local buckling stress for equal angle columns. According to (Rasmussen K. J., 2003) equal-leg angle is a unique type of cross section for which the local buckling mode is the same as critical overall buckling mode at short length. Only short length applies due to the fact that at short lengths the flexural-torsional buckling load approaches the torsional buckling load.

2. Variation of effective length depending on buckling mode.

Moreover, according to (Popovic, Hancock, & Rasmussen, 1999) it is stated that for fixed-ended specimens the use of effective length (L_e) value differs depending on the real length (L) and slenderness of the cross section. It is correct to assume $L_e=0.5L$ in case of non-slender and long specimens due to the fact that in this case the failure mode is flexural buckling. However, at short lengths the critical overall mode becomes torsional or flexural-torsional and torsional component is length independent. That is why for short lengths it is less meaningful to use $L_e=0.5L$.

5.6 Elastic critical load evaluation

The discussed theory regarding buckling phenomena is used in evaluation of elastic critical load. To clearly describe the procedure one selected specimen is calculated via hand calculation in mathematical editor (see **Attachment 14 “Calculation procedure according to EN for cross-sections P1-4 (Class 4) and P1-10 (Class 3)”**). Remaining specimens are evaluated in Microsoft Excel to speed up the whole procedure (see **Attachment 4 “Determination of elastic critical force (fixed BC)”**).

Considered parameters:

- 1) Geometrical properties of profile
- 2) Fixed supports => $k = 0.5$ (effective length is half of actual one)

or

Pinned supports => $k = 1$ (effective length is equal to actual length)

- 3) Steel elastic modulus $E = 210\,000\text{ MPa}$
- 4) Shear elastic modulus $G = 80\,700\text{ MPa}$

Main formulas used during calculation:

- 1) Flexural buckling:
$$N_{CR} = \frac{\pi^2 \cdot E \cdot I}{k \cdot L^2}$$

- 2) Torsional buckling:
$$N_{CR,T} = \frac{1}{i_c^2} \left(GI_T + \frac{\pi^2 EI_w}{L_{ET}^2} \right)$$

- 3) Lateral-torsional b.:
$$N_{CR,TF} = \frac{1}{2\beta} \left[(N_{CR,y} + N_{CR,T}) - \sqrt{(N_{CR,y} + N_{CR,T})^2 - 4\beta N_{CR,y} N_{CR,T}} \right]$$

- 4) Local buckling:

$$\sigma_{cr} = \frac{k_\sigma \pi^2 E}{12 \cdot (1 - \nu^2)} \cdot \left(\frac{t}{b} \right)^2$$

$$N_{cr,loc} = \sigma_{cr} \cdot A$$

Steel profiles are evaluated according to their real shape (with rounded corner), but also shape with straight corner, neglecting rounded corners (**see Attachment 4a – Determination of geometrical properties and elastic critical force - fixed BC (neglecting rounded corners)**). This evaluation is performed to see difference in final elastic critical force. Results may answer the question if it is safe to neglect rounding, since it can simplify the whole process of evaluation of L-shaped specimen.

It can be observed, that difference for straight and rounded corner in case of elastic critical force is almost negligible for groups P4, P5, P6 (140°, 160°, 170°). Thickness of element is not playing crucial role, at least for evaluated range 4 to 20 mm.

In case of groups P1, P2, P3 (90°, 100°, 120°) the value of critical force is more dependent on the shape of the corner. Results also vary according to the thickness and final difference can be more than 50% higher in favour for element with straight corner.

According to the results it is therefore not safe to neglect rounded shape of corner in case of angles, which are close to 90-100° angle, for evaluation of elastic critical load.

6 IMPERFECTIONS AND DESIGN ACCORDING EN

6.1 Imperfections in columns (theory)

Theory regarding elastic critical load creates an idealized straight strut (column) concentrically loaded, on which the magnitude is calculated. Unfortunately in real world conditions it is impossible to achieve such a perfect member, nor to apply the load in the centre of gravity of the cross-section. Therefore there is a need to introduce a value, which will describe the non-straightness of strut and other deviations.

Those values are known as imperfections and according to their magnitude, the final elastic critical load is reduced. In other words due to imperfections it is not possible to reach the maximum (idealized) value of elastic critical load.

We recognize three main types of imperfections (Narayanan, et al., 1999):

1. Initial imperfection (initial bow of a strut).
2. Load application eccentricity.
3. Residual stresses in cross-section.

In next paragraphs, each of listed imperfections will be described more in detail to fully understand its effect on final resistance of strut (column).

6.1.1 Initial imperfection / out of straightness

Euler defined ideal strut as fully straight member, but in practice there is always a slight disturbance. In various books regarding member stability this issue is named initial imperfection, initial bow or out of straightness. In fact, the meaning is same for all of them.

Let's have a strut, which is pin-ended and has an initial imperfection (Figure 6.1.1). In the time, when we apply the load, the member is subjected not only to axial force, but also to the bending moment in every cross-section along the length. This bending moment leads to additional deformation.

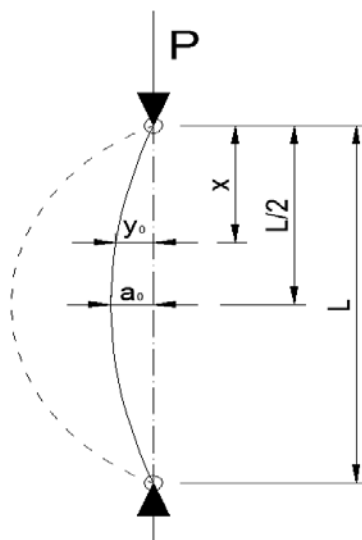


Figure 6.1.1: Strut with initial imperfection

To express this behaviour in terms of calculations, let's have an initial shape of the strut described by equation:

$$y_0 = a_0 \cdot \sin \frac{\pi \cdot x}{L}$$

Where:

L – overall length of the strut (column)

P – force applied at the top support

x – position of measured imperfection from the top support

a_0 – maximum imperfection at the middle of span ($x = L/2$)

Represented buckling shape isn't the only one, which can appear on compressed element, yet previous calculations clearly stated, that shape of half-sine wave corresponds to the lowest buckling mode and therefore is the safest.

If the material remains in elastic range, there is also possibility to see, that application of force P increases the initial deflection at any point along the whole length of the strut by a multiplier factor:

$$\frac{1}{1 - \frac{P}{P_{cr}}}$$

Theoretically, as P is reaching the value of P_{cr} , the deflection of the strut will tend to infinity. More can be seen the graph below (Figure 6.1.2), where this behaviour is described with dashed curve A.

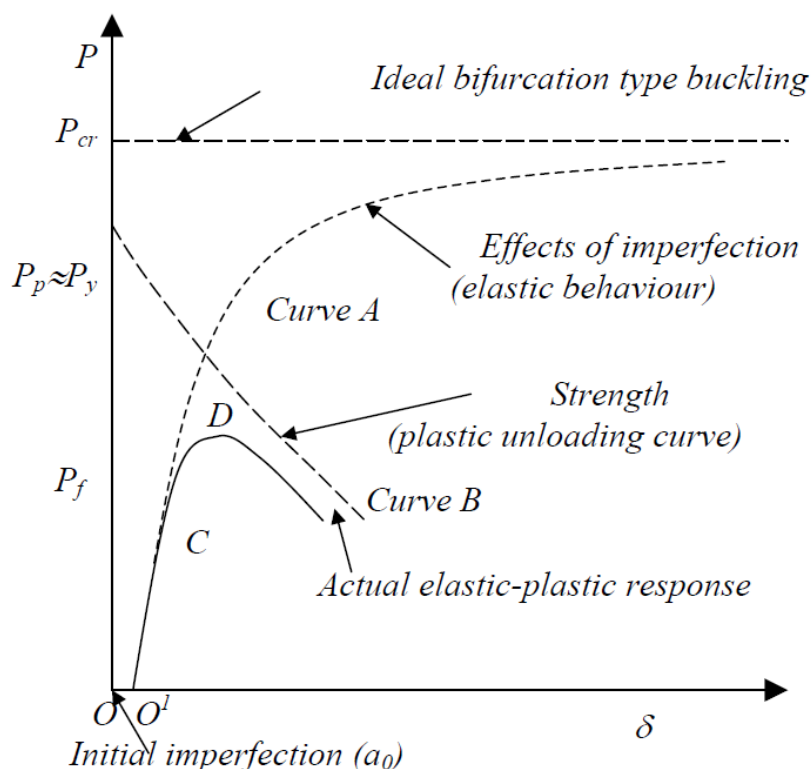


Figure 6.1.2: Load deflection response of a strut (Narayanan, et al., 1999)

In real world conditions the strut (column) behaves differently. Member subjected to increasing load deflects and therefore the moment on the cross-section increases. This causes, that at certain magnitude of force P , the cross-section reaches equivalent stress distribution and yields. In the graph this situation is showed as point C.

While increasing the load, the bending stiffness is reduced and therefore ideal shape (curve A) can't be followed anymore. After certain time the maximum load P_f is reached and column collapses.

From the graph (Figure 6.1.2) theoretical rigid plastic response of loaded member can be seen on the dashed curve B. Its maximum is defined by point P_p and under certain conditions the strut can reach similar values. Such strut (column) is called stocky and its failure is triggered by yielding of the section ($P_p = P_y$). For the other columns, which are slender, the collapse is due to elastic buckling.

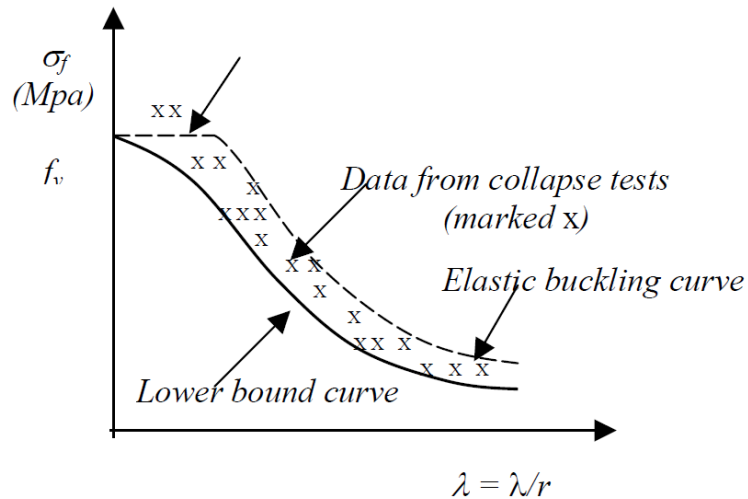


Figure 6.1.3: Strength curves according to slenderness (Narayanan, et al., 1999)

Tests showed (Figure 6.1.3), that stocky columns are not sensitive to initial out of straightness and their failure is mostly by plastic squash load. For slender columns, the effect of initial bow is very significant and the distance between lower bound curve and elastic buckling curve depends on the magnitude of slenderness.

6.1.2 Eccentricity of applied load

From the geometrical point of view, the load should be applied directly at the centre gravity of the cross-section. In case of angles this is almost impossible as in most of the cases centre of gravity is located out of the cross-section. Therefore the load, which is applied on the surface of element lies at certain distance from the centre of gravity (Figure 6.1.4).

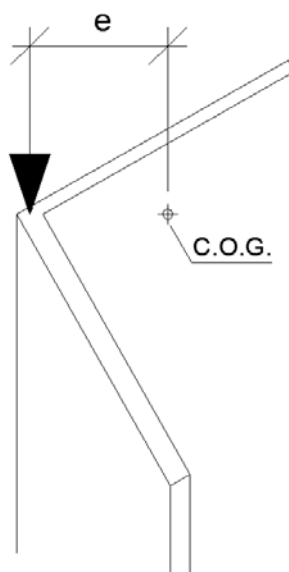


Figure 6.1.4: Eccentricity in load application

This value is called eccentricity and causes another increase of the bending moment and consequently raise the compressive stress on the concave face of the column at middle section. For some sections the eccentricity can be reduced to almost negligible magnitude, but in case of tested L shaped profiles it must be checked carefully.

6.1.3 Residual stresses in cross-section

During production of structural steel, the element undergoes several forming procedures before it obtains its final shape. Those procedures involve applying of different temperatures or external force. The cross-section of the element is therefore subjected to external loading and as a result, internal (residual) stresses are developed. Mostly those additional stresses remain locked in the element forever and can affect the final resistance. Generally residual stresses reduce the strength of the element, but in some situations their effect can be also positive with respect to fatigue strength.

Residual stresses are mostly considered for hot rolled profiles, due to uneven cooling down of the cross-section or forming (rolling) procedure. Profiles described in this thesis are cold formed and even in this forming process residual stresses are developed and affect behaviour and final resistance of the profile. (Karren, 1967)

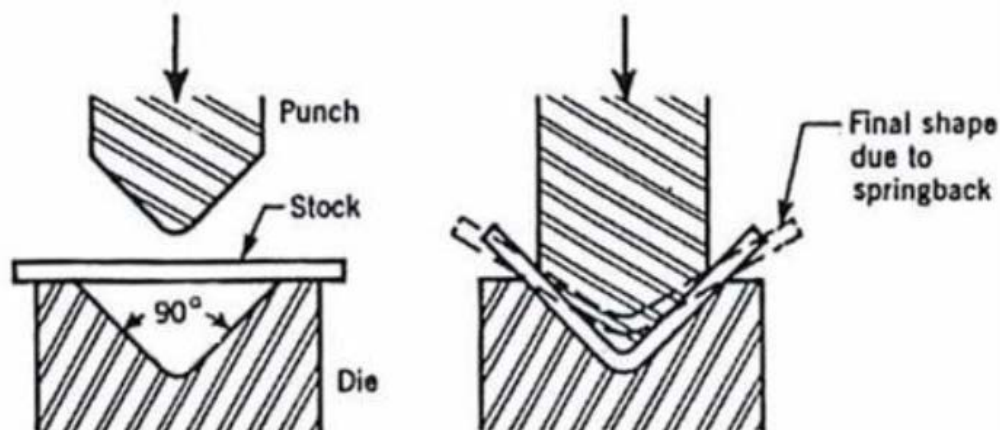
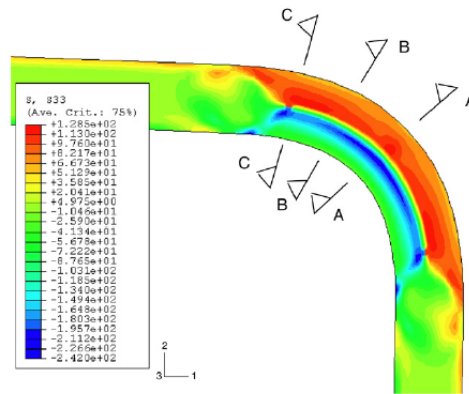
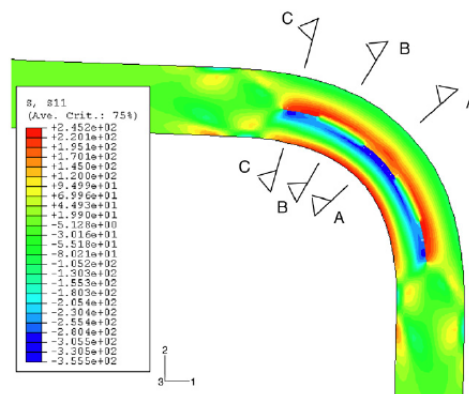


Figure 6.1.5: Press-braking method introduces residual stresses (Anis, Bjork, & Heinilla, 2012)

The press-braking method involves a cold bending of steel plate (Figure 6.1.5), where firstly plastic loading appears, followed by elastic unloading. As stated before, newly shaped product has residual stresses locked inside the cross-section. The maximum residual stresses of press-braked section appear in the corner part. The distribution along thickness of material is not linear and biggest concentration of stresses is close to the centre of element (Figure 6.1.6). (Quach W.M., 2006)



(a) Longitudinal residual stress.



(b) Transverse residual stress.

Figure 6.1.6: Nonlinear distribution of residual stresses at corner area (Quach W.M., 2006)

Evaluation of induced residual stresses is possible by two methods. First method is destructive one and consists of measuring stresses in specimen before and after cutting, since splitting of steel cross-section releases residual stresses. Second method is non-destructive, since elements are modelled and evaluated by finite element method.

Both methods mentioned above are difficult and require significant knowledge regarding steel and residual stresses. However to achieve correct judgement regarding all effects, which may lower the buckling resistance of L-profile, residual stresses will be simulated using FEA for one cross-section P1-6. More information will be given in appropriate paragraph later on.

According to research made by (Ellobody & Young, 2005) on brake-pressed high-strength steel angles the effect of residual stress has got negligible effect on ultimate load, stiffness of columns, load-shortening behaviour and failure mode in case of plain angle columns. This investigation has been made using FEA. Load versus axial shortening diagram for column (plate thickness - 1.9 mm, length - 2500 mm) with and without simulation of residual stresses is presented in Figure 6.1.7. The behaviour and ultimate load of the column is practically identical. It is expected to achieve similar negligible effect of residual stresses in case of this thesis as well.

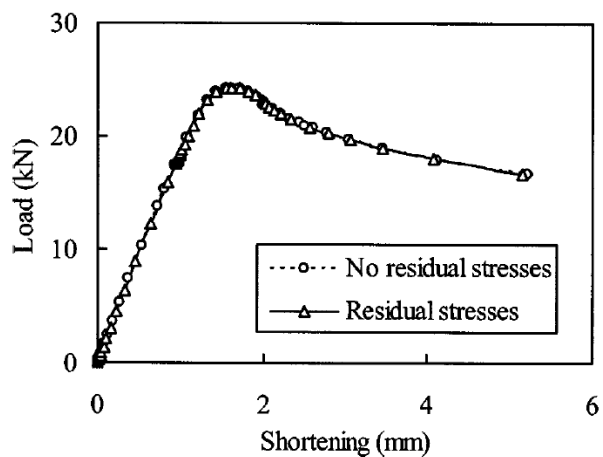


Figure 6.1.7: Load-axial shortening curve with and without simulation of residual stresses (Young, 2005).

This statement is also in line with the researches made by (Shi, Liu, & Chung, 2009) and (Silvestre, Dinis, & Camotim, 2013).

6.2 Current design according Eurocode

6.2.1 General

Current version of Eurocode provides step-by-step procedure to evaluate buckling resistance of a member. All formulas and coefficients are based on theoretical and practical experience with steel, which yield strength varies between 235 to 460 MPa, therefore there is a question, whether the same procedure and namely coefficients, can be used in case of steel with higher yield strength.

To have a direct comparison with FEM analysis and real tests in laboratory, it was decided to evaluate buckling strength of L profiles according to current version of Eurocode. In the next paragraphs all recommended formulas and coefficients will be presented, followed by evaluation of buckling resistance for each specimen.

6.2.2 Compression

Buckling resistance of the cross-sections will be evaluated on the basis of EN 1993-1-3, ch.6.2; EN 1993-1-1, ch.6.3.1; EN 1993-1-12, ch. 2.1 and 2.3. In Eurocode 1993-1-1, chapter 6.3.1.1 for members in uniform compression is stated a check, which must be met to get sufficient resistance of a member and prevent collapse of the structure:

$$\frac{N_{Ed}}{N_{b,Rd}} \leq 1.0$$

Where:

N_{Ed} – is the design value of the compression force,

$N_{b,Rd}$ – is the design buckling resistance of the compressed member.

Evaluation of $N_{b,Rd}$ is dependent on the class of the cross-section and in case of angles (L profiles) it is distinguished between Class 3 and Class 4, or in the other words between profile with full cross-section resisting the load (Class 3) or with profile with effective cross-section (Class 4). For class 4 elements the effects of local buckling are taken into account as specified in EN 1993-1-3, clause 5.5.

Moreover, in Class 4, due to the reduction of cross-section, there is a shift in position of centre of gravity and additional moment occurs. This combination of loads (N + M) will be described later on.

To take into account the interaction between local and global buckling of thin-walled sections (class 4), the calculation of the load bearing capacity is based upon the effective cross-section, calculated for uniform compression.

Formulas for design buckling resistance are given as follows:

$$N_{b,Rd} = \frac{\chi \cdot A \cdot f_y}{\gamma_{M1}} \quad \text{for cross-section Class 1,2 and 3}$$

$$N_{b,Rd} = \frac{\chi \cdot A_{eff} \cdot f_y}{\gamma_{M1}} \quad \text{for cross-section Class 4}$$

Where:

χ – the reduction factor for the relevant buckling mode (Figure 6.2.2)

A – gross cross-section area of the evaluated member

A_{eff} – effective cross-section area of the evaluated member

f_y – yield strength of used steel grade

γ_{M1} – partial safety factor

As can be observed from formulas above, it is crucial to use appropriate cross-sectional area, but also relevant buckling mode. For evaluation of buckling reduction factor is prepared chapter 6.3.1.2, which describes formulas in case of axial compression:

$$\chi = \frac{1}{\phi + \sqrt{\phi^2 - \lambda^2}}, \text{ but } \chi \leq 1.0$$

Where:

$$\phi = 0.5[1 + \alpha(\lambda - 0.2) + \lambda^2]$$

λ – non-dimensional slenderness coefficient

α – the imperfection factor (Figure 6.2.1)

Table 6.1: Imperfection factors for buckling curves

Buckling curve	a ₀	a	b	c	d
Imperfection factor α	0,13	0,21	0,34	0,49	0,76

Figure 6.2.1: Imperfection factor (EN 1993-1-1, table 6.1)

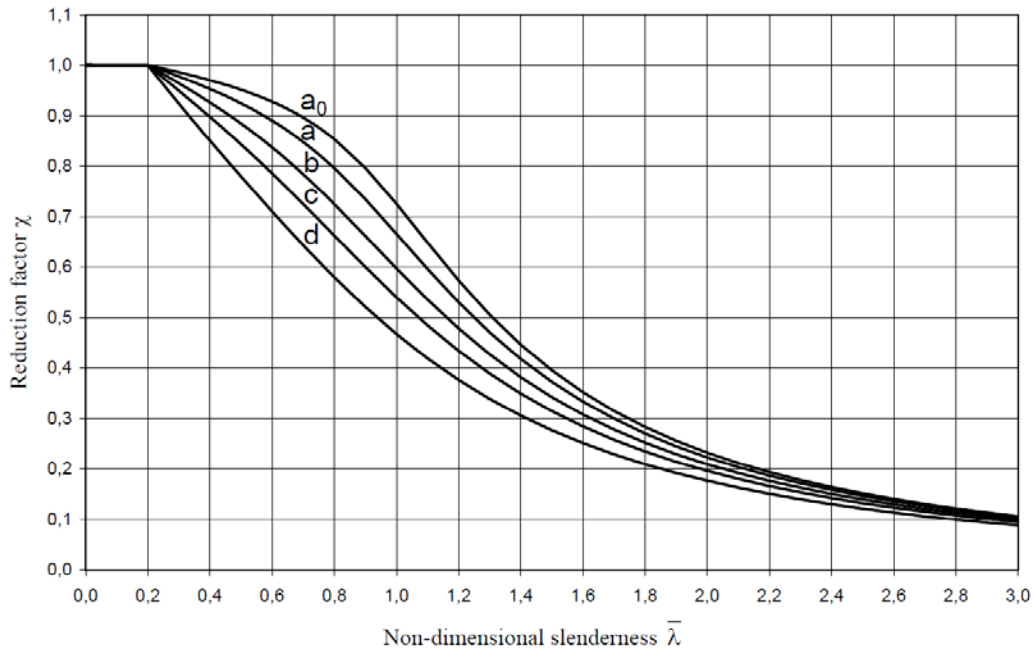


Figure 6.2.2: Buckling curves according Eurocode (EN 1993-1-1, Figure 6.4)

According to EN 1993-1-3, Table 6.3 buckling curve c will be used for the cross-sections P1-P6.

While:

$$\chi = \sqrt{\frac{A \cdot f_y}{N_{cr}}} \quad \text{for cross-section Class 1,2 and 3}$$

$$\chi = \sqrt{\frac{A_{eff} \cdot f_y}{N_{cr}}} \quad \text{for cross-section Class 4}$$

Formulas for non-dimensional slenderness coefficient for flexural buckling can be furthermore simplified to (Simoes da Silva, Simoes, & Gervasio, 2010):

$$\chi = \sqrt{\frac{A \cdot f_y}{N_{cr}}} = \frac{L_{cr}}{i} \cdot \frac{1}{\lambda_1} \quad \text{for cross-section Class 1,2 and 3}$$

$$\chi = \sqrt{\frac{A_{eff} \cdot f_y}{N_{cr}}} = \frac{L_{cr}}{i} \cdot \frac{\sqrt{A_{eff}/A}}{\lambda_1} \quad \text{for cross-section Class 4}$$

Non-dimensional slenderness will be evaluated on the basis of critical load which will be taken as the lowest of the values for flexural, torsional or flexural-torsional critical load.

For members with mono-symmetric open cross-sections according to EN 1993-1-3, clause 6.2.3 (2) account will be taken of the possibility that the resistance of the member to torsional-flexural buckling might be less than its resistance to flexural buckling.

6.2.3 Bending

For members with non-symmetric class 4 sections, the additional moment ΔM_{Ed} should be taken into account due to the eccentricity of the centroidal axis of the effective section according to §6.2.2.5(4) of EN1993-1-1

According to EN 1993-1-1, ch. 6.2.2.5(4) additional moment is calculated as follows:

$$\Delta M_{Ed} = N_{Ed} e_N$$

Where:

e_N – shift of the centroid of the effective area relative to the centre of gravity of the gross cross section.

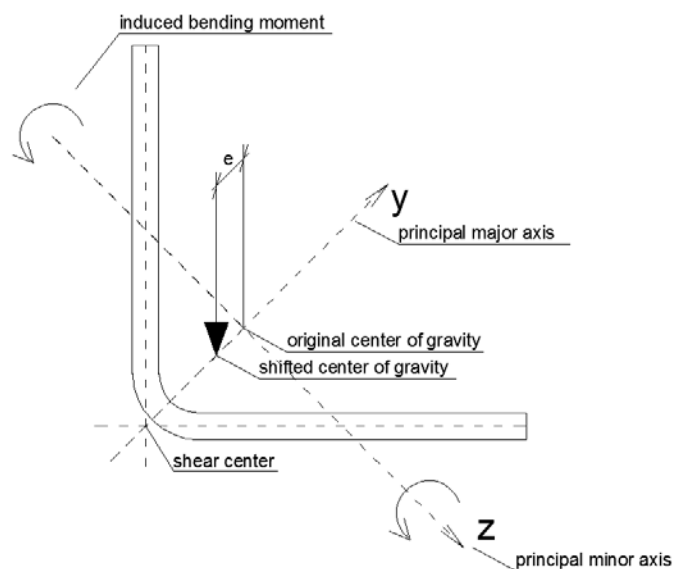


Figure 6.2.3: Load causing bending around weaker axis

According to EN 1993-1-3, ch. 6.1.4.1(1) design moment resistance of a cross-section about one principal axis for the case when effective section modulus is less than the gross elastic section modulus is determined as follows:

$$M_{c,Rd} = \frac{W_{eff} f_{yb}}{\gamma_{M0}}$$

Where:

W_{eff} – effective section modulus of cross-section,

f_{yb} – basic yield strength,

γ_{M0} – partial factor of cross-section resistance.

Moreover, according to EN 1993-1-3, ch.6.2.4 and EN 1993-1-1, ch. 6.3.2.1(1) members which are laterally unrestrained and subjected to bending about major axis should be verified against lateral-torsional buckling as follows:

$$\frac{M_{Ed}}{M_{b,Rd}} \leq 1$$

Where:

M_{Ed} – design value of bending moment,

$M_{b,Rd}$ – design buckling resistance moment.

According to EN 1993-1-1, ch.6.3.2.1(3) for Class 4 cross-sections design buckling resistance is calculated as follows:

$$M_{b,Rd} = \frac{\chi_{LT} W_{eff} f_y}{\gamma_{M1}}$$

Where:

χ_{LT} – the reduction factor for lateral-torsional buckling,

γ_{M1} – partial factor for resistance of members to instability.

However, in case of occurrence of additional moment in slender angles it can be seen from figure 6.2.3 that the cross-section is subjected to bending about weak axis. Therefore, it can be stated that cross-section is not susceptible to lateral-torsional buckling due to shift of centroid and $\chi_{LT} = 1$.

Effective section modulus is calculated using software SCIA by introducing the effective cross-section.

6.2.4 Combined compression and bending

As long as Class 4 cross-sections are subjected to compression and bending they should be designed as beam-columns. The approach for verification of stability for interaction of bending and axial compression is provided in EN 1993-1-3, ch.6.2.5. The calculation will be based on the alternative method which is described as follows:

$$\left(\frac{N_{Ed}}{N_{b,Rd}}\right)^{0.8} + \left(\frac{M_{Ed}}{M_{b,Rd}}\right)^{0.8} \leq 1$$

Where:

$N_{b,Rd}$ – the design buckling resistance of the member (flexural, torsional or flexural-torsional),

$M_{b,Rd}$ – the design bending moment resistance,

N_{Ed} – acting axial force,

M_{Ed} – acting moment (in case of angles moment due to shift of centroid).

For slender angles under concentrically applied compression formula will look as follows:

$$\left(\frac{N_{Ed}}{N_{b,Rd}}\right)^{0.8} + \left(\frac{N_{Ed}e_N}{M_{b,Rd}}\right)^{0.8} \leq 1$$

Where:

e_N – shift of centroid.

This approach provides possibility to assess resistance capacity of cross-section. This is done using Excel.

6.3 Buckling resistance evaluation

Evaluation of buckling resistance was done by procedures suggested by Eurocode and is shown in two methods. First method is hand calculation on randomly selected profile to explain step by step procedure, how final buckling resistance was achieved (**Attachment 14 – Calculation procedure according to EN for cross-sections P1-4 (Class 4) and P1-10 (Class 3)**). Second method covers rest of the profiles and for their evaluation was used Microsoft Excel to speed up the whole process of computation. The results of calculations are presented in following chapters:

Attachment 5 – Determination of flexural buckling resistance (fixed BC);

Attachment 6 – Determination of torsional buckling resistance (fixed BC);

Attachment 7 – Determination of torsional buckling resistance (fixed BC);

Attachment 8 – Determination of moment buckling resistance for Class 4 cross-sections for bending about weak axis;

Attachment 9 – Determination of member resistance for combined compression and bending interaction (fixed BC);

Attachment 10 – Combined table of buckling resistance according to EN (fixed BC);

Attachment 11 – Combined table of buckling resistance according to EN for fixed BC (neglecting additional moment for Class 4 cross-sections);

Pinned support specimens have also been evaluated. The results are presented in following attachments:

Attachment 12 - Combined table of buckling resistance according to EN (pinned BC);

Attachment 13 – Combined table of buckling resistance according to EN for pinned BC (neglecting additional moment for Class 4 cross-sections);

7 FINITE ELEMENT MODELLING

7.1 Introduction

According to the requirements of the research it is necessary to compute analysis of the cross-section using Finite Element Modelling. In the frame of this study Finite Element Analysis will help to predict elastic critical loads, design ultimate loads and failure modes of studied specimens. This type of analysis plays increasingly important role in engineering practice because of the benefits it has got compared to the real experiments. Firstly, it is time efficient and secondly, it is relatively inexpensive. These facts are vital especially in case of involvement of parametric study of cross-section. However, it is important to have accurate finite element model and verification of the model with experimental results is necessary. Therefore, the results of the performed FEA will be validated with the tests and parametric study will be held to develop buckling curves for different length of the columns. For this purpose sensitivity analysis of the geometrical imperfections will be held in order to obtain the most accurate result. Experimental determination of the imperfections has been performed in the frame of this research but FEA based on these results is not provided in the scope of this work. Moreover, the results from FEA are compared with the results obtained by hand calculation using Eurocode.

All finite element modelling was performed in ABAQUS 6.13.

7.2 General

Finite element analysis for buckling requires two types of analysis. Firstly, linear elastic buckling analysis has been performed to evaluate elastic critical load and buckling modes. This analysis provides the factor by which the applied load should be multiplied to reach the elastic critical load. The second is called load-displacement nonlinear analysis (RIKS). This procedure allows determination of ultimate buckling load using initial imperfections from the buckling analysis. The nonlinear geometry parameter was included to deal with nonlinear behaviour of the model. Residual stresses are not taken into account in the analysis. For shell modelling centreline dimension was taken as a basis for analysis.

7.3 Finite element type and mesh

Shell elements have been used as a main type of elements for modelling. However, few models were checked using solid elements either.

For **solid** modelling an 8-node linear brick **C3D8R** element with reduced integration was used. Parametric study of appropriate meshing is performed. The meshing of the element

was used as follows: **5 x b x b mm**, where b varies with the thickness of the element. It is required to have at least two elements through the thickness.

For **shell** modelling 4-node shell element with reduced integration **S4R** has been used. In Abaqus manual it is mentioned that this type of elements are suitable for complex buckling behaviour. The meshing of the element was used as follows: **5 x 1 mm**. It has been noticed that this type of mesh gives good processing time and accuracy.

7.4 Boundary conditions and load application

The most necessary part of simulation in FEM analysis is to achieve the similar behaviour of simulation model to the experimental one. In the experiment boundary conditions are close to fixed-fixed and the load is applied to the edge of cross-sections. Implementation of these requirements in Abaqus differs depending on the type of elements used (3D or 2D). Modelling of the given specimens has been based on the “trial and error” method. Therefore, in the following list will be presented the approaches which did not truly represent the required results:

1. Solid model with load applied at the edge. Fixed boundary conditions in solid model included fixing the ends of the column against displacements except the displacement at loaded end in the direction of the applied load. Boundary conditions were applied at the edge of the cross-section. The load has also been applied at the edge of cross-section: for eigenvalue analysis – unit load, for RIKS analysis – unit displacement. Obtained output has shown that elastic critical loads differ significantly from hand calculation; rotation of the end of cross-section with applied load is observed despite being fixed (Figure 7.4.1); failure modes differ from the ones predicted by hand calculation.

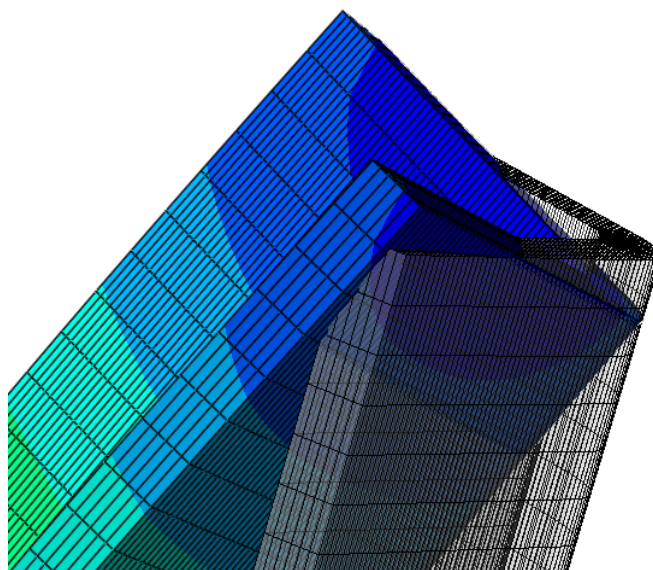


Figure 7.4.1: Unwanted rotation of fixed end with applied load

2. Solid model with attached slab (Figure 7.4.2). The bottom edge of the cross-section has been fixed against all the displacements, the upper part of slab has been prevented from lateral displacements but it is free to move longitudinally. L-specimen has been tied to the slab. The load has been applied at top surface of the slab: for eigenvalue analysis – unit load, for RIKS analysis – unit displacement. Obtained output has shown that elastic critical loads differ significantly.

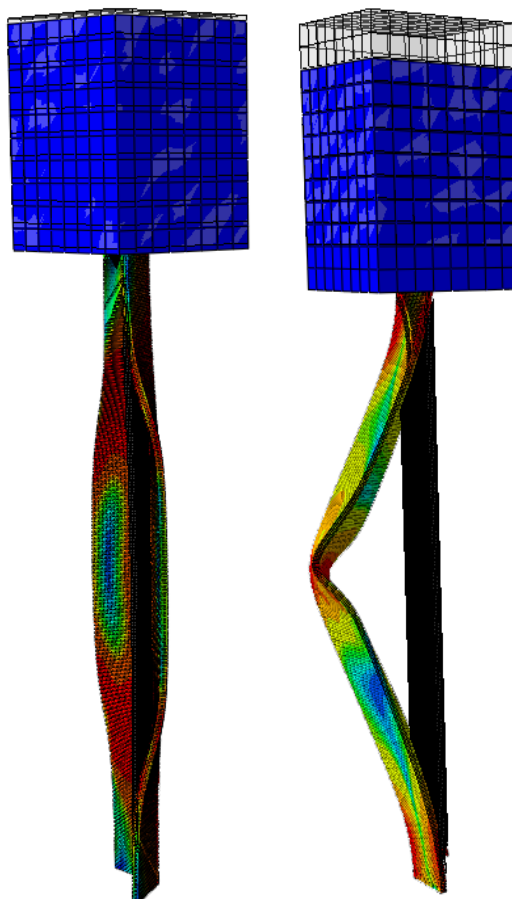


Figure 7.4.2: Solid model loaded through slab

3. Shell model with load applied at the edge. Fixed boundary conditions in shell model included fixing the ends of the columns against displacements except the displacement at loaded end in the direction of the applied load. Boundary conditions were applied at the edge of the cross-section. The load has also been applied at the edge of cross-section: for eigenvalue analysis – unit load, for RIKS analysis – unit displacement. Obtained output has shown that elastic critical loads differ significantly from hand calculation; rotation of the end of cross-section with applied load is observed despite being fixed (Figure 7.4.3)

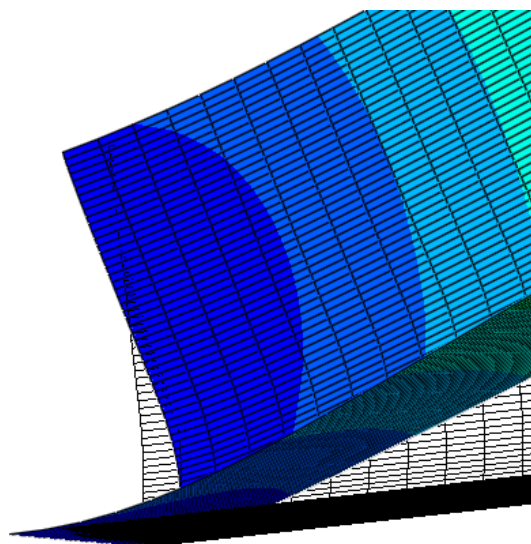


Figure 7.4.3: Unwanted rotation of fixed end with applied load

Description of the most precise approach for fixed-ended angles is provided further. Shell model has been used. Fixed boundary conditions have been applied to the centre of gravity of cross-section (Figure 7.4.4). It has been modelled as a reference point with coordinates determined in AutoCAD. Afterwards it has been coupled to the edge of the cross-section. Fixed boundary conditions has been ensured by restricting reference points on both sides of cross-section **against all degrees of freedom except the displacement at loaded end in the direction of the applied load**. The nodes other than the two ends were free to translate and rotate in any direction. The **application of load** differs according to the step of analysis. For the eigenvalue analysis the load is applied as a unit load to the top reference point. For non-linear analysis load is substituted with the unit displacement what represents displacement control method identical to the one in tests. The main representations of model are shown in Figure 7.4.4-7.4.7.

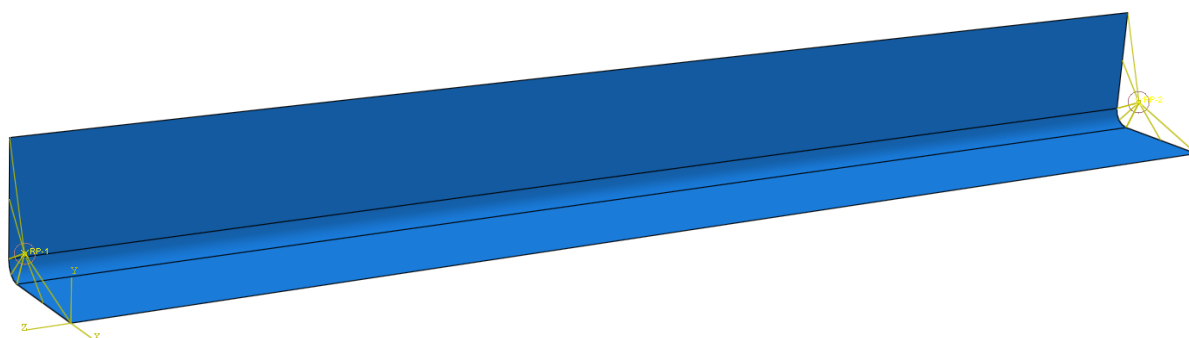


Figure 7.4.4: Final model – Reference point (located at c.o.g) coupled to the edge of cross-section.

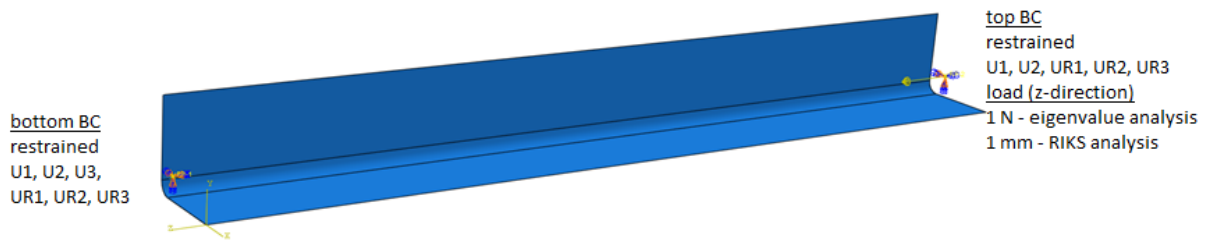


Figure 7.4.5: Final model (fixed-fixed BC) – Load and boundary conditions are applied to the reference points.

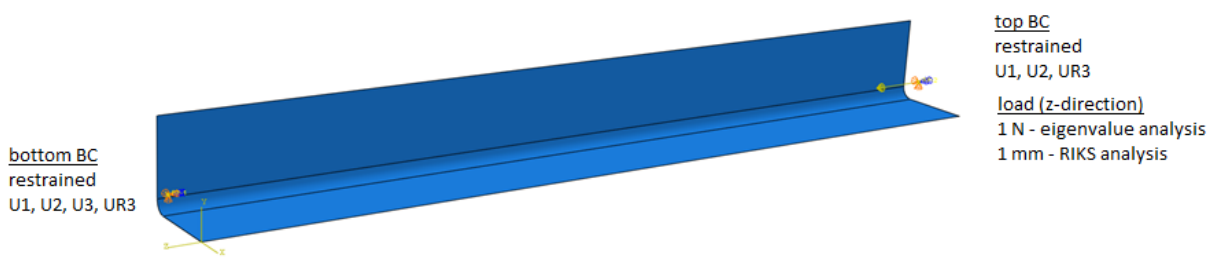


Figure 7.4.6: Final model (pinned-pinned BC) – Load and boundary conditions are applied to the reference points.

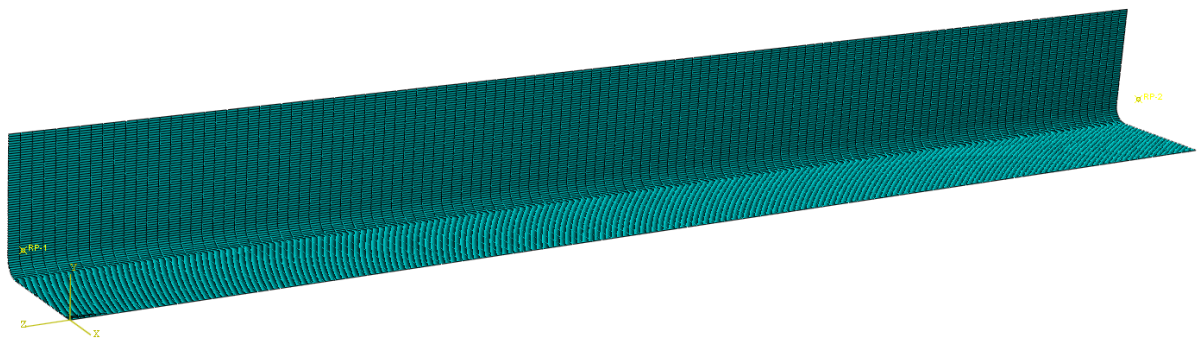


Figure 7.4.7: Final model – Meshed shell element.

As long as the results of tests are only expected to be fixed it has also been decided to simulate model with pinned boundary conditions. This might assist if the expected boundary conditions will not be achieved. Moreover, it will help to assess if the behaviour of the cross-section is closer to the one with pinned supports. In case of pinned boundary conditions all displacements were restricted in the bottom, displacements U1 and U2 were restricted at the top edge. Moreover, at both ends rotation UR3 was restricted due to the fact that the model was not converging and exhibited rotation about z-axis.

7.5 Material modelling

First part of the modelling consists of linear analysis which is characterized by linear dependency between load application and response of structure. Therefore, only elastic modulus ($E=210$ GPa) and Poisson's ratio ($\nu=0.3$) are used. The second stage of simulation is non-linear analysis in which stiffness of the structure changes with deformations. Material non-linearity is introduced by a true stress and true plastic strain curve which is converted from nominal (engineering) static stress-strain curve.

The material properties for steel S650MC has been obtained from previous researches on this type of steel in LTU.

The properties for grade S500MC has been calculated numerically. The material behaviour was assumed according to Swedish Regulations for Steel Structures, BSK 99:

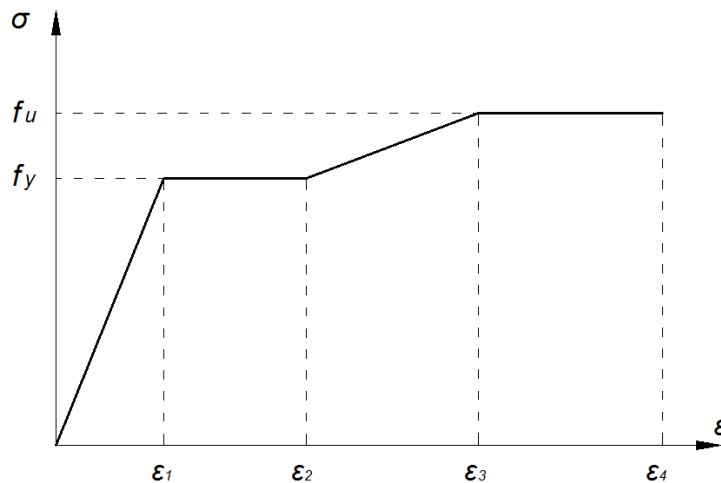


Figure 7.5.1. Material behaviour according BSK 99

According to BSK 99 strains are calculated as follows:

1. Steel 500MC, $t=16$ mm

Stress σ	Strains	
0	0	0
$f_y=500$ MPa	$\varepsilon_1 = \frac{f_y}{E}$	0.0024
$f_y=500$ MPa	$\varepsilon_2 = 0.025 - 5 \cdot \frac{f_u}{E}$	0.0110
$f_u=590$ MPa	$\varepsilon_3 = 0.02 + 50 \cdot \frac{f_u - f_y}{E}$	0.0410
$f_u=590$ MPa	∞	0.2000

2. Steel 500MC, t=20 mm

Stress σ	Strains	
0	0	0
$f_y=480$ MPa	$\varepsilon_1 = \frac{f_y}{E}$	0.0023
$f_y=480$ MPa	$\varepsilon_2 = 0.025 - 5 \cdot \frac{f_u}{E}$	0.0110
$f_u=590$ MPa	$\varepsilon_3 = 0.02 + 50 \cdot \frac{f_u - f_y}{E}$	0.0460
$f_u=590$ MPa	∞	0.2000

The true stress and plastic true strain were calculated according to EN 1993-1-5, Annex C:

$$\sigma_{true} = \sigma(1 + \varepsilon)$$

$$\varepsilon_{true} = \ln(1 + \varepsilon)$$

True plastic strain is obtained as follows:

$$\varepsilon_{pl.true} = \varepsilon_{true} - \frac{\sigma_{true}}{E}$$

Where:

σ and ε are values of engineering stress and strain obtained according to BSK 99.

Following values were introduced in non-linear analysis:

1. Plasticity data for 650MC, t=4; 6 and 10mm (obtained from previous tests in LTU):

σ_{true} [MPa]	$\varepsilon_{pl.true}$
652.113	0.000000
652.275	0.000233
922.350	0.065380

2. Plasticity data for 500MC, t=16mm:

σ_{true} [MPa]	$\varepsilon_{pl.true}$
501.190	0.000
505.476	0.008
614.443	0.038
708.000	0.179

3. Plasticity data for 500MC, t=20mm:

σ_{true} [MPa]	$\varepsilon_{pl.true}$
481.100	0.000
485.257	0.009
617.252	0.042
708.000	0.179

7.6 Modelling of imperfection

As it has been stated before, geometrical imperfections have been measured experimentally but the results will not be processed in the scope of this work. The procedure of measuring the imperfections will be described further. Therefore, eigenvalue analysis will be used as the input for analytical values of imperfections in RIKS analysis and sensitivity analysis of imperfections will be carried out. As a result of the manufacturing process both initial local and overall geometric imperfections are found in columns. Therefore, a linear superposition of local and global buckling modes will be applied for accurate finite element analysis. Moreover, the imperfection sensitivity of specimens will be assessed by applying different magnitudes of imperfections.

The sensitivity analysis and choice of imperfections will be based on two types of imperfections:

1. recommended values of imperfections proposed in literature for equal-leg angle cross-section,
2. variations of recommended values used in order to see the influence of imperfections.

Recommended values are described as follows:

1. The approach proposed by (Silvestre, Dinis, & Camotim, 2013) will be applied. In this work the magnitudes of imperfections are in line with the mean values of amplitudes measured in tests which were performed by (Young B. , 2004) and (Popovic, Hancock, & Rasmussen, 1999). For the specimens where local buckling mode is critical, imperfection of 10 % of wall thickness will be adopted. In case when global buckling mode is critical the applied initial imperfections combine local imperfections with magnitude 10 % of wall thickness; and global imperfections, with amplitudes equal to $L/750$.
2. The approach is based on information obtained from (Simoes da Silva, Simoes, & Gervasio, 2010) and EN 1993-1-5, Annex C-Finite Element Analysis. Even though latter gives guidance on the use of FE-methods only for plated structures it is considered to be applicable to the case of equal angles. For local type of imperfection magnitude of $b/200$ is used, where b – is the notional width of the leg according to EN 1993-1-3. For global critical buckling mode will be used superposition of global mode imperfection with amplitude $L/1000$ and local mode imperfection with amplitude $b/200$.
3. According to (Mesacasa, E., Dinis, P., Camotim, D., and Malite, M. , 2013) amplitude of $L/1000$ will be used for both local and global imperfections.

Variations of recommended values will be described as follows:

1. For local type of imperfection value of $b/200$ will be used, where b – is the notional width of the leg according to EN 1993-1-3. For global type of imperfection superposition of global mode imperfection will be used with amplitude $L/200$ and

local mode imperfection with amplitude $b/200$. This mode is intended to provide significant reduction in buckling resistance for global mode.

2. Extreme values will be used for the sake of checking values which are not expected to appear in reality. It will help to assess the influence of imperfections. For local mode it is $L/200$ and for global mode it is $L/6000$ for global component and $L/6000$ for local component. It is expected to obtain significant reduction in local mode and negligible reduction in global mode.

Application of imperfections is summarized in the following table:

№	Approach	Local mode	Global mode	
			Global component	Local component
1	Mesacasa (2013)	$L/1000$	$L/1000$	$L/1000$
2	Silvestre (2013)	10 % of wall thickness	$L/750$	10% of wall thickness
3	EN, ECCS	$b/200$	$L/1000$	$b/200$
4	Variation 1	$b/200$	$L/200$	$b/200$
5	Variation 2	$L/200$	$L/6000$	$L/6000$

Table 7.6.1: Application of imperfections for sensitivity analysis.

7.8 Tracking of shear centre movement

It has already been stated that at short length of angle specimen flexural-torsional mode tends to torsional mode which is equal to local. However, in case of studied specimens it is hard to distinguish between torsional and flexural-torsional mode visually in FEM and it is hard to say if specimen of 600 mm can be called short to equalize these two modes. Therefore, the movement of shear centre of the cross-section has been tracked in Finite Element Analysis during elastic buckling analysis. In case of movement of shear centre this mode will be called torsional-flexural. Otherwise it will be considered as torsional. It is expected that even for torsional mode there might be slight movement. It is suggested to neglect this displacement if it is less or equal to 3% of maximum displacement.

Tracking of movement will be performed only in case when the critical eigenmode shows torsional behaviour. It has been decided to track the displacements of the point in the middle of the specimen. As a result, the reference point has been created at the mid-length with coordinates of shear centre obtained from AutoCAD. Afterwards, the cross-section has been partitioned in the middle in order to create lines to tie reference point. Furthermore,

reference point has been coupled to the node region at the middle of cross-section to make sure that it is able to displace in case of rotation due to flexural-torsional mode.

The visualization of applied method is shown on example of specimen P1-4 in Figure 7.8.1 and 7.8.2. The direction of axis can be seen in Figure 7.8.2.



Figure 7.8.1: Reference point for tracking of shear centre (RP-3).

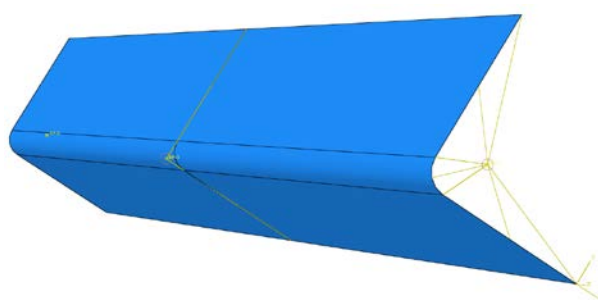


Figure 7.8.2: Reference point for tracking of shear centre (RP-3).

7.9 Modelling output

7.9.1 General

For the completion of finite element analysis it is required to simulate 30 L-shape profiles with fixed-fixed boundary conditions and the same amount with pinned-pinned boundary conditions. Moreover, each specimen was modelled with 5 different imperfections for sensitivity analysis. Validation of finite element model has to be done using results of tests. Shell modelling was taken as a basis. Solid models were calculated for some cross-sections for verification of the approach but not presented in the work because shell modelling showed the most realistic results.

Presenting of Finite Element results without comparison them with test output and hand calculation does not provide sufficient information. Therefore, in this chapter tracking of shear centre movement and failure modes will be described. Presenting of results obtained in Finite Element Analysis with comparison of results from hand calculation and tests will be given in chapter 9 “Output comparison”.

7.9.2 Tracking of shear centre movement

In case of fixed conditions buckling mode with torsional component appears to take place in following cross-sections with length 600 mm: P1-4, P1-6, P2-4, P2-6, P3-4, P3-6, P4-4.

In case of pinned conditions and length 600 mm buckling mode with torsional component appears only in P1-4, P2-4, P3-4.

The results for fixed boundary conditions are shown in Table 7.9.1. It can be seen that all translations are less than 1% of maximum (100%) displacement. Therefore, the buckling modes can be considered as torsional (no shift of shear centre) which is equal to local mode.

Axis	P1-4	P1-6	P2-4	P2-6	P3-4	P3-6	P4-4
X	-0.31%	-0.76%	-0.37%	-0.88%	-0.37%	-0.87%	-0.28%
Y	0.31%	0.76%	0.31%	0.74%	0.21%	0.50%	0.10%
Z	0%	0%	0%	0%	0%	0%	0%

Table 7.9.1: Displacement of shear centre. Percentage of maximum (100%) displacement.
Fixed BC.

The results for pinned conditions show that specimens P1-6, P2-6, P3-6, P4-4 changed mode to flexural buckling. Moreover, from results in Table 7.9.2 flexural component in torsional mode has increased up to 2.4% as maximum. It can be stated that this influence of flexure can be neglected and therefore mode can be equalized to torsional which is identical to local in case of equal angles.

Axis	P1-4	P2-4	P3-4
X	-2.40%	-2.09%	-1.52%
Y	2.40%	1.75%	0.88%
Z	0%	0%	0%

Table 7.9.2: Displacement of shear centre.
 Percentage of maximum (100%) displacement. Pinned BC.

7.9.3 Failure modes

In this chapter failure modes obtained using FEA will be shown by Misses stresses. The main interest in this chapter is the failure mode of the specimen. The output will be shown at the increment at which column fails. The deformed shape will be plotted together with initial shape of cross-section in order to compare them. The magnitude of visualization will be set as 10. This will enable to see the cross-sections at the peak load and at the same magnitude of deformations. For some cross-sections the magnitude will be too big but it is inevitable to use this magnification factor because some specimens exhibit small displacements. The failure modes will be shown only for fixed boundary conditions.

Group P1

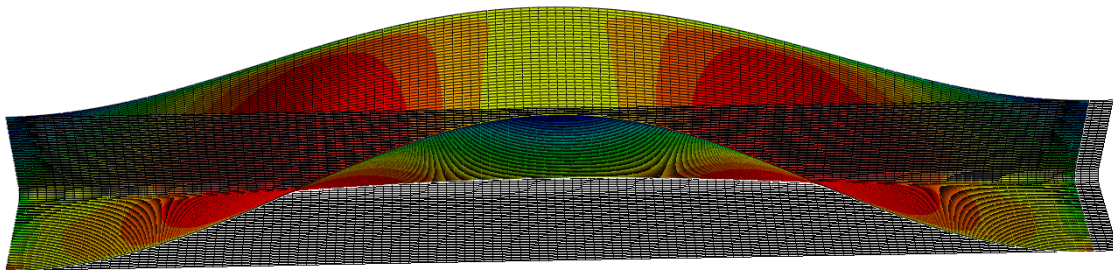


Figure 7.9.1. Failure of P1-4 (local).

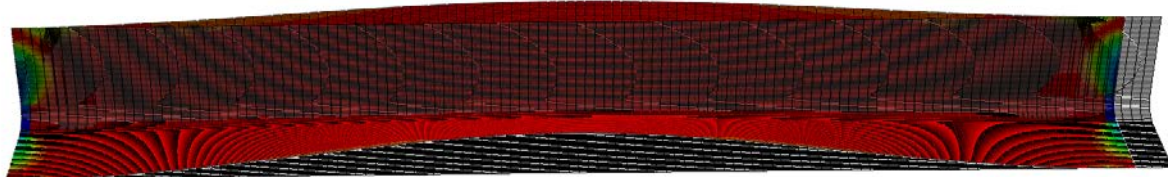


Figure 7.9.2. Failure of P1-6 (local).

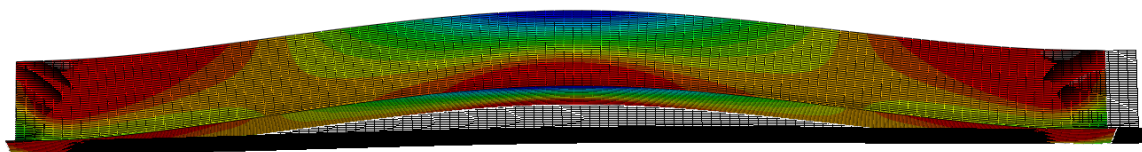


Figure 7.9.3. Failure of P1-10 (flexural).

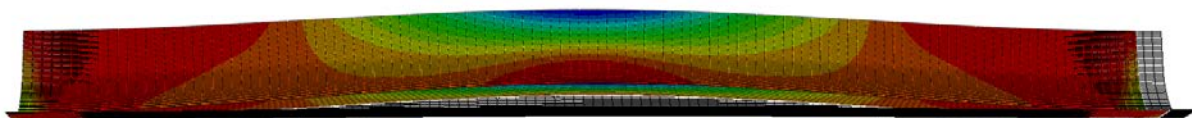


Figure 7.9.4. Failure of P1-16 (flexural).

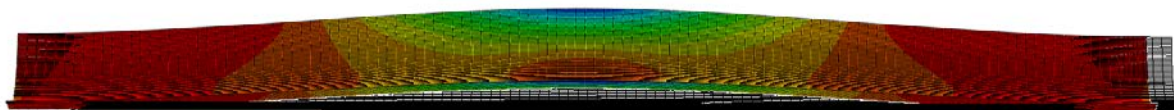


Figure 7.9.5. Failure of P1-20 (flexural).

Group P2

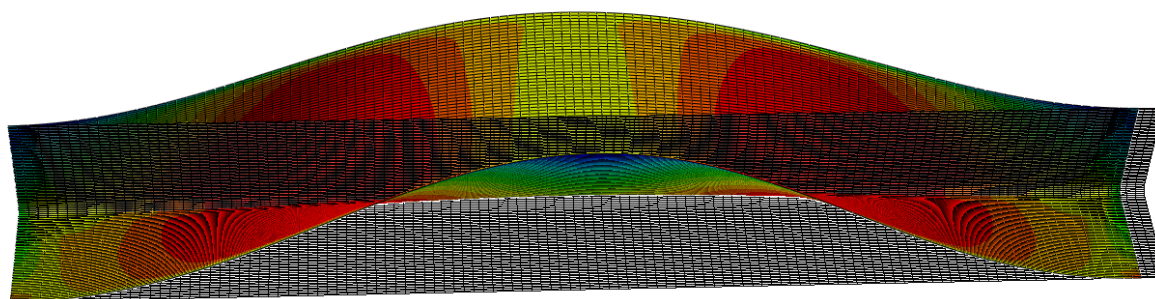


Figure 7.9.6. Failure of P2-4 (local).

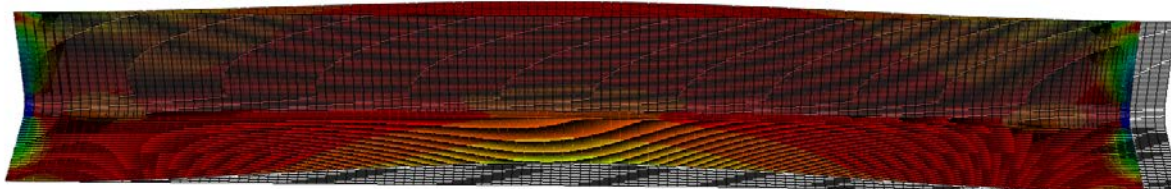


Figure 7.9.7. Failure of P2-6 (local).

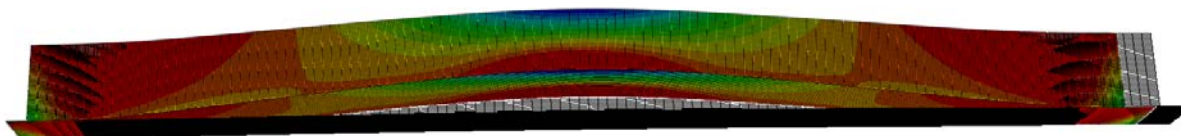


Figure 7.9.8. Failure of P2-10 (flexural).

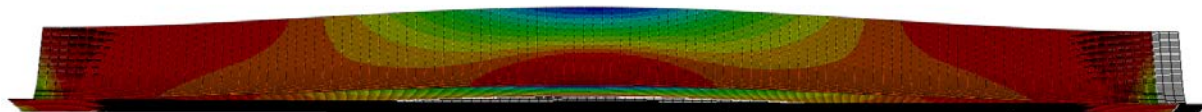


Figure 7.9.9. Failure of P2-16 (flexural).

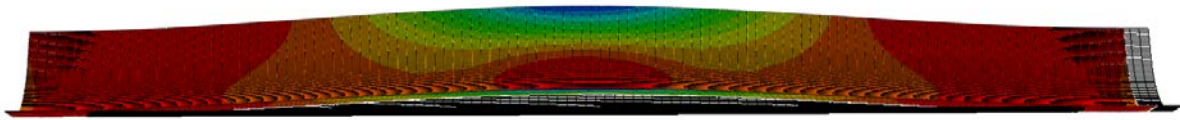


Figure 7.9.10. Failure of P2-20 (flexural).

Group P3

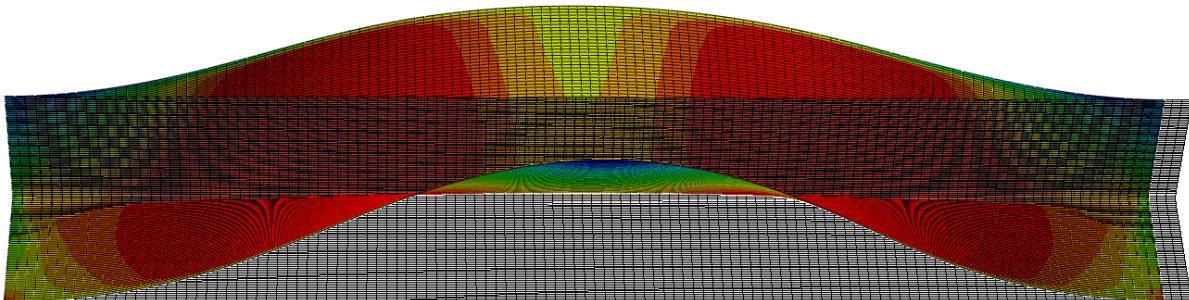


Figure 7.9.11. Failure of P3-4 (local).

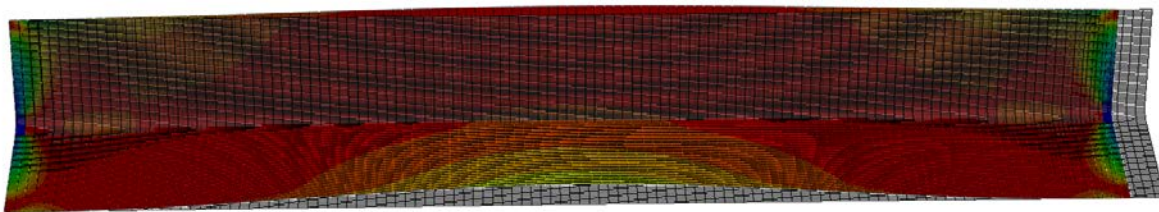


Figure 7.9.12. Failure of P3-6 (local).

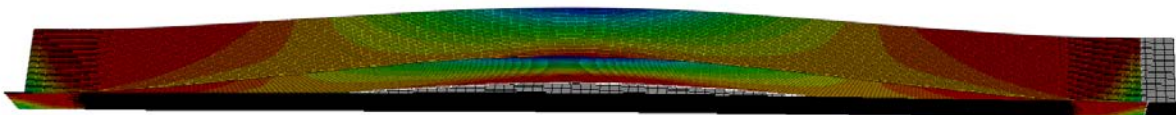


Figure 7.9.13. Failure of P3-10 (flexural).

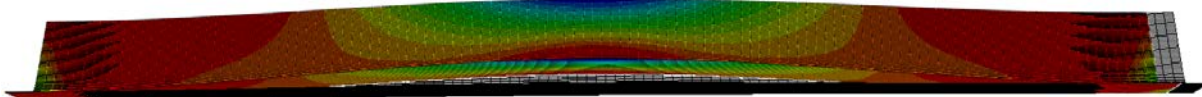


Figure 7.9.14. Failure of P3-16 (flexural).

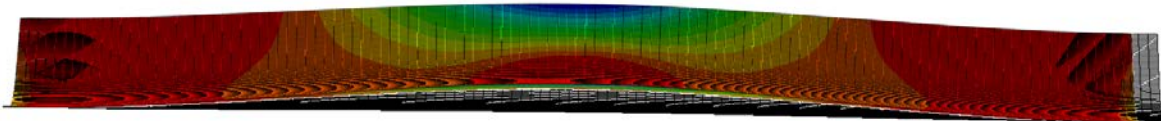


Figure 7.9.15. Failure of P3-20 (flexural).

Group P4

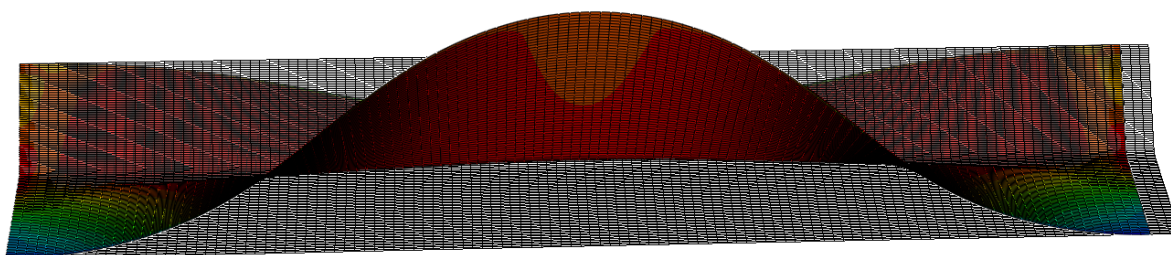


Figure 7.9.16. Failure of P4-4 (local).

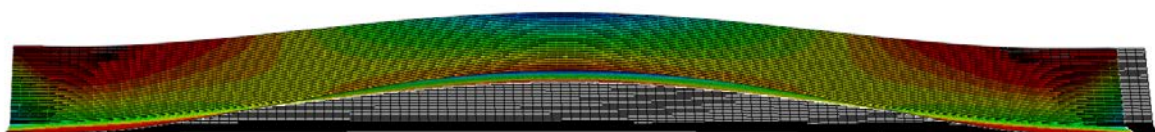


Figure 7.9.17. Failure of P4-6 (flexural).

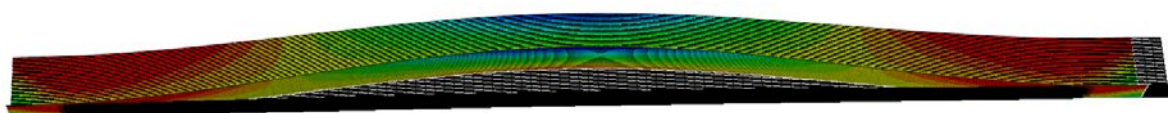


Figure 7.9.18. Failure of P4-10 (flexural).

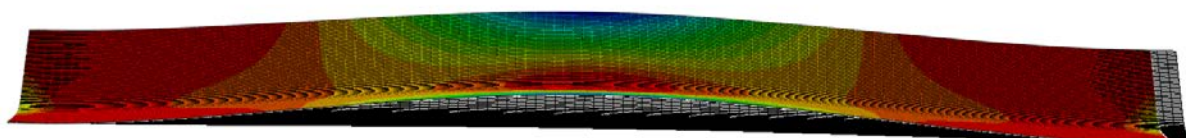


Figure 7.9.19. Failure of P4-16 (flexural).



Figure 7.9.20. Failure of P4-20 (flexural).

Group P5

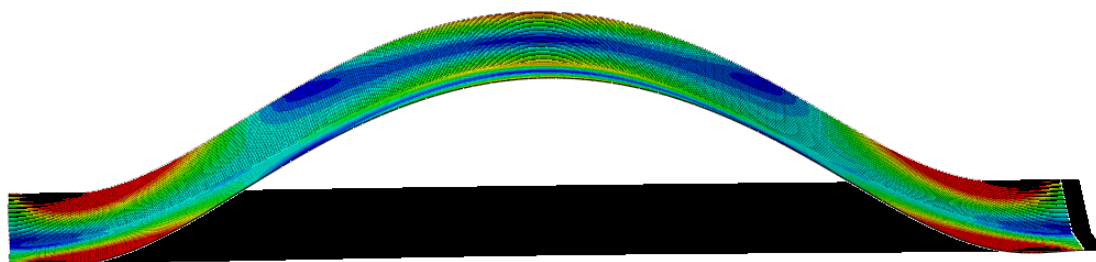


Figure 7.9.21. Failure of P5-4 (flexural).

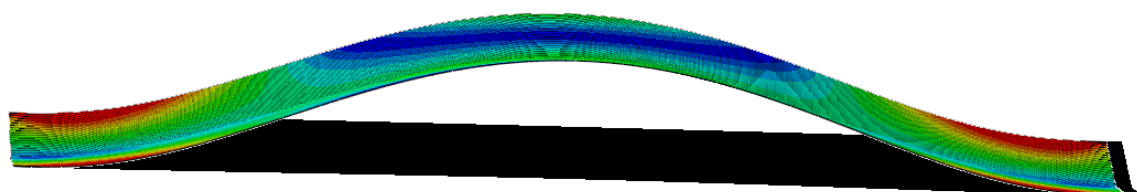


Figure 7.9.22. Failure of P5-6 (flexural).

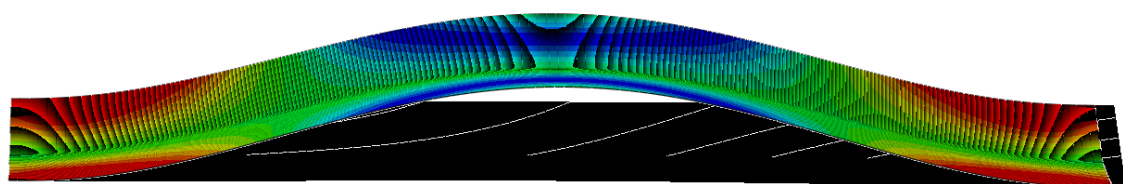


Figure 7.9.23. Failure of P5-10 (flexural).

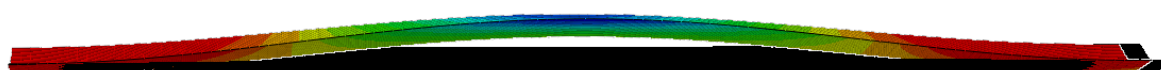


Figure 7.9.24. Failure of P5-16 (flexural).



Figure 7.9.25. Failure of P5-20 (flexural).

Group P6

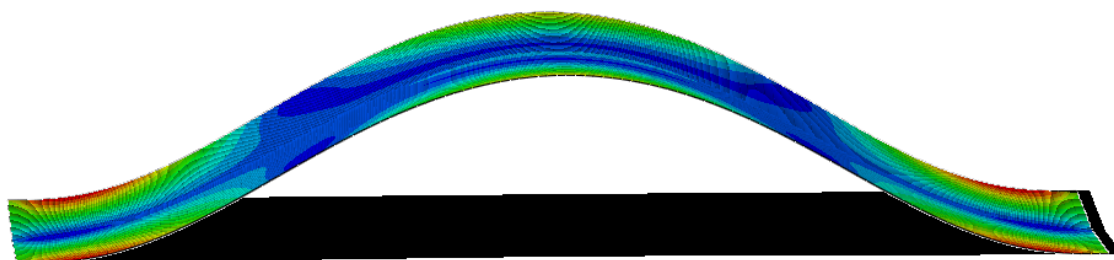


Figure 7.9.26. Failure of P6-4 (flexural).

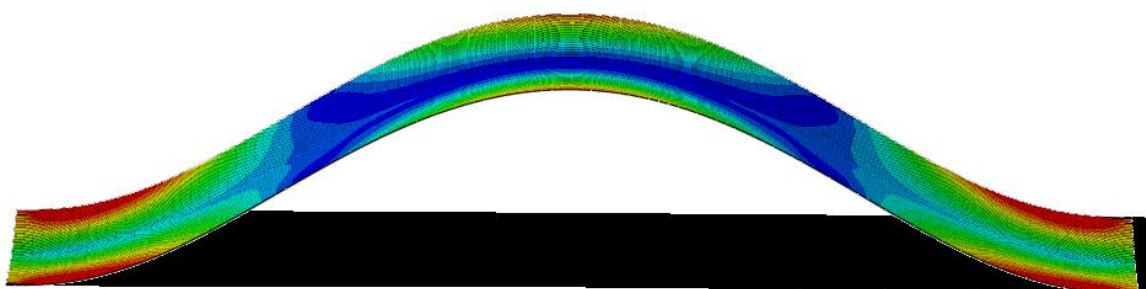


Figure 7.9.27. Failure of P6-6 (flexural).

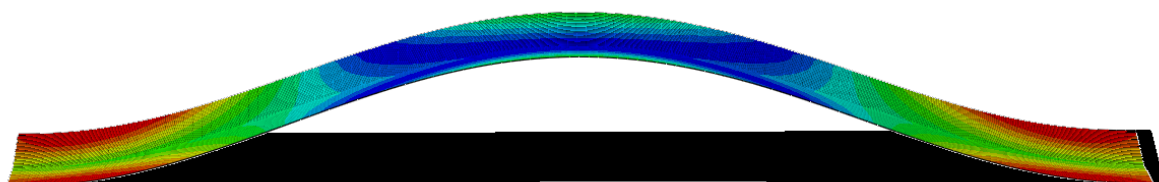


Figure 7.9.28. Failure of P6-10 (flexural).

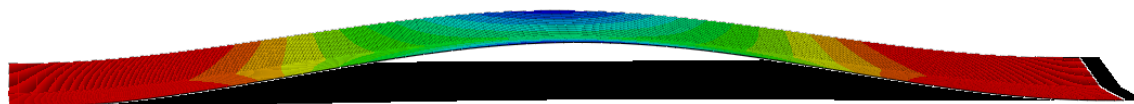


Figure 7.9.29. Failure of P6-16 (flexural).

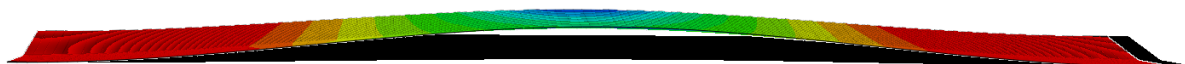


Figure 7.9.30. Failure of P6-20 (flexural).

From analysis of failure modes it can be seen that cross-sections P1-4, P1-6, P2-4, P2-6, P3-4, P3-6, P4-4 exhibit local deformations and fail due to this mode. Whereas, all other specimens fail in flexural mode. Moreover, from analysis of failure modes it can be seen that the buckling of junction between plates of the angle occurs only during flexural failure.

8 EXPERIMENTAL INVESTIGATION

8.1 Experimental evaluation of imperfections

8.1.1 Introduction

During the period of conducting thesis the experimental determination of initial imperfections has been performed. This procedure was the part of development of new technique in this field. The uniqueness of this method is in the type of used equipment for measurements and the precision of obtained output. Determination of initial imperfections has been performed using 3D scanner VIUscan Handyscan 3D Handheld by CREAFORM. Brief summary of technical characteristics for this type of scanner is given below:

- Weight – 1.3 kg;
- Dimensions – 172x260x216 mm;
- Measurement rate – 18000 measures/s;
- Laser Class – II (eye-safe);
- Resolution – 0.100 mm;
- Accuracy – up to 0.050 mm;
- Volumetric accuracy – 0.020 mm + 0.200 mm/m;
- Stand-off distance – 300 mm;
- Laser cross area – 210 mm x 210 mm;
- Software – Vxelements;

Using this type of equipment in measurements provides ability to obtain the spatial scanned model of the specimen. Therefore, it is possible to obtain the magnitude of imperfections in every point of the scanned surface. This fact combined with high accuracy of measurements (up to 0.050 mm) gives bigger benefits compared with the measurement techniques which are currently used for such type of applications.

Determination of initial imperfections has been performed for 36 L-shaped specimens with thicknesses 4 and 6 mm. This amount included 3 specimens of each type P1 to P6. Remaining cross sections are not currently in the scope of this work.

8.1.2 Scanning methodology

The methodology of scanning consisted of following steps:

1. preparation of specimens for painting;
2. painting;
3. scanning;
4. analysis of results.

The **preparation of specimens** included cleaning of the surface using sandpaper. According to the technical specifications of the scanner its accuracy is up to 0.050 mm. Therefore, it is vital to remove the small particles of dust from the surface and to make the results obtained from further measurements more precise and realistic.

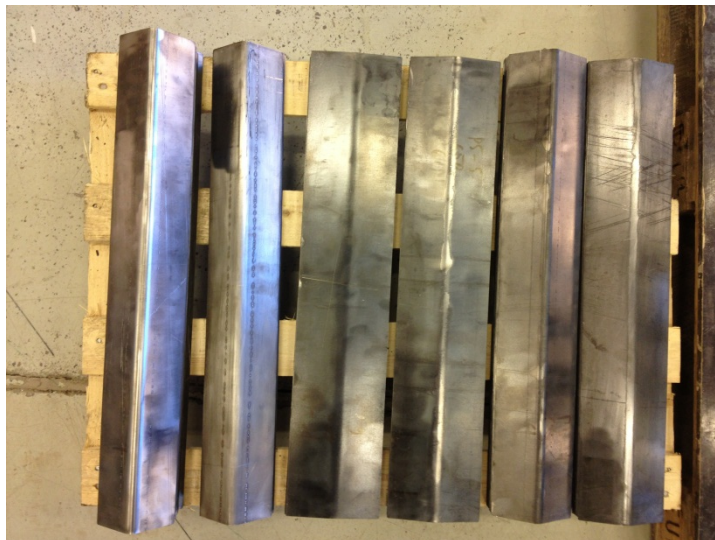


Figure 8.1.1: Specimens after preparation



Figure 8.1.2: Specimens after preparation

The next step was **painting of the specimens**. The scanned surface is required to be not reflective in order to obtain quality measurement. Therefore, the specimens were painted in mat grey colour using spray paint.



Figure 8.1.3: Painted specimens

The **scanning** procedure includes following steps:

1. Application of positioning targets.

It is required to apply sufficient number of positioning targets on surface of the specimen. According to the support documentation the distance between the targets should vary between 2 and 10 cm and the distance from the edge of the specimen to the target should be more than 2 cm. However, these values differ according to geometry of scanned object. The most efficient way of targets positioning is achieved using “trial and error” method.

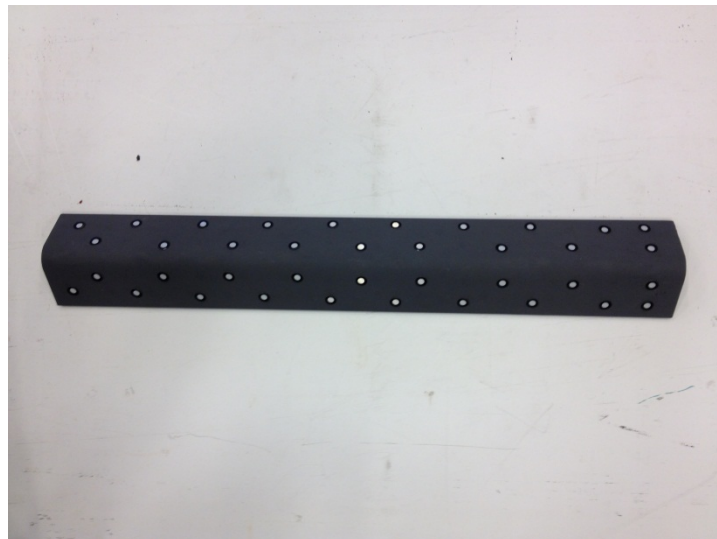


Figure 8.1.4: Positioning targets

2. *Adjusting of the height of the specimens above horizontal surface.*

The specimen has to be placed on the stable surface. In performed measurements the base shown on the picture was used in order to achieve comfortable positioning of the specimens.



Figure 8.1.5: Stable base for positioning of specimens

During scanning it was found out that the surface of the specimen has to be placed over the level of axis (axis positioning is described below). Therefore, additional supports were used for placement of the specimen.

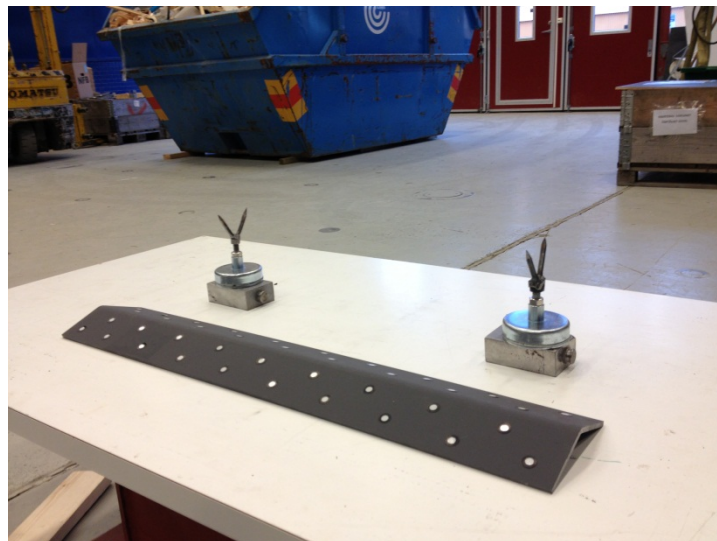


Figure 8.1.6: Supports for the specimen

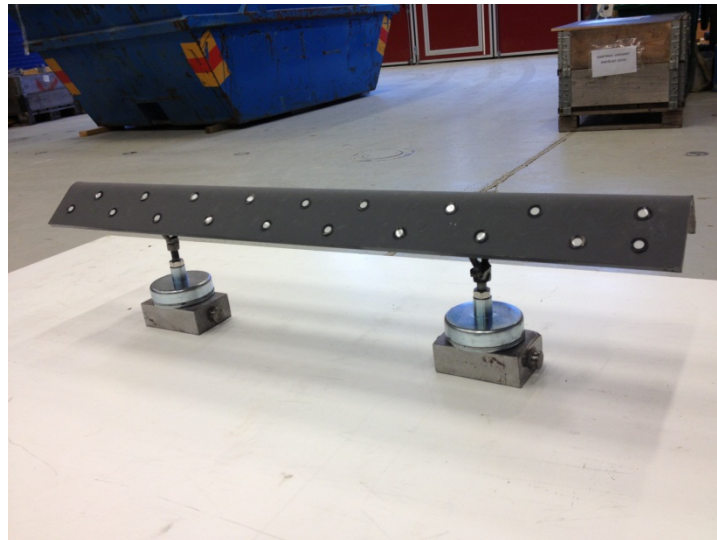


Figure 8.1.7: Supports for the specimen

3. Positioning of the member axis.

In order to locate and match the direction of the specimen in the software and reality it is required to use the axis. It is represented by metal frame with positioning targets on it.

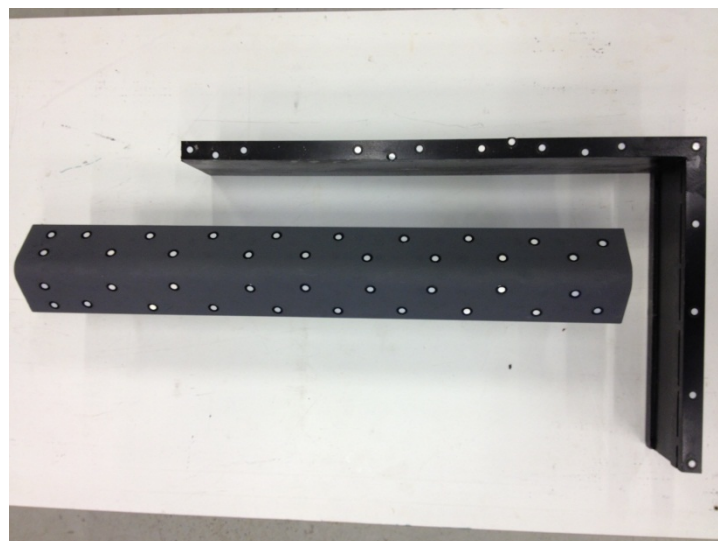


Figure 8.1.8: Member axis

Furthermore, the edges of the axis and the specimen will be located parallel to each other. For this purpose the wooden plates with equal thickness were used.

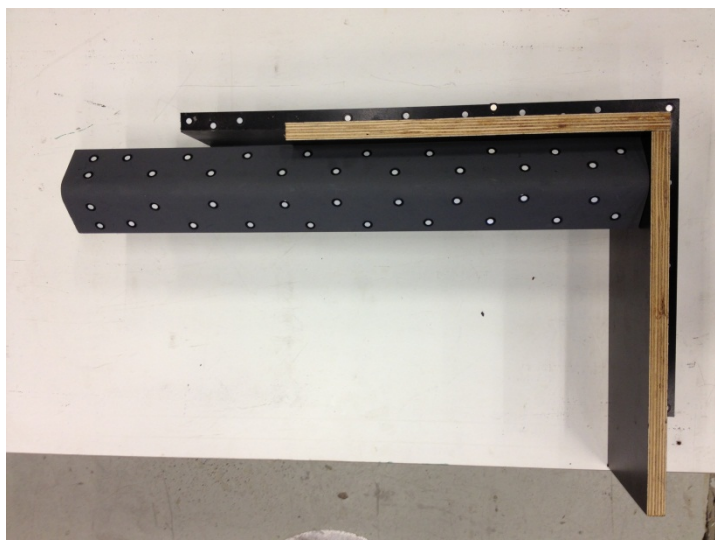


Figure 8.1.9: Equal positioning of specimen and axis

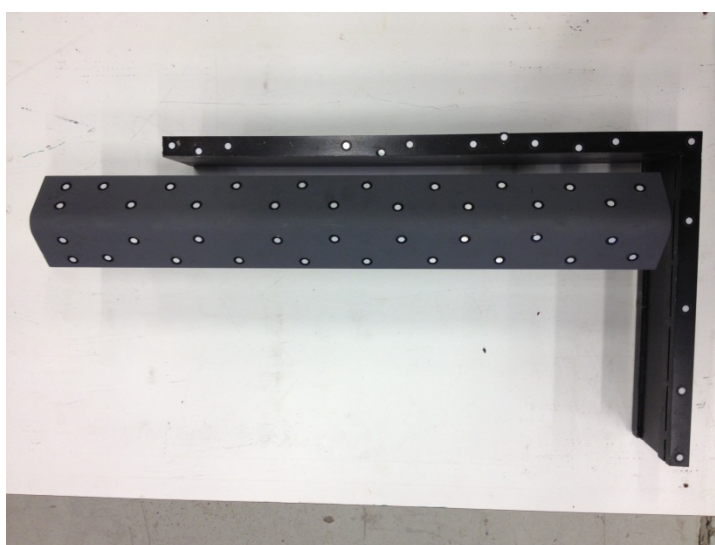


Figure 8.1.10: Equal positioning of specimen and axis

4. Scanning of positioning targets.

During this step positioning targets have to be scanned to the software VElements by Creaform. The software recognizes the location of the targets and the axis.

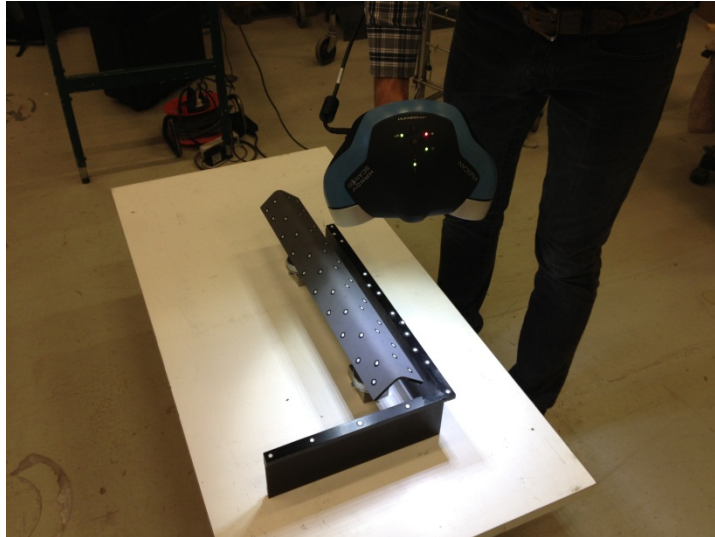


Figure 8.1.11: Scanning of positioning targets

5. Removal of axis.

After scanning of positioning targets the axis has to be removed from the scanning location.

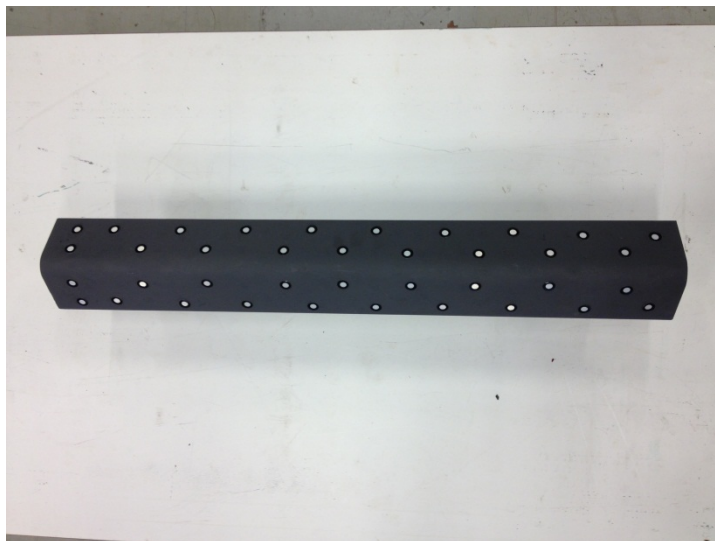


Figure 8.1.12: Removal of axis

6. Scanning of specimen`s surface.

In this step the surface of the specimen is scanned. The output from this scanning should be used for determination of initial imperfections.

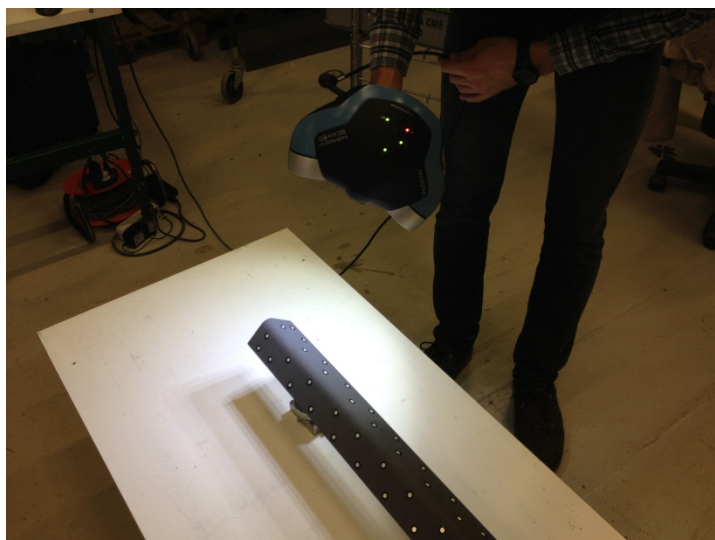


Figure 8.1.13: Scanning of specimen's surface.

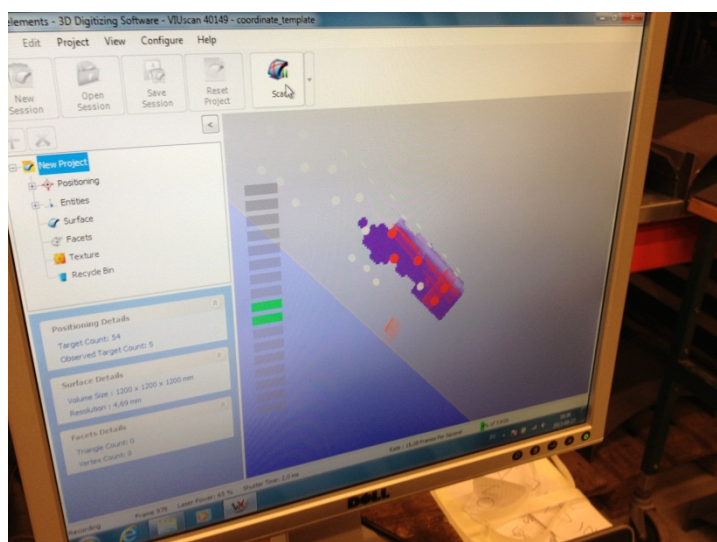


Figure 8.1.14: User interface of VXelements software. Representation of scanned positioning targets and specimen's surface.

7. Locating of the coordinate system on the specimen.

After performing of all mentioned steps it is necessary to locate the direction of coordinate system on the specimen. It will be beneficial for future analysis and it will help to match the location of axis in software and in reality.



Figure 8.1.15: Locating of the coordinate system on the specimen.

Following step of the procedure is **analysis** of the obtained measurements and calculating of initial imperfections.

8.1.3 Evaluation of measured imperfections

The obtained files afterwards are processed using AutoCAD Alias Automotive software. Afterwards scanned cross sections are compared with idealized geometry created in AutoCAD. As a result the difference between real surface and idealized one is obtained for the number of required points. The next step is to introduce obtained results in Finite Element software. As one of ways for defining imperfections in Abaqus this software offers possibility of introducing imperfections directly. This is performed by specifying imperfections as a table of node numbers and coordinate perturbations in the global coordinate system or, optionally, in a cylindrical or spherical coordinate system. Alternatively, the imperfection data can be read from a separate input file.

The evaluation of obtained results is not included in the scope of work of this thesis and it will be done during further investigation of the L-profile behaviour.

8.2 Compression test

8.2.1 Specimen labelling

The labelling of specimens in this work has been described in chapter 4.1 “Tested specimens”. However, additional labelling is used during experimental investigation in the laboratory. Experimental labelling includes identification of angle of folding, thickness of material and number of the specimen (from total available number of given type). For example, “P1-5-6mm” define specimen as follows:

1. Angle of folding refers to group “P1” - 90°. All angles of folding and appropriate groups are presented in chapter 4.1 “Tested specimens”.
2. “5” indicates the index number of specimen tested.
3. “6mm” indicates thickness of material.

8.2.2 Test rig and operation

Compression test has been performed using laboratory facilities of Lulea University of Technology. The 600kN servo-controlled hydraulic testing machine was used to apply compressive axial force to specimen. The ends of cross-sections have been milled flat before test. This was done to ensure that the end-surface will be parallel to bearing plate and no imperfection will be introduced to the results due to unsmoothness of surface. The compression force was applied through upper moveable end support which allowed to test specimens of 300 and 600 mm.

The specimen was placed between two rigid bearing plates which were mounted to the test rig. Calculated centre of gravity of specimen was aligned with the centre of the bottom bearing plate. The boundary conditions used in the test are expected to be fixed-ended (displacements and rotations restrained in the ends of cross-section, except displacement of upper end in the direction of applied load).

The upper bearing of test rig has been moved slowly towards the specimen with application of initial load of approximately 1-2 kN. This was performed to make sure that no possible gaps between surface of specimen and bearing plate appear.

Four displacement transducers (LVDT1, 2, 3 and 4) were used to measure axial shortening of the member. The transducers consist of measuring device and carbon-fibre strut. This strut allows to eliminate the deformations of the transducer due to high stiffness and light weight. The location of LVDT is shown on Figure 8.2.1.

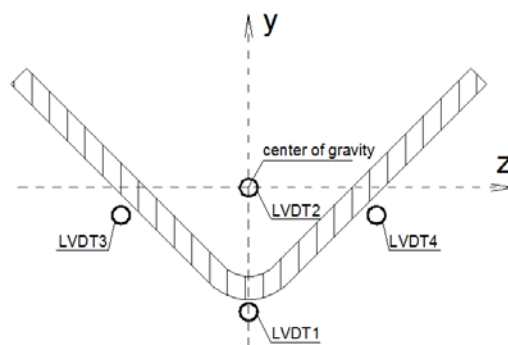


Figure 8.2.1: Location of displacement transducers (LVDT1, 2, 3, 4).

According to Figure 1 displacement transducers were placed as follows:

1. LVDT1 was placed in the outer corner of the specimen between two thin plates welded to the cross-section. This approach enables to measure only shortening of specimen. This is beneficial comparing to measurement of shortening between bearing plates of test rig when error might be introduced by displacements of these plates.
2. LVDT2 was placed in centre of gravity of cross-section between bearing plates of test rig. The transducer has been located at its position by mounting strong magnet at upper and lower end
3. LVDT3 and 4 were placed in the middle of cross-section leg between bearing plates of test rig. The transducers have been located at its position by mounting strong magnet at upper and lower end.

The test has been performed using displacement control what enabled test to be continued in post-ultimate range. The load was applied at constant speed 0.001 mm/s. Load has been applied after failure until the load dropped by 15-20%. This enabled to see higher deformation of specimen.

PC software has been used to record data obtained from the test: applied load and information from displacement transducers at regular intervals during performed experiment.

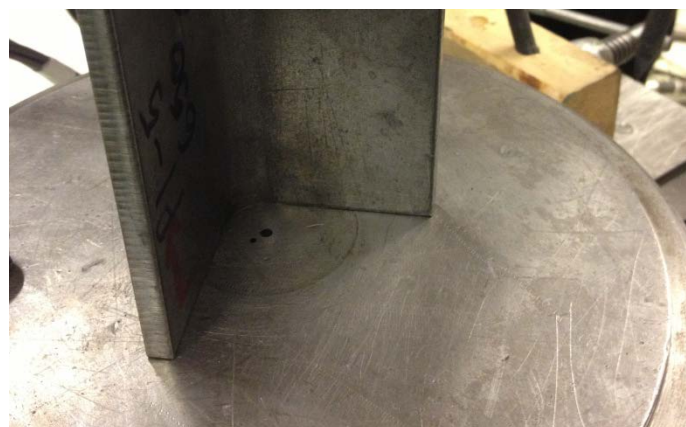


Figure 8.2.2: Centre of gravity is aligned with the centre of lower bearing.

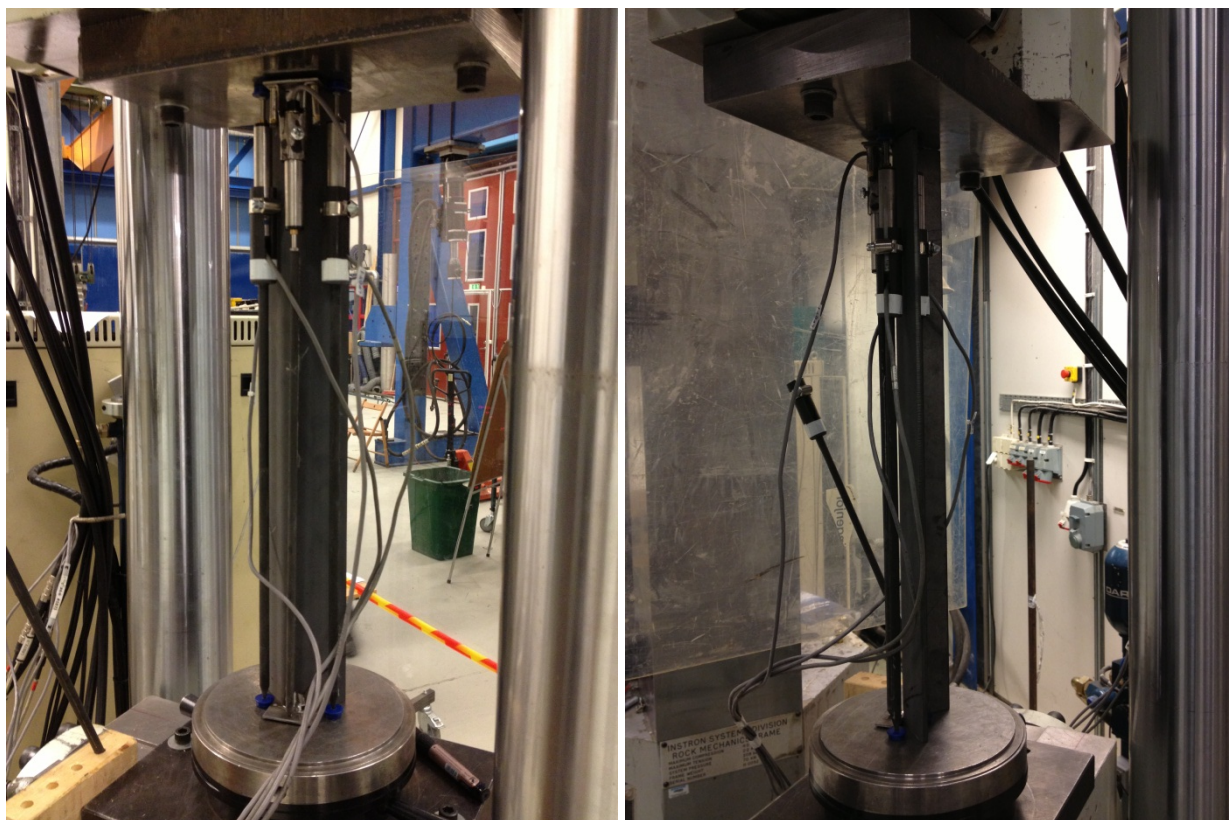


Figure 8.2.3: Test rig



Figure 8.2.4: Additional plate welded to the specimen for installation of LVDT1. Magnets used for LVDT3 and 4.

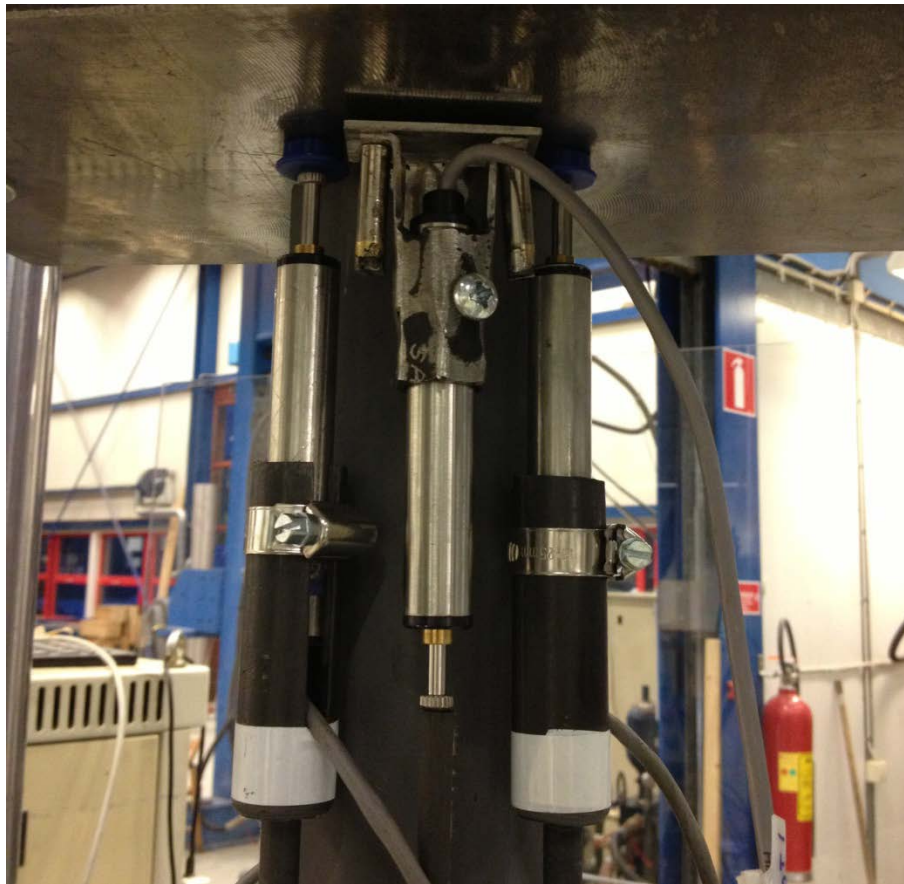


Figure 8.2.5: Mounting of LVDT1 to welded plate in upper part.
Magnets used for LVDT3 and 4.

8.2.3 Test results

This chapter will represent results which were obtained during experiments. Table 8.2.1 provides information about following:

1. ultimate load P_{test} at which section failed during test,
2. ultimate stress σ_{test} (dividing ultimate load with section area measured in AutoCAD)
3. Comparison of ultimate stress with nominal yield stress.

Group	Profile number	Class	Test			Nominal yield stress f_y [MPa]	σ_{test}/f_y
			P_{test} [kN]	Area [mm ²]	Ultimate stress σ_{test} [MPa]		
P1-6	P1-5-6mm	Class 4	443	652.52	679	650	1.04
	P1-6-6mm	Class 4	446	652.52	684	650	1.05
	P1-7-6mm	Class 4	445	652.52	682	650	1.05
P2-4	P2-7-4mm	Class 4	207	457.33	453	650	0.70
P2-6	P2-5-6mm	Class 4	454	668.98	678	650	1.04
	P2-6-6mm	Class 4	469	668.98	701	650	1.08
	P2-7-6mm	Class 4	456	668.98	681	650	1.05
P3-6	P3-5-6mm	Class 4	454	691.09	656	650	1.01
	P3-6-6mm	Class 4	444	691.09	642	650	0.99
	P3-7-6mm	Class 4	450	691.09	651	650	1.00
P4-6	P4-5-6mm	Class 4	369	704.5	523	650	0.81
	P4-6-6mm	Class 4	389	704.5	552	650	0.85
	P4-7-6mm	Class 4	343	704.5	487	650	0.75

Table 8.2.1: Test output results

The representative column deformation after test for cross-section P1-7-6 can be seen in Figure 8.2.6. It can be seen that local deformation takes place in cross-section. In case of P1-6 specimen the deformations are similar for all 3 cross-sections. Similar deformations take place in cross-sections P2-4, P2-6, P3-6.

In case of cross-section P4-6 the failure occurs due to flexural buckling. Typical deformation for this mode is shown in Figure 8.2.7.

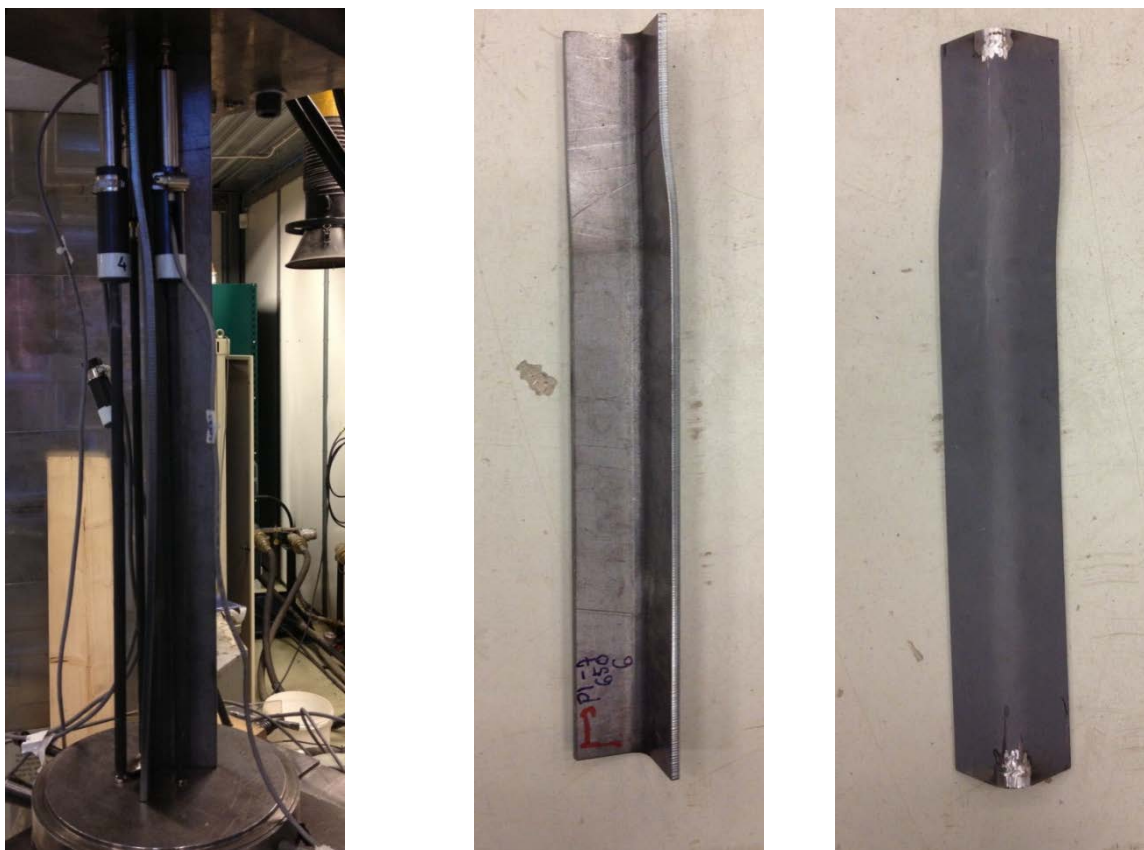


Figure 8.2.6: Deformation of specimen P1-7-6mm (typical failure for P1-6, P2-4, P2-6, P3-6).



Figure 8.2.7: Deformation of specimen P4-5-6mm (typical failure for P4-6).

From table 8.2.2 it can be seen that the difference in ultimate loads between 3 identical specimens is small (only for cross-section P4-6 the difference is up to 13% in ultimate resistance). Therefore, this indicates reliability of results. Moreover, it can be seen that ultimate stress for specimens P1-6, P2-6 and P3-6 is higher than the nominal yield stress. This fact might indicate that steel yielding occurs before local buckling. However, this fact might be justified truthfully in case of comparing results with the actual yield stress obtained experimentally.

The results of the test are obtained in the form of load-displacement curve. This curve has to be normalized due to initial errors which provide displacement transducers. Normalization procedure will be described on the example of specimen P1-6-6mm. Figure 8.2.8 represents the initial output which is obtained directly from PC software connected to test rig. It can be seen that displacement transducers LVDT2, 3 and 4 show almost identical results. Therefore, for final analysis the single average curve will be created for these 3 displacement transducers. However, LVDT1 shows different results in terms of displacement. It can be explained by the fact that it was mounted between plates welded to the specimen. Therefore, this result is expected to show real axial shortening of specimen without influence of test rig deformations.

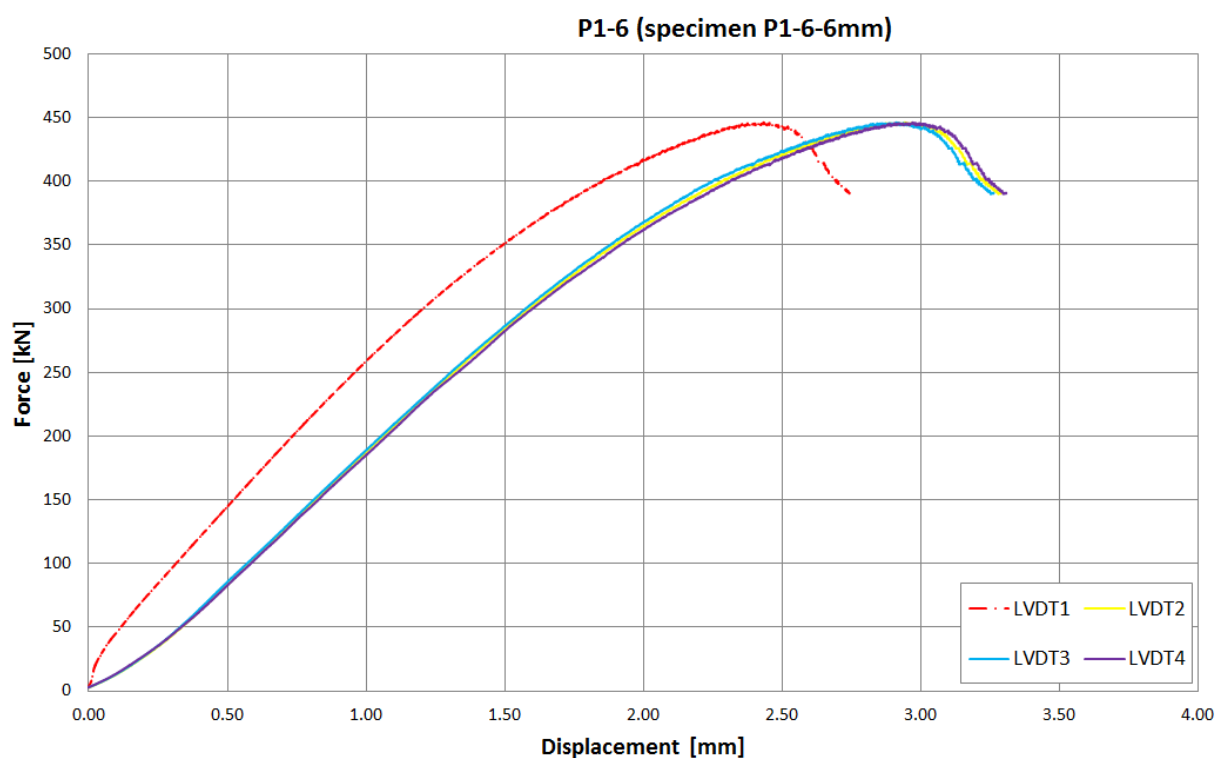


Figure 8.2.8: Initial force-displacement curve for P1-6-6mm

The Figure 8.2.9 shows force-displacement curve for LVDT1 and for obtained average between LVDT2, 3, 4.

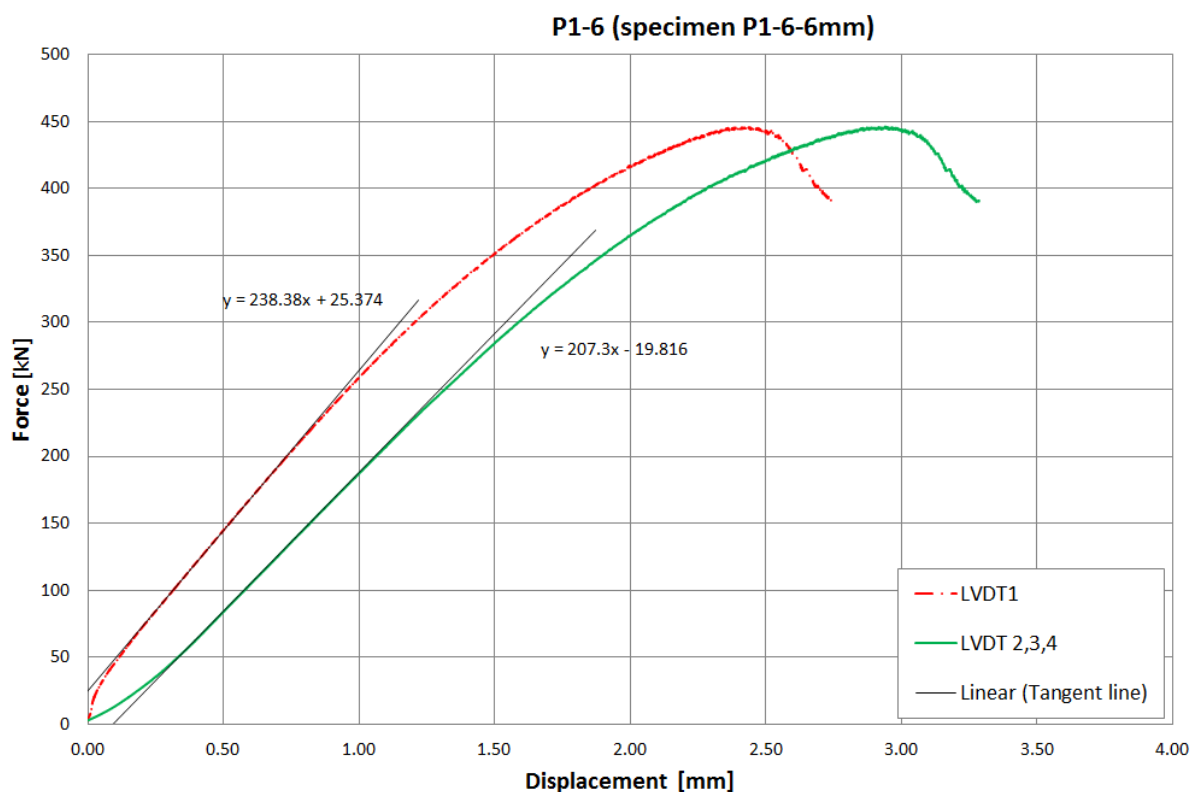


Figure 8.2.9: Force-displacement curve for LVDT1 and average LVDT2, 3, 4. P1-6-6mm

The initial part of load-displacement curve has to be linear as long as the behaviour is elastic in this part. From Figure 8.2.8 it can be seen that the initial part of curve obtained from test is non-linear. It can be observed if the tangent line to curve is plotted. The fact of non-linearity can be explained by initial settling of displacement transducers during start of the test. Therefore, this error has to be eliminated. This will be done by substituting the initial curved part with the appropriate linear behaviour what corresponds to tangent line. Furthermore, the graphs will be shifted so that the starting point of linear part will coincide with the start of coordinate system. Precise shifting of the graph is performed using the equation of tangent line shown in Figure 8.2.8. The final normalized force-displacement curve is plotted in Figure 8.2.10.

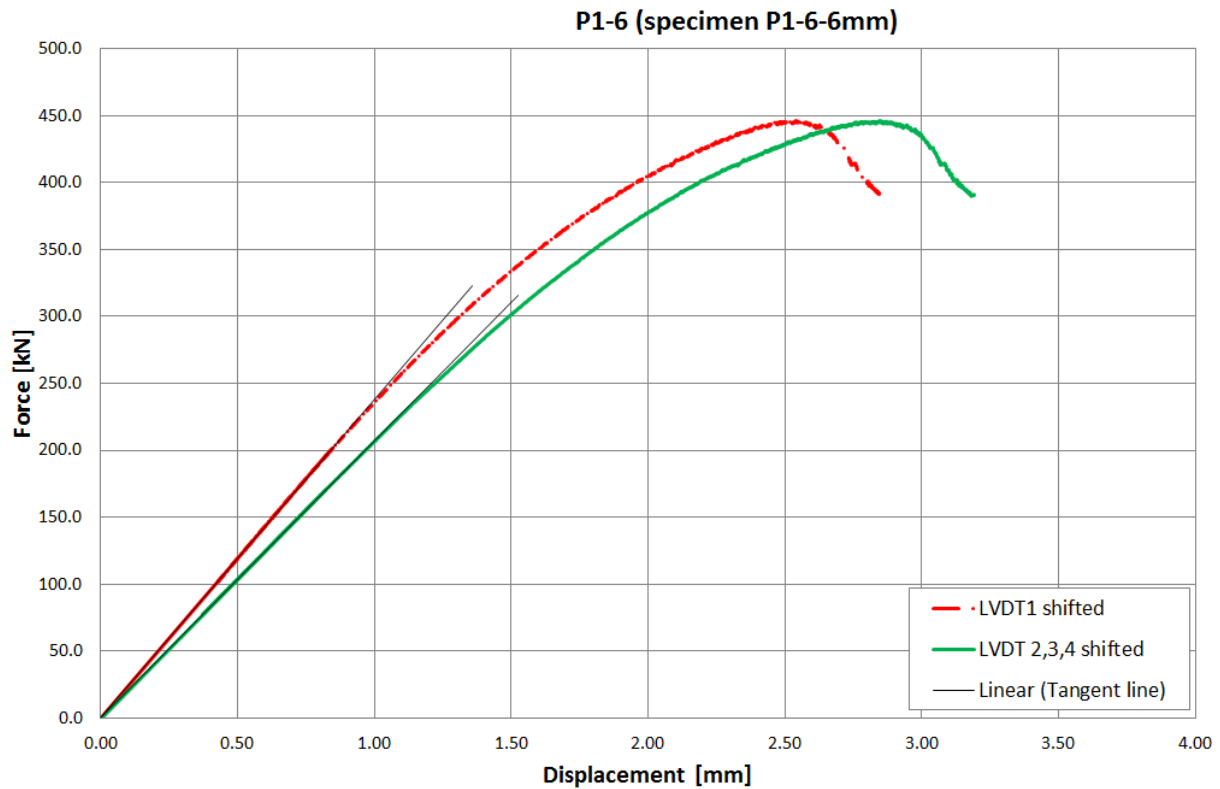


Figure 8.2.10: Normalized force-displacement curve for P1-6-6mm

Specimens P1-5-6mm, P1-6-6mm and P1-7-6mm exhibit similar behaviour and that is why the normalized graph for P1-6-6mm will be used for group P1-6 for further investigation and comparison.

Not normalized load-displacement curves for other tests are presented in **Attachment 19 - Load-displacement curves**. This document illustrates the output for LVDT1 and average curve for LVDT2, 3 and 4.

9 OUTPUT COMPARISON

9.1 Summary of calculation according to EN

The procedures for obtaining results of hand calculation according to EN have been described in previous chapters. The results can be found in relevant attachments:

Attachment 1 – Determination of average yield strength;

Attachment 2 – Classification of cross-sections;

Attachment 3 – Determination of effective width for Class 4 cross-sections;

Attachment 4 – Determination of elastic critical force (fixed BC);

Attachment 5 – Determination of flexural buckling resistance (fixed BC);

Attachment 6 – Determination of torsional buckling resistance (fixed BC);

Attachment 7 – Determination of torsional buckling resistance (fixed BC);

Attachment 8 – Determination of moment buckling resistance for Class 4 cross-sections for bending about weak axis;

Attachment 9 – Determination of member resistance for combined compression and bending interaction (fixed BC);

Attachment 10 – Combined table of buckling resistance according to EN (fixed BC);

Attachment 11 – Combined table of buckling resistance according to EN for fixed BC (neglecting additional moment for Class 4 cross-sections);

Attachment 12 - Combined table of buckling resistance according to EN (pinned BC);

Attachment 13 – Combined table of buckling resistance according to EN for pinned BC (neglecting additional moment for Class 4 cross-sections);

Attachment 14 – Calculation procedure according to EN for cross-sections P1-4 (Class 4) and P1-10 (Class 3).

9.2 Comparison of elastic critical load according to hand calculations and FEA

For hand calculations elastic critical load has been obtained using stability theory. From Finite Element Analysis elastic critical load was obtained using eigenvalue analysis. The lowest eigenmode was considered to be the most critical and corresponding eigenvalue has been used. Table 9.2.1 represents results obtained for the case of fixed boundary conditions.

The lowest elastic critical load is coloured. Column “Diff” represents difference between FEM and hand calculation results in percentage. In the table buckling modes are denominated as

follows: L – local, T – torsional, TF – torsional-flexural, F – flexural. T/L means torsional or local mode which is equal for equal-leg angles for short and intermediate length.

Group	Profile number	Class	Hand calculation				FEM		
			Local buckling	Flexural buckling	Torsional buckling	Torsional flexural buckling	Critical force [kN]	Buckl mode	Diff
			Ncr.L [kN]	Ncr.F [kN]	Ncr.T [kN]	Ncr.TF [kN]			
P1	P1-4	Class 4	190	1351	174	172	178	T/L	3%
	P1-6	Class 4	670	1805	601	585	583	T/L	0%
	P1-10	Class 3	-	2340	2821	2599	2139	F	-9%
	P1-16	Class 3	-	2447	12356	9597	2241	F	-9%
	P1-20	Class 3	-	2346	25865	15830	2187	F	-7%
P2	P2-4	Class 4	185	1179	173	172	180	T/L	4%
	P2-6	Class 4	647	1631	607	596	593	T/L	-1%
	P2-10	Class 3	-	2304	2793	2642	2089	F	-10%
	P2-16	Class 3	-	2855	11971	10203	2600	F	-10%
	P2-20	Class 3	-	3080	23863	17765	2822	F	-9%
P3	P3-4	Class 4	180	771	175	174	183	T/L	5%
	P3-6	Class 4	618	1123	612	607	608	T/L	0%
	P3-10	Class 3	-	1800	2774	2704	1620	F	-11%
	P3-16	Class 3	-	2834	11339	10575	2573	F	-10%
	P3-20	Class 3	-	3620	21693	19126	3297	F	-10%
P4	P4-4	Class 4	177	384	180	180	185	T/L	4%
	P4-6	Class 4	602	588	609	607	520	F	-13%
	P4-10	Class 3	-	1068	2771	2743	972	F	-10%
	P4-16	Class 3	-	2095	11084	10795	1933	F	-8%
	P4-20	Class 3	-	3081	21248	20374	2860	F	-8%
P5	P5-4	Class 4	175	113	180	180	101	F	-11%
	P5-6	Class 4	593	195	608	608	180	F	-8%
	P5-10	Class 3	-	464	2763	2758	441	F	-5%
	P5-16	Class 3	-	1283	10889	10821	1246	F	-3%
	P5-20	Class 3	-	2225	20608	20377	2168	F	-3%
P6	P6-4	Class 4	175	40	179	179	38	F	-5%
	P6-6	Class 4	590	87	604	603	84	F	-3%
	P6-10	Class 3	-	290	2741	2739	289	F	0%
	P6-16	Class 3	-	1029	10809	10799	1033	F	0%
	P6-20	Class 3	-	1934	20502	20469	1939	F	0%

Table 9.2.1: Elastic critical load assessment for fixed boundary conditions (hand calculation vs FEM).

From table 9.2.1 it can be observed that difference between values of elastic critical load according to FEM and hand calculation is very small in most cases (around 5%) and for few specimens this difference reaches 13%. It is considered that these results are acceptable in

terms of deviations. Moreover, comparing results from hand calculation for different modes it can be noticed that for 600 mm specimen torsional and torsional flexural elastic critical loads are almost similar for Class 4 elements. Moreover, local buckling elastic critical load is similar to torsional and flexural-torsional mode for the case of 4 mm specimen. Torsional-flexural mode (or torsional – because values are similar) is dominant for Class 4 specimens of Groups P1-P3 and for P4 with $t=4\text{mm}$. Results for all the other specimens show that flexural mode is dominant. The predicted buckling modes coincide for hand calculation and FEM considering the fact that for short length specimen torsional mode is equal to local and tends to be equal to flexural-torsional mode.

As it has already been stated specimens were also considered to have pinned support. Therefore, this investigation has been done separately. Table 9.2.2 represents results obtained for the case of pinned supports.

Group	Profile number	Class	Hand calculation				FEM		
			Local buckling	Flexural buckling	Torsional buckling	Torsional flexural buckling	Critical force [kN]	Buckl mode	Diff
			Ncr.L [kN]	Ncr [kN]	Ncr.T [kN]	Ncr.TF [kN]			
P1	P1-4	Class 4	190	338	165	158	174	T/L	9%
	P1-6	Class 4	670	451	568	509	438	F	-3%
	P1-10	Class 3	-	585	2674	1840	561	F	-4%
	P1-16	Class 3	-	612	11852	3851	573	F	-7%
	P1-20	Class 3	-	586	25090	4510	553	F	-6%
P2	P2-4	Class 4	185	295	165	161	177	T/L	9%
	P2-6	Class 4	647	408	576	534	395	F	-3%
	P2-10	Class 3	-	576	2649	2033	552	F	-4%
	P2-16	Class 3	-	714	11435	4780	669	F	-7%
	P2-20	Class 3	-	770	22963	5887	718	F	-7%
P3	P3-4	Class 4	180	193	167	165	182	T/L	10%
	P3-6	Class 4	618	281	580	561	271	F	-4%
	P3-10	Class 3	-	450	2628	2315	431	F	-4%
	P3-16	Class 3	-	709	10773	6472	667	F	-6%
	P3-20	Class 3	-	905	20696	8499	845	F	-7%
P4	P4-4	Class 4	177	96	171	170	93	F	-4%
	P4-6	Class 4	602	147	575	568	142	F	-3%
	P4-10	Class 3	-	267	2618	2488	256	F	-4%
	P4-16	Class 3	-	524	10497	8100	498	F	-5%
	P4-20	Class 3	-	770	20177	11317	730	F	-6%
P5	P5-4	Class 4	175	28	170	170	27	F	-3%
	P5-6	Class 4	593	49	574	572	47	F	-3%
	P5-10	Class 3	-	116	2606	2579	113	F	-3%
	P5-16	Class 3	-	321	10282	9503	313	F	-2%
	P5-20	Class 3	-	556	19488	13961	543	F	-2%
P6	P6-4	Class 4	175	10	169	169	10	F	-2%
	P6-6	Class 4	590	22	569	569	21	F	-1%
	P6-10	Class 3	-	73	2583	2574	72	F	-1%
	P6-16	Class 3	-	257	10200	10071	255	F	-1%
	P6-20	Class 3	-	484	19355	15538	480	F	-1%

Table 9.2.2: Elastic critical load assessment for pinned boundary conditions
(hand calculation vs FEM)

From table 9.2.2 it can be seen the difference between results from hand calculation and FEM is up to 10% and in most cases is around 4%. Dominating buckling modes change in some specimens compared to fixed boundary conditions. For pinned-supported specimen flexural-torsional (or torsional – because values are similar) mode is dominant only in specimens P1-4, P2-4, P3-4. Results for all the other specimens show that flexural mode is dominant.

To demonstrate changes of buckling modes in fixed-supported specimens buckling curves have been plotted for specimens P1-P6 with $t=4, 6$ and 10 mm. The explanation of changes depicted in these graphs is presented in chapter 10.2.2 where the curves are used to solve the problem of cross-section classification. All the curves can be seen in the Attachment 17 “Elastic critical loads curves”.

9.3 Sensitivity analysis. Comparing design strength according to EN, FEA and tests

Fixed boundary conditions

The background for sensitivity analysis has been presented in chapter 7.6 “Modelling of imperfections”. The results of sensitivity analysis are provided in Attachment 15 “Combined table of buckling resistance – fixed BC”. This document provides comparison of design resistance according to EN and FEA. Five different approaches to model imperfections in FEA are used. EN calculation of design buckling resistance includes interaction between compression and additional moment for cross-sections Class 4. Class 3 cross-sections are calculated in pure compression.

Sensitivity analysis presented in Attachment 16 shows that in case of local imperfections and thickness of material $t=4$ mm the model is not sensitive to imperfections. In case of local imperfections for $t=6$ mm model is slightly influenced by imperfections (difference between design strength with different imperfections is up to 7%). In case when global imperfections are dominant the model is sensitive to imperfections (the difference in design resistance is up to 38%). To choose the most appropriate imperfections it is required to validate FEA model with test results.

Moreover, comparison of EN and FEA results show big deviation between values of design strength for Class 4 elements (up to 78%). This difference can be explained partly by the big influence of additional moment on final buckling resistance according to EN. Whereas for Class 3 elements and groups P1, P2, P3 the average deviation is up to 16%. Elements of Class 3 in Groups P4, P5, P6 show difference up to 27% when compared to imperfections recommended in literature. The difference in design resistance for angles with slender sections has been described in literature review. Therefore, this particular problem has been previously discovered in presented scholar articles.

Pinned boundary conditions

As it has already been discussed the model with pinned boundary conditions has also been run. This would help to see the deviations in test results due to boundary conditions. The results for pinned model can be seen in Attachment 16 “Combined table of buckling resistance – pinned BC”.

The sensitivity analysis shows that for pinned boundary conditions the influence of imperfections slightly differs from fixed. In case of dominant local mode and thickness $t=4$ mm, the sensitivity is small (up to 8%). In case when global mode is dominant the model is sensitive to imperfections (in some cases up to 32%).

The deviations between Finite Element Analysis and results are quite similar to fixed conditions. In case of Class 4 elements the difference is up to 71% for $t=4$ mm and up to 34 % for $t=6$ mm. In case of Class 3 elements the deviation is smaller and it is up to 21 % for the recommended values of imperfections.

Test results

Table 9.3.1 provides comparison of test results with sensitivity analysis for fixed boundary conditions. It has been seen that results for fixed supports are closer than for pinned. Therefore, it can be concluded that test rig provides fixed boundary conditions in case of tested specimens. From this table it can be seen that imperfection $b/200$ gives closer result to experimental value in case of cross-sections P1-6, P2-4, P2-6, P3-6. Therefore, this imperfection is recommended for parametric study of mentioned specimens.

In case of P4-6 the cross-section fails in flexural mode that is why imperfections are presented in following format: $b/200+L/1000$. The first imperfection is used for local mode and second is used for global mode. It can be seen that the values obtained from test differ up to 13% and that is why it is complicated to justify use of appropriate set of imperfections. Further tests are required for similar specimens.

Profile number	Test		Abaqus shell model COG									
	P _{test} [kN]	Mode	Mesacasa (2013)			EN, ECCS			Silvestre (2013)			Mode
			Imperfection	P _{FEA} [kN]	P _{test} /P _{FEA}	Imperfection	P _{FEA} [kN]	P _{test} /P _{FEA}	Imperfection	P _{FEA} [kN]	P _{test} /P _{FEA}	
P1-5-6mm	443	L	L/1000	419	1.06	b/200	428	1.03	10% t	419	1.06	L
P1-6-6mm	446	L	L/1000	419	1.06	b/200	428	1.04	10% t	419	1.06	L
P1-7-6mm	445	L	L/1000	419	1.06	b/200	428	1.04	10% t	419	1.06	L
P2-7-4mm	207	L	L/1000	193	1.07	b/200	195	1.06	10% t	193	1.07	L
P2-5-6mm	454	L	L/1000	431	1.05	b/200	435	1.04	10% t	431	1.05	L
P2-6-6mm	469	L	L/1000	431	1.09	b/200	435	1.08	10% t	431	1.09	L
P2-7-6mm	456	L	L/1000	431	1.06	b/200	435	1.05	10% t	431	1.06	L
P3-5-6mm	454	L	L/1000	446	1.02	b/200	448	1.01	10% t	446	1.02	L
P3-6-6mm	444	L	L/1000	446	0.99	b/200	448	0.99	10% t	446	0.99	L
P3-7-6mm	450	L	L/1000	446	1.01	b/200	448	1.00	10% t	446	1.01	L
P4-5-6mm	369	F	L/1000 +L/1000	366	1.01	b/200+ L/1000	369	1.00	10%t+ L/750	354	1.04	F
P4-6-6mm	389	F	L/1000 +L/1000	366	1.06	b/200+ L/1000	369	1.05	10%t+ L/750	354	1.10	F
P4-7-6mm	343	F	L/1000 +L/1000	366	0.94	b/200+ L/1000	369	0.93	10%t+ L/750	354	0.97	F

Table 9.3.1: Test results and FEA sensitivity analysis.

Table 9.3.2 provides comparison of test result with predicted strength according to EN. The latter was calculated considering the member under compression and additional moment due to shift of centroid.

Group	Profile number	Class	Test		EN		
			P_{test} [kN]	Buckling mode	P_{EN} [kN]	P_{test}/P_{EN}	Buckling mode
P1-6	P1-5-6mm	Class 4	443	L	218	2.03	L
	P1-6-6mm	Class 4	446	L	218	2.05	L
	P1-7-6mm	Class 4	445	L	218	2.04	L
P2-4	P2-7-4mm	Class 4	207	L	46	4.50	L
P2-6	P2-5-6mm	Class 4	454	L	208	2.18	L
	P2-6-6mm	Class 4	469	L	208	2.25	L
	P2-7-6mm	Class 4	456	L	208	2.19	L
P3-6	P3-5-6mm	Class 4	454	L	184	2.46	L
	P3-6-6mm	Class 4	444	L	184	2.41	L
	P3-7-6mm	Class 4	450	L	184	2.45	L
P4-6	P4-5-6mm	Class 4	369	F	181	2.04	F
	P4-6-6mm	Class 4	389	F	181	2.15	F
	P4-7-6mm	Class 4	343	F	181	1.89	F

Table 9.3.2: Test results and EN calculations.

It can be seen that the predictions according to EN are very conservative.

9.4 Force-displacement curve analysis for EN, FEA and tests

This chapter will describe the comparison of force-displacement curves obtained from test, FEA and EN. This curve can provide information about axial shortening, stiffness of member and maximum load which can be applied to specimen.

Before discussing obtained results it is important to mention that there are five main factors which might influence the obtained results from FEA and tests. Therefore, they might introduce errors in validation of the FEA model. They can be listed as follows:

1. initial imperfections,
2. residual stresses,
3. inaccuracy of using S4R shell element,
4. undesirable eccentricity of applied load in test,
5. flexibility of test setup.

First three points are the possible factors which introduce error directly in the Finite Element Model. Points 4 and 5 might produce errors in results obtained from test rig. The affecting of

initial imperfections and residual stresses has been covered in previous chapters. Points 3, 4 and 5 will be described further in this chapter. However, detailed description of these problems will be given in separate chapter 10.1 “Factors which influence results of tests and FEA”. The analysis of load-displacement curve will be presented on the basis of cross-section P1-6.

Initial results provided by laboratory equipment contained several errors, which needed to be removed or corrected in the post-processing. Main issue was in the beginning of load application, where is material assumed to behave in elastic way, therefore the load-displacement curve should be linear till the yielding point.

Another issue was observed in output of displacement from LVDT sensors, where LVDT 2, 3, 4 measured different values, than LVDT1. Values obtained from LVDT 2,3,4 were averaged to one final displacement, while LVDT1 was plotted according to test output. For both curves nonlinear initial part of graph was removed and linearly interpolated by tangent line, afterwards shifted to the origin of the graph.

Results for all numerical methods and laboratory test are combined in one graph (Figure 9.4.1), which is presented below this paragraph. Eurocode approach is expecting elastic behaviour with combination of additional moment, while final value of strength is almost 50% lower, than real one. As stated in previous chapters, Eurocode tends to be very conservative in case of Class 4 cross-section and short length of element.

On the other hand Finite Element Analysis predicted behaviour of element with very good precision. In case of initial imperfection equal to 10% of thickness (Silvestre approach) the curve starts to differ from LVDT1 at magnitude of force close to its ultimate value and expected strength 419 kN is bit conservative compared to the final results from the real test.

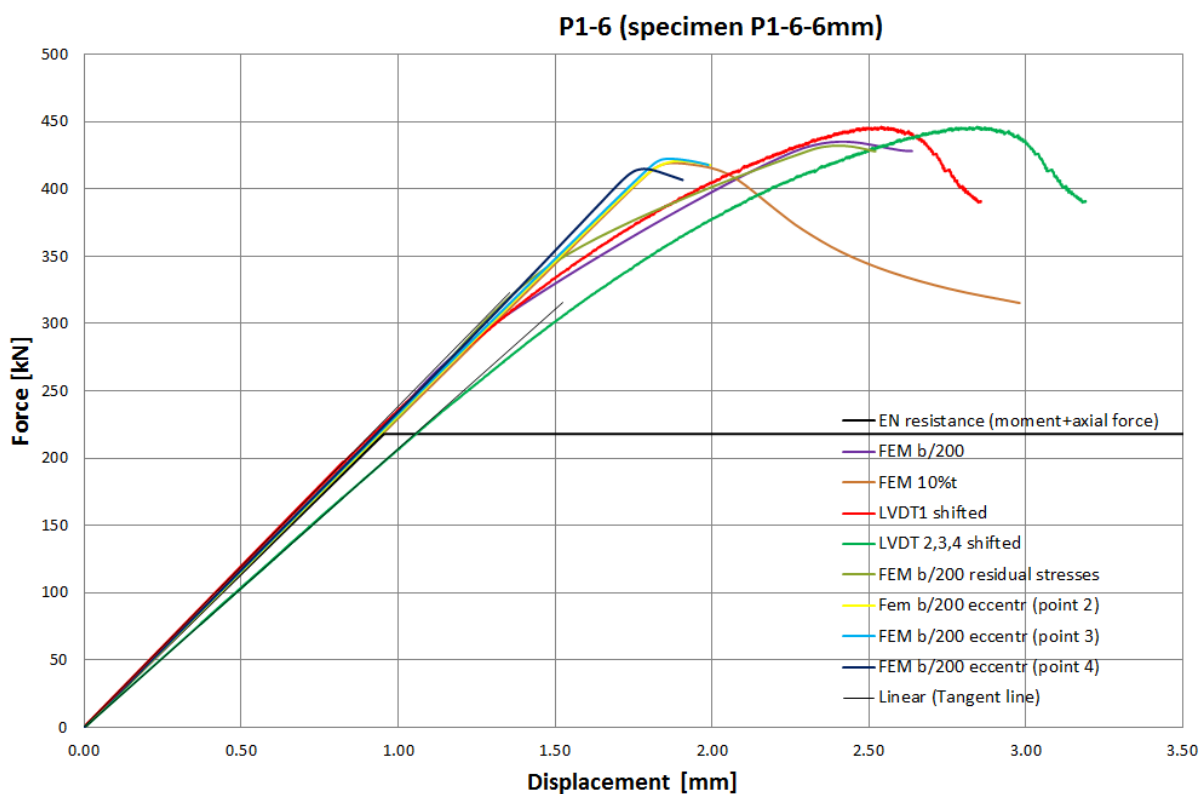


Figure 9.4.1: Load-displacement curve according to test, FEA and EN for specimen P1-6

The effect of residual stresses has been studied in the separate model. Residual stresses were introduced as follows: flat parts of L-profile were subjected to body force causing compression and rounded part was loaded by body force causing tension. The statements by (Shi, Liu, & Chung, 2009) and (Silvestre, Dinis, & Camotim, 2013) were proved and it was observed that residual stresses have negligible effect on the design strength in case of considered specimens.

The effect of introduced eccentricity has shown that the load-displacement curves from FEA do not match test results. Therefore, it can be assumed that eccentricities do not affect the results of test in case of fixed-fixed boundary conditions.

Best match is provided by initial imperfection $b/200$ (Eurocode), where both curves (FEM $b/200$ and measured LVDT1) are almost identical.

Figure 9.4.2 shows best match of test results and FEA. It depicts results from LVDT 1, Finite Element Analysis with imperfections $b/200$ and EN.

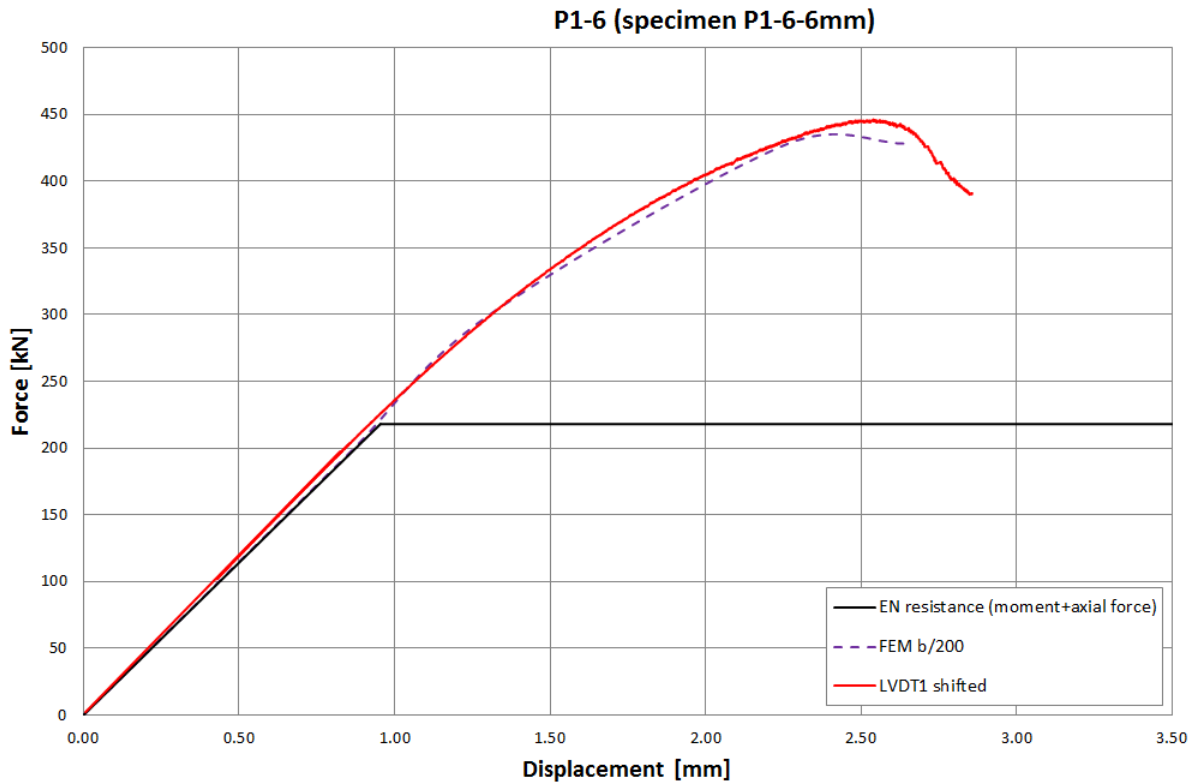


Figure 9.4.2: Best match of results according to test, FEA and EN for specimen P1-6.

Therefore, it can be stated that for given cross-section P1-6 imperfection with magnitude $b/200$ is the most appropriate. As a result, it will be used further for parametric study. Moreover, predictions according to Eurocode have shown to be over conservative.

On the basis of normalized load-displacement curve it is possible to compare the axial shortening of specimen for results of FEA with imperfections $b/200$ and test for LVDT1. The comparison will be provided only for cross-section P1-6-6mm as long as the normalized curve is done only for this specimen in the scope of this work. The shortening is taken only from LVDT1 because it provides more realistic results (axial shortening of specimen without considering the flexibility of test setup). The results are presented in Table 9.4.2.

Group	Profile number	Class	Test (LVDT1)		FEM ($b/200$)		
			e_{test} [mm]	Buckling mode	e_{FEM} [mm]	e_{test}/e_{FEM}	Buckling mode
P1-6	P1-6-6mm	Class 4	2.54	L	2.64	0.96	L

Table 9.4.2: Comparison of axial shortening results from FEA and test

From Table 9.4.2 it can be seen that the axial shortening is very close for FEA and test result. Therefore, it proves again that the results from FEA (imperfection $b/200$) and test (LVDT1) are in good agreement.

9.5 Buckling curves - parametric study

Important aim of this thesis was to compare buckling curves (expected member strength) provided by current Eurocode (Figure 9.5.1) with simulation in Finite Element analysis. Finite Element Analysis was performed for 5 different lengths for each thickness and group of cross-section. More precise explanation is given further. Theory behind Eurocode approach in case of different buckling curves was described in previous chapters, so for now the text will focus mainly on description of possible complications and their solutions and later on results evaluation.

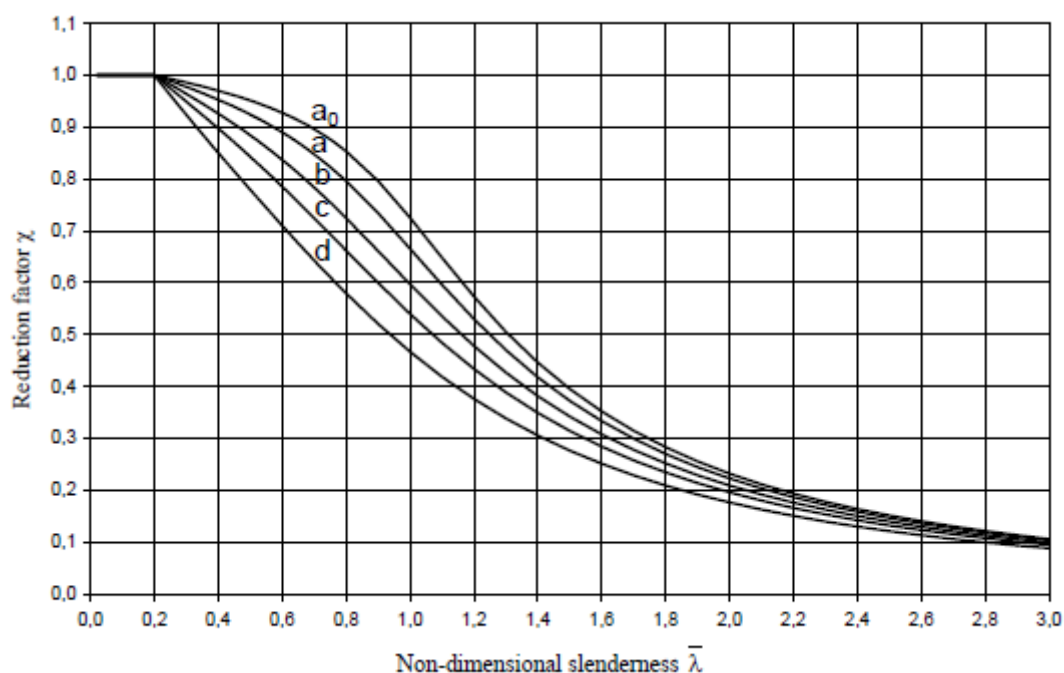


Figure 9.5.1: Buckling curves according Eurocode

Comparison between Eurocode results and FEA was prepared for all specimens from groups P1 to P6 and thicknesses 4, 6, 10, 16 and 20 mm. Boundary conditions were assumed as fixed and imperfection for FEA analysis used 10% of thickness for local buckling mode and $L/750$ for global buckling mode. Lengths of simulated specimens differ since for better comparison with graph provided in Eurocode, non-dimensional slenderness was used with fixed values (0.2, 0.75, 1.5 and 2.5). According to validated results of specimen P1-6, P2-4, P2-6 and P3-6 the imperfections $b/200$ will be used for parametric study. On the basis of tests it was decided to use this imperfection for all cross-sections which fail in local mode.

In first attempt, same procedure of evaluation was used for Class 4 and Class 3 cross-section. For horizontal axis non-dimensional slenderness ($\bar{\lambda}$) and for vertical axis buckling reduction factor (χ). Non-dimensional slenderness was plotted as follows:

$$\bar{\lambda} = \sqrt{\frac{Af_y}{N_{cr}}} \quad \text{- For Class 3 cross-sections}$$

$$\bar{\lambda} = \sqrt{\frac{A_{eff}f_y}{N_{cr}}} \quad \text{- For Class 4 cross-sections}$$

Where:

A – gross area of cross-section,

A_{eff} – effective area of cross-section,

f_y – yield strength,

N_{cr} – critical force (the lowest value of flexural, torsional and flexural-torsional critical forces).

However graphs for Class 4 were showing results of FEA under the Eurocode buckling curve and that would lead to conclusion, that EN approach isn't safe (Figure 9.5.2). Comparing absolute values of strength obtained from EN and FEA showed exactly opposite behaviour and therefore, it was concluded, that usage of same graph for Class 4 and Class 3 isn't possible.

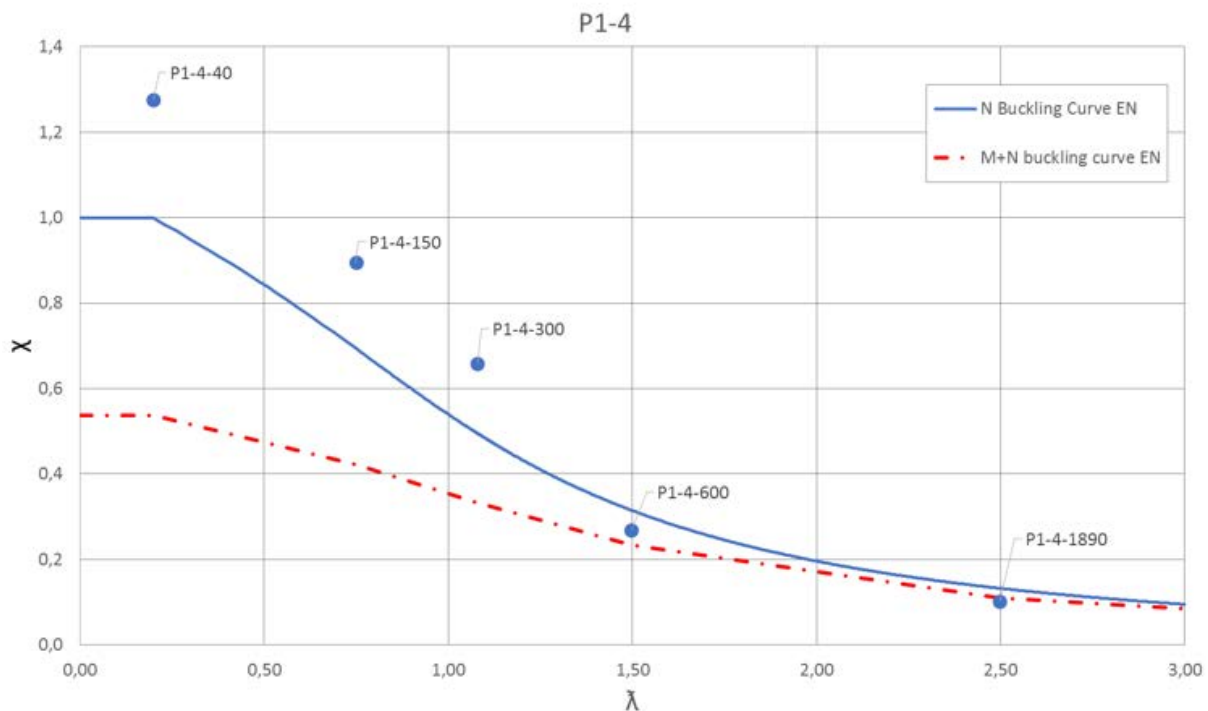


Figure 9.5.2: FEA below EN curve isn't correct interpretation of results

For Class 4 with effective cross-section properties, it is more convenient to use on vertical axis instead of buckling reduction factor (χ), ratio N/N_{pl} (Figure 9.5.3). Where N stands for buckling resistance of member according Eurocode based on effective cross-section

properties ($N = N_{bRd} = N_{cRd} \cdot \chi$, while $N_{cRd} = F_y \cdot A_{eff}$) and N_{pl} is maximum applicable plastic force for the gross cross-section properties ($N_{pl} = F_y \cdot A_g$).

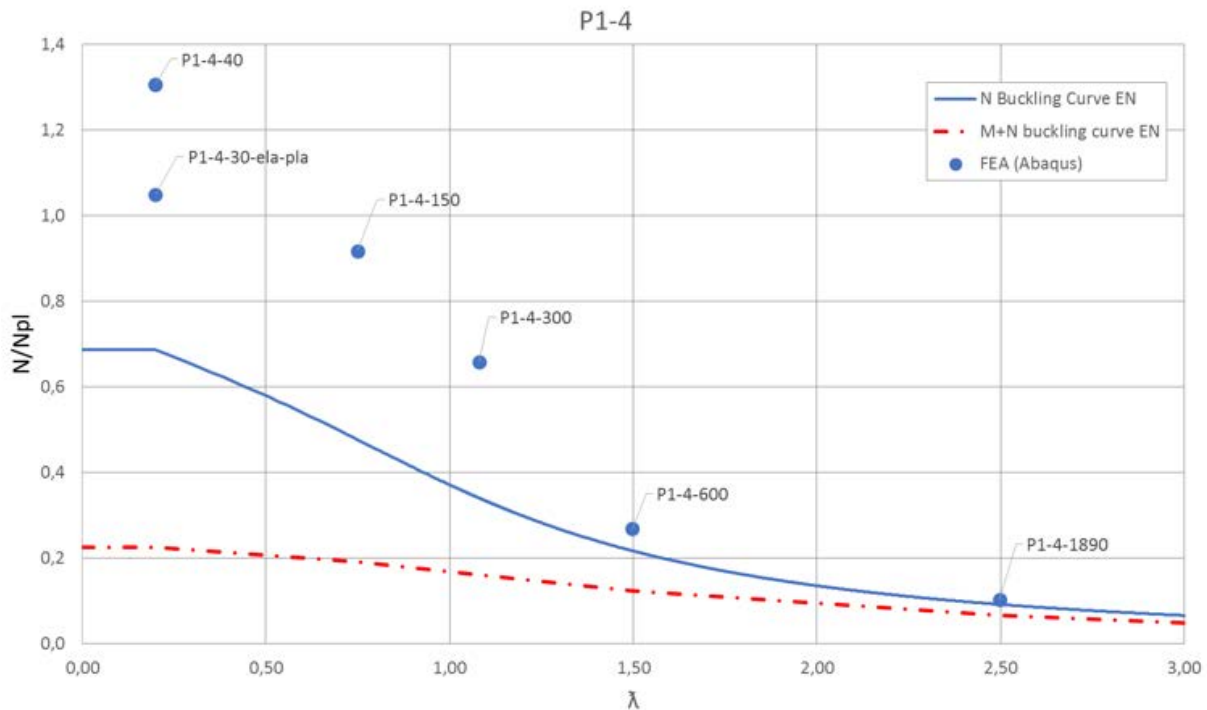


Figure 9.5.3: Correct setup for Class 4 results with N/N_{pl} ratio

Since Class 4 cross-section expects movement of centre of gravity, it was discussed to include N+M interaction curve to the graph, to observe additional moment effect on the strength of the cross-section. All tested L-profiles Class 4 should bend about its weaker axis and therefore no lateral buckling will occur, as described before, Eurocode provides simplified formula in such a case.

Results after all necessary changes and improvements will be discussed separately for Class 4 and Class 3, since their behaviour and obtained values differ significantly. For Class 4 it is visible from figures 9.5.4-9.5.6 below this paragraph, that Eurocode approach in case of uniaxial compression can lead to very conservative result in case of shorter lengths compared to FEA analysis. Moreover, when plastic strain hardening is considered, the resulting strength from FEA can be almost twice bigger compared to plotted buckling EN curve.

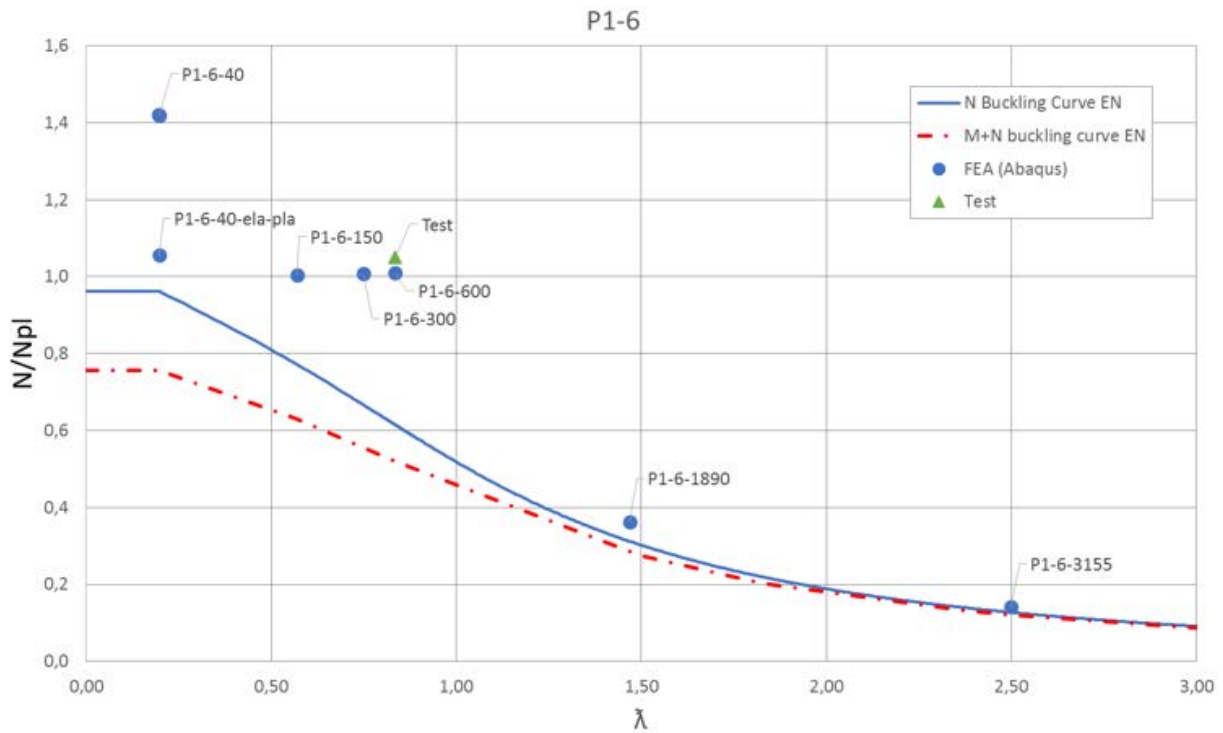


Figure 9.5.4: Correct setup for Class 4 results with N/N_{pl} ratio

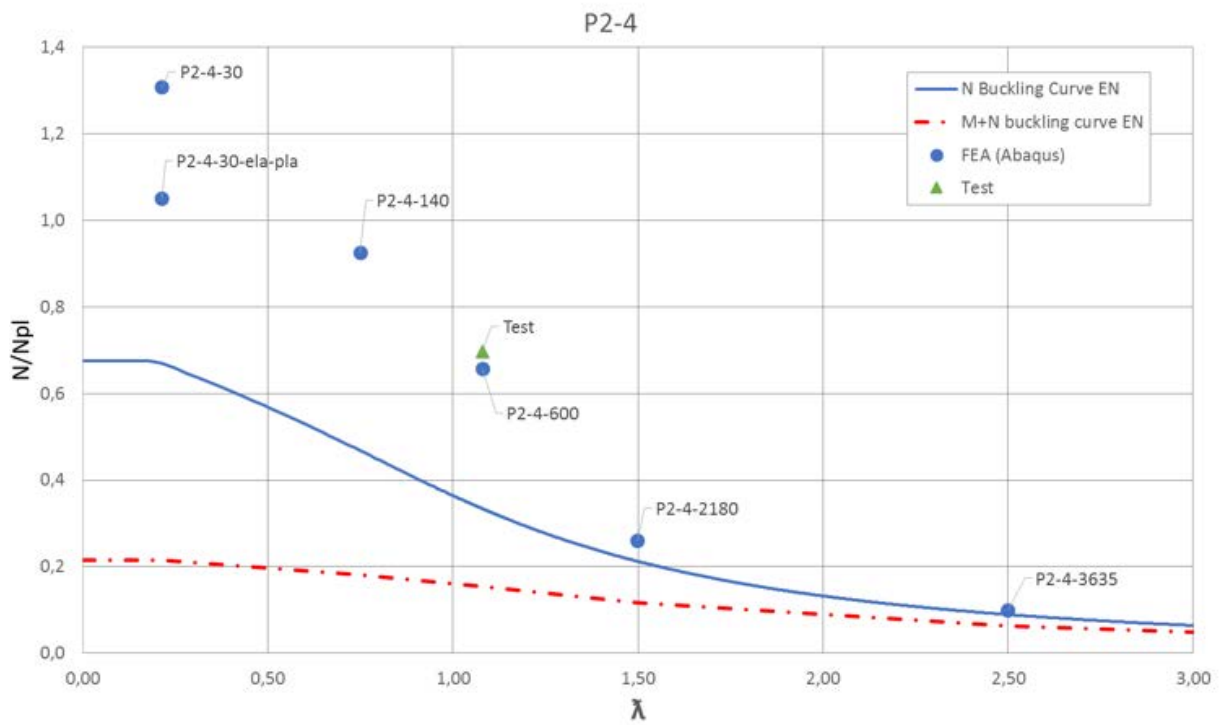


Figure 9.5.5: Correct setup for Class 4 results with N/N_{pl} ratio

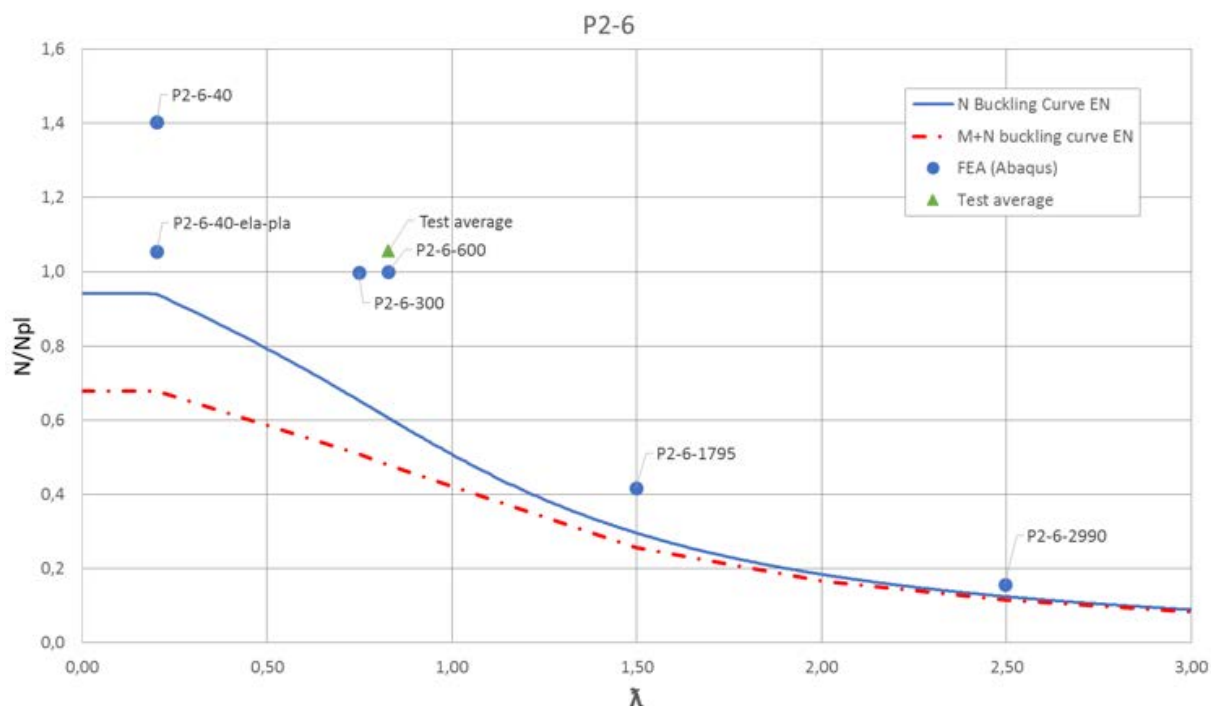


Figure 9.5.6: Correct setup for Class 4 results with N/N_{pl} ratio

However this increased strength is happening for very short specimens (up to 100 mm) and therefore measured inaccuracy is more theoretical, than practically applicable. If strain hardening is neglected and elasto-plastic behaviour of material is assumed, then obtained values are much more close to expected strength according Eurocode.

In case of evaluation of N+M combination (red curve in above graphs) the resulting strength of a member is very small compared both to EN curve and FEA in case of 4 mm thickness and short length. For thicker specimen with 6 mm the results tend to be more close to EN curve, but still very far from FEA analysis.

Overall conclusion for Class 4 is following, design procedure provided by Eurocode provides conservative results.

For Class 3 results of Eurocode and FEA are closer, than in case of Class 4 cross-section. Generally it can be observed, that in case of gross cross-section properties, results from Eurocode formulas tend to be within 10-20% from results obtained in ABAQUS. More can be seen on Figures 9.5.7-9.5.9 below this paragraph.

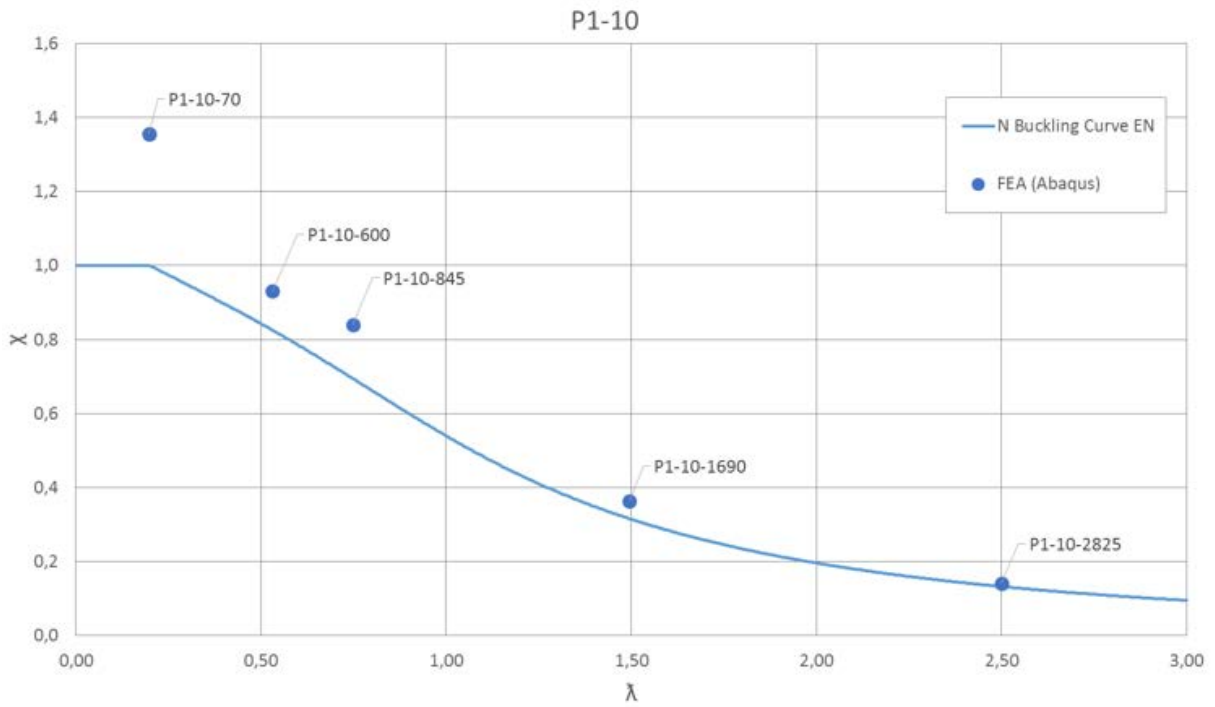


Figure 9.5.7: Buckling curve in case of Class 3 with FEA results

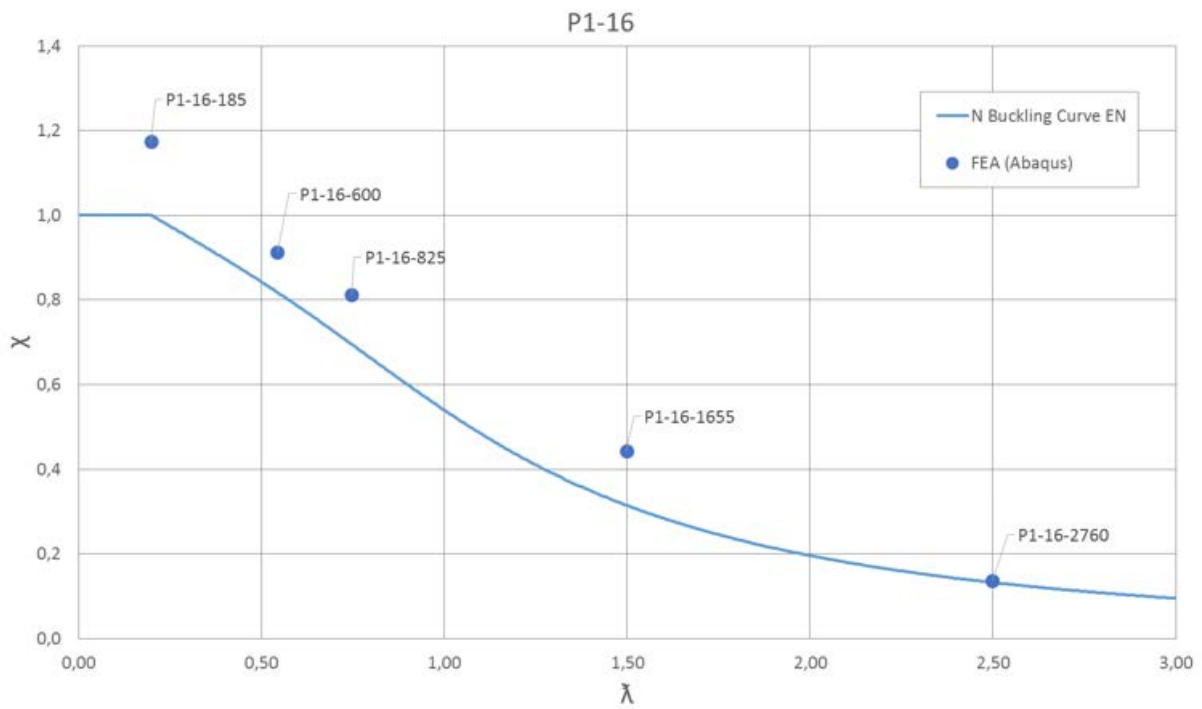


Figure 9.5.8: Buckling curve in case of Class 3 with FEA results

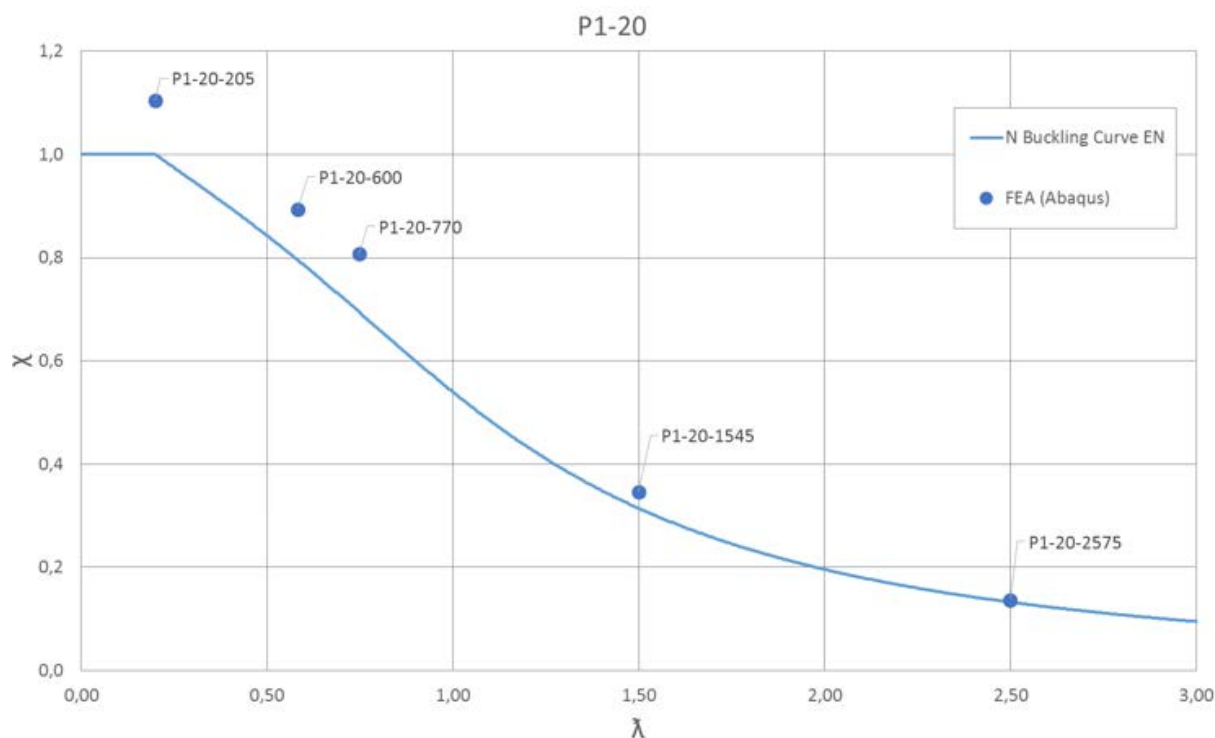


Figure 9.5.9: Buckling curve in case of Class 3 with FEA results

Conclusion for Class 3 cross-section is therefore much simpler, than in case of Class 4. Thanks to fully active cross-section, there are neither effective parameters, nor shift of centroid with additional moment. At longer lengths (above 2.0 m) evaluated L-profiles tend to have almost identical strength both for FEA and EN approach. However for shorter lengths (below 2.0 m) Eurocode is conservative and may lead to uneconomical design.

Buckling curves for all evaluated cross-sections can be found in **Attachment 18 –Buckling curves**.

10 DISCUSSIONS AND SUGGESTIONS

10.1 Factors which influence results of tests and FEA

In the chapter 9.4 “Force-displacement curve analysis for FEA, test and EN” it has been described that there are five main factors which might influence the obtained results from FEA and tests. Therefore, they might introduce errors in validation of the FEA model. They can be listed as follows:

1. initial imperfections,
2. residual stresses,
3. inaccuracy of using S4R shell element,
4. undesirable eccentricity of applied load in test,
5. flexibility of test setup.

Points 3, 4 and 5 will be described further as long as points 1 and 2 has been covered in previous chapters.

10.1.1 The inaccuracy of using S4R shell element

For conventional shell elements analysed by ABAQUS, it is recommended to use shell element type S4R, which is three dimensional stress/displacement method having 4 nodes (quadrilateral) and 6 available degrees of freedom per node (shift and rotation around X/Y/Z axis).

S4R is considered as a robust and generally applicable computational method for thin shells in many applications (Figure 10.1.1). However letter R stands for reduced integration and this can lead to certain inaccuracy of final result, or in case of this thesis the magnitude of element resistance.

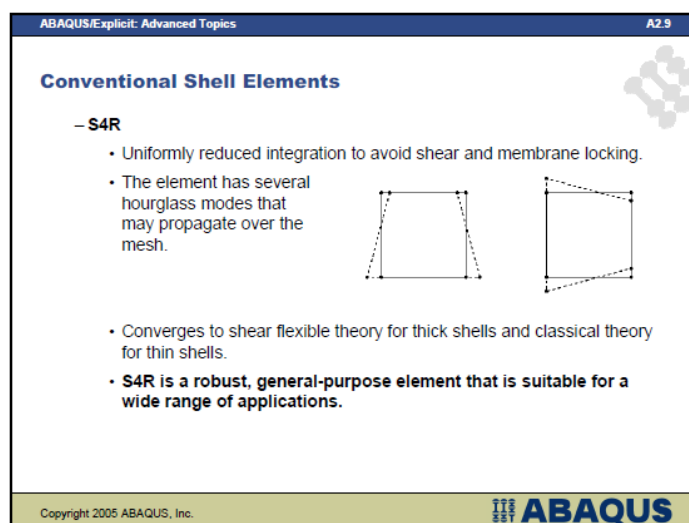


Figure 10.1.1: Element type S4R used by ABAQUS software

Producer of software isn't describing inaccuracy of such reduction and therefore research, which was done at Johns Hopkins University (Moen & Schafer, 2006) will be used to evaluate the possible inexactness of S4R compared to other methods. Research compared S4R, S9R5 and S4 in case of uniaxially loaded and fully stiffened plate, which isn't exactly comparable to this thesis, since tested L-profiles have one side unrestrained.

However results provided in study can at least serve as partial guide to estimate inaccuracy of S4R in case of this thesis. On Figure 10.1.2 below is graphically represented the difference between element types (S4R, S9R5 and S4) and theoretical buckling load (full line). In certain situations, where ratio a/b (length/width of element) is between 1 and 2, then results from S4R are very different (20-25%) from the theory and S9R5.

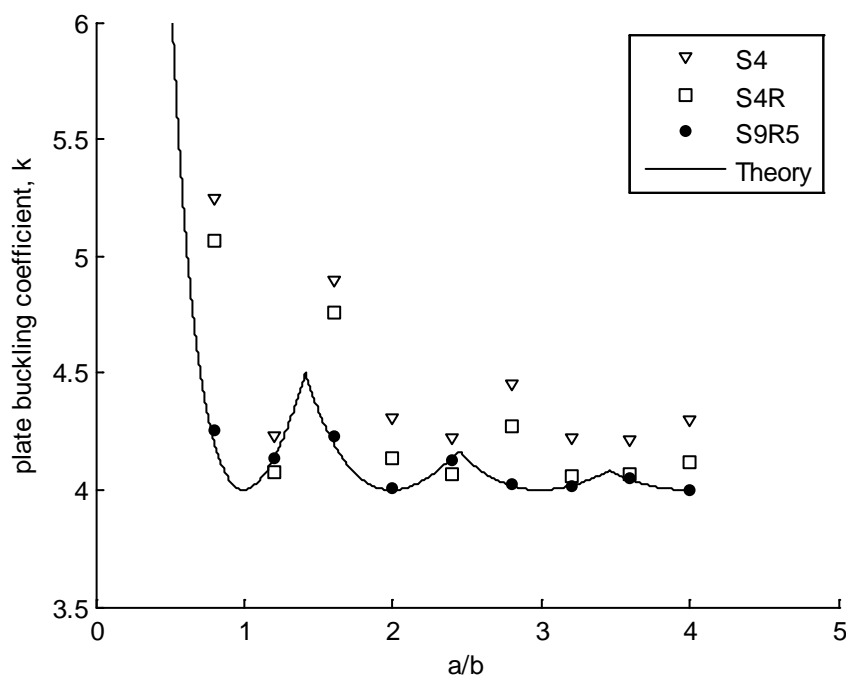


Figure 10.1.2: Comparison of S4/S4R/S9R5 accuracy

In case of bigger value of ratio, which is also applicable on tested L-profiles, all calculation methods seems to converge and their difference from theory is very small, sometimes negligible. Therefore it can be assumed, that in case of this thesis, usage of S4R can lead to certain difference from theoretical value, but its impact on final buckling resistance won't be significant.

10.1.2 Eccentricity of applied load

As discussed before, structures are mostly loaded out from its centre of gravity and additional load is produced. In laboratory the conditions are almost perfect and compressive force can be generally assumed with equal distribution along the whole cross-section. Unfortunately in some situations it can be observed, that the element wasn't grinded properly at its contact surface with the machine isn't the same along the whole cross-section and therefore during loading, some unequal distribution of applied load can occur.

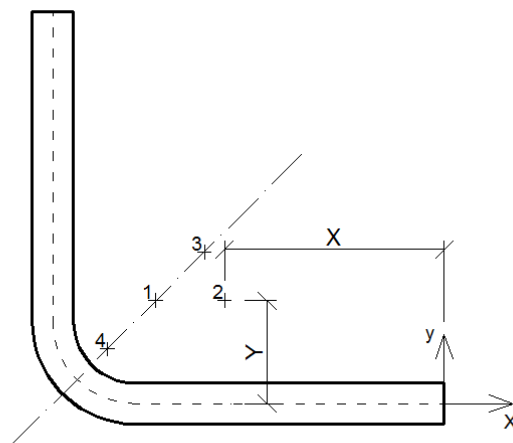


Figure 10.1.3: Possible shift of load

The effect of eccentricity of applied load will be studied for fixed and pinned boundary conditions using Finite Element Analysis.

For purpose of this thesis, possible eccentricity was evaluated for element P1-6, which is equal angle with 90° internal angle and 6 mm thickness. Together 4 possible applications of load were assumed (Figure 10.1.3), including original position of force in the centre of gravity as a reference point. The boundary conditions were assumed to be fixed as in the test.

Point 1 was located at centre of gravity. Points 2, 3 and 4 were located on the distance 10 mm from centre of gravity.

All calculations were simulated in ABAQUS using non-linear analysis with material properties and material orientation included. The simulation has been done using additional slab for application of load. This enabled to introduce eccentricity in the model. Moreover, it helped to introduce fixed boundary conditions. Results are given below in table 10.1.1

Point	Movement	X coordinate	Y coordinate	FEM [kN]
1	Load at COG	-42.01	14.99	428.4
2	10 mm on X axis	-32.01	14.99	420.7
3	10 mm along strong axis	-34.94	22.06	422.4
4	(-)10 mm along strong axis	-49.08	7.92	414.8

Table 10.1.1: Resistance with different point load application for fixed boundary conditions

It can be seen that for fixed boundary conditions the eccentricity provides not significant decrease in design resistance.

The influence of eccentricity has been studied with pinned boundary conditions. The model has been used without slab and load with boundary conditions have been applied to reference points. The results of the investigation are shown in table 10.1.2.

Point	Movement	X coordinate	Y coordinate	FEM [kN]
1	Load at COG	-42.01	14.99	345.6
2	10 mm on X axis	-32.01	14.99	163.6
3	10 mm along strong axis	-34.94	22.06	150.5
4	(-)10 mm along strong axis	-49.08	7.92	153

Table 10.1.2: Resistance with different point load application for pinned boundary conditions

In case of pinned boundary conditions it can be seen that the resistance drops significantly due to eccentricity of applied load (up to 56% for 10 mm eccentricity).

Therefore, it can be concluded that cross-sections with pinned supports are very sensitive to eccentricity of applied load. Whereas specimens with fixed boundary conditions are not sensitive to this factor.

10.1.3 Flexibility of the setup

Another reason for difference between the FEM and real laboratory results can be the flexibility of the setup. Furthermore these effects can be divided in two groups. First group is the actual stiffness of the compression machine. In case of tested L-profiles expected values of resistance are reaching almost 450 kN while the maximum allowed load for the testing device is 600 kN (Figure 10.1.4), therefore robustness isn't several times greater, than maximum resistance.



Figure 10.1.4: Maximum possible load during test

Usage of more robust machine for compression tests will provide significant assurance that obtained values of element resistance aren't affected by stiffness of machine, on the other hand it is generally expected, that all testing device in laboratory are designed to effect the results in negligible scale.

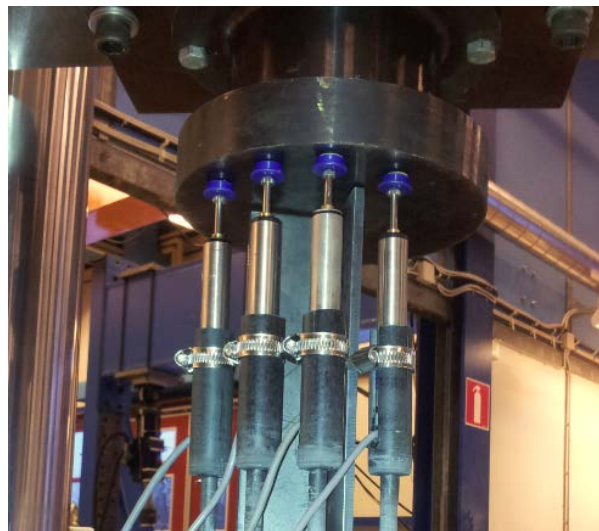


Figure 10.1.5: Initially LVDT were not attached to L-profile

Second group, which can cause some disturbance is position of LVDT sensors, which are measuring the actual displacement. During the test 4 sensors were used, while majority of them measured displacement between two compressing slabs of the laboratory device and that is not fully representing the behaviour of the element itself (Figure 10.1.5).



Figure 10.1.6: Final solution, LVDT 1 welded to the specimen

It was decided to weld small plates directly on the L-profile (perpendicularly outside to the folded corner) and measure the displacement there as well (Figure 10.1.6). Obtained results compared with FEM analysis are showing, that attaching LVDT to the element is the best possible solution for achieving optimal results.

10.2 Suitability of classification according EN 1993-1-1

According to the research question it is necessary to study if classification of cross-section classes according to EN 1993-1-1 is suitable for considered specimens. In Eurocode it is stated that the aim of cross-section classification is to find in which extent the rotation capacity and resistance are lowered due to occurrence of local buckling. In case of compressed members only the problem of resistance limitations will be solved. However, rotation capacity problem might need further investigation in case of accounting additional moment due to shift of centroid.

Firstly, it is necessary to mention that the problem of classification justification does not have straightforward explanation. Mainly the answer for this research question can be obtained through observation of experimental results. However, extensive theoretical and numerical investigation using Finite Element Analysis has been also performed in order to find solution for this considered problem. It is also necessary to mention that all numerical calculations have been done using nominal material properties without accounting for changes in corner parts. Therefore, experimental results might differ from predicted results using FEA.

According to EN 1993-1-1 class of cross-section is dependent on the dimensions of cross-section (width-to-thickness ratio), stress distribution and yield strength. It has been shown in previous chapters that in case of $t=4$ mm and 6 mm cross-sections should be designed as class 4 elements. Therefore local buckling phenomena is expected to occur first during loading and as a result the gross cross-section has to be reduced to effective cross-section.

According to EN 1993-1-1 cross-section classification is independent from length of member. However, during analysis it has been noticed that depending on the angle of folding and the length global buckling may occur before local buckling in case of class 4 elements. As a result in these cases consideration of reduction in cross-section dimensions through effective area approach might lead to conservative results in terms of design resistance.

The plates are known to be characterized by a stable post-critical behaviour. However, to achieve this, elastic critical buckling load has to be lower than yield stress. This fact is described in Figure 10.2.1 for slender plates in compression.

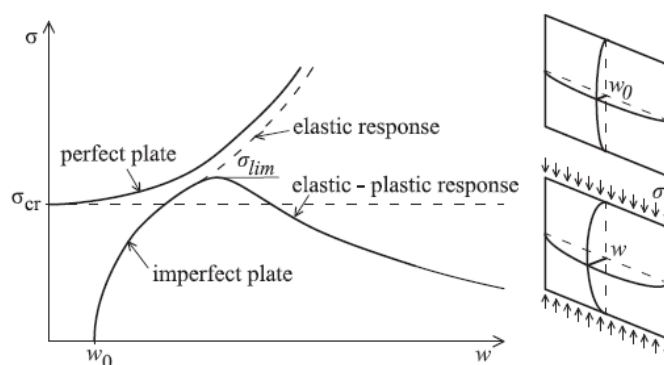


Figure 10.2.1. Post-critical response of slender plates in compression (Beg, Kuhlmann, Davaine, & Braun, 2012)

In case of post-critical response after reaching elastic critical stress the resistance is not exhausted but increases until plastic collapse. In this region redistribution of stresses takes place and it is accounted for by using of “effective width method”.

2 approaches will be used to investigate the classification of cross-sections:

1. At minimum allowable length to neglect influence of member length.
2. With length variation to provide recommendations for use of reduced cross-section.

10.2.1 1st approach

In order to investigate the occurrence of local buckling it has been decided to base initial study on cross-sections with the minimum allowable length. This approach would allow to neglect the effect of length on justification of cross-section class. This length should enable appearance of the local buckling waves. In case of considered cross-sections with fixed supports ($L_e=0.5L$) and width of flat part $b=60$ mm (neglecting rounded corners) this length should be equal at least

$$L_e = 2b = 120 \text{ mm}$$

$$L = 2L_e = 240 \text{ mm}$$

Where:

L – actual column length,

L_e – effective column length.

Therefore, local buckling can be investigated minimum on specimens of length 240 mm. As long as the main justification should be based on the experimental results it has been decided to investigate specimens of 300 mm what is equal to half-length of tested specimens. Therefore, the tests will be performed on length 300 mm and 600 mm.

According to description of local buckling occurrence following equations should be satisfied for classification in case of imperfect elastic-plastic plate:

$$\sigma_{cr} < \sigma_u \leq f_y \quad \text{– Class 4}$$

$$\sigma_{cr} > \sigma_u \text{ and } \sigma_u > f_y \text{ or } \sigma_u < f_y \text{ (for global buckling)} \quad \text{– Class 3, 2, 1}$$

Where:

σ_{cr} – elastic critical stress for local buckling,

σ_u – ultimate strength stress,

f_y – yield stress.

As long as rotation capacity is not considered for investigation, distinguishing between classes 3, 2 and 1 will not be performed.

Elastic critical stress for local buckling, ultimate strength stress and yield stress will be compared for cross-sections which were classified as Class 4 according to EN 1993-1-1. Elastic critical stress for local buckling has been evaluated according to equation presented in consequent chapter. Ultimate strength has been evaluated using FEA with imperfections equal to $b/200$. This comparison is shown in **Table 10.2.1**.

Profile	L [mm]	σ_{cr} [MPa]		σ_u [MPa]		f_y [MPa]	Failure mode
P1-4	600	422	<	427	<	650	Local
	300	422	<	489	<	650	Local
P1-6	600	1027	>	656	>	650	Yielding
	300	1027	>	655	>	650	Yielding
P2-4	600	405	<	425	<	650	Local
	300	405	<	487	<	650	Local
P2-6	600	967	>	650	≈	650	Yielding
	300	967	>	649	≈	650	Yielding
P3-4	600	385	<	424	<	650	Local
	300	385	<	485	<	650	Local
P3-6	600	894	>	649	≈	650	Yielding
	300	894	>	649	≈	650	Yielding
P4-4	600	374	<	422	<	650	Local
	300	374	<	484	<	650	Local
P4-6	600	854	>	523	<	650	Flexural
	300	854	>	649	≈	650	Yielding
P5-4	600	367	>	197	<	650	Flexural
	300	367	<	481	<	650	Local
P5-6	600	832	>	231	<	650	Flexural
	300	832	>	521	<	650	Flexural
P6-4	600	365	>	74	<	650	Flexural
	300	365	>	241	<	650	Flexural
P6-6	600	824	>	112	<	650	Flexural
	300	824	>	351	<	650	Flexural

Table 10.2.1: Comparison of elastic critical stress for local buckling, ultimate strength stress and yield stress for Class 4 cross-sections.

It can be seen that cross-sections P1-4, P2-4, P3-4 and P4-4 are suitable for Class 4 classification: elastic critical stress is less than ultimate strength stress, local buckling occurs before the yield stress is reached. However, for P1-6, P2-6 and P3-6 elastic critical load is higher than ultimate strength stress, ultimate strength is more or equal to yield stress, yield

stress is reached before local buckling occurs in cross-section. In case of cross-section P4-6 elastic critical load is higher than ultimate strength stress but at length 600 mm global flexural buckling dominates the local buckling. However, at length 300 mm cross-section P4-6 exhibits local buckling which occurs after yield stress is reached. In case of cross-sections P5-6, P6-4, P6-6 local buckling does not occur and global flexural buckling dominates.

The stress distribution has also been studied in specimens in longitudinal direction. For comparison the same magnitude of displacements visualization has been used. The stress in longitudinal direction has been extracted for the middle line of the specimen. The stresses have been limited by yield stress 650 MPa, values which exceed this value are represented in black colour. The visualization of stresses will be presented for specimens typical for their group: P1-4 (local buckling), P1-6 (yielding) and P5-6 (flexural buckling).

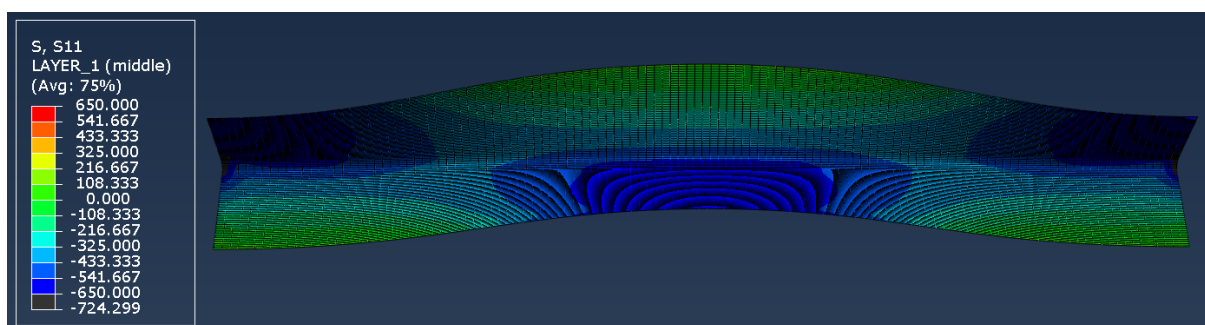


Figure 10.2.2: P1-4, L=600 mm, local buckling

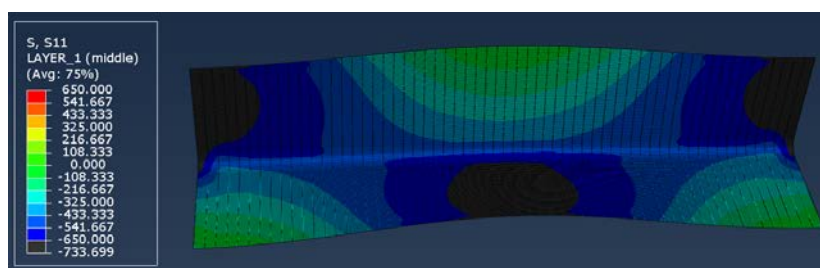


Figure 10.2.3: P1-4, L=300 mm, local buckling

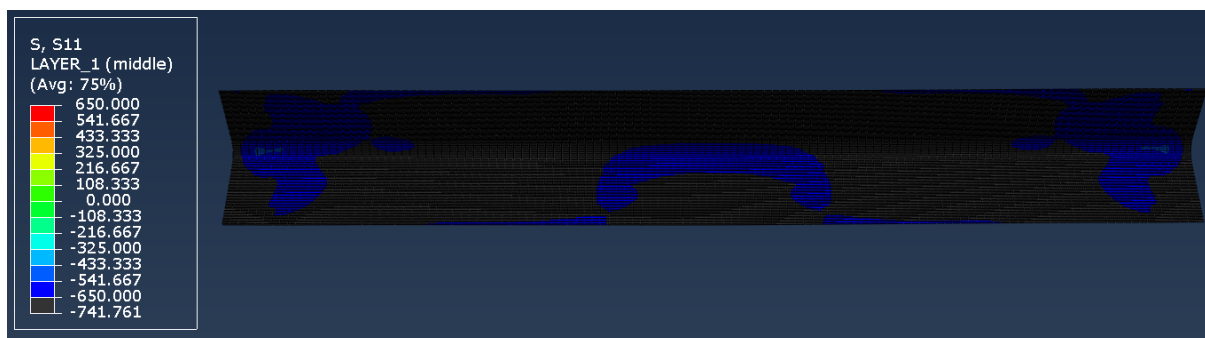


Figure 10.2.4: P1-6, L=600 mm, yielding

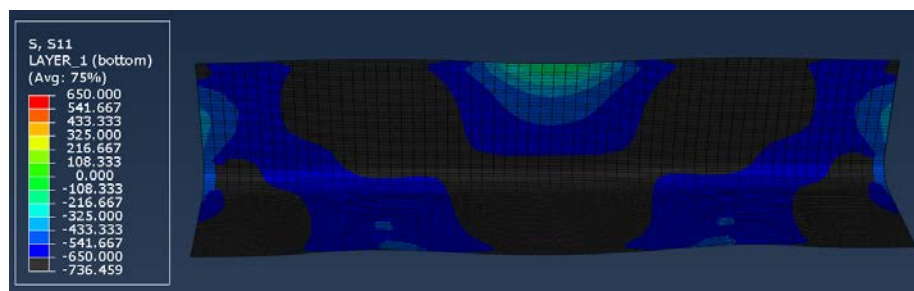


Figure 10.2.5: P1-6, L=300 mm, yielding

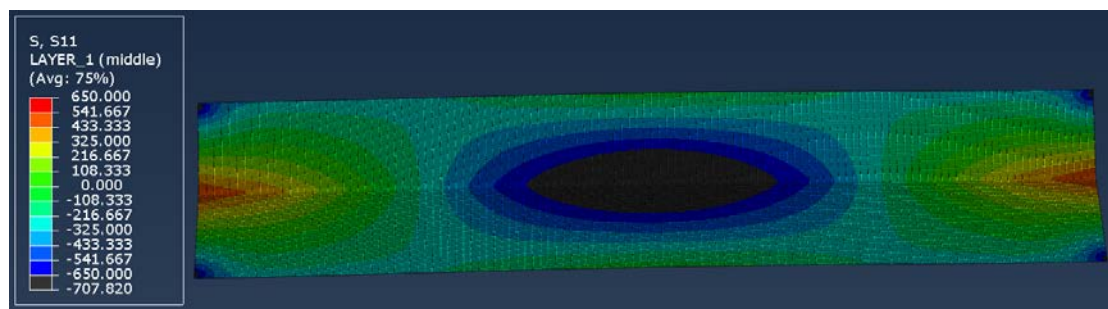


Figure 10.2.6: P5-6, L=600 mm, flexural buckling

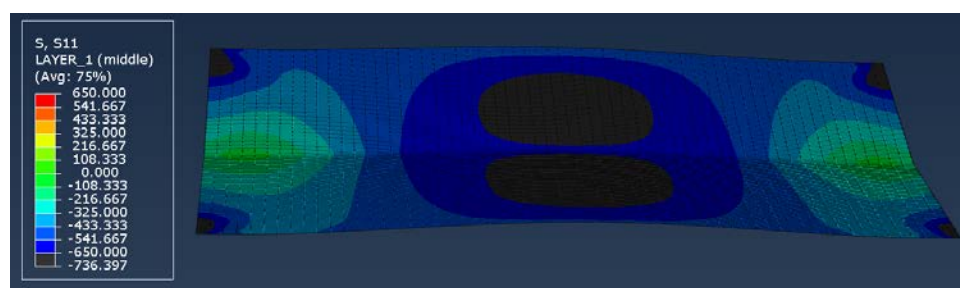


Figure 10.2.7: P5-6, L=300 mm, flexural buckling

In case of P1-4 and P5-6 it can be seen that local yielding occurs but the overall failure mode is local for P1-4 and flexural for P5-6. In case of P1-6 overall yielding of cross-section can be observed without local deformations prior to this state.

It has been stated that for classification the most reliable justification can be done based on the experiments. According to performed tests following observations have been made. In case of cross-section P1-6, P2-6, P3-6 deformation of specimen happens after reaching of ultimate design strength without occurrence of local deformations. Moreover, it has been shown in Figure 10.2.8 for cross-section P1-6 that theoretical elastic critical load is not reached. From Table 10.2.2 it can be seen that failure stress exceeds yield stress what can be explained by possible strain-hardening.

Group	Profile number	Class	Test			Nominal yield stress f_y [MPa]	σ_{test}/f_y
			P_{test} [kN]	Area [mm ²]	Ultimate stress σ_{test} [MPa]		
P1-6	P1-5-6mm	Class 4	443	652.52	679	650	1.04
	P1-6-6mm	Class 4	446	652.52	684	650	1.05
	P1-7-6mm	Class 4	445	652.52	682	650	1.05
P2-4	P2-7-4mm	Class 4	207	457.33	453	650	0.70
P2-6	P2-5-6mm	Class 4	454	668.98	678	650	1.04
	P2-6-6mm	Class 4	469	668.98	701	650	1.08
	P2-7-6mm	Class 4	456	668.98	681	650	1.05
P3-6	P3-5-6mm	Class 4	454	691.09	656	650	1.01
	P3-6-6mm	Class 4	444	691.09	642	650	0.99
	P3-7-6mm	Class 4	450	691.09	651	650	1.00
P4-6	P4-5-6mm	Class 4	369	704.5	523	650	0.81
	P4-6-6mm	Class 4	389	704.5	552	650	0.85
	P4-7-6mm	Class 4	343	704.5	487	650	0.75

Table 10.2.2: Test results vs yield stress.

Following considerations might indicate that classification of cross-section P1-6, P2-6, P3-6 as Class 4 might be conservative: 1. local buckling of individual components of member does not happen before yield stress, 2. deformations and failure of cross-section happens at the point when actual stress exceeds yield stress. However, it should be stressed that nominal value of yield stress has been used. From results of tensile test it might appear that actual yield stress is higher than nominal. As a result it will be possible to conclude that cross-section fails before reaching yield stress and therefore fails by local buckling.

However, for cross-section P2-4 it can be seen that the ultimate stress is less than yield stress and local buckling happens before yielding of cross-section. Therefore, it can be stated that classification as Class 4 according to EN 1993-1-1 is suitable for this cross-section.

In case of cross-section P4-6 it is observed that the specimen fails in flexural mode before occurrence of local buckling what is not typical for Class 4 cross-sections. However, as long as classification is not dependent on the length it is necessary to test specimen with length 300 mm.

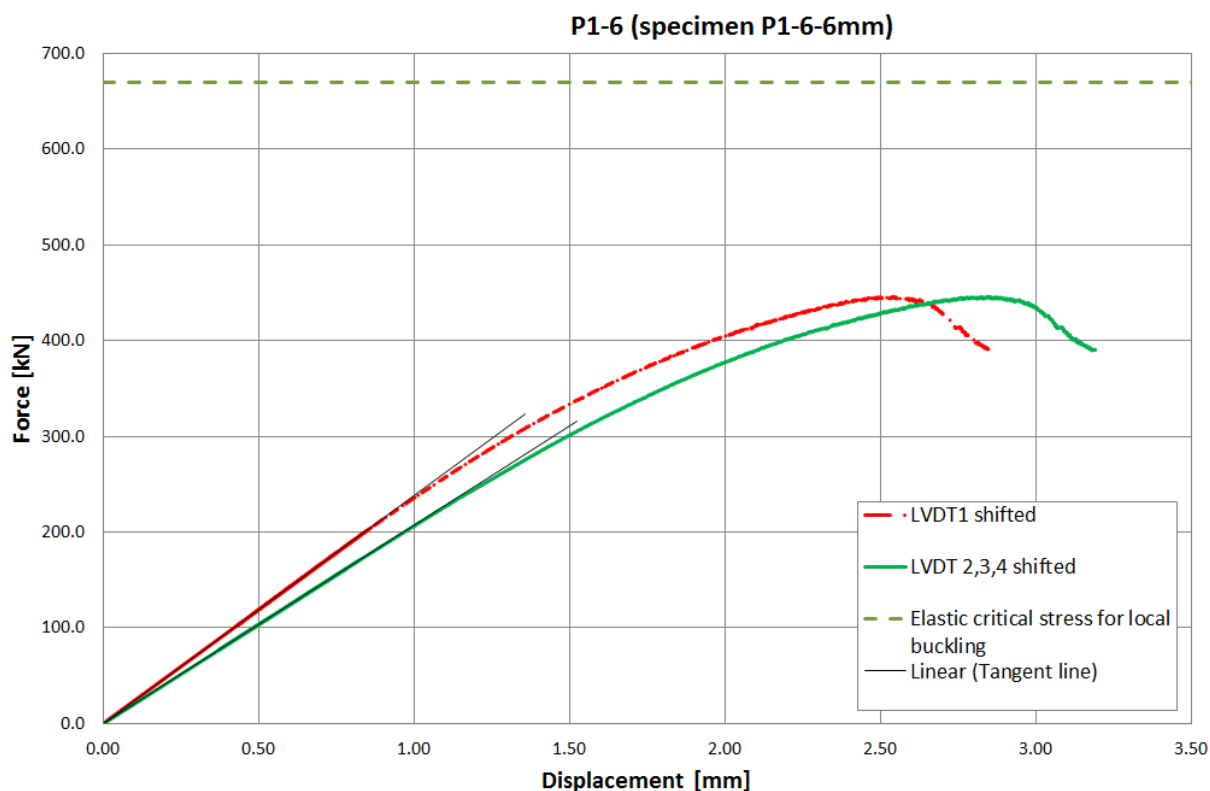


Figure 10.2.8: Normalized force-displacement curves from test and elastic critical stress for local buckling.

10.2.2 2nd approach

It has already been stated that cross-section classification does not depend on the length of the member. However, considered cross-sections tend to change local buckling to global buckling mode at specific lengths or sometimes not to exhibit local buckling mode at all. Accounting for these facts may lead to making possible design of class 4 cross-sections without reduction of cross-section area. As a result less conservative predictions of design strength might be obtained. Therefore, the parametric study was held using stability theory and plotting of different buckling curves for flexural, torsional, torsional-flexural and local buckling modes. Secondly, parametric study was performed using Finite Element Modelling.

Stability theory

For stability theory approach the elastic buckling curves have been plotted in axis stress over slenderness ($\lambda=L_e/i$, where L_e - effective length, i – radius of gyration about weak axis). Elastic buckling curves have been plotted for specimens with thickness 4 mm, 6 mm and 10 mm. Here will be presented curves only for P1-4, P1-6 and P5-6 specimens as an example. Other ones can be found in Attachment 17 – Elastic critical load curves.

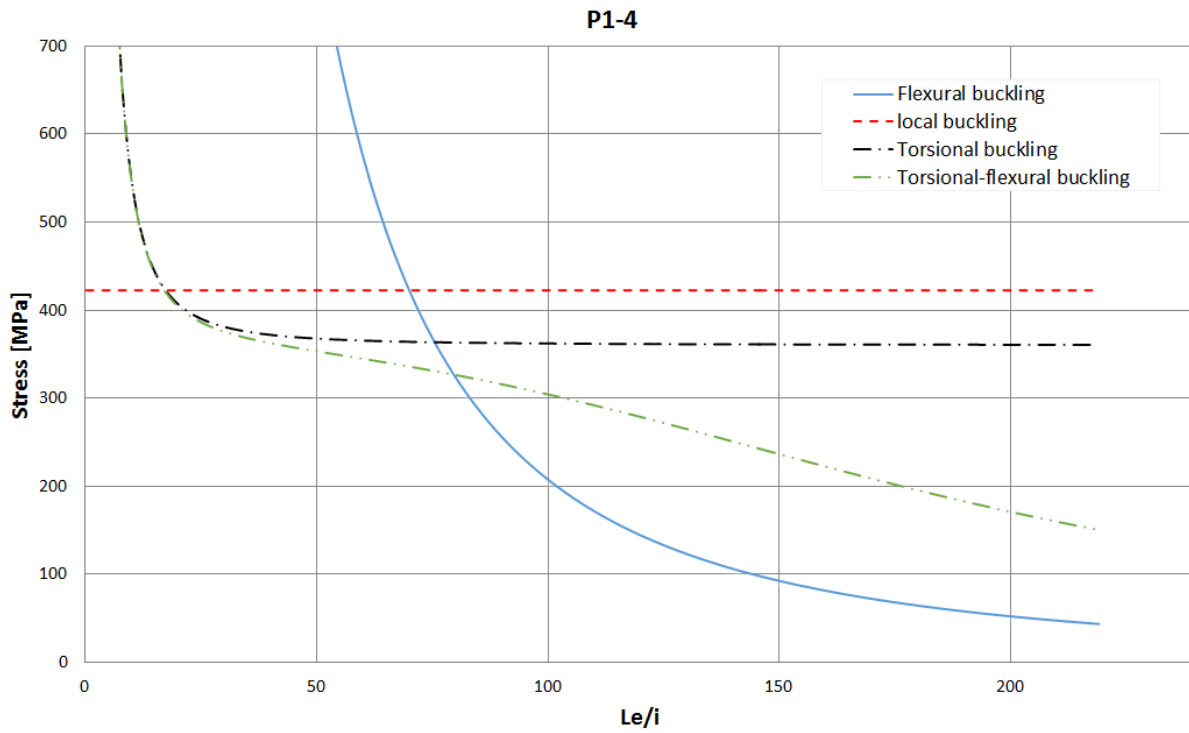


Figure 10.2.9: Elastic critical load assessment. Specimen P1-4.

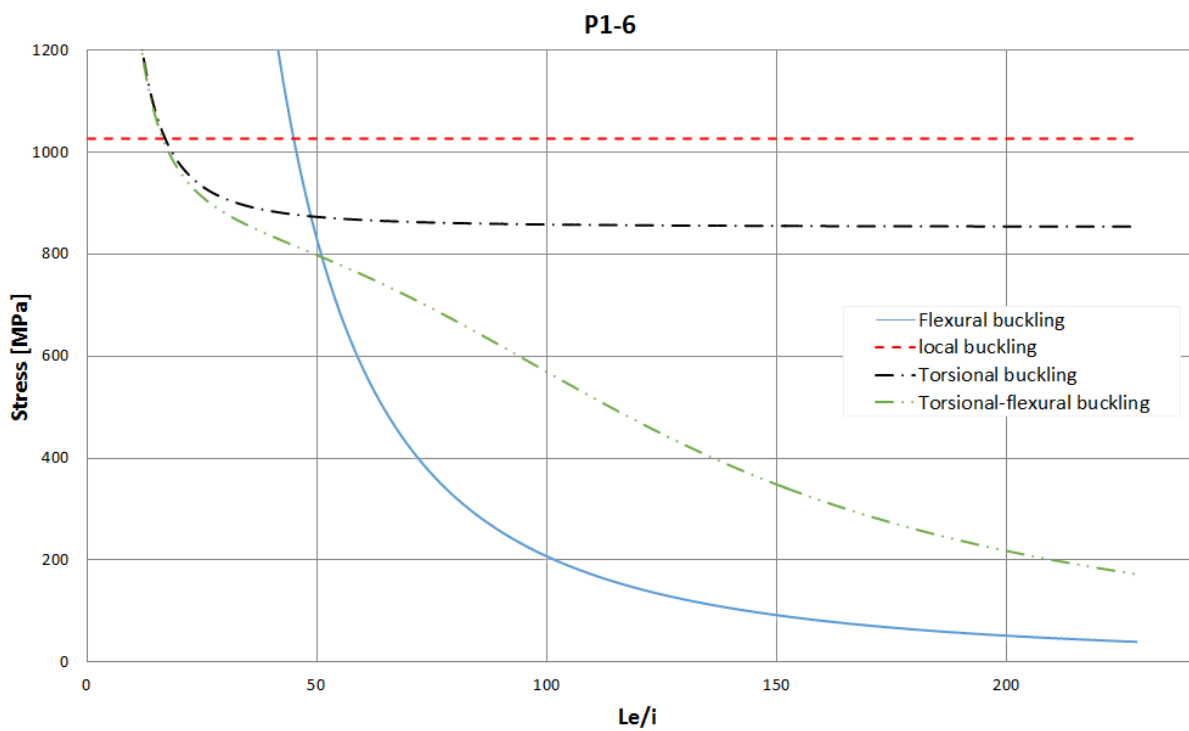


Figure 10.2.10: Elastic critical load assessment. Specimen P1-6.

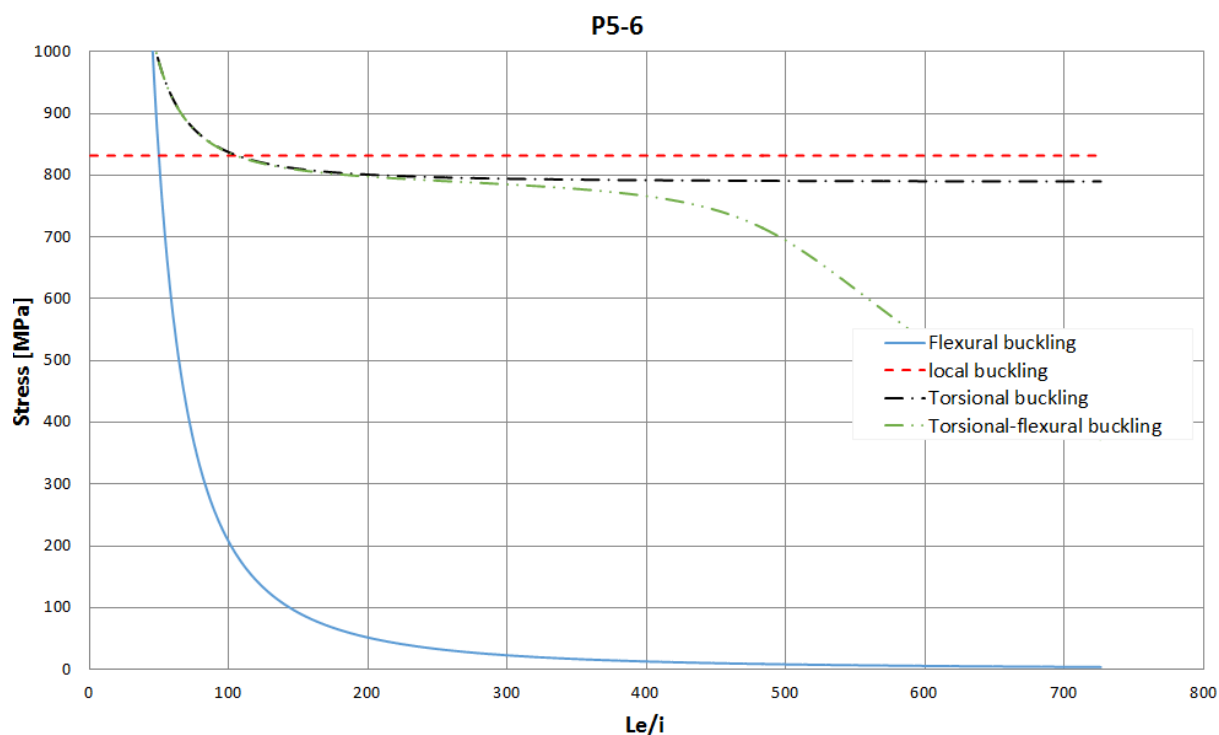


Figure 10.2.11: Elastic critical load assessment. Specimen P5-6.

From these curves it can be seen that depending on the slenderness members different types of buckling dominate. For cross-sections P1-4, P1-6 the graph shows that at low slenderness ratios local buckling changes into torsional (which is equal to local for equal-leg angles). Moreover, torsional and flexural-torsional critical loads are equal at low slenderness values but with its increase they tend to deviate. As a result flexural-torsional mode becomes dominant at certain range of slenderness. However, it is hard to distinguish between torsional and torsional-flexural mode in case of considered cross-sections. Therefore, it is complicated to state at which exact length buckling mode switches from torsional (local) to flexural-torsional (global) mode. With increase of slenderness flexural mode becomes dominant which is truly global mode in case of equal-leg angles.

In case of specimen P5-6 from Figure 10.2.11 it can be seen that torsional and torsional-flexural modes do not influence the behaviour of cross-section. Moreover, the most of slenderness range is dominated by global flexural mode. Local buckling mode can be observed only for low slenderness ratio and for high critical loads.

In case of classification cross-section as Class 4 the use of “effective width concept” is required to allow for local buckling of cross-section. However, it can be seen from presented graphs that the actual buckling mode tends to become global at certain slenderness. As a result the use of reduced cross-section area is not relevant in this case because global buckling mode dominates over local buckling mode. As a supplementary research on this topic FEM analysis will be used. Moreover, recommendations regarding limits of buckling modes will be presented on basis of Finite Element Analysis.

FEM analysis

It has been decided to perform elastic analysis of cross-sections using Finite Element Analysis to investigate the influence of length on appearance of local buckling. The models have been created for different lengths in order to distinguish changes of buckling modes with change of length. As it has been stated it is hard to distinguish torsional and flexural-torsional mode for considered cross-sections. In order to solve this problem the change between these two modes was considered to be influenced by the movement of shear centre. In previous chapters it has already been described how this procedure is performed in Abaqus. Therefore it will be possible to see where the lateral component of flexural-torsional buckling moment will become sufficiently large, so that the overall mode can be considered as global.

Following assumption have been made:

- 1) Torsional-flexural with shear centre movement till 3% -> local mode -> Class 4
- 2) Torsional-flexural with shear centre movement above 3% -> global mode -> Class 3

The results of performed studied is presented in **Table 10.2.3**.

Profile	Buckling modes				
	Torsional		Flexural-torsional		Flexural
	Torsional	Shear centre movement	Flexural-torsional	Shear centre movement	Length
P1-4	up to 900 mm	3%	900 mm - 1700 mm	5.70%	from 1700 mm
P1-6	up to 900 mm	3%	900 mm - 1100 mm	5%	from 1200 mm
P2-4	up to 1400 mm	3%	1400 mm - 1600 mm	4.30%	from 1600 mm
P2-6	up to 1000 mm	3%	-	-	from 1000 mm
P3-4	up to 1250 mm	1.7%	-	-	from 1250 mm
P3-6	up to 800 mm	1.6%	-	-	from 800 mm
P4-4	up to 850 mm	0.5%	-	-	from 850 mm
P4-6	up to 500 mm	0.5%	-	-	from 500 mm
P5-4	up to 350 mm	0.2%	-	-	from 350 mm
P5-6	-	-	-	-	all length
P6-4	-	-	-	-	all length
P6-6	-	-	-	-	all length

Table 10.2.3: Research on changes of buckling modes using FEM.

Table 10.2.3 can be used as a recommendation for use of gross cross-section area in calculation of design resistance in case considered specimens Class 4 according to EN 1993-1-1. According to assumptions made before gross area could be used for cross-sections with global buckling modes: flexural-torsional and flexural. However, it is hard to justify using of assumed 3 % of shear movement as a boundary for occurrence of global flexural-torsional

mode. Therefore, the safe approach would be to consider using gross cross-section area in case of flexural buckling mode.

10.2.3 Conclusion

Suitability of cross-section classification according to EN 1993-1-1 has been studied. It can be concluded that this problem is very versatile and straightforward solution can hardly be obtained only on the basis of theoretical research.

However, it was shown that theoretical definition of Class 4 cross-section is not always applicable for following cross-sections: groups P1-P6 with $t = 6$ mm and group P6 with $t = 4$ mm. Therefore, considering them as Class 4 might lead to conservative results in terms of design resistance. The experimental result in case of P1-6, P2-6, P3-6 cross-section proves developed theory because deformation of specimen takes place only after reaching failure stress which is more than yield stress. However, it should be mentioned that these results were derived on the basis of assumed nominal yield stress equal to 650 MPa. From results of tensile test it might appear that actual yield stress is higher than nominal. As a result it will be possible to conclude that cross-section fails before reaching yield stress and therefore fails by local buckling.

However, for cross-section P2-4 classification proves to be suitable.

In case of cross-section P4-6 at 600 mm failure occurs due to flexural buckling. Therefore, it is required to perform tests on 300 mm specimens to investigate local buckling behaviour.

Moreover, the influence of length on the buckling behaviour has been studied. Despite the fact that cross-sections classification is not dependent on length, recommendations have been proposed for neglecting of "effective width" concept. This has been proposed in case when global buckling mode dominates over local buckling mode.

10.3 Influence of angle of folding and thickness of material on resistance

10.3.1 Influence of folding angle on resistance

Internal angle of L-profile is one of many parameters, which is involved in the final magnitude of strength. Evaluated specimens, were sorted in six groups regarding their internal angle, starting from 90° and finishing with 170°, which is almost flat plate shape. It is interesting to observe, which values of angles are suitable for design and for what angles the reduction of member resistance is simply too large.

Since tests in laboratory aren't fully completed, this evaluation will focus on results obtained from hand calculation by Eurocode approach and Finite Element Analysis from ABAQUS software. It is important to note, that compared values are based on expectations and may differ from those, which will be obtained from real tests in future. However, already obtained test results are very close to predicted by FEA and that is why the statements apply for these cross-sections.

Based on hand calculation provided by Eurocode for Class 4 cross-section with fixed boundary conditions it can be observed in Attachment 10 "Combined table of buckling resistance according to EN (fixed BC)" that for internal angles 90°, 100°, 120° and 140° (Group P1-P4) the strength is almost the same, around 100 kN for 4 mm thickness and around 260 kN for 6 mm thickness. For bigger angles (160°, 170°) the reduction of member resistance is more than 50%. For Class 3 the behaviour is very similar, smaller internal angles 90°-140° are delivering consistent values of strength, but larger angle 160° and 170° are again responsible for resistance reduction, however the drop isn't so significant, as in case of Class 4.

Results from Finite Element Analysis provided in Attachment 10 "Combined table of buckling resistance according to EN (fixed BC)" are in generally providing bigger value of member strength, however the tendency is very similar to the one, described in previous paragraph. Again it is more suitable to design smaller internal angles 90°-140°, instead of 160° and 170°, which are decreasing several times.

Conclusion of influence of folding angle in case of tested L-profiles is following: for final strength of member with cross-section of same thickness different internal angle can produce significant decrease. Based on obtained results, the highest value of resistance was achieved for Class 3 and internal angles 120° and 140°, while the lowest value of member strength is observed in case of large internal angles 160° and 170°.

10.3.2 Influence of material thickness on resistance

Based on hand calculation and FEM analysis, it can be also observed the influence of thickness on final resistance of the member. For tested L-profiles thickness vary from 4 mm up to 20 mm. While the increase of strength isn't always linear, as it may be expected. The

final magnitude of strength is however depended on combination of thickness and internal angle.

Highest improvement in resistance is observed between 4 mm and 6 mm, where the magnitude, no matter the internal angle, is always around 50% higher in favour of 6mm thick element. For thickness 10 mm and 16 mm resulting resistance is very similar in small internal angles ($90^\circ - 120^\circ$) and significant difference is observed at large angles ($140^\circ - 170^\circ$).

For thickness 20 mm result are showing, that in case of smaller angles, the magnitude of resistance isn't significantly different from 10 and 16 mm, however in larger angles the strength of element with 20 mm is much more bigger compared to smaller thicknesses.

Conclusion of designing appropriate thickness of element is dependent on internal angle, thickness itself and material properties, therefore it may be recommended to design several thicknesses of one element and compare the difference between obtained magnitudes of strength.

10.4 Suggestions

10.4.1 Proposed changes in design procedure for cross-sections with fixed BC

On the basis of performed analysis it has been seen that for cross-sections which are classified as Class 4 (according to EN 1993-1-1) the design resistance according to Eurocode is too conservative. Moreover, it is more conservative when cross-section exhibits local buckling and critical load for torsional or flexural-torsional buckling is used for calculation of design strength. On the other hand, it is less conservative when cross-section fails in purely global mode and flexural critical load is used for calculations.

In chapter 3 "Review of performed researches" it has been shown that the problem of overestimating the design resistance for equal-leg angles with slender legs is typical for American, Australian/New Zealand design codes. The procedures of design according to these codes have similarities to EN in the way that for purely compressed members the reduction of cross-section is used and critical loads influence the design strength. Moreover, the critical load is taken as the lowest from flexural, torsional or torsional-flexural.

In the state-of-art review it has been shown that there are different directions in trying to solve this particular problem for slender equal-leg angles. It has been decided to try changes by following approach which was studied by Young (2004), Ellobody E. and Young B. (2005). Moreover, this approach was a modified version of conclusions which were made by Popovic et al. The method proposed by Young (2004), Ellobody E. and Young B. (2005) included changes in coefficients for design equations. However, this will not be done in this attempt of adjusting the design strength according EN. Only basic principles will be applied:

1. Ignore additional moment due to shift of the centroid.

2. Torsional and flexural-torsional critical load should be ignored and calculation of design strength should be based only on minor flexural mode.

According to the proposed changes additional moment is not considered and the cross-section is considered to be uniformly compressed. Calculation of non-dimensional slenderness is performed as follows:

$$\lambda_F = \sqrt{\frac{A_{eff} \cdot f_y}{N_{cr,F}}}$$

where

A_{eff} – effective cross-section area,

f_y – yield strength,

$N_{cr,F}$ – elastic critical load for minor flexural buckling.

Moreover, it has been decided to investigate if the possibility of using alternative buckling curve from EN 1993-1-1 is feasible. According to EN 1993-1-3 the choice of buckling curve c is prescribed for the case of considered cross-sections. However, buckling curves a and b will be considered for comparison. Due to the fact that not all results from FEA are validated with test results, these suggestions will be based only on assumptions. For definite changes in the design rules further investigation will be needed. Following imperfection factors will apply for buckling curves according to EN 1993-1-1, ch.6.3.1.2(2):

Buckling curve	a	b	c
Imperfection factor α	0.21	0.34	0.49

Table 10.4.1: Imperfection factor for buckling curves a, b and c (EN 1993-1-1, ch.6.3.1.2(2)).

The results will be plotted similarly as was shown in chapter 9.5 “Buckling curves. Parametric study”. On the vertical axis ratio N/N_{pl} will be used. On horizontal axis - non-dimensional slenderness. As it has been stated, for this modified procedure the latter will be based only on minor flexural critical load. Two graphs will be presented separately: one from chapter 9.5 and second with modified curve. Figure 10.4.2 illustrates the dependency between results according EN, FEA and test with non-dimensional slenderness plotted using the lowest elastic critical load. The curves will be plotted for cross-sections P2-4 and P2-6.

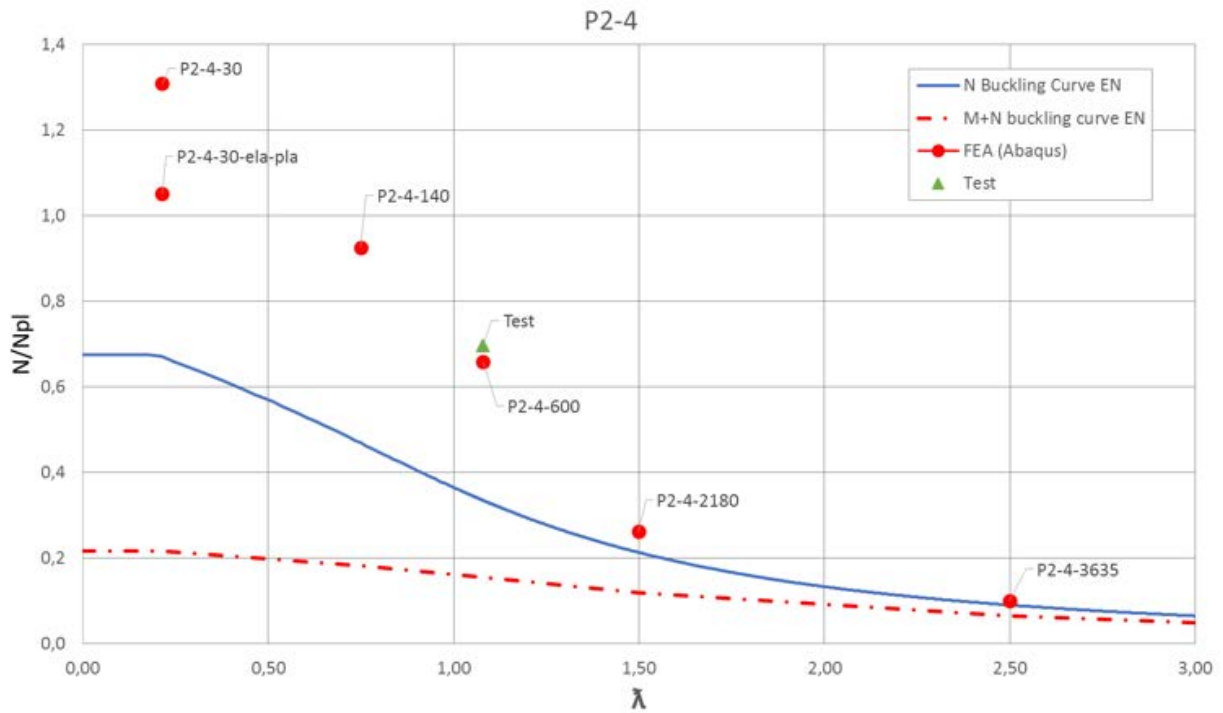


Figure 10.4.1: P2-4. EN design resistance versus test and FEA (non-dimensional slenderness based on lowest critical load)

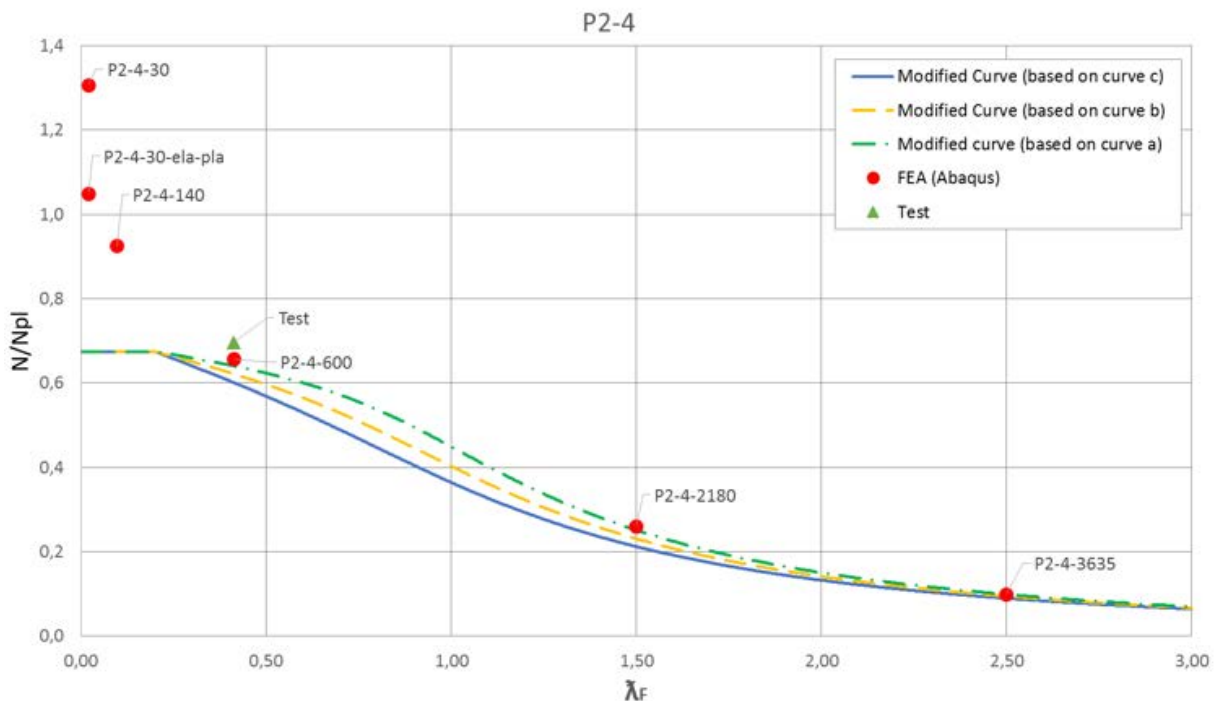


Figure 10.4.2: P2-4. Modified buckling curves versus test and FEA (non-dimensional slenderness based on flexural critical load)

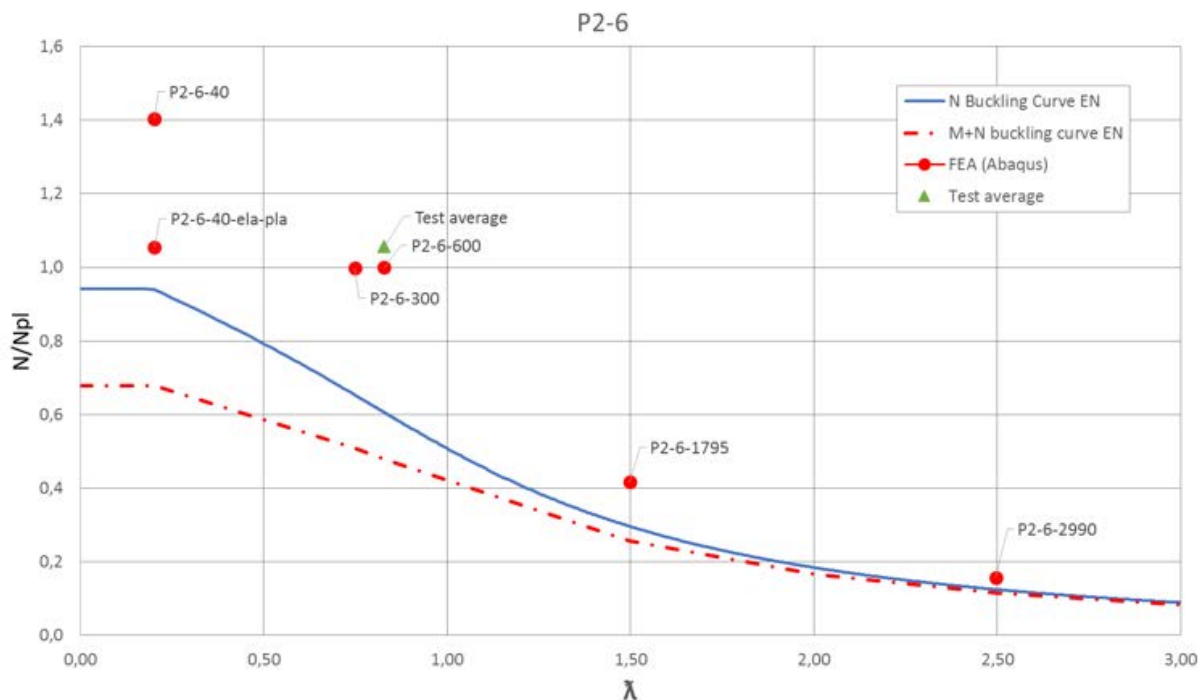


Figure 10.4.3: P2-6. EN design resistance versus test and FEA (non-dimensional slenderness based on lowest critical load)

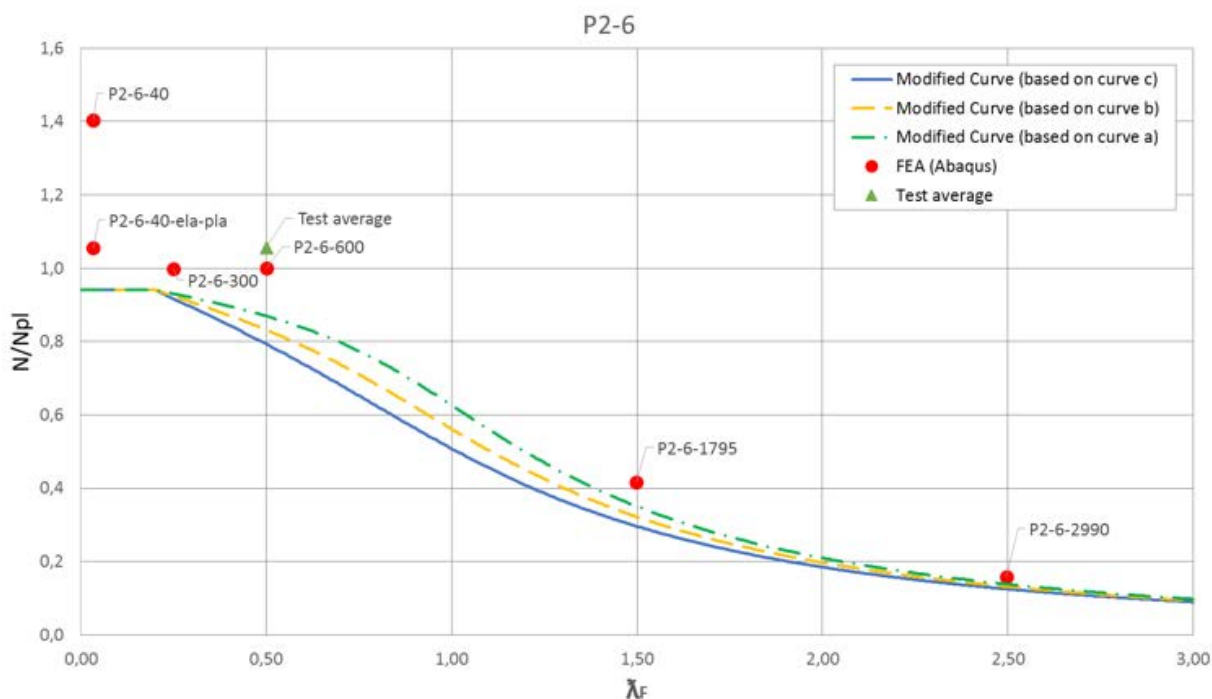


Figure 10.4.4: P2-6. Modified buckling curves versus test and FEA (non-dimensional slenderness based on flexural critical load)

It can be seen that these modifications make the predictions according to hand calculations less conservative. Moreover, for the case of application of curves a and b the results are still safe. However, in case of using curves a and b different behaviour is observed for bigger

thicknesses (10, 16 and 20 mm). The results for cross-section P2-10, P2-16 and P2-20 can be seen in Figures 10.4.5-10.4.7 respectively. For these cross-sections on the vertical axis $\chi = N/N_{pl}$ will be used to plot the graphs.

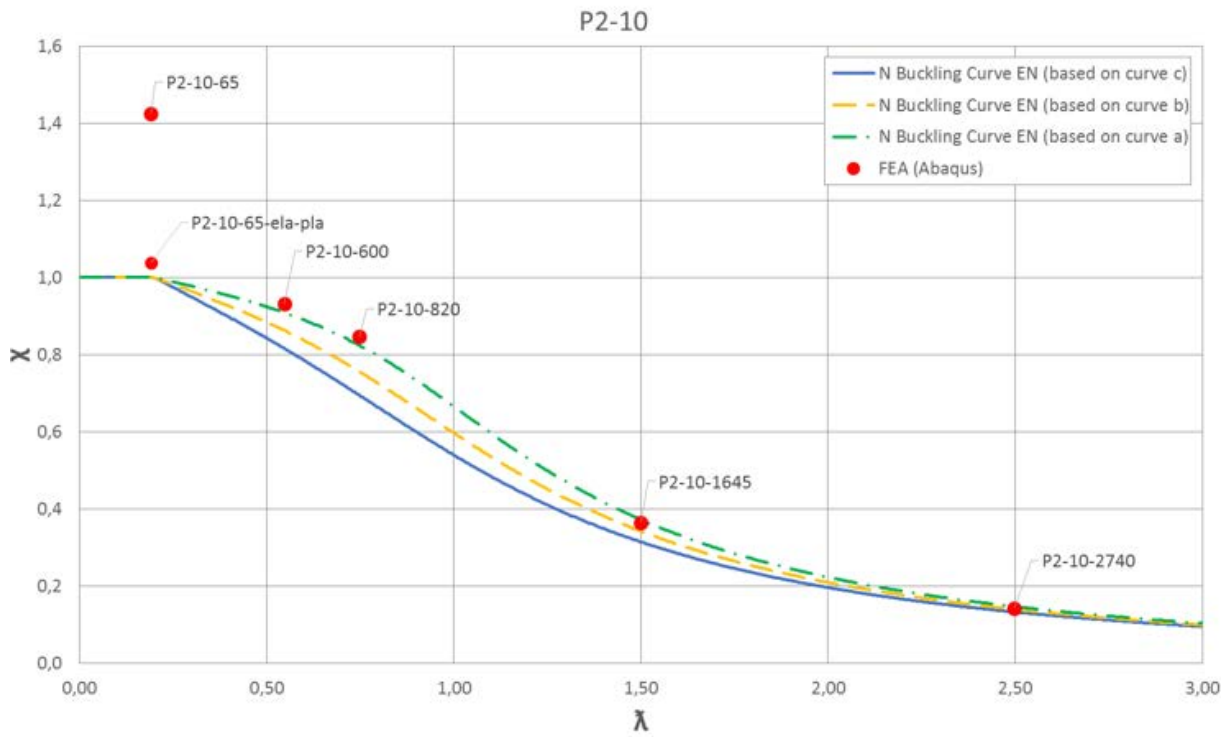


Figure 10.4.5: P2-10. EN design resistance (buckling curves a, b and c) versus FEA.

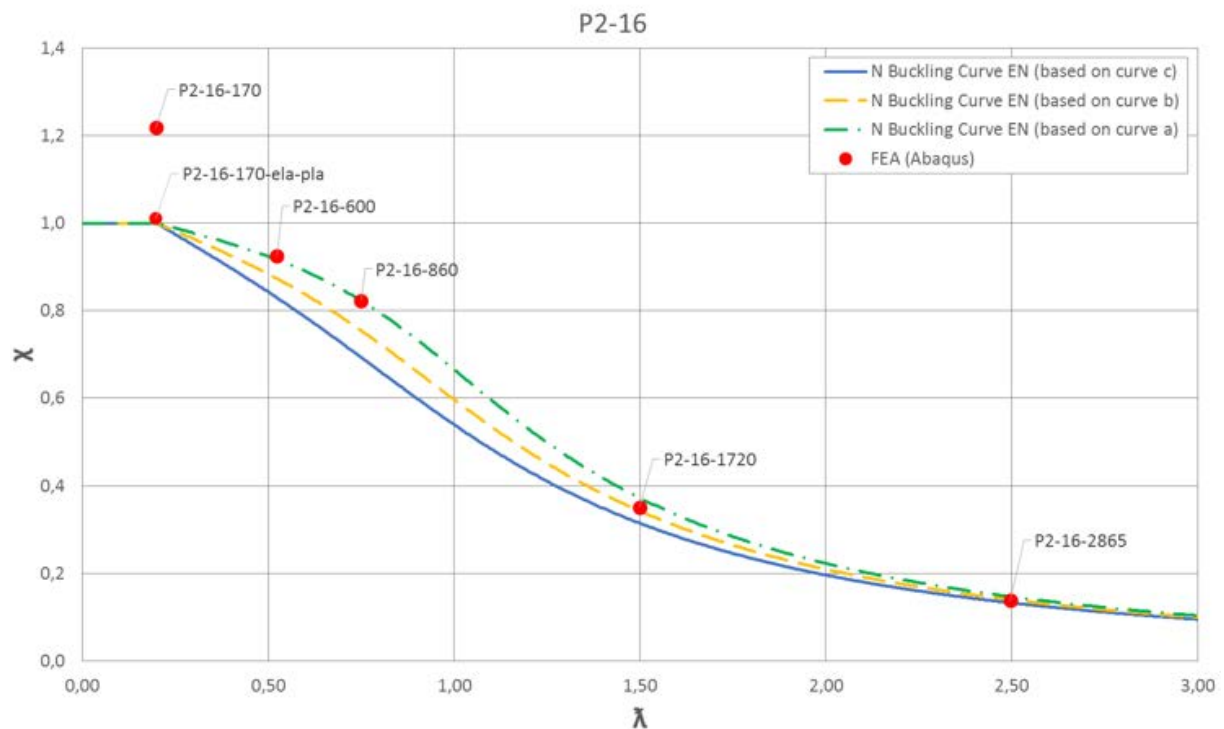


Figure 10.4.6: P2-16. EN design resistance (buckling curves a, b and c) versus FEA.

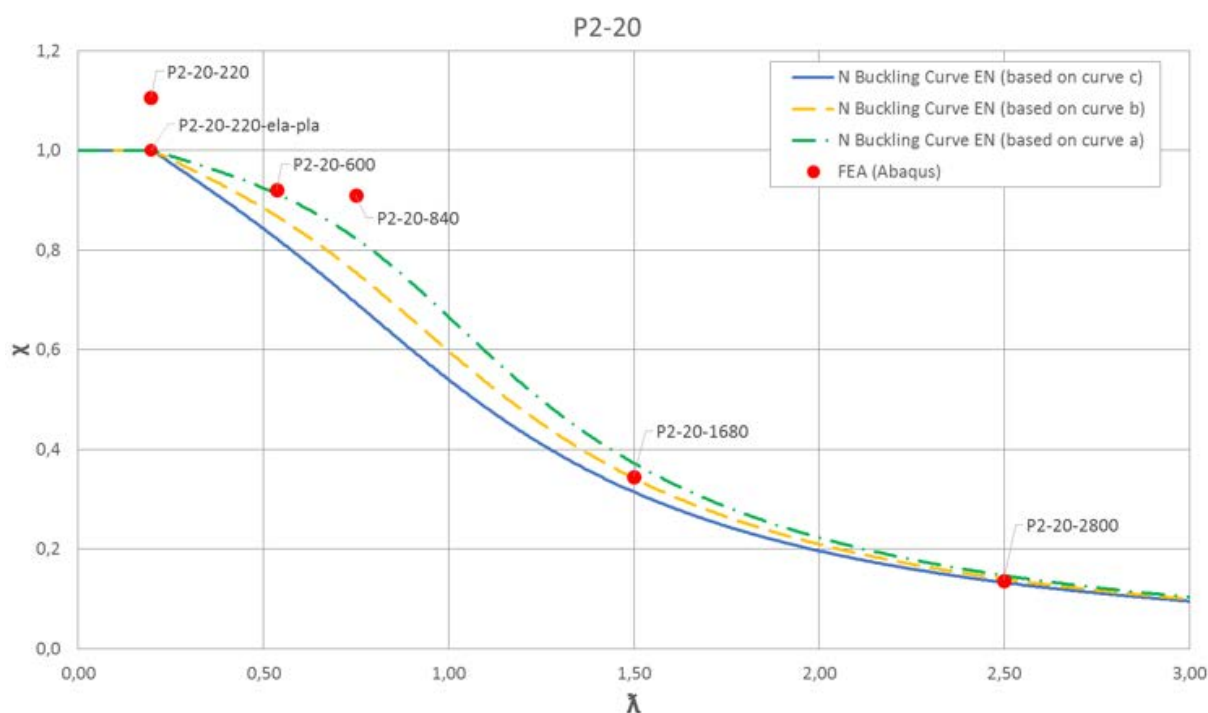


Figure 10.4.7: P2-20. EN design resistance (buckling curves a, b and c) versus FEA.

It can be observed that choice of buckling curve a in case of thicknesses 10, 16 and 20 mm show unconservative results. Moreover, for specimens with bigger length the results for curve b are also unsafe. However, as it has been stated the resistance for these cross-sections have not been validated with test results and it has been seen that FEA model is sensitive to imperfections. Therefore, to make conclusions regarding choice of buckling curve it is required to perform tests for all specimens. Moreover, it would be appropriate to test specimens with bigger length (up to 3000 mm) where it can be seen that the results might be unsafe.

Therefore, the recommendations for change in design will be based on curve c and on the amendments described in the beginning of this chapter.

Similar evaluations have been performed for other cross-sections. However, the tendency of curves is similar. Therefore, the results of suggested improvements (disregarding additional moment, using only flexural elastic critical load) will be presented only for length 600 mm for tested specimens in table 10.4.2.

Group	Profile number	Class	Test	EN		Suggested	
			P_{test} , kN	P_{EN} , kN	$\frac{P_{test}}{P_{EN}}$	P_S , kN	$\frac{P_{test}}{P_S}$
P1-6	P1-5-6mm	Class 4	443	218	2.03	349	1.27
	P1-6-6mm	Class 4	446	218	2.05	349	1.28
	P1-7-6mm	Class 4	445	218	2.04	349	1.28
P2-4	P2-7-4mm	Class 4	207	46	4.50	179	1.16
P2-6	P2-5-6mm	Class 4	454	208	2.18	345	1.31
	P2-6-6mm	Class 4	469	208	2.25	345	1.36
	P2-7-6mm	Class 4	456	208	2.19	345	1.32
P3-6	P3-5-6mm	Class 4	454	184	2.46	321	1.41
	P3-6-6mm	Class 4	444	184	2.41	321	1.38
	P3-7-6mm	Class 4	450	184	2.45	321	1.40
P4-6	P4-5-6mm	Class 4	369	181	2.04	263	1.40
	P4-6-6mm	Class 4	389	181	2.15	263	1.48
	P4-7-6mm	Class 4	343	181	1.89	263	1.30

Table 10.4.2: Comparison of test results, EN prediction and suggested improvements to EN.

It can be seen that suggested procedure for improvements increases the design strength significantly and the deviation with test results is smaller compared to EN results. Nevertheless, the results are still conservative. Therefore, it is necessary to develop more precise method of evaluation of design resistance and investigate the choice of appropriate buckling curves.

10.4.2 Suggestions for further research

The research on equal-leg angles with different angles of folding and thickness is very new perspective on old research of typical cold-formed 90 degree equal-leg angles. And it can be stated that this is the first research in this field. Therefore, there are a lot of questions which can be studied. Some of the questions which need further investigation will be described below.

Firstly, it is necessary to investigate the change of material properties in corners of cross-sections on the basis of tensile coupon test's results. Moreover, it is important to study the influence of these changes on buckling resistance of cross-section.

Secondly, it is necessary to finish tests on all the specimens to be able to validate all results obtained in FEA.

Thirdly, changes in classification of considered cross-sections might be proposed. Furthermore, already proposed changes should be investigated on validated models and further changes might apply. Application of different buckling curves from EN 1993-1-1

should be studied on validated results. As an alternative, Direct Strength Method can be studied for design of considered specimens.

Moreover, the experimentally measured imperfections should be introduced to Finite Element Model and the design resistance should be investigated based on this data.

It can be also recommended to test specimen with different lengths, than only 600 mm. With laboratory test results obtained for various lengths, the FEA and hand calculation can be verified more precisely and final recommendations, therefore more definite.

Finally, tests can be performed with pinned boundary conditions to investigate the influence of this supports on design resistance.

11 CONCLUSIONS

As long as discussions and conclusions concerning research questions have been presented in relevant chapters, this chapter will summarize the fulfilled objectives of the thesis. It can be stated that the method used in the research has proved to be convenient and efficient as long as it gives the possibility to compare effectively results obtained through hand calculations, FEA and tests. The work has been performed according to limitation of scope presented in the beginning, except the fact that during performance of thesis it has been possible to obtain results from compression tests not for all cross-sections of 4 mm and 6 mm thickness.

The fulfilled objectives can be listed as follows:

1. Review of literature has been performed. Suggested improvements for design procedures in case of cold-formed slender equal-leg angles have been outlined.
2. The classic theory of elastic stability has been reviewed on the basis of studied specimens. The curves for elastic critical loads have been plotted for cross-sections with different angles and thicknesses. This assisted in observing which buckling mode is dominant for certain slenderness of the member.
3. Design strength of cross-sections has been calculated according to Eurocode.
4. Eigenvalue Finite Element Analysis has been performed using software Abaqus. Results were compared with analytical results based on theory of elastic stability. It has been shown that both results are in good agreement for fixed-ended and pin-ended boundary conditions.
5. Non-linear Finite Element Analysis has been performed using software Abaqus. Sensitivity analysis has been done using different values of imperfections. Different approaches to modelling have been used to find the model which would represent expected results (solid and shell model; application of load on the cross-section edge and on centre of gravity; application of additional slab to transfer the load to the specimen).
6. Compression tests have been performed. The Finite Element Model has been validated with these results. It has been shown that both results are in good agreement.
7. All aspects affecting the precision of the laboratory test results (namely: initial imperfections, residual stresses, inaccuracy of using S4R shell element, undesirable eccentricity of applied load in test and flexibility of test setup) have been described and their influence of final result of resistance evaluated.
8. Comparison of ultimate resistances according to Eurocode, FEA and tests has been done. It has been shown that Eurocode is too conservative in case of Class 4 elements (more in case of $t=4$ mm and less in case $t=6$ mm). The comparison for Class 3 elements show quite close results. Similar behaviour of cross-sections has been studied during review of literature. Therefore, results can be considered reasonable.
9. Parametric study for different length of specimens has been done using software Abaqus. Buckling curves on the basis of EN prediction of design strength have been plotted. The results from parametric study have been incorporated in the graphs with

buckling curves. Comparison has been performed. The outcome has proved the conclusions made in paragraph 7.

10. The influence of angle of folding and thickness on ultimate resistance has been shown.
11. Suitability of classification of considered specimens according EN 1993-1-1 has been studied. Recommendations in use of gross area for design of Class 4 elements have been proposed.
12. The changes in design procedure of Class 4 elements (fixed boundary conditions) have been proposed on the basis of the information studied in Review of literature.
13. Suggestions for further research have been made.

12 ATTACHMENTS

Average yield strength

Group	Profile number	t,mm	Ag, mm2	Cross-section	fyb, MPa	fu,MPa	k	n	fya,MPa		(fu+fyb)/2, MPa	fya, MPa
P1	P1-4	4	450.01	Effective	650	700	-	-	-	-	-	none
	P1-6	6	652.52	Effective	650	700	-	-	-	-	-	none
	P1-10	10	1015.00	Full	650	700	5	1	674.6	<	675.00	674.63
	P1-16	16	1444.10	Full	500	570	5	1	562.0	>	535.00	none
	P1-20	20	1656.40	Full	480	570	5	1	588.7	>	525.00	none
P2	P2-4	4	457.33	Effective	650	700	-	-	-	-	-	none
	P2-6	6	668.98	Effective	650	700	-	-	-	-	-	none
	P2-10	10	1060.40	Full	650	700	5	1.11	676.2	>	675.00	none
	P2-16	16	1560.70	Full	500	570	5	1.11	563.8	>	535.00	none
	P2-20	20	1838.60	Full	480	570	5	1.11	588.8	>	525.00	none
P3	P3-4	4	467.15	Effective	650	700	-	-	-	-	-	none
	P3-6	6	691.09	Effective	650	700	-	-	-	-	-	none
	P3-10	10	1121.30	Full	650	700	5	1.33	679.7	>	675.00	none
	P3-16	16	1717.00	Full	500	570	5	1.33	569.6	>	535.00	none
	P3-20	20	2082.90	Full	480	570	5	1.33	595.2	>	525.00	none
P4	P4-4	4	473.11	Effective	650	700	-	-	-	-	-	none
	P4-6	6	704.50	Effective	650	700	-	-	-	-	-	none
	P4-10	10	1158.00	Full	650	700	5	1.56	683.6	>	675.00	none
	P4-16	16	1811.50	Full	500	570	5	1.56	576.9	>	535.00	none
	P4-20	20	2230.50	Full	480	570	5	1.56	605.5	>	525.00	none
P5	P5-4	4	477.05	Effective	650	700	-	-	-	-	-	none
	P5-6	6	713.36	Effective	650	700	-	-	-	-	-	none
	P5-10	10	1181.70	Full	650	700	5	1.78	687.6	>	675.00	none
	P5-16	16	1873.00	Full	500	570	5	1.78	585.0	>	535.00	none
	P5-20	20	2326.50	Full	480	570	5	1.78	617.5	>	525.00	none
P6	P6-4	4	478.58	Effective	650	700	-	-	-	-	-	none
	P6-6	6	716.81	Effective	650	700	-	-	-	-	-	none
	P6-10	10	1191.20	Full	650	700	5	1.89	689.6	>	675.00	none
	P6-16	16	1897.40	Full	500	570	5	1.89	589.2	>	535.00	none
	P6-20	20	2364.60	Full	480	570	5	1.89	623.8	>	525.00	none

Classification of cross-sections

Group	Codename	f_y , MPa	b [mm]	h [mm]	t [mm]	angle [°]	ϵ	h/t		15 ϵ	$b+h/2t$		11,5 ϵ	CLASS	Cross-section
P1	P1-4	650	57.07	57.07	4	90	0.601	14.27	>	9.019	14.27	>	6.915	4	Effective
	P1-6	650	55.61	55.61	6	90	0.601	9.27	>	9.019	9.27	>	6.915	4	Effective
	P1-10	650	52.68	52.68	10	90	0.601	5.27	<	9.019	5.27	<	6.915	3	Full
	P1-16	500	48.28	48.28	16	90	0.686	3.02	<	10.283	3.02	<	7.884	3	Full
	P1-20	480	45.36	45.36	20	90	0.700	2.27	<	10.496	2.27	<	8.047	3	Full
P2	P2-4	650	58.04	58.04	4	100	0.601	14.51	>	9.019	14.51	>	6.915	4	Effective
	P2-6	650	57.06	57.06	6	100	0.601	9.51	>	9.019	9.51	>	6.915	4	Effective
	P2-10	650	55.09	55.09	10	100	0.601	5.51	<	9.019	5.51	<	6.915	3	Full
	P2-16	500	52.15	52.15	16	100	0.686	3.26	<	10.283	3.26	<	7.884	3	Full
	P2-20	480	50.18	50.18	20	100	0.700	2.51	<	10.496	2.51	<	8.047	3	Full
P3	P3-4	650	59.23	59.23	4	120	0.601	14.81	>	9.019	14.81	>	6.915	4	Effective
	P3-6	650	58.84	58.84	6	120	0.601	9.81	>	9.019	9.81	>	6.915	4	Effective
	P3-10	650	58.07	58.07	10	120	0.601	5.81	<	9.019	5.81	<	6.915	3	Full
	P3-16	500	56.91	56.91	16	120	0.686	3.56	<	10.283	3.56	<	7.884	3	Full
	P3-20	480	56.13	56.13	20	120	0.700	2.81	<	10.496	2.81	<	8.047	3	Full
P4	P4-4	650	59.1	59.1	4	140	0.601	14.78	>	9.019	14.78	>	6.915	4	Effective
	P4-6	650	58.64	58.64	6	140	0.601	9.77	>	9.019	9.77	>	6.915	4	Effective
	P4-10	650	57.74	57.74	10	140	0.601	5.77	<	9.019	5.77	<	6.915	3	Full
	P4-16	500	56.39	56.39	16	140	0.686	3.52	<	10.283	3.52	<	7.884	3	Full
	P4-20	480	55.48	55.48	20	140	0.700	2.77	<	10.496	2.77	<	8.047	3	Full
P5	P5-4	650	59.63	59.63	4	160	0.601	14.91	>	9.019	14.91	>	6.915	4	Effective
	P5-6	650	59.44	59.44	6	160	0.601	9.91	>	9.019	9.91	>	6.915	4	Effective
	P5-10	650	59.06	59.06	10	160	0.601	5.91	<	9.019	5.91	<	6.915	3	Full
	P5-16	500	58.5	58.5	16	160	0.686	3.66	<	10.283	3.66	<	7.884	3	Full
	P5-20	480	58.13	58.13	20	160	0.700	2.91	<	10.496	2.91	<	8.047	3	Full
P6	P6-4	650	59.82	59.82	4	170	0.601	14.96	>	9.019	14.96	>	6.915	4	Effective
	P6-6	650	59.73	59.73	6	170	0.601	9.96	>	9.019	9.96	>	6.915	4	Effective
	P6-10	650	59.56	59.56	10	170	0.601	5.96	<	9.019	5.96	<	6.915	3	Full
	P6-16	500	59.29	59.29	16	170	0.686	3.71	<	10.283	3.71	<	7.884	3	Full
	P6-20	480	59.11	59.11	20	170	0.700	2.96	<	10.496	2.96	<	8.047	3	Full

Effective width

Group	Profile number	bp, mm	t,mm	Cross-section	fyb, Mpa	ψ	$k\sigma$	ϵ	$\lambda\rho$		$\lambda\rho$	ρ	beff, mm
P1	P1-4	55.6	4	Effective	650	1	0.43	0.601	1.241	>	0.748	0.683584	38.01
	P1-6	53.49	6	Effective	650	1	0.43	0.601	0.796	>	0.748	0.959452	51.32
P2	P2-4	56.75	4	Effective	650	1	0.43	0.60	1.267	>	0.748	0.672154	38.14
	P2-6	55.13	6	Effective	650	1	0.43	0.60	0.821	>	0.748	0.939471	51.79
P3	P3-4	58.23	4	Effective	650	1	0.43	0.601	1.300	>	0.748	0.657971	38.31
	P3-6	57.34	6	Effective	650	1	0.43	0.601	0.853	>	0.748	0.913609	52.39
P4	P4-4	59.1	4	Effective	650	1	0.43	0.601	1.319	>	0.748	0.649899	38.41
	P4-6	58.64	6	Effective	650	1	0.43	0.601	0.873	>	0.748	0.89895	52.71
P5	P5-4	59.63	4	Effective	650	1	0.43	0.601	1.331	>	0.748	0.645073	38.47
	P5-6	59.44	6	Effective	650	1	0.43	0.601	0.885	>	0.748	0.890128	52.91
P6	P6-4	59.82	4	Effective	650	1	0.43	0.601	1.336	>	0.748	0.64336	38.49
	P6-6	59.73	6	Effective	650	1	0.43	0.601	0.889	>	0.748	0.886967	52.98

Properties of cross-sections for critical force assessment

Group	Profile number	Class	Specimen length	Buckling length		Warping length		Material properties		Gross cross-section parameters			Shear center to center of gravity		Torsion constant	Warping constant
			Length [mm]	k	LE [mm]	kET	LET [mm]	E [MPa]	G [MPa]	A [mm ²]	Iz [mm ⁴]	Iy [mm ⁴]	dz [mm]	dy [mm]	It [mm ⁴]	Iw [mm ⁶]
P1	P1-4	Class 4	600.00	0.5	300.00	0.5	300.00	210000	80700	450.01	58664	260350	0.00	21.00	2310	611960
	P1-6	Class 4	600.00	0.5	300.00	0.5	300.00	210000	80700	652.52	78386	370850	0.00	20.00	7509	2071700
	P1-10	Class 3	600.00	0.5	300.00	0.5	300.00	210000	80700	1015.00	101620	555120	0.00	18.00	31583	8266900
	P1-16	Class 3	600.00	0.5	300.00	0.5	300.00	210000	80700	1444.10	106240	740890	0.00	13.00	109400	22064000
	P1-20	Class 3	600.00	0.5	300.00	0.5	300.00	210000	80700	1656.40	101860	801320	0.00	8.00	187470	27339000
P2	P2-4	Class 4	600.00	0.5	300.00	0.5	300.00	210000	80700	457.33	51194	310630	0.00	19.00	2325	530220
	P2-6	Class 4	600.00	0.5	300.00	0.5	300.00	210000	80700	668.98	70812	446390	0.00	18.00	7685	2003200
	P2-10	Class 3	600.00	0.5	300.00	0.5	300.00	210000	80700	1060.40	100040	681570	0.00	17.00	33073	8555000
	P2-16	Class 3	600.00	0.5	300.00	0.5	300.00	210000	80700	1560.70	123980	947950	0.00	13.00	119370	26571000
	P2-20	Class 3	600.00	0.5	300.00	0.5	300.00	210000	80700	1838.60	133730	1069300	0.00	10.00	211840	39285000
P3	P3-4	Class 4	600.00	0.5	300.00	0.5	300.00	210000	80700	467.15	33479	407680	0.00	15.00	2381	540220
	P3-6	Class 4	600.00	0.5	300.00	0.5	300.00	210000	80700	691.09	48750	593940	0.00	14.00	7945	2080300
	P3-10	Class 3	600.00	0.5	300.00	0.5	300.00	210000	80700	1121.30	78171	933400	0.00	14.00	35097	9287100
	P3-16	Class 3	600.00	0.5	300.00	0.5	300.00	210000	80700	1717.00	123070	1365200	0.00	12.00	132570	33112000
	P3-20	Class 3	600.00	0.5	300.00	0.5	300.00	210000	80700	2082.90	157180	1604900	0.00	11.00	244010	55784000
P4	P4-4	Class 4	600.00	0.5	300.00	0.5	300.00	210000	80700	473.11	16682	490400	0.00	10.00	2434	654260
	P4-6	Class 4	600.00	0.5	300.00	0.5	300.00	210000	80700	704.50	25522	722270	0.00	10.00	8121	2269300
	P4-10	Class 3	600.00	0.5	300.00	0.5	300.00	210000	80700	1158.00	46384	1160400	0.00	10.00	36327	10123000
	P4-16	Class 3	600.00	0.5	300.00	0.5	300.00	210000	80700	1811.50	90972	1756600	0.00	9.00	140530	37414000
	P4-20	Class 3	600.00	0.5	300.00	0.5	300.00	210000	80700	2230.50	133800	2115600	0.00	8.00	263400	66505000
P5	P5-4	Class 4	600.00	0.5	300.00	0.5	300.00	210000	80700	477.05	4893	548860	0.00	5.00	2449	666720
	P5-6	Class 4	600.00	0.5	300.00	0.5	300.00	210000	80700	713.36	8456	816040	0.00	5.00	8234	2337800
	P5-10	Class 3	600.00	0.5	300.00	0.5	300.00	210000	80700	1181.70	20129	1336200	0.00	5.00	37117	10660000
	P5-16	Class 3	600.00	0.5	300.00	0.5	300.00	210000	80700	1873.00	55723	2081800	0.00	5.00	145670	40949000
	P5-20	Class 3	600.00	0.5	300.00	0.5	300.00	210000	80700	2326.50	96603	2556400	0.00	5.00	276030	75539000
P6	P6-4	Class 4	600.00	0.5	300.00	0.5	300.00	210000	80700	478.58	1722	566640	0.00	3.00	2459	673080
	P6-6	Class 4	600.00	0.5	300.00	0.5	300.00	210000	80700	716.81	3768	846250	0.00	3.00	8260	2369800
	P6-10	Class 3	600.00	0.5	300.00	0.5	300.00	210000	80700	1191.20	12594	1398100	0.00	3.00	37411	10913000
	P6-16	Class 3	600.00	0.5	300.00	0.5	300.00	210000	80700	1897.40	44668	2207700	0.00	2.00	147540	42043000
	P6-20	Class 3	600.00	0.5	300.00	0.5	300.00	210000	80700	2364.60	83984	2735500	0.00	2.00	281260	79483000

Critical force assessment (fixed BC)

Group	Profile number	Radius of polar gyration	Factor	Flexural buckling		Torsional buckling	Torsional flexural buckling
		i_c [mm]	β [-]	N_{crz} [kN]	N_{cry} [kN]	$N_{cr.T}$ [kN]	$N_{cr.TF}$ [kN]
P1	P1-4	33.9102	0.6165	1350.978	5995.620	174.350	172.393
	P1-6	32.9919	0.6325	1805.157	8540.333	600.573	584.777
	P1-10	31.1614	0.6663	2340.215	12783.901	2820.834	2599.455
	P1-16	27.4884	0.7763	2446.609	17062.013	12356.425	9596.973
	P1-20	24.6833	0.8950	2345.742	18453.660	25864.563	15830.272
P2	P2-4	33.9436	0.6867	1178.951	7153.522	173.417	172.088
	P2-6	33.1228	0.7047	1630.735	10279.950	607.291	596.442
	P2-10	32.0326	0.7183	2303.829	15695.928	2793.133	2642.470
	P2-16	29.2545	0.8025	2855.145	21830.413	11970.961	10202.997
	P2-20	27.4649	0.8674	3079.678	24624.992	23862.845	17764.587
P3	P3-4	34.1959	0.8076	770.990	9388.494	174.977	174.342
	P3-6	33.5554	0.8259	1122.668	13677.890	611.945	607.037
	P3-10	33.1382	0.8215	1800.206	21495.340	2773.961	2704.487
	P3-16	31.7928	0.8575	2834.188	31439.296	11338.649	10575.050
	P3-20	31.0962	0.8749	3619.710	36959.366	21692.675	19125.940
P4	P4-4	34.2316	0.9147	384.171	11293.459	180.455	180.206
	P4-6	34.0801	0.9139	587.748	16633.211	609.225	607.243
	P4-10	33.7954	0.9124	1068.181	26722.941	2770.892	2743.411
	P4-16	33.1800	0.9264	2095.001	40452.877	11083.876	10794.796
	P4-20	32.7486	0.9403	3081.290	48720.315	21248.012	20374.123
P5	P5-4	34.4352	0.9789	112.684	12639.739	179.631	179.577
	P5-6	34.3627	0.9788	194.732	18792.648	608.304	607.874
	P5-10	34.2458	0.9787	463.552	30771.453	2763.381	2757.595
	P5-16	34.1501	0.9786	1283.249	47941.932	10888.582	10820.963
	P5-20	34.1371	0.9785	2224.678	58871.532	20607.889	20376.500
P6	P6-4	34.5919	0.9925	39.654	13049.196	178.764	178.746
	P6-6	34.5664	0.9925	86.778	19488.356	603.541	603.396
	P6-10	34.5436	0.9925	290.028	32196.952	2740.707	2738.786
	P6-16	34.5120	0.9966	1028.663	50841.293	10809.245	10799.464
	P6-20	34.5886	0.9967	1934.074	62996.040	20502.061	20469.121

Properties of cross-sections for critical force assessment (neglecting rounded corners)

Group	Profile number	Class	Specimen length	Buckling length		Warping length		Material properties		Gross cross-section parameters			Shear center to center of gravity		Torsion constant	Warping constant
			Length [mm]	k	Le [mm]	kET	LET [mm]	E [MPa]	G [MPa]	A [mm ²]	Iz [mm ⁴]	Iy [mm ⁴]	dz [mm]	dy [mm]	It [mm ⁴]	Iw [mm ⁶]
P1	P1-4	Class 4	600.00	0.5	300.00	0.5	300.00	210000	80700	464.00	65810	260460	0.00	20.00	2310	611960
	P1-6	Class 4	600.00	0.5	300.00	0.5	300.00	210000	80700	684.00	95159	371410	0.00	20.00	7509	2071700
	P1-10	Class 3	600.00	0.5	300.00	0.5	300.00	210000	80700	1100.00	150080	559170	0.00	19.00	31583	8266900
	P1-16	Class 3	600.00	0.5	300.00	0.5	300.00	210000	80700	1664.00	231540	767660	0.00	16.00	109400	22064000
	P1-20	Class 3	600.00	0.5	300.00	0.5	300.00	210000	80700	2000.00	290670	866670	0.00	14.00	187470	27339000
P2	P2-4	Class 4	600.00	0.5	300.00	0.5	300.00	210000	80700	466.57	55356	310690	0.00	19.00	2325	530220
	P2-6	Class 4	600.00	0.5	300.00	0.5	300.00	210000	80700	689.79	80847	446700	0.00	18.00	7685	2003200
	P2-10	Class 3	600.00	0.5	300.00	0.5	300.00	210000	80700	1116.10	130310	683710	0.00	17.00	33073	8555000
	P2-16	Class 3	600.00	0.5	300.00	0.5	300.00	210000	80700	1705.20	208180	962150	0.00	15.00	119370	26571000
	P2-20	Class 3	600.00	0.5	300.00	0.5	300.00	210000	80700	2064.40	267490	1104000	0.00	14.00	211840	39285000
P3	P3-4	Class 4	600.00	0.5	300.00	0.5	300.00	210000	80700	470.76	34615	407690	0.00	15.00	2381	540220
	P3-6	Class 4	600.00	0.5	300.00	0.5	300.00	210000	80700	699.22	51642	594010	0.00	14.00	7945	2080300
	P3-10	Class 3	600.00	0.5	300.00	0.5	300.00	210000	80700	1142.30	87532	933870	0.00	14.00	35097	9287100
	P3-16	Class 3	600.00	0.5	300.00	0.5	300.00	210000	80700	1772.20	152530	1368300	0.00	13.00	132570	33112000
	P3-20	Class 3	600.00	0.5	300.00	0.5	300.00	210000	80700	2169.10	207910	1612600	0.00	12.00	244010	55784000
P4	P4-4	Class 4	600.00	0.5	300.00	0.5	300.00	210000	80700	474.18	16876	490410	0.00	10.00	2434	654260
	P4-6	Class 4	600.00	0.5	300.00	0.5	300.00	210000	80700	706.90	26050	722280	0.00	10.00	8121	2269300
	P4-10	Class 3	600.00	0.5	300.00	0.5	300.00	210000	80700	1163.60	48164	1160500	0.00	10.00	36327	10123000
	P4-16	Class 3	600.00	0.5	300.00	0.5	300.00	210000	80700	1826.80	97278	1757000	0.00	9.00	140530	37414000
	P4-20	Class 3	600.00	0.5	300.00	0.5	300.00	210000	80700	2254.40	145430	2116600	0.00	9.00	263400	66505000
P5	P5-4	Class 4	600.00	0.5	300.00	0.5	300.00	210000	80700	477.18	4903	548860	0.00	5.00	2449	666720
	P5-6	Class 4	600.00	0.5	300.00	0.5	300.00	210000	80700	713.65	8484	816040	0.00	5.00	8234	2337800
	P5-10	Class 3	600.00	0.5	300.00	0.5	300.00	210000	80700	1182.40	20241	1336200	0.00	5.00	37117	10660000
	P5-16	Class 3	600.00	0.5	300.00	0.5	300.00	210000	80700	1874.90	56180	2081800	0.00	5.00	145670	40949000
	P5-20	Class 3	600.00	0.5	300.00	0.5	300.00	210000	80700	2329.50	97514	2556400	0.00	5.00	276030	75539000
P6	P6-4	Class 4	600.00	0.5	300.00	0.5	300.00	210000	80700	478.60	1723	566640	0.00	3.00	2459	673080
	P6-6	Class 4	600.00	0.5	300.00	0.5	300.00	210000	80700	716.85	3770	846250	0.00	3.00	8260	2369800
	P6-10	Class 3	600.00	0.5	300.00	0.5	300.00	210000	80700	1191.30	12602	1398100	0.00	3.00	37411	10913000
	P6-16	Class 3	600.00	0.5	300.00	0.5	300.00	210000	80700	1897.60	44706	2207700	0.00	2.00	147540	42043000
	P6-20	Class 3	600.00	0.5	300.00	0.5	300.00	210000	80700	2365.00	84063	2735500	0.00	2.00	281260	79483000

Critical force assessment (neglecting rounded corners)

Group	Profile number	Radius of polar gyration	Factor	Flexural buckling		Torsional buckling	Torsional flexural buckling
		i_c [mm]	β [-]	N _{crz} [kN]	N _{cry} [kN]	N _{cr.T} [kN]	N _{cr.TF} [kN]
P1	P1-4	33.2140	0.6374	1515.544	5998.153	181.736	179.723
	P1-6	32.8956	0.6304	2191.424	8553.229	604.094	588.047
	P1-10	31.7139	0.6411	3456.204	12877.169	2723.406	2506.054
	P1-16	29.2657	0.7011	5332.152	17678.501	10901.230	8526.700
	P1-20	27.8329	0.7470	6693.862	19958.610	20342.108	13404.928
P2	P2-4	33.8459	0.6849	1274.798	7154.904	174.419	173.068
	P2-6	32.9969	0.7024	1861.832	10287.089	611.935	600.844
	P2-10	31.9115	0.7162	3000.919	15745.210	2814.380	2660.819
	P2-16	30.1882	0.7531	4794.193	22157.426	11241.882	9487.735
	P2-20	29.3318	0.7722	6160.048	25424.101	20921.864	15458.776
P3	P3-4	34.1256	0.8068	797.151	9388.724	175.699	175.057
	P3-6	33.4573	0.8249	1189.268	13679.502	615.540	610.546
	P3-10	33.0176	0.8202	2015.781	21506.164	2794.263	2723.275
	P3-16	32.0493	0.8355	3512.625	31510.686	11157.897	10329.152
	P3-20	31.3575	0.8536	4787.975	37136.689	21332.670	18599.624
P4	P4-4	34.2026	0.9145	388.639	11293.690	180.762	180.511
	P4-6	34.0383	0.9137	599.907	16633.442	610.719	608.723
	P4-10	33.7450	0.9122	1109.172	26725.244	2779.164	2751.433
	P4-16	33.1065	0.9261	2240.223	40462.088	11133.137	10839.980
	P4-20	32.9300	0.9253	3349.119	48743.344	21014.621	19978.175
P5	P5-4	34.4309	0.9789	112.900	12639.739	179.676	179.622
	P5-6	34.3564	0.9788	195.386	18792.648	608.526	608.095
	P5-10	34.2373	0.9787	466.132	30771.453	2764.760	2758.964
	P5-16	34.1367	0.9785	1293.774	47941.932	10897.111	10829.319
	P5-20	34.1213	0.9785	2245.657	58871.532	20626.961	20394.831
P6	P6-4	34.5912	0.9925	39.668	13049.196	178.771	178.753
	P6-6	34.5655	0.9925	86.817	19488.356	603.574	603.428
	P6-10	34.5423	0.9925	290.212	32196.952	2740.920	2738.999
	P6-16	34.5105	0.9966	1029.538	50841.293	10810.199	10800.415
	P6-20	34.5862	0.9967	1935.893	62996.040	20504.945	20471.989

Critical buckling load for local buckling

Group	Profile number	A, mm ²	bp, mm	t,mm	$k\sigma$	σ_{cr} , MPa	P _{cr} ,kN
P1	P1-4	450.01	55.6	4	0.43	422.4	190.1
	P1-6	652.52	53.49	6	0.43	1026.9	670.1
P2	P2-4	457.33	56.75	4	0.43	405.5	185.4
	P2-6	668.98	55.13	6	0.43	966.7	646.7
P3	P3-4	467.15	58.23	4	0.43	385.1	179.9
	P3-6	691.09	57.34	6	0.43	893.6	617.6
P4	P4-4	473.11	59.1	4	0.43	373.9	176.9
	P4-6	704.50	58.64	6	0.43	854.4	601.9
P5	P5-4	477.05	59.63	4	0.43	367.2	175.2
	P5-6	713.36	59.44	6	0.43	831.6	593.2
P6	P6-4	478.58	59.82	4	0.43	364.9	174.6
	P6-6	716.81	59.73	6	0.43	823.5	590.3

E= 210000 Mpa

v= 0.3

Flexural buckling resistance (fixed BC)

Group	Profile number	Class	γ_{M1}	f_{yb} , Mpa	f_{ya}	A_g , mm ²	A_{eff} , mm ²	N_{cr} , kN	Buckling curve	α	λ	Φ	χ	N_{bRd} , kN
P1	P1-4	Class 4	1	650	-	-	309.1	1350.98	c	0.49	0.386	0.620	0.90	181.80
	P1-6	Class 4	1	650	-	-	627.1	1805.16	c	0.49	0.475	0.680	0.86	349.23
	P1-10	Class 3	1	-	674.6	1015.00	-	2340.21	c	0.49	0.541	0.730	0.82	561.37
	P1-16	Class 3	1	500	-	1444.10	-	2446.61	c	0.49	0.543	0.732	0.82	590.99
	P1-20	Class 3	1	480	-	1656.40	-	2345.74	c	0.49	0.582	0.763	0.80	632.79
P2	P2-4	Class 4	1	650	-	-	308.7	1178.95	c	0.49	0.413	0.637	0.89	178.70
	P2-6	Class 4	1	650	-	-	629.4	1630.73	c	0.49	0.501	0.699	0.84	344.70
	P2-10	Class 3	1	650	-	1060.40	-	2303.83	c	0.49	0.547	0.735	0.82	562.68
	P2-16	Class 3	1	500	-	1560.70	-	2855.14	c	0.49	0.523	0.716	0.83	647.81
	P2-20	Class 3	1	480	-	1838.60	-	3079.68	c	0.49	0.535	0.725	0.82	726.35
P3	P3-4	Class 4	1	650	-	-	308.0	770.99	c	0.49	0.510	0.706	0.84	167.69
	P3-6	Class 4	1	650	-	-	632.1	1122.67	c	0.49	0.605	0.782	0.78	321.47
	P3-10	Class 3	1	650	-	1121.30	-	1800.21	c	0.49	0.636	0.809	0.76	556.60
	P3-16	Class 3	1	500	-	1717.00	-	2834.19	c	0.49	0.550	0.737	0.81	699.16
	P3-20	Class 3	1	480	-	2082.90	-	3619.71	c	0.49	0.526	0.718	0.83	828.42
P4	P4-4	Class 4	1	650	-	-	307.7	384.17	c	0.49	0.722	0.888	0.71	142.28
	P4-6	Class 4	1	650	-	-	633.5	587.75	c	0.49	0.837	1.006	0.64	263.11
	P4-10	Class 3	1	650	-	1158.00	-	1068.18	c	0.49	0.839	1.009	0.64	479.79
	P4-16	Class 3	1	500	-	1811.50	-	2095.00	c	0.49	0.658	0.828	0.75	680.03
	P4-20	Class 3	1	480	-	2230.50	-	3081.29	c	0.49	0.589	0.769	0.79	847.53
P5	P5-4	Class 4	1	650	-	-	307.8	112.68	c	0.49	1.333	1.665	0.38	75.10
	P5-6	Class 4	1	650	-	-	635.0	194.73	c	0.49	1.456	1.868	0.33	135.91
	P5-10	Class 3	1	650	-	1181.70	-	463.55	c	0.49	1.287	1.595	0.39	302.82
	P5-16	Class 3	1	500	-	1873.00	-	1283.25	c	0.49	0.854	1.025	0.63	588.27
	P5-20	Class 3	1	480	-	2326.50	-	2224.68	c	0.49	0.708	0.876	0.72	803.39
P6	P6-4	Class 4	1	650	-	-	307.9	39.65	c	0.49	2.247	3.525	0.16	32.07
	P6-6	Class 4	1	650	-	-	635.8	86.78	c	0.49	2.182	3.367	0.17	69.68
	P6-10	Class 3	1	650	-	1191.20	-	290.03	c	0.49	1.634	2.186	0.27	212.80
	P6-16	Class 3	1	500	-	1897.40	-	1028.66	c	0.49	0.960	1.147	0.56	534.37
	P6-20	Class 3	1	480	-	2364.60	-	1934.07	c	0.49	0.766	0.932	0.68	775.74

Torsional buckling resistance (fixed BC)

Group	Profile number	Class	γ_{M1}	f_{yb} , Mpa	f_{ya}	A_g , mm ²	A_{eff} , mm ²	N_{crT} , kN	Buckling curve	α	λ	Φ	χ	N_{brdT} , kN
P1	P1-4	Class 4	1	650	-	-	309.1	174.35	c	0.49	1.073	1.290	0.50	100.16
	P1-6	Class 4	1	650	-	-	627.1	600.57	c	0.49	0.824	0.992	0.65	263.81
	P1-10	Class 3	1	-	674.6	1015.00	-	2820.83	c	0.49	0.493	0.693	0.85	580.03
	P1-16	Class 3	1	500	-	1444.10	-	12356.42	c	0.49	0.242	0.539	0.98	706.72
	P1-20	Class 3	1	480	-	1656.40	-	25864.56	c	0.49	0.175	0.509	1.01	805.12
P2	P2-4	Class 4	1	650	-	-	308.7	173.42	c	0.49	1.076	1.293	0.50	99.79
	P2-6	Class 4	1	650	-	-	629.4	607.29	c	0.49	0.821	0.989	0.65	265.57
	P2-10	Class 3	1	650	-	1060.40	-	2793.13	c	0.49	0.497	0.696	0.84	582.29
	P2-16	Class 3	1	500	-	1560.70	-	11970.96	c	0.49	0.255	0.546	0.97	758.40
	P2-20	Class 3	1	480	-	1838.60	-	23862.84	c	0.49	0.192	0.517	1.00	885.99
P3	P3-4	Class 4	1	650	-	-	308.0	174.98	c	0.49	1.070	1.285	0.50	100.22
	P3-6	Class 4	1	650	-	-	632.1	611.94	c	0.49	0.819	0.987	0.65	267.05
	P3-10	Class 3	1	650	-	1121.30	-	2773.96	c	0.49	0.513	0.708	0.84	609.26
	P3-16	Class 3	1	500	-	1717.00	-	11338.65	c	0.49	0.275	0.556	0.96	825.70
	P3-20	Class 3	1	480	-	2082.90	-	21692.68	c	0.49	0.215	0.527	0.99	992.31
P4	P4-4	Class 4	1	650	-	-	307.7	180.46	c	0.49	1.053	1.263	0.51	102.00
	P4-6	Class 4	1	650	-	-	633.5	609.22	c	0.49	0.822	0.990	0.65	266.95
	P4-10	Class 3	1	650	-	1158.00	-	2770.89	c	0.49	0.521	0.715	0.83	625.54
	P4-16	Class 3	1	500	-	1811.50	-	11083.88	c	0.49	0.286	0.562	0.96	866.22
	P4-20	Class 3	1	480	-	2230.50	-	21248.01	c	0.49	0.224	0.531	0.99	1057.30
P5	P5-4	Class 4	1	650	-	-	307.8	179.63	c	0.49	1.055	1.266	0.51	101.74
	P5-6	Class 4	1	650	-	-	635.0	608.30	c	0.49	0.824	0.992	0.65	267.17
	P5-10	Class 3	1	650	-	1181.70	-	2763.38	c	0.49	0.527	0.719	0.83	635.72
	P5-16	Class 3	1	500	-	1873.00	-	10888.58	c	0.49	0.293	0.566	0.95	892.09
	P5-20	Class 3	1	480	-	2326.50	-	20607.89	c	0.49	0.233	0.535	0.98	1098.09
P6	P6-4	Class 4	1	650	-	-	307.9	178.76	c	0.49	1.058	1.270	0.51	101.47
	P6-6	Class 4	1	650	-	-	635.8	603.54	c	0.49	0.827	0.996	0.64	266.51
	P6-10	Class 3	1	650	-	1191.20	-	2740.71	c	0.49	0.532	0.722	0.83	638.94
	P6-16	Class 3	1	500	-	1897.40	-	10809.25	c	0.49	0.296	0.567	0.95	902.27
	P6-20	Class 3	1	480	-	2364.60	-	20502.06	c	0.49	0.235	0.536	0.98	1114.63

Torsional-flexural buckling resistance (fixed BC)

Group	Profile number	Class	γ_{M1}	f_{yb} , Mpa	f_{ya}	A_g , mm ²	A_{eff} , mm ²	N_{crTF} , kN	Buckling curve	α	λ	Φ	χ	N_{brdTF} , kN
P1	P1-4	Class 4	1	650	-	-	309.1	172.39	c	0.49	1.080	1.298	0.50	99.50
	P1-6	Class 4	1	650	-	-	627.1	584.78	c	0.49	0.835	1.004	0.64	260.99
	P1-10	Class 3	1	-	674.6	1015.00	-	2599.45	c	0.49	0.513	0.708	0.84	572.15
	P1-16	Class 3	1	500	-	1444.10	-	9596.97	c	0.49	0.274	0.556	0.96	694.78
	P1-20	Class 3	1	480	-	1656.40	-	15830.27	c	0.49	0.224	0.531	0.99	785.31
P2	P2-4	Class 4	1	650	-	-	308.7	172.09	c	0.49	1.080	1.298	0.50	99.34
	P2-6	Class 4	1	650	-	-	629.4	596.44	c	0.49	0.828	0.997	0.64	263.67
	P2-10	Class 3	1	650	-	1060.40	-	2642.47	c	0.49	0.511	0.707	0.84	576.89
	P2-16	Class 3	1	500	-	1560.70	-	10203.00	c	0.49	0.277	0.557	0.96	749.98
	P2-20	Class 3	1	480	-	1838.60	-	17764.59	c	0.49	0.223	0.530	0.99	872.24
P3	P3-4	Class 4	1	650	-	-	308.0	174.34	c	0.49	1.072	1.288	0.50	100.01
	P3-6	Class 4	1	650	-	-	632.1	607.04	c	0.49	0.823	0.991	0.65	266.20
	P3-10	Class 3	1	650	-	1121.30	-	2704.49	c	0.49	0.519	0.713	0.83	606.57
	P3-16	Class 3	1	500	-	1717.00	-	10575.05	c	0.49	0.285	0.561	0.96	821.44
	P3-20	Class 3	1	480	-	2082.90	-	19125.94	c	0.49	0.229	0.533	0.99	985.22
P4	P4-4	Class 4	1	650	-	-	307.7	180.21	c	0.49	1.054	1.264	0.51	101.91
	P4-6	Class 4	1	650	-	-	633.5	607.24	c	0.49	0.823	0.992	0.65	266.60
	P4-10	Class 3	1	650	-	1158.00	-	2743.41	c	0.49	0.524	0.717	0.83	624.43
	P4-16	Class 3	1	500	-	1811.50	-	10794.80	c	0.49	0.290	0.564	0.95	864.46
	P4-20	Class 3	1	480	-	2230.50	-	20374.12	c	0.49	0.229	0.533	0.99	1054.71
P5	P5-4	Class 4	1	650	-	-	307.8	179.58	c	0.49	1.056	1.267	0.51	101.72
	P5-6	Class 4	1	650	-	-	635.0	607.87	c	0.49	0.824	0.992	0.65	267.09
	P5-10	Class 3	1	650	-	1181.70	-	2757.59	c	0.49	0.528	0.720	0.83	635.48
	P5-16	Class 3	1	500	-	1873.00	-	10820.96	c	0.49	0.294	0.566	0.95	891.65
	P5-20	Class 3	1	480	-	2326.50	-	20376.50	c	0.49	0.234	0.536	0.98	1097.34
P6	P6-4	Class 4	1	650	-	-	307.9	178.75	c	0.49	1.058	1.270	0.51	101.47
	P6-6	Class 4	1	650	-	-	635.8	603.40	c	0.49	0.828	0.996	0.64	266.49
	P6-10	Class 3	1	650	-	1191.20	-	2738.79	c	0.49	0.532	0.723	0.83	638.85
	P6-16	Class 3	1	500	-	1897.40	-	10799.46	c	0.49	0.296	0.568	0.95	902.20
	P6-20	Class 3	1	480	-	2364.60	-	20469.12	c	0.49	0.235	0.536	0.98	1114.52

Moment buckling resistance of Class 4 cross-sections for bending about z-axis

Group	Profile number	b_p , mm	t, mm	Cross-section	f_{yb} , Mpa	W_{effz} , mm ³	χ_{LT}	M_{bRd} , kNm
P1	P1-4	55.6	4	Effective	650	1251.9	1	0.814
	P1-6	53.49	6	Effective	650	3388.8	1	2.203
P2	P2-4	56.75	4	Effective	650	1127.1	1	0.733
	P2-6	55.13	6	Effective	650	3086.2	1	2.006
P3	P3-4	58.23	4	Effective	650	855.35	1	0.556
	P3-6	57.34	6	Effective	650	2377.5	1	1.545
P4	P4-4	59.1	4	Effective	650	566.97	1	0.369
	P4-6	58.64	6	Effective	650	1592.4	1	1.035
P5	P5-4	59.63	4	Effective	650	291.98	1	0.190
	P5-6	59.44	6	Effective	650	841.24	1	0.547
P6	P6-4	59.82	4	Effective	650	190.36	1	0.124
	P6-6	59.73	6	Effective	650	572.57	1	0.372

Combined compression and bending interaction (fixed BC)

Group	Profile number	Moment buckling resistance	Compressionb uckling resistance	e _n , mm	Acting axial force	Acting moment	Member stability check		
		M _{bRd} , kNm	N _{bRd} , kN		N _{ed} , kN	M _{ed} , kNm			
P1	P1-4	0.814	99.498	6.21	48	0.295	0.998	<	1
	P1-6	2.203	260.986	0.76	218	0.166	0.992	<	1
P2	P2-4	0.733	99.34	5.96	46	0.274	0.994	<	1
	P2-6	2.006	263.67	1.07	208	0.223	0.999	<	1
P3	P3-4	0.556	100.012	4.97	44	0.219	0.992	<	1
	P3-6	1.545	266.196	1.23	192	0.236	0.992	<	1
P4	P4-4	0.369	101.914	3.54	43	0.152	0.994	<	1
	P4-6	1.035	263.107	1.02	181	0.184	0.991	<	1
P5	P5-4	0.190	75.105	1.84	37	0.067	0.999	<	1
	P5-6	0.547	135.907	0.57	106	0.060	0.991	<	1
P6	P6-4	0.124	32.067	0.93	22	0.021	0.991	<	1
	P6-6	0.372	69.683	0.3	62	0.018	0.995	<	1

Combined table of compression buckling resistance according to EN (fixed BC)

Group	Profile number	Class	Hand calculation			
			Flexural buckling	Torsional buckling	Torsional-flexural buckling	Buckl mode
			N _{brdF} , kN	N _{brdT} , kN	N _{brdTF} , kN	
P1	P1-4	Class 4	182	100	99	FT
	P1-6	Class 4	349	264	261	FT
	P1-10	Class 3	561	580	572	F
	P1-16	Class 3	591	707	695	F
	P1-20	Class 3	633	805	785	F
P2	P2-4	Class 4	179	100	99	FT
	P2-6	Class 4	345	266	264	FT
	P2-10	Class 3	563	582	577	F
	P2-16	Class 3	648	758	750	F
	P2-20	Class 3	726	886	872	F
P3	P3-4	Class 4	168	100	100	FT
	P3-6	Class 4	321	267	266	FT
	P3-10	Class 3	557	609	607	F
	P3-16	Class 3	699	826	821	F
	P3-20	Class 3	828	992	985	F
P4	P4-4	Class 4	142	102	102	FT
	P4-6	Class 4	263	267	267	F
	P4-10	Class 3	480	626	624	F
	P4-16	Class 3	680	866	864	F
	P4-20	Class 3	848	1057	1055	F
P5	P5-4	Class 4	75	102	102	F
	P5-6	Class 4	136	267	267	F
	P5-10	Class 3	303	636	635	F
	P5-16	Class 3	588	892	892	F
	P5-20	Class 3	803	1098	1097	F
P6	P6-4	Class 4	32	101	101	F
	P6-6	Class 4	70	267	266	F
	P6-10	Class 3	213	639	639	F
	P6-16	Class 3	534	902	902	F
	P6-20	Class 3	776	1115	1115	F

L- local
F- flexural
T- torsional
FT- flexural-torsional

**Combined table of compression buckling resistance according to EN for fixed BC
(neglecting additional moment for Class 4 cross-sections)**

Group	Profile number	Class	Hand calculation			
			Flexural buckling	Torsional buckling	Torsional-flexural buckling	Buckl mode
			N _{bRdF} , kN	N _{bRdT} , kN	N _{bRdTF} , kN	
P1	P1-4	Class 4	64	48	48	FT
	P1-6	Class 4	280	222	218	FT
	P1-10	Class 3	561	580	572	F
	P1-16	Class 3	591	707	695	F
	P1-20	Class 3	633	805	785	F
P2	P2-4	Class 4	61	46	46	FT
	P2-6	Class 4	256	208	208	FT
	P2-10	Class 3	563	582	577	F
	P2-16	Class 3	648	758	750	F
	P2-20	Class 3	726	886	872	F
P3	P3-4	Class 4	56	44	43	FT
	P3-6	Class 4	223	192	184	FT
	P3-10	Class 3	557	609	607	F
	P3-16	Class 3	699	826	821	F
	P3-20	Class 3	828	992	985	F
P4	P4-4	Class 4	50	43	43	FT
	P4-6	Class 4	181	184	184	F
	P4-10	Class 3	480	626	624	F
	P4-16	Class 3	680	866	864	F
	P4-20	Class 3	848	1057	1055	F
P5	P5-4	Class 4	37	43	43	F
	P5-6	Class 4	106	181	181	F
	P5-10	Class 3	303	636	635	F
	P5-16	Class 3	588	892	892	F
	P5-20	Class 3	803	1098	1097	F
P6	P6-4	Class 4	22	48	48	F
	P6-6	Class 4	62	193	193	F
	P6-10	Class 3	213	639	639	F
	P6-16	Class 3	534	902	902	F
	P6-20	Class 3	776	1115	1115	F

L- local
 F- flexural
 T- torsional
 FT- flexural-torsional

Combined table of compression buckling resistance according to EN (pinned BC)

Group	Profile number	Class	Hand calculation			
			Flexural buckling	Torsional buckling	Torsional-flexural buckling	Buckl mode
			N _{brdF} , kN	N _{brdT} , kN	N _{brdTF} , kN	
P1	P1-4	Class 4	137	97	94	FT
	P1-6	Class 4	232	258	246	F
	P1-10	Class 3	338	575	534	F
	P1-16	Class 3	355	705	635	F
	P1-20	Class 3	359	804	705	F
P2	P2-4	Class 4	130	97	95	FT
	P2-6	Class 4	220	260	252	F
	P2-10	Class 3	336	577	549	F
	P2-16	Class 3	401	756	699	F
	P2-20	Class 3	441	884	798	F
P3	P3-4	Class 4	106	97	97	FT
	P3-6	Class 4	176	261	258	F
	P3-10	Class 3	292	603	589	F
	P3-16	Class 3	415	823	786	F
	P3-20	Class 3	511	990	927	F
P4	P4-4	Class 4	67	99	98	F
	P4-6	Class 4	109	261	259	F
	P4-10	Class 3	198	619	613	F
	P4-16	Class 3	346	863	844	F
	P4-20	Class 3	475	1054	1012	F
P5	P5-4	Class 4	24	98	98	F
	P5-6	Class 4	41	261	261	F
	P5-10	Class 3	97	629	628	F
	P5-16	Class 3	239	888	882	F
	P5-20	Class 3	383	1094	1070	F
P6	P6-4	Class 4	9	98	98	F
	P6-6	Class 4	20	260	260	F
	P6-10	Class 3	63	632	631	F
	P6-16	Class 3	199	898	897	F
	P6-20	Class 3	345	1111	1094	F

L- local
F- flexural
T- torsional
FT- flexural-torsional

**Combined table of compression buckling resistance according to EN -pinned BC
(neglecting additional moment for Class 4 cross-sections)**

Group	Profile number	Class	Hand calculation			
			Flexural buckling	Torsional buckling	Torsional-flexural buckling	Buckl mode
			N _{brdF} , kN	N _{brdT} , kN	N _{brdTF} , kN	
P1	P1-4	Class 4	56	46	46	FT
	P1-6	Class 4	197	216	208	F
	P1-10	Class 3	338	575	534	F
	P1-16	Class 3	355	705	635	F
	P1-20	Class 3	359	804	705	F
P2	P2-4	Class 4	53	45	45	FT
	P2-6	Class 4	178	205	200	F
	P2-10	Class 3	336	577	549	F
	P2-16	Class 3	401	756	699	F
	P2-20	Class 3	441	884	798	F
P3	P3-4	Class 4	45	43	43	FT
	P3-6	Class 4	139	189	188	F
	P3-10	Class 3	292	603	589	F
	P3-16	Class 3	415	823	786	F
	P3-20	Class 3	511	990	927	F
P4	P4-4	Class 4	34	42	42	F
	P4-6	Class 4	89	180	180	F
	P4-10	Class 3	198	619	613	F
	P4-16	Class 3	346	863	844	F
	P4-20	Class 3	475	1054	1012	F
P5	P5-4	Class 4	16	42	42	F
	P5-6	Class 4	37	178	178	F
	P5-10	Class 3	97	629	628	F
	P5-16	Class 3	239	888	882	F
	P5-20	Class 3	383	1094	1070	F
P6	P6-4	Class 4	8	47	47	F
	P6-6	Class 4	19	188	188	F
	P6-10	Class 3	63	632	631	F
	P6-16	Class 3	199	898	897	F
	P6-20	Class 3	345	1111	1094	F

L- local
 F- flexural
 T- torsional
 FT- flexural-torsional

Attachment 14

This calculation procedure shows the way how the data calculated in Excel sheets was obtained.

Following characteristics are calculated on the basis of cross-sections P1-4 (Class 4) and P1-10 (Class 3) taken as an example:

1. Evaluation of increased average yield strength:
2. Classification of cross-section.
3. Determination of effective width of unstiffened elements (EN 1993-1-3, ch.5.5.2)
4. Critical force assessment
5. Determination of buckling resistance of members.

All the data for specimens P1-P6 with thicknesses $t=4\text{mm}$, 6mm , 10mm , 16mm and 20mm can be found in Attachments. Fixed boundary conditions are used.

1. Evaluation of increased average yield strength:

Evaluation of increased average yield strength is performed on the basis of EN 1993-1-3, ch.3.2.2(3).

It is impossible to determine average yield strength for specimen **P1-4** according to EN 1993-1-3 because following requirement is not satisfied:

- The average yield strength f_{ya} may be utilised in determining the cross-section resistance and the buckling resistance of an axially loaded compression member with a fully effective cross-section.

Example of calculation of average yield strength will be shown for P1-10:

Cross-section P1-10

$f_{yb} := 650\text{MPa}$ - basic yield strength

$f_u := 700\text{MPa}$ - tensile strength

$t_{P1.10} := 10\text{mm}$ - thickness of leg

$k := 5$ - numerical coefficient

$n := 1$ - number of 90 deg bends

$A_g := 1015\text{mm}^2$ - gross area of cross-section

$$f_{ya} := f_{yb} + (f_u - f_{yb}) \cdot \frac{k \cdot n \cdot (t_{P1.10})^2}{A_g} = 674.631 \cdot \text{MPa}$$

$$f_{ya} = 674.631 \cdot \text{MPa} < \frac{f_u + f_{yb}}{2} = 675 \cdot \text{MPa}$$

Average yield strength can be used for calculations.

2. Classification of cross-secection (EN 1993-1-3, ch.5.5.2)

Classification has been performed according to EN 1993-1-1, Table 5.2 for angles in compression. The dimensions of legs were taken as the distance from the edge of profile to the midpoint of outer corner.

Cross-section P1-4

a) Classification according to Table 5.2 for angles

$$f_{yb} = 650 \cdot \text{MPa}$$

$$b_{P1.4} := 57.05 \text{ mm} \quad \text{- dimensions of the leg}$$

$$h_{P1.4} := 57.07 \text{ mm}$$

$$t_{P1.4} := 4 \text{ mm}$$

$$\varepsilon := \sqrt{\frac{235 \text{ MPa}}{f_{yb}}} = 0.601$$

Verification:

$$\frac{h_{P1.4}}{t_{P1.4}} = 14.268 > 15 \cdot \varepsilon = 9.019$$

$$\frac{b_{P1.4} + h_{P1.4}}{2t_{P1.4}} = 14.265 > 11.5 \cdot \varepsilon = 6.915$$

Section is Class 4

a) Classification according to Table 5.2 for outstand flanges

$$c_{P1.4} := b_{P1.4} = 57.05 \cdot \text{mm} \quad \text{- dimension of leg}$$

$$\frac{c_{P1.4}}{t_{P1.4}} = 14.262 > 14 \cdot \varepsilon = 8.418$$

Section is Class 4

Cross-section P1-10

a) Classification according to Table 5.2 for angles

$$f_{yb} = 650 \cdot \text{MPa}$$

$$b_{P1.10} := 52.68 \text{ mm} \quad \text{- dimensions of the leg}$$

$$h_{P1.10} := 52.68 \text{ mm}$$

$$t_{P1.10} = 10 \cdot \text{mm}$$

$$\varepsilon := \sqrt{\frac{235 \text{ MPa}}{f_{yb}}} = 0.601$$

Verification:

$$\frac{h_{P1.10}}{t_{P1.10}} = 5.268 < 15 \cdot \varepsilon = 9.019$$

$$\frac{b_{P1.4} + h_{P1.4}}{2t_{P1.4}} = 14.265 < 11.5 \cdot \varepsilon = 6.915$$

Section is Class 3

a) Classification according to Table 5.2 for outstand flanges

$$c_{P1.10} := b_{P1.10} = 52.68 \cdot \text{mm} \quad \text{dimension of leg}$$

$$\frac{c_{P1.10}}{t_{P1.10}} = 5.268 < 9 \cdot \varepsilon = 5.412$$

Section is Class 2

3. Determination of effective width of unstiffened elements (EN 1993-1-3, ch.5.5.2)

This chapter applies only to cross-sections Class 4. Calculation is performed according to EN 1993-1-3, ch.5.5.2.

Cross-section P 1-4

$$f_{yb} := 650 \text{ MPa}$$

$$E := 210 \text{ GPa}$$

$$\nu := 0.3$$

$$t_{P1.4} = 4 \cdot \text{mm} \quad \text{- thickness of the flat part}$$

$$b_p := 55.6 \text{ mm} \quad \text{- notional width}$$

$$A_{P1.4} := 450.01 \text{ mm}^2 \quad \text{- gross area of cross section}$$

Outstand compression element:

$$\psi := 1 \quad k_{\sigma} := 0.43$$

$$\varepsilon := \sqrt{\frac{235 \text{ MPa}}{f_{yb}}} = 0.601$$

$$\lambda_p := \frac{\frac{b_p}{t_{P1.4}}}{28.4 \cdot \varepsilon \cdot \sqrt{k_{\sigma}}} = 1.241 > 0.748$$

$$\rho := \frac{\lambda_p - 0.188}{\lambda_p^2} = 0.684$$

$$b_{\text{eff}} := \rho \cdot b_p = 38.007 \cdot \text{mm}$$

4. Determination of buckling critical stress for local buckling of Class 4 cross-sections

Elastic buckling stress has been calculated for P1-4 cross-section according to Darko Beg (2010):

$$\sigma_{cr} := \frac{k_{\sigma} \cdot \pi^2 \cdot E}{12(1 - \nu^2) \cdot \left(\frac{b_p}{t_{P1.4}}\right)^2} = 422.411 \cdot \text{MPa}$$

$$P_{cr} := \sigma_{cr} \cdot A_{P1.4} = 190.089 \cdot \text{kN} \quad - \text{ elastic critical load for local buckling.}$$

5. Critical force assessment

Cross-section P 1-4

$L := 600\text{mm}$ - real length of specimen

$k := 0.5$ - coefficient for buckling length for fixed-fixed conditions

$L_E := k \cdot L = 300 \cdot \text{mm}$ - buckling length.

$L_{ET} := k \cdot L = 300 \cdot \text{mm}$ - warping and torsion length.

$E := 210000\text{MPa}$ - elastic modulus

$G := 80700\text{MPa}$ - shear modulus

$I_y := 260350\text{mm}^4$ - moments of inertia of cross-section about y and z axis

$I_z := 58664\text{mm}^4$

$I := \min(I_y, I_z) = 5.866 \times 10^4 \cdot \text{mm}^4$

$I_t := 2310\text{mm}^4$ - torsional constant

$I_w := 611960\text{mm}^6$ - warping constant

$A := 450.11\text{mm}^2$ - gross area of cross-section

$y_c := 21\text{mm}$ - distance between shear centre and centre of gravity

$i_c := \sqrt{y_c^2 + \frac{(I_y + I_z)}{A}} = 33.908 \cdot \text{mm}$ - radius of polar gyration

$\beta := 1 - \left(\frac{y_c}{i_c}\right)^2 = 0.616$

Elastic critical load for flexural buckling:

$$N_{\text{cr.z.P1.4}} := \frac{\pi^2 \cdot E \cdot I_z}{L_E^2} = 1351 \cdot \text{kN}$$

$$N_{\text{cr.y.P1.4}} := \frac{\pi^2 \cdot E \cdot I_y}{L_E^2} = 5996 \cdot \text{kN}$$

$$N_{cr.F.P1.4} := \min(N_{cr.z.P1.4}, N_{cr.y.P1.4}) = 1351 \cdot \text{kN}$$

Elastic critical load for torsional buckling:

$$N_{cr.T.P1.4} := \frac{1}{i_c^2} \cdot \left(G \cdot I_t + \frac{\pi^2 \cdot E \cdot I_w}{L_{ET}^2} \right) = 174 \cdot \text{kN}$$

Elastic critical load for flexural-torsional buckling:

$$N_{cr.TF.P1.4} := \frac{1}{2\beta} \left[(N_{cr.y.P1.4} + N_{cr.T.P1.4}) - \sqrt{(N_{cr.y.P1.4} + N_{cr.T.P1.4})^2 - 4\beta \cdot N_{cr.y.P1.4} \cdot N_{cr.T.P1.4}} \right] = 172 \cdot \text{kN}$$

Cross-section P 1-10

$L = 600 \cdot \text{mm}$ - real length of the specimen

$k = 0.5$ - coefficient for buckling length

$L_E := k \cdot L = 0.3 \text{ m}$ - buckling length.

$L_{ET} := k \cdot L = 0.3 \text{ m}$ - warping and torsion length.

$E := 210000 \text{ MPa}$ - elastic modulus

$G := 80700 \text{ MPa}$ - shear modulus

$I_y := 555120 \text{ mm}^4$
- moments of inertia of cross-section about y and z axis

$I_z := 101620 \text{ mm}^4$

$I := \min(I_y, I_z) = 1.016 \times 10^5 \cdot \text{mm}^4$

$I_t := 31583 \text{ mm}^4$ - torsional constant

$I_w := 8266900 \text{ mm}^6$ - warping constant

$A := 1015 \text{ mm}^2$ - gross area of cross-section

$y_c := 18 \text{ mm}$ - distance between shear centre and centre of gravity

$$i_c := \sqrt{y_c^2 + \frac{(I_y + I_z)}{A}} = 31.161 \cdot \text{mm} \quad - \text{radius of polar gyration}$$

$$\beta := 1 - \left(\frac{y_c}{i_c} \right)^2 = 0.666$$

Elastic critical load for flexural buckling:

$$N_{\text{cr.z.P1.10}} := \frac{\pi^2 \cdot E \cdot I_z}{L_E^2} = 2340 \cdot \text{kN}$$

$$N_{\text{cr.y.P1.10}} := \frac{\pi^2 \cdot E \cdot I_y}{L_E^2} = 12784 \cdot \text{kN}$$

$$N_{\text{cr.F.P1.10}} := \min(N_{\text{cr.z.P1.10}}, N_{\text{cr.y.P1.10}}) = 2340 \cdot \text{kN}$$

Elastic critical load for torsional buckling:

$$N_{\text{cr.T.P1.10}} := \frac{1}{i_c^2} \cdot \left(G \cdot I_t + \frac{\pi^2 \cdot E \cdot I_w}{L_{ET}^2} \right) = 2821 \cdot \text{kN}$$

Elastic critical load for flexural-torsional buckling:

$$N_{\text{cr.TF.P1.10}} := \frac{1}{2\beta} \left[(N_{\text{cr.y.P1.10}} + N_{\text{cr.T.P1.10}}) - \sqrt{(N_{\text{cr.y.P1.10}} + N_{\text{cr.T.P1.10}})^2 - 4\beta \cdot N_{\text{cr.y.P1.10}} \cdot N_{\text{cr.T.P1.10}}} \right] = 2599 \cdot \text{kN}$$

6. Verification of resistance of members:

Cross-section P 1-4

$f_{yb} := 650 \text{ MPa}$ - basic yield strength

$A_{\text{eff.P1.4}} := 309.1 \text{ mm}^2$ - effective area of cross-section

$W_{\text{eff.z}} := 1251.9 \text{ mm}^3$ - minimum effective section modulus for bending about z-axis

$\gamma_{M0} := 1$
- partial factors

$\gamma_{M1} := 1$

Compression

Cross-section resistance is verified according to EN 1993-1-3, ch. 6.1.3(1):

$$N_{c.Rd} := \frac{A_{\text{eff.P1.4}} \cdot f_{yb}}{\gamma_{M0}} = 200.915 \cdot \text{kN}$$

In compression members buckling resistance according to EN 1993-1-3, ch. 6.2 and EN 1993-1-1, ch.6.3.1. Buckling resistance should be taken as the minimum value of flexural, torsional or torsional-flexural buckling resistance. It can be done by choosing the minimum value of elastic critical load. However, further for the sake of analysis all three buckling resistances will be shown. Minimum value will provide buckling resistance of the member.

1. Flexural buckling resistance:

$$N_{\text{cr.F.P1.4}} = 1351 \cdot \text{kN}$$

buckling curve c

$$\alpha := 0.49$$

$$\lambda := \sqrt{\frac{A_{\text{eff.P1.4}} \cdot f_{yb}}{N_{\text{cr.F.P1.4}}}} = 0.386$$

$$\phi := 0.5 \left[1 + \alpha \cdot (\lambda - 0.2) + \lambda^2 \right] = 0.62$$

$$\chi := \frac{1}{\phi + \sqrt{\phi^2 - \lambda^2}} = 0.905$$

$$N_{\text{bRdF.P1.4}} := \frac{\chi \cdot A_{\text{eff.P1.4}} \cdot f_{yb}}{\gamma_{M1}} = 181.8 \cdot \text{kN}$$

2. Torsional buckling resistance:

$$N_{cr,T,P1.4} = 174.4 \cdot \text{kN}$$

buckling curve c

$$\alpha := 0.49$$

$$\lambda := \sqrt{\frac{A_{eff,P1.4} \cdot f_{yb}}{N_{cr,T,P1.4}}} = 1.073$$

$$\phi := 0.5 \left[1 + \alpha \cdot (\lambda - 0.2) + \lambda^2 \right] = 1.29$$

$$\chi := \frac{1}{\phi + \sqrt{\phi^2 - \lambda^2}} = 0.499$$

$$N_{bRdT,P1.4} := \frac{\chi \cdot A_{eff,P1.4} \cdot f_{yb}}{\gamma_{M1}} = 100.2 \cdot \text{kN}$$

3. Torsional-flexural buckling resistance:

$$N_{cr,TF,P1.4} = 172.4 \cdot \text{kN}$$

buckling curve c

$$\alpha := 0.49$$

$$\lambda := \sqrt{\frac{A_{eff,P1.4} \cdot f_{yb}}{N_{cr,TF,P1.4}}} = 1.079$$

$$\phi := 0.5 \left[1 + \alpha \cdot (\lambda - 0.2) + \lambda^2 \right] = 1.298$$

$$\chi := \frac{1}{\phi + \sqrt{\phi^2 - \lambda^2}} = 0.495$$

$$N_{bRdTF,P1.4} := \frac{\chi \cdot A_{eff,P1.4} \cdot f_{yb}}{\gamma_{M1}} = 99.5 \cdot \text{kN}$$

Buckling resistance of the member is:

$$N_{b,Rd,P1.4} := \min(N_{bRdF,P1.4}, N_{bRdF,P1.4}, N_{bRdTF,P1.4}) = 99.514 \cdot \text{kN}$$

Bending

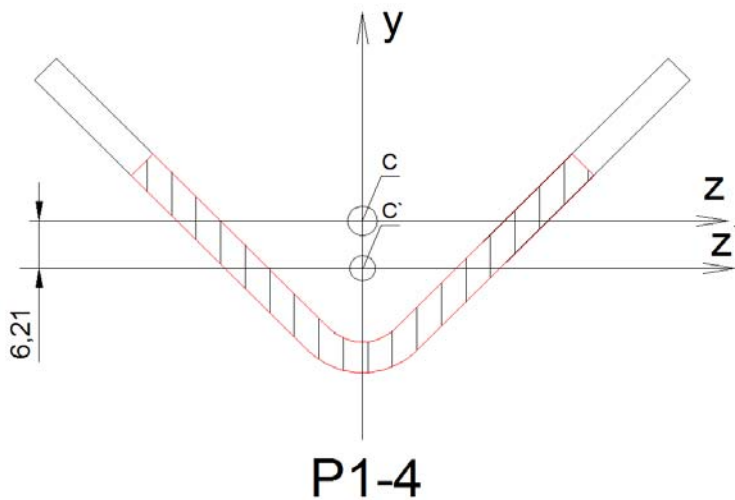
Due to shift of centroid of effective cross-section in cross-section P1-4 appears shift of centroid. As a result account should be taken of additional moment.

According to EN 1993-1-1, ch.6.2.2.5(4) additional moment is calculated as follows:

$$\Delta M_{Ed} = N_{Ed} \cdot e_N$$

where

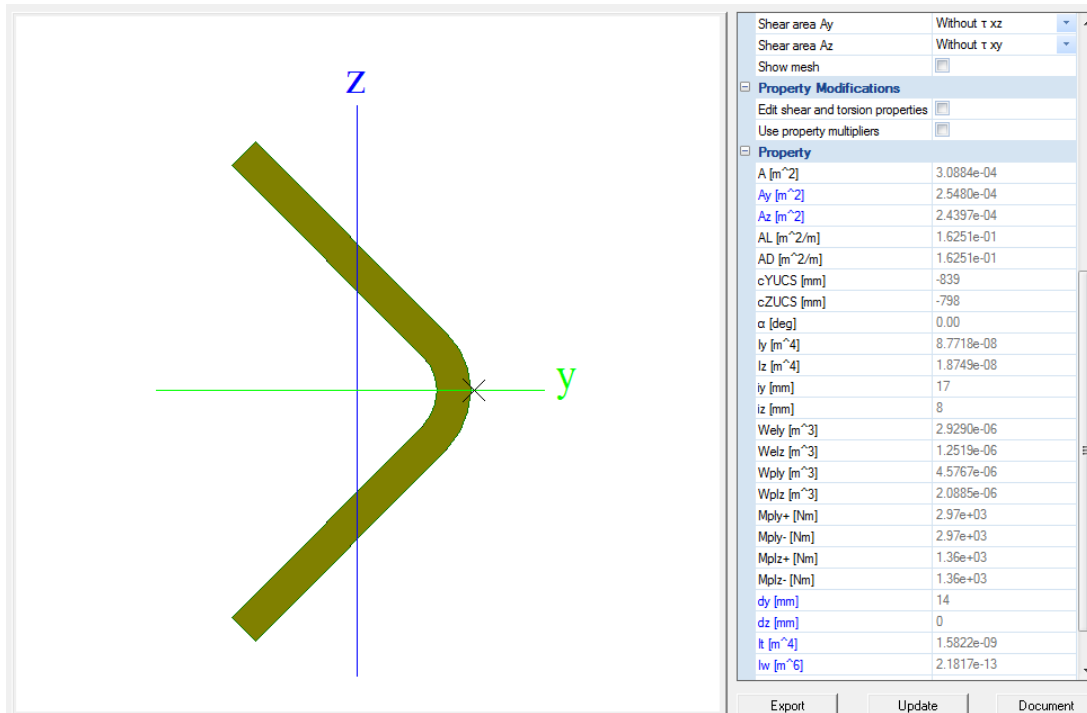
$e_N := 6.21\text{mm}$ - shift of centroid along y-axis (measured in AutoCAD)



Firstly cross-section resistance is calculated according to EN 1993-1-3, ch.6.1.4.1(1):

$$M_{zRk.P1.4} := \frac{f_{yb} \cdot W_{eff.z}}{\gamma_{M0}} = 0.814 \cdot \text{kN} \cdot \text{m}$$

$W_{eff.z} = 1.252 \times 10^3 \cdot \text{mm}^3$ - effective section modulus calculated in software SCIA for effective cross-section and bending about z axis.



Wely [m ³]	2.9290e-06
Welz [m ³]	1.2519e-06
Wply [m ³]	4.5767e-06
Wplz [m ³]	2.0885e-06

Effective section modulus has been taken as Welz from SCIA software.

As long as L-sections are symmetric about strong axis and bent about weak axis it can be stated verification of lateral-torsional buckling is not needed.

$$\chi_{LT} := 1$$

Therefore, it can be stated that buckling resistance is equal to cross-section resistance.

$$M_{b.Rd.P1.4} := M_{zRk.P1.4} = 0.814 \cdot \text{kN} \cdot \text{m}$$

Combination of bending and compression

For combination of bending and compression will verified stability of the member as long its governing verification. Calculation is made on the basis of alternative method described in EN 1993-1-3, ch.6.2.5:

$$\left(\frac{N_{Ed}}{N_{b.R}} \right)^{0.8} + \left(\frac{M_{Ed}}{M_{b.R}} \right)^{0.8} < 1$$

where

$$M_{Ed} = N_{Ed} \cdot e_N \quad \text{in particular case.}$$

This approach is used to determine maximum resistance of the member:

$$\text{Lets assume } N_{Ed} := 47.5 \text{ kN}$$

$$N_{Ed} \cdot e_N = 0.295 \cdot \text{kN} \cdot \text{m}$$

$$\left(\frac{N_{Ed}}{N_{b,Rd.P1.4}} \right)^{0.8} + \left(\frac{N_{Ed} \cdot e_N}{M_{b,Rd.P1.4}} \right)^{0.8} = 0.997 < 1$$

Therefore, assumed axial force is the maximum resistance of the member.

The drop in resistance can be seen as follows:

$$\frac{N_{Ed}}{N_{b,Rd.P1.4}} = 0.477$$

Cross-section P 1-10

$$f_{yb} := 650 \text{ MPa} \quad \text{- basic yield strength}$$

$$f_{ya} = 674.631 \cdot \text{MPa} \quad \text{- average yield strength}$$

$$A_{P1.10} := 1015 \text{ mm}^2 \quad \text{- area of cross-section}$$

$$\gamma_{M0} := 1 \quad \text{- partial factors}$$

$$\gamma_{M1} := 1$$

Cross-section P1-10 is subjected only to compression. Therefore only resistance to compression will be verified. As long as buckling resistance is governing cross-section resistance check is not required.

Compression

In compression members buckling resistance is verified according to EN 1993-1-3, ch. 6.2 and EN 1993-1-1, ch.6.3.1. Buckling resistance should be taken as the minimum value of flexural, torsional or torsional-flexural buckling resistance. It can be done by choosing the minimum value of elastic critical load. However, further for the sake of analysis all three buckling resistances will be shown. Minimum value will provide buckling resistance of the member.

1. Flexural buckling resistance:

$$N_{cr,F.P1.10} = 2340 \cdot \text{kN}$$

buckling curve c

$$\alpha := 0.49$$

$$\lambda := \sqrt{\frac{A \cdot f_{ya}}{N_{cr.F.P1.10}}} = 0.541$$

$$\phi := 0.5 \left[1 + \alpha \cdot (\lambda - 0.2) + \lambda^2 \right] = 0.73$$

$$\chi := \frac{1}{\phi + \sqrt{\phi^2 - \lambda^2}} = 0.82$$

$$N_{bRdF.P1.10} := \frac{\chi \cdot A \cdot f_{ya}}{\gamma_{M1}} = 561.4 \cdot \text{kN}$$

2. Torsional buckling resistance:

$$N_{cr.T.P1.10} = 2820.8 \cdot \text{kN}$$

buckling curve c

$$\alpha := 0.49$$

$$\lambda := \sqrt{\frac{A_{P1.10} \cdot f_{ya}}{N_{cr.T.P1.10}}} = 0.493$$

$$\phi := 0.5 \left[1 + \alpha \cdot (\lambda - 0.2) + \lambda^2 \right] = 0.693$$

$$\chi := \frac{1}{\phi + \sqrt{\phi^2 - \lambda^2}} = 0.847$$

$$N_{bRdT.P1.4} := \frac{\chi \cdot A_{P1.10} \cdot f_{ya}}{\gamma_{M1}} = 580 \cdot \text{kN}$$

3. Torsional-flexural buckling resistance:

$$N_{cr.TF.P1.10} = 2599.5 \cdot \text{kN}$$

buckling curve c

$$\alpha := 0.49$$

$$\lambda := \sqrt{\frac{A_{P1.10} \cdot f_{ya}}{N_{cr.TF.P1.10}}} = 0.513$$

$$\phi := 0.5 \left[1 + \alpha \cdot (\lambda - 0.2) + \lambda^2 \right] = 0.708$$

$$\chi := \frac{1}{\phi + \sqrt{\phi^2 - \lambda^2}} = 0.836$$

$$N_{bRdTF.P1.10} := \frac{\chi \cdot A_{P1.10} \cdot f_{ya}}{\gamma_{M1}} = 572.1 \cdot \text{kN}$$

Buckling resistance of the member is:

$$N_{b.Rd.P1.10} := \min(N_{bRdF.P1.10}, N_{bRdF.P1.10}, N_{bRdTF.P1.10}) = 561.4 \cdot \text{kN}$$

**Combined table of buckling resistance - fixed BC
(additional moment and compression for Class 4)**

Group	Profile number	Class	Hand calculation				Abaqus shell model COG										
			Flexural buckling	Torsional buckling	Torsional-flexural buckling	Buckl mode	Mesacasa (2013)					EN, ECCS					Buckl mode
							Imperfection		Imperf, mm	fu, kN	Diff (EN vs FEA)	Imperfection		Imperf, mm	fu, kN	Diff (EN vs FEA)	
							Local	Global				Local	Global				
N _{brdF} , kN	N _{brdT} , kN	N _{brdTF} , kN															
P1	P1-4	Class 4	64	48	48	FT	L/1000	-	0.6	190	75%	b/200	-	0.28	192	75%	T/L
	P1-6	Class 4	280	222	218	FT	L/1000	-	0.6	419	48%	b/200	-	0.27	428	49%	T/L
	P1-10	Class 3	561	580	572	F	L/1000	L/1000	0.6+0.6	625	10%	b/200	L/1000	0.25+0.6	626	10%	F
	P1-16	Class 3	591	707	695	F	L/1000	L/1000	0.6+0.6	675	12%	b/200	L/1000	0.21+0.6	675	12%	F
	P1-20	Class 3	633	805	785	F	L/1000	L/1000	0.6+0.6	732	14%	b/200	L/1000	0.19+0.6	733	14%	F
P2	P2-4	Class 4	61	46	46	FT	L/1000	-	0.6	193	76%	b/200	-	0.28	195	76%	T/L
	P2-6	Class 4	256	208	208	FT	L/1000	-	0.6	431	52%	b/200	-	0.28	435	52%	T/L
	P2-10	Class 3	563	582	577	F	L/1000	L/1000	0.6+0.6	654	14%	b/200	L/1000	0.26+0.6	654	14%	F
	P2-16	Class 3	648	758	750	F	L/1000	L/1000	0.6+0.6	737	12%	b/200	L/1000	0.24+0.6	737	12%	F
	P2-20	Class 3	726	886	872	F	L/1000	L/1000	0.6+0.6	829	12%	b/200	L/1000	0.22+0.6	830	12%	F
P3	P3-4	Class 4	56	44	43	FT	L/1000	-	0.6	197	78%	b/200	-	0.29	198	78%	T/L
	P3-6	Class 4	223	192	184	FT	L/1000	-	0.6	446	59%	b/200	-	0.29	448	59%	T/L
	P3-10	Class 3	557	609	607	F	L/1000	L/1000	0.6+0.6	678	18%	b/200	L/1000	0.28+0.6	678	18%	F
	P3-16	Class 3	699	826	821	F	L/1000	L/1000	0.6+0.6	811	14%	b/200	L/1000	0.26+0.6	811	14%	F
	P3-20	Class 3	828	992	985	F	L/1000	L/1000	0.6+0.6	950	13%	b/200	L/1000	0.26+0.6	950	13%	F
P4	P4-4	Class 4	50	43	43	FT	L/1000	-	0.6	198	78%	b/200	-	0.30	200	78%	T/L
	P4-6	Class 4	181	184	184	F	L/1000	L/1000	0.6+0.6	366	51%	b/200	L/1000	0.29+0.6	369	51%	F
	P4-10	Class 3	480	626	624	F	L/1000	L/1000	0.6+0.6	628	24%	b/200	L/1000	0.29+0.6	628	24%	F
	P4-16	Class 3	680	866	864	F	L/1000	L/1000	0.6+0.6	831	18%	b/200	L/1000	0.28+0.6	831	18%	F
	P4-20	Class 3	848	1057	1055	F	L/1000	L/1000	0.6+0.6	1006	16%	b/200	L/1000	0.28+0.6	1006	16%	F
P5	P5-4	Class 4	37	43	43	F	L/1000	L/1000	0.6+0.6	94	61%	b/200	L/1000	0.3+0.6	94	61%	F
	P5-6	Class 4	106	181	181	F	L/1000	L/1000	0.6+0.6	165	36%	b/200	L/1000	0.3+0.6	165	36%	F
	P5-10	Class 3	303	636	635	F	L/1000	L/1000	0.6+0.6	388	22%	b/200	L/1000	0.3+0.6	388	22%	F
	P5-16	Class 3	588	892	892	F	L/1000	L/1000	0.6+0.6	782	25%	b/200	L/1000	0.29+0.6	782	25%	F
	P5-20	Class 3	803	1098	1097	F	L/1000	L/1000	0.6+0.6	1014	21%	b/200	L/1000	0.29+0.6	1014	21%	F
P6	P6-4	Class 4	22	48	48	F	L/1000	L/1000	0.6+0.6	35	37%	b/200	L/1000	0.3+0.6	35	37%	F
	P6-6	Class 4	62	193	193	F	L/1000	L/1000	0.6+0.6	81	24%	b/200	L/1000	0.3+0.6	81	24%	F
	P6-10	Class 3	213	639	639	F	L/1000	L/1000	0.6+0.6	266	20%	b/200	L/1000	0.3+0.6	266	20%	F
	P6-16	Class 3	534	902	902	F	L/1000	L/1000	0.6+0.6	734	27%	b/200	L/1000	0.3+0.6	734	27%	F
	P6-20	Class 3	776	1115	1115	F	L/1000	L/1000	0.6+0.6	1019	24%	b/200	L/1000	0.3+0.6	1019	24%	F

F-flexural; T-torsional; FT-flexural-torsional; T/L-local or torsional

**Combined table of buckling resistance - fixed BC
(additional moment and compression for Class 4)**

Group	Profile number	Class	Hand calculation				Abaqus shell model COG										
			Flexural buckling	Torsional buckling	Torsional-flexural buckling	Buckl mode	Silvestre (2013)					Variation 1					Buckl mode
							Imperfection		Imperf, mm	fu, kN	Diff (EN vs FEA)	Imperfection		Imperf, mm	fu, kN	Diff (EN vs FEA)	
							Local	Global				Local	Global				
N _{brdF} , kN	N _{brdT} , kN	N _{brdTF} , kN															
P1	P1-4	Class 4	64	48	48	FT	10% t	-	0.4	193	75%	b/200	-	0.28	192	75%	T/L
	P1-6	Class 4	280	222	218	FT	10% t	-	0.6	419	48%	b/200	-	0.27	428	49%	T/L
	P1-10	Class 3	561	580	572	F	10% t	L/750	1+0.8	614	9%	b/200	L/200	0.25+3	525	-7%	F
	P1-16	Class 3	591	707	695	F	10% t	L/750	1.6+0.8	659	10%	b/200	L/200	0.21+3	548	-8%	F
	P1-20	Class 3	633	805	785	F	10% t	L/750	2+0.8	711	11%	b/200	L/200	0.19+3	582	-9%	F
P2	P2-4	Class 4	61	46	46	FT	10% t	-	0.4	193	76%	b/200	-	0.28	195	76%	T/L
	P2-6	Class 4	256	208	208	FT	10% t	-	0.6	431	52%	b/200	-	0.28	435	52%	T/L
	P2-10	Class 3	563	582	577	F	10% t	L/750	1+0.8	642	12%	b/200	L/200	0.26+3	550	-2%	F
	P2-16	Class 3	648	758	750	F	10% t	L/750	1.6+0.8	722.3	10%	b/200	L/200	0.24+3	613	-6%	F
	P2-20	Class 3	726	886	872	F	10% t	L/750	2+0.8	812	11%	b/200	L/200	0.22+3	685	-6%	F
P3	P3-4	Class 4	56	44	43	FT	10% t	-	0.4	199	78%	b/200	-	0.29	198	78%	T/L
	P3-6	Class 4	223	192	184	FT	10% t	-	0.6	446	59%	b/200	-	0.29	448	59%	T/L
	P3-10	Class 3	557	609	607	F	10% t	L/750	1+0.8	663	16%	b/200	L/200	0.28+3	554	-1%	F
	P3-16	Class 3	699	826	821	F	10% t	L/750	1.6+0.8	795.5	12%	b/200	L/200	0.26+3	677	-3%	F
	P3-20	Class 3	828	992	985	F	10% t	L/750	2+0.8	932.1	11%	b/200	L/200	0.26+3	802.9	-3%	F
P4	P4-4	Class 4	50	43	43	FT	10% t	-	0.4	198.7	78%	b/200	-	0.30	200	78%	T/L
	P4-6	Class 4	181	184	184	F	10% t	L/750	0.6+0.8	354	49%	b/200	L/200	0.29+3	277	35%	F
	P4-10	Class 3	480	626	624	F	10% t	L/750	1+0.8	608	21%	b/200	L/200	0.29+3	475	-1%	F
	P4-16	Class 3	680	866	864	F	10% t	L/750	1.6+0.8	811	16%	b/200	L/200	0.28+3	665	-2%	F
	P4-20	Class 3	848	1057	1055	F	10% t	L/750	2+0.8	986	14%	b/200	L/200	0.28+3	834	-2%	F
P5	P5-4	Class 4	37	43	43	F	10% t	L/750	0.4+0.8	92	60%	b/200	L/200	0.3+3	75	51%	F
	P5-6	Class 4	106	181	181	F	10% t	L/750	0.6+0.8	162	35%	b/200	L/200	0.3+3	132	20%	F
	P5-10	Class 3	303	636	635	F	10% t	L/750	1+0.8	376	19%	b/200	L/200	0.3+3	297	-2%	F
	P5-16	Class 3	588	892	892	F	10% t	L/750	1.6+0.8	754	22%	b/200	L/200	0.29+3	581	-1%	F
	P5-20	Class 3	803	1098	1097	F	10% t	L/750	2+0.8	992	19%	b/200	L/200	0.29+3	804	0%	F
P6	P6-4	Class 4	22	48	48	F	10% t	L/750	0.4+0.8	35	36%	b/200	L/200	0.3+3	30	25%	F
	P6-6	Class 4	62	193	193	F	10% t	L/750	0.6+0.8	80	23%	b/200	L/200	0.3+3	69	11%	F
	P6-10	Class 3	213	639	639	F	10% t	L/750	1+0.8	260	18%	b/200	L/200	0.3+3	215	1%	F
	P6-16	Class 3	534	902	902	F	10% t	L/750	1.6+0.8	702	24%	b/200	L/200	0.3+3	539	1%	F
	P6-20	Class 3	776	1115	1115	F	10% t	L/750	2+0.8	991	22%	b/200	L/200	0.3+3	789	2%	F

F-flexural; T-torsional; FT-flexural-torsional; T/L-local or torsional

**Combined table of buckling resistance - fixed BC
(additional moment and compression for Class 4)**

Group	Profile number	Class	Hand calculation				Abaqus shell model COG					
			Flexural buckling	Torsional buckling	Torsional-flexural buckling	Buckl mode	Variation 2					Buckl mode
							Imperfection		Imperf, mm	fu, kN	Diff (EN vs FEA)	
							Local	Global				
N _{bRdF} , kN	N _{bRdT} , kN	N _{bRdTF} , kN										
P1	P1-4	Class 4	64	48	48	FT	L/200	-	3	183	74%	T/L
	P1-6	Class 4	280	222	218	FT	L/200	-	3	374	42%	T/L
	P1-10	Class 3	561	580	572	F	L/6000	L/6000	0.1+0.1	655	14%	F
	P1-16	Class 3	591	707	695	F	L/6000	L/6000	0.1+0.1	714	17%	F
	P1-20	Class 3	633	805	785	F	L/6000	L/6000	0.1+0.1	783	19%	F
P2	P2-4	Class 4	61	46	46	FT	L/200	-	3	186	75%	T/L
	P2-6	Class 4	256	208	208	FT	L/200	-	3	384	46%	T/L
	P2-10	Class 3	563	582	577	F	L/6000	L/6000	0.1+0.1	692	19%	F
	P2-16	Class 3	648	758	750	F	L/6000	L/6000	0.1+0.1	773	16%	F
	P2-20	Class 3	726	886	872	F	L/6000	L/6000	0.1+0.1	873.2	17%	F
P3	P3-4	Class 4	56	44	43	FT	L/200	-	3	191	77%	T/L
	P3-6	Class 4	223	192	184	FT	L/200	-	3	400	54%	T/L
	P3-10	Class 3	557	609	607	F	L/6000	L/6000	0.1+0.1	734	24%	F
	P3-16	Class 3	699	826	821	F	L/6000	L/6000	0.1+0.1	849	18%	F
	P3-20	Class 3	828	992	985	F	L/6000	L/6000	0.1+0.1	990.7	16%	F
P4	P4-4	Class 4	50	43	43	FT	L/200	-	3	189	77%	T/L
	P4-6	Class 4	181	184	184	F	L/200	L/6000	0.1+0.1	424	57%	F
	P4-10	Class 3	480	626	624	F	L/6000	L/6000	0.1+0.1	763	37%	F
	P4-16	Class 3	680	866	864	F	L/6000	L/6000	0.1+0.1	889	23%	F
	P4-20	Class 3	848	1057	1055	F	L/6000	L/6000	0.1+0.1	1058	20%	F
P5	P5-4	Class 4	37	43	43	F	L/200	L/6000	0.1+0.1	101	64%	F
	P5-6	Class 4	106	181	181	F	L/200	L/6000	0.1+0.1	179	41%	F
	P5-10	Class 3	303	636	635	F	L/6000	L/6000	0.1+0.1	430	30%	F
	P5-16	Class 3	588	892	892	F	L/6000	L/6000	0.1+0.1	889	34%	F
	P5-20	Class 3	803	1098	1097	F	L/6000	L/6000	0.1+0.1	1095	27%	F
P6	P6-4	Class 4	22	48	48	F	L/200	L/6000	0.1+0.1	37	40%	F
	P6-6	Class 4	62	193	193	F	L/200	L/6000	0.1+0.1	84.5	27%	F
	P6-10	Class 3	213	639	639	F	L/6000	L/6000	0.1+0.1	286	26%	F
	P6-16	Class 3	534	902	902	F	L/6000	L/6000	0.1+0.1	858	38%	F
	P6-20	Class 3	776	1115	1115	F	L/6000	L/6000	0.1+0.1	1097	29%	F

F-flexural; T-torsional; FT-flexural-torsional; T/L-local or torsional

**Combined table of buckling resistance - pinned BC
(additional moment and compression for Class 4)**

Group	Profile number	Class	Hand calculation				Abaqus shell model COG										
			Flexural buckling	Torsional buckling	Torsional-flexural buckling	Buckl mode	Mesacasa (2013)					EN, ECCS					Buckl mode
							Imperfection		Imperf, mm	fu, kN	Diff	Imperfection		Imperf, mm	fu, kN	Diff	
							Local	Global				Local	Global				
NbRdF, kN	NbRdT, kN	NbRdTF, kN															
P1	P1-4	Class 4	56	46	46	FT	L/1000	-	0.6	157	71%	b/200	-	0.28	164	72%	T/L
	P1-6	Class 4	197	216	208	F	L/1000	L/1000	0.6+0.6	313	37%	b/200	L/1000	0.27+0.6	313	37%	F
	P1-10	Class 3	338	575	534	F	L/1000	L/1000	0.6+0.6	426	21%	b/200	L/1000	0.25+0.6	426	21%	F
	P1-16	Class 3	355	705	635	F	L/1000	L/1000	0.6+0.6	412	14%	b/200	L/1000	0.21+0.6	412	14%	F
	P1-20	Class 3	359	804	705	F	L/1000	L/1000	0.6+0.6	386	7%	b/200	L/1000	0.19+0.6	386	7%	F
P2	P2-4	Class 4	53	45	45	FT	L/1000	-	0.6	158	71%	b/200	-	0.28	165	73%	T/L
	P2-6	Class 4	178	205	200	F	L/1000	L/1000	0.6+0.6	301	41%	b/200	L/1000	0.28+0.6	301	41%	F
	P2-10	Class 3	336	577	549	F	L/1000	L/1000	0.6+0.6	431	22%	b/200	L/1000	0.26+0.6	431	22%	F
	P2-16	Class 3	401	756	699	F	L/1000	L/1000	0.6+0.6	477	16%	b/200	L/1000	0.24+0.6	477	16%	F
	P2-20	Class 3	441	884	798	F	L/1000	L/1000	0.6+0.6	494	11%	b/200	L/1000	0.22+0.6	494	11%	F
P3	P3-4	Class 4	45	43	43	FT	L/1000	-	0.6	149	71%	b/200	-	0.29	159	73%	T/L
	P3-6	Class 4	139	189	188	F	L/1000	L/1000	0.6+0.6	236	41%	b/200	L/1000	0.29+0.6	236	41%	F
	P3-10	Class 3	292	603	589	F	L/1000	L/1000	0.6+0.6	370	21%	b/200	L/1000	0.28+0.6	370	21%	F
	P3-16	Class 3	415	823	786	F	L/1000	L/1000	0.6+0.6	506	18%	b/200	L/1000	0.26+0.6	506	18%	F
	P3-20	Class 3	511	990	927	F	L/1000	L/1000	0.6+0.6	599	15%	b/200	L/1000	0.26+0.6	599	15%	F
P4	P4-4	Class 4	34	42	42	F	L/1000	L/1000	0.6+0.6	88	62%	b/200	L/1000	0.30+0.6	88	62%	F
	P4-6	Class 4	89	180	180	F	L/1000	L/1000	0.6+0.6	134	34%	b/200	L/1000	0.29+0.6	134	34%	F
	P4-10	Class 3	198	619	613	F	L/1000	L/1000	0.6+0.6	236	16%	b/200	L/1000	0.29+0.6	236	16%	F
	P4-16	Class 3	346	863	844	F	L/1000	L/1000	0.6+0.6	413	16%	b/200	L/1000	0.28+0.6	413	16%	F
	P4-20	Class 3	475	1054	1012	F	L/1000	L/1000	0.6+0.6	572	17%	b/200	L/1000	0.28+0.6	572	17%	F
P5	P5-4	Class 4	16	42	42	F	L/1000	L/1000	0.6+0.6	27	40%	b/200	L/1000	0.30+0.6	27	40%	F
	P5-6	Class 4	37	178	178	F	L/1000	L/1000	0.6+0.6	47	21%	b/200	L/1000	0.30+0.6	47	21%	F
	P5-10	Class 3	97	629	628	F	L/1000	L/1000	0.6+0.6	109	11%	b/200	L/1000	0.30+0.6	109	11%	F
	P5-16	Class 3	239	888	882	F	L/1000	L/1000	0.6+0.6	284	16%	b/200	L/1000	0.29+0.6	284	16%	F
	P5-20	Class 3	383	1094	1070	F	L/1000	L/1000	0.6+0.6	465	18%	b/200	L/1000	0.29+0.6	465	18%	F
P6	P6-4	Class 4	8	47	47	F	L/1000	L/1000	0.6+0.6	10	23%	b/200	L/1000	0.30+0.6	10	23%	F
	P6-6	Class 4	19	188	188	F	L/1000	L/1000	0.6+0.6	22	15%	b/200	L/1000	0.30+0.6	22	15%	F
	P6-10	Class 3	63	632	631	F	L/1000	L/1000	0.6+0.6	71	11%	b/200	L/1000	0.30+0.6	71	11%	F
	P6-16	Class 3	199	898	897	F	L/1000	L/1000	0.6+0.6	236	16%	b/200	L/1000	0.30+0.6	236	16%	F
	P6-20	Class 3	345	1111	1094	F	L/1000	L/1000	0.6+0.6	411	16%	b/200	L/1000	0.30+0.6	411	16%	F

F-flexural; T-torsional; FT-flexural-torsional; T/L-local or torsional

**Combined table of buckling resistance - pinned BC
(additional moment and compression for Class 4)**

Group	Profile number	Class	Hand calculation				Abaqus shell model COG										
			Flexural buckling	Torsional buckling	Torsional-flexural buckling	Buckl mode	Silvestre (2013)					Variation 1					Buckl mode
							Imperfection		Imperf, mm	fu, kN	Diff	Imperfection		Imperf, mm	fu, kN	Diff	
							Local	Global				Local	Global				
NbRdF, kN	NbRdT, kN	NbRdTF, kN															
P1	P1-4	Class 4	56	46	46	FT	10% t	-	0.4	161	71%	b/200	-	0.28	164	72%	T/L
	P1-6	Class 4	197	216	208	F	10% t	L/750	0.6+0.8	300	34%	b/200	L/200	0.27+3.0	223	12%	F
	P1-10	Class 3	338	575	534	F	10% t	L/750	1.0+0.8	404	16%	b/200	L/200	0.25+3.0	307	-10%	F
	P1-16	Class 3	355	705	635	F	10% t	L/750	1.6+0.8	394	10%	b/200	L/200	0.21+3.0	299	-19%	F
	P1-20	Class 3	359	804	705	F	10% t	L/750	2.0+0.8	372	3%	b/200	L/200	0.19+3.0	281	-28%	F
P2	P2-4	Class 4	53	45	45	FT	10% t	-	0.4	162	72%	b/200	-	0.28	165	73%	T/L
	P2-6	Class 4	178	205	200	F	10% t	L/750	0.6+0.8	288	38%	b/200	L/200	0.28+3.0	217	18%	F
	P2-10	Class 3	336	577	549	F	10% t	L/750	1.0+0.8	413	19%	b/200	L/200	0.26+3.0	316	-6%	F
	P2-16	Class 3	401	756	699	F	10% t	L/750	1.6+0.8	457	12%	b/200	L/200	0.24+3.0	349	-15%	F
	P2-20	Class 3	441	884	798	F	10% t	L/750	2.0+0.8	473	7%	b/200	L/200	0.22+3.0	363	-21%	F
P3	P3-4	Class 4	45	43	43	FT	10% t	-	0.4	154	72%	b/200	-	0.29	159	73%	T/L
	P3-6	Class 4	139	189	188	F	10% t	L/750	0.6+0.8	229	39%	b/200	L/200	0.29+3.0	178	22%	F
	P3-10	Class 3	292	603	589	F	10% t	L/750	1.0+0.8	358	18%	b/200	L/200	0.28+3.0	281	-4%	F
	P3-16	Class 3	415	823	786	F	10% t	L/750	1.6+0.8	486	14%	b/200	L/200	0.26+3.0	373	-11%	F
	P3-20	Class 3	511	990	927	F	10% t	L/750	2.0+0.8	574	11%	b/200	L/200	0.26+3.0	444	-15%	F
P4	P4-4	Class 4	34	42	42	F	10% t	L/750	0.4+0.8	86	60%	b/200	L/200	0.30+3.0	72	53%	F
	P4-6	Class 4	89	180	180	F	10% t	L/750	0.6+0.8	130	31%	b/200	L/200	0.29+3.0	108	18%	F
	P4-10	Class 3	198	619	613	F	10% t	L/750	1.0+0.8	231	14%	b/200	L/200	0.29+3.0	189	-5%	F
	P4-16	Class 3	346	863	844	F	10% t	L/750	1.6+0.8	403	14%	b/200	L/200	0.28+3.0	316	-10%	F
	P4-20	Class 3	475	1054	1012	F	10% t	L/750	2.0+0.8	550	14%	b/200	L/200	0.28+3.0	426	-11%	F
P5	P5-4	Class 4	16	42	42	F	10% t	L/750	0.4+0.8	26	39%	b/200	L/200	0.30+3.0	23	32%	F
	P5-6	Class 4	37	178	178	F	10% t	L/750	0.6+0.8	46	20%	b/200	L/200	0.30+3.0	41	10%	F
	P5-10	Class 3	97	629	628	F	10% t	L/750	1.0+0.8	108	11%	b/200	L/200	0.30+3.0	95	-2%	F
	P5-16	Class 3	239	888	882	F	10% t	L/750	1.6+0.8	274	13%	b/200	L/200	0.29+3.0	224	-7%	F
	P5-20	Class 3	383	1094	1070	F	10% t	L/750	2.0+0.8	450	15%	b/200	L/200	0.29+3.0	360	-6%	F
P6	P6-4	Class 4	8	47	47	F	10% t	L/750	0.4+0.8	10	22%	b/200	L/200	0.30+3.0	9	14%	F
	P6-6	Class 4	19	188	188	F	10% t	L/750	0.6+0.8	22	14%	b/200	L/200	0.30+3.0	20	7%	F
	P6-10	Class 3	63	632	631	F	10% t	L/750	1.0+0.8	69	10%	b/200	L/200	0.30+3.0	63	-1%	F
	P6-16	Class 3	199	898	897	F	10% t	L/750	1.6+0.8	230	13%	b/200	L/200	0.30+3.0	192	-4%	F
	P6-20	Class 3	345	1111	1094	F	10% t	L/750	2.0+0.8	426	19%	b/200	L/200	0.30+3.0	335	-3%	F

F-flexural; T-torsional; FT-flexural-torsional; T/L-local or torsional

**Combined table of buckling resistance - pinned BC
(additional moment and compression for Class 4)**

Group	Profile number	Class	Hand calculation				Abaqus shell model COG					
			Flexural buckling	Torsional buckling	Torsional-flexural buckling	Buckl mode	Variation 2				Buckl mode	
							Imperfection		Imperf, mm	fu, kN		Diff
			NbRdF, kN	NbRdT, kN	NbRdTF, kN		Local	Global				
P1	P1-4	Class 4	56	46	46	FT	L/200	-	3	128	64%	T/L
	P1-6	Class 4	197	216	208	F	L/6000	L/6000	0.1+0.1	369	47%	F
	P1-10	Class 3	338	575	534	F	L/6000	L/6000	0.1+0.1	496	32%	F
	P1-16	Class 3	355	705	635	F	L/6000	L/6000	0.1+0.1	468	24%	F
	P1-20	Class 3	359	804	705	F	L/6000	L/6000	0.1+0.1	436	18%	F
P2	P2-4	Class 4	53	45	45	FT	L/200	-	3	127	65%	T/L
	P2-6	Class 4	178	205	200	F	L/6000	L/6000	0.1+0.1	358	50%	F
	P2-10	Class 3	336	577	549	F	L/6000	L/6000	0.1+0.1	496	32%	F
	P2-16	Class 3	401	756	699	F	L/6000	L/6000	0.1+0.1	544	26%	F
	P2-20	Class 3	441	884	798	F	L/6000	L/6000	0.1+0.1	557	21%	F
P3	P3-4	Class 4	45	43	43	FT	L/200	-	3	113	62%	T/L
	P3-6	Class 4	139	189	188	F	L/6000	L/6000	0.1+0.1	264	47%	F
	P3-10	Class 3	292	603	589	F	L/6000	L/6000	0.1+0.1	412	29%	F
	P3-16	Class 3	415	823	786	F	L/6000	L/6000	0.1+0.1	575	28%	F
	P3-20	Class 3	511	990	927	F	L/6000	L/6000	0.1+0.1	676	24%	F
P4	P4-4	Class 4	34	42	42	F	L/6000	L/6000	0.1+0.1	94	64%	F
	P4-6	Class 4	89	180	180	F	L/6000	L/6000	0.1+0.1	142	37%	F
	P4-10	Class 3	198	619	613	F	L/6000	L/6000	0.1+0.1	253	22%	F
	P4-16	Class 3	346	863	844	F	L/6000	L/6000	0.1+0.1	465	25%	F
	P4-20	Class 3	475	1054	1012	F	L/6000	L/6000	0.1+0.1	639	26%	F
P5	P5-4	Class 4	16	42	42	F	L/6000	L/6000	0.1+0.1	28	42%	F
	P5-6	Class 4	37	178	178	F	L/6000	L/6000	0.1+0.1	48	23%	F
	P5-10	Class 3	97	629	628	F	L/6000	L/6000	0.1+0.1	113	15%	F
	P5-16	Class 3	239	888	882	F	L/6000	L/6000	0.1+0.1	305	21%	F
	P5-20	Class 3	383	1094	1070	F	L/6000	L/6000	0.1+0.1	514	25%	F
P6	P6-4	Class 4	8	47	47	F	L/6000	L/6000	0.1+0.1	10	25%	F
	P6-6	Class 4	19	188	188	F	L/6000	L/6000	0.1+0.1	22	17%	F
	P6-10	Class 3	63	632	631	F	L/6000	L/6000	0.1+0.1	73	14%	F
	P6-16	Class 3	199	898	897	F	L/6000	L/6000	0.1+0.1	251	21%	F
	P6-20	Class 3	345	1111	1094	F	L/6000	L/6000	0.1+0.1	463	25%	F

F-flexural; T-torsional; FT-flexural-torsional; T/L-local or torsional

Elastic curves – change of buckling modes

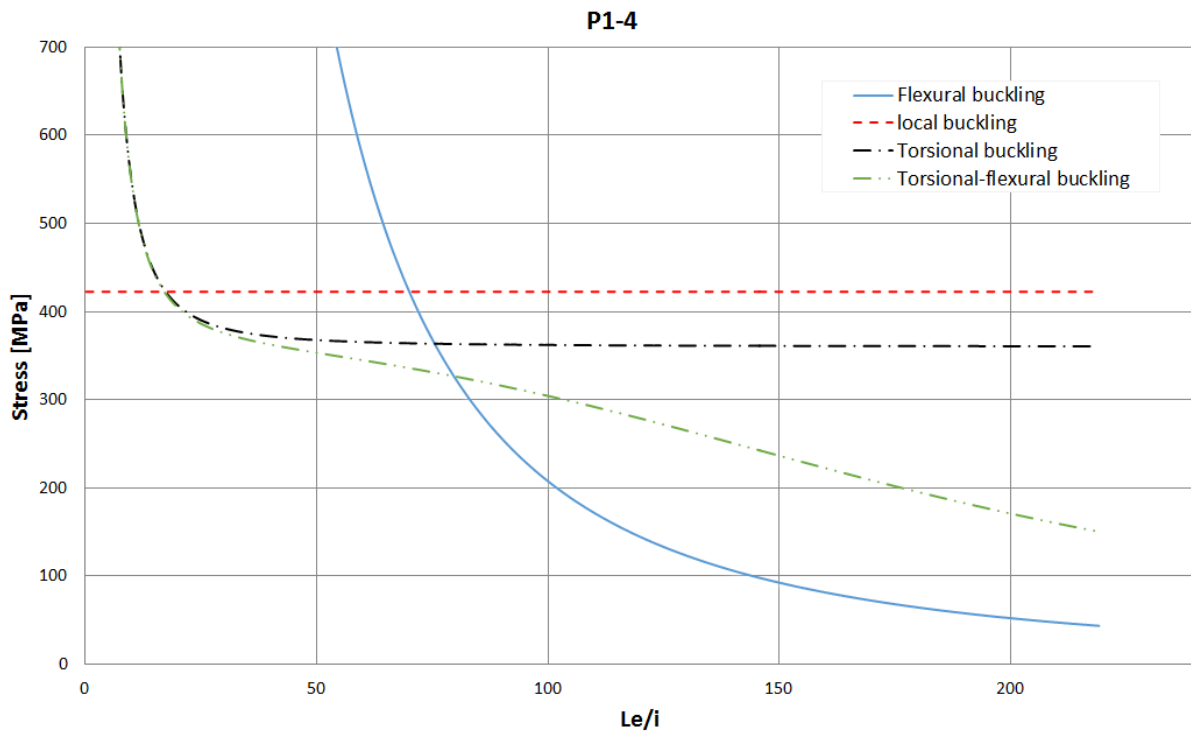


Figure 17.1: Elastic critical load assessment. Cross-section P1-4.

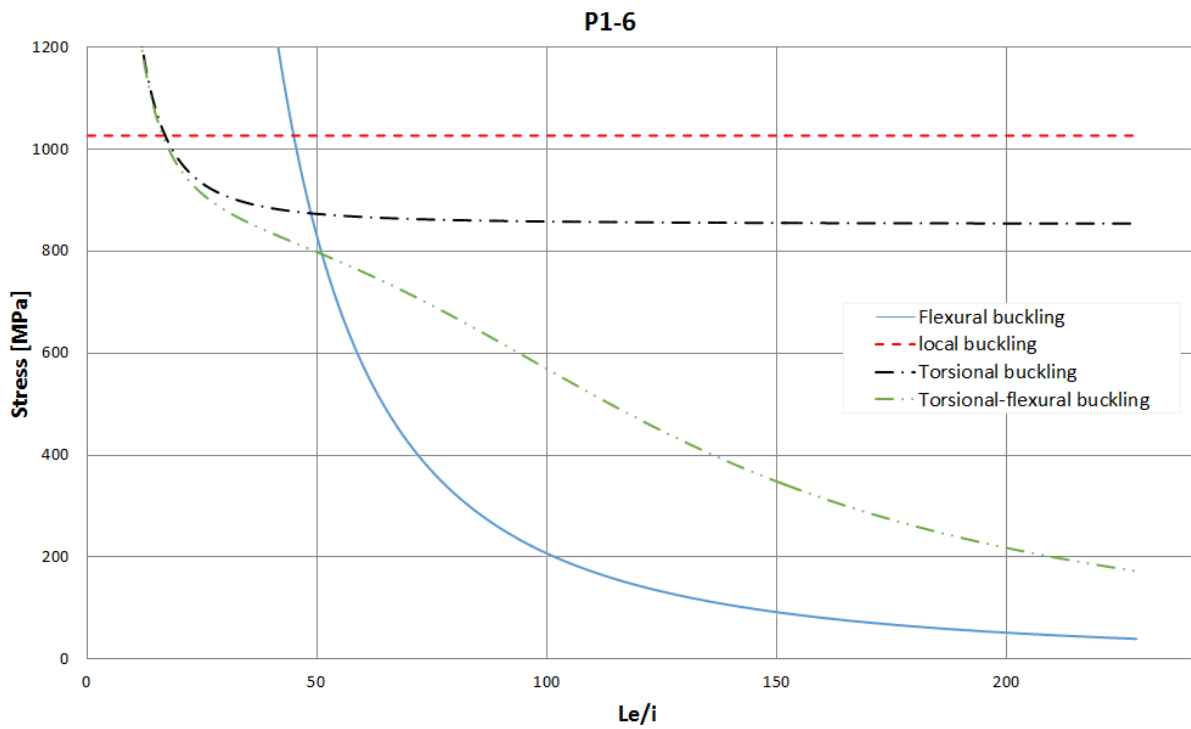


Figure 17.2: Elastic critical load assessment. Cross-section P1-6.

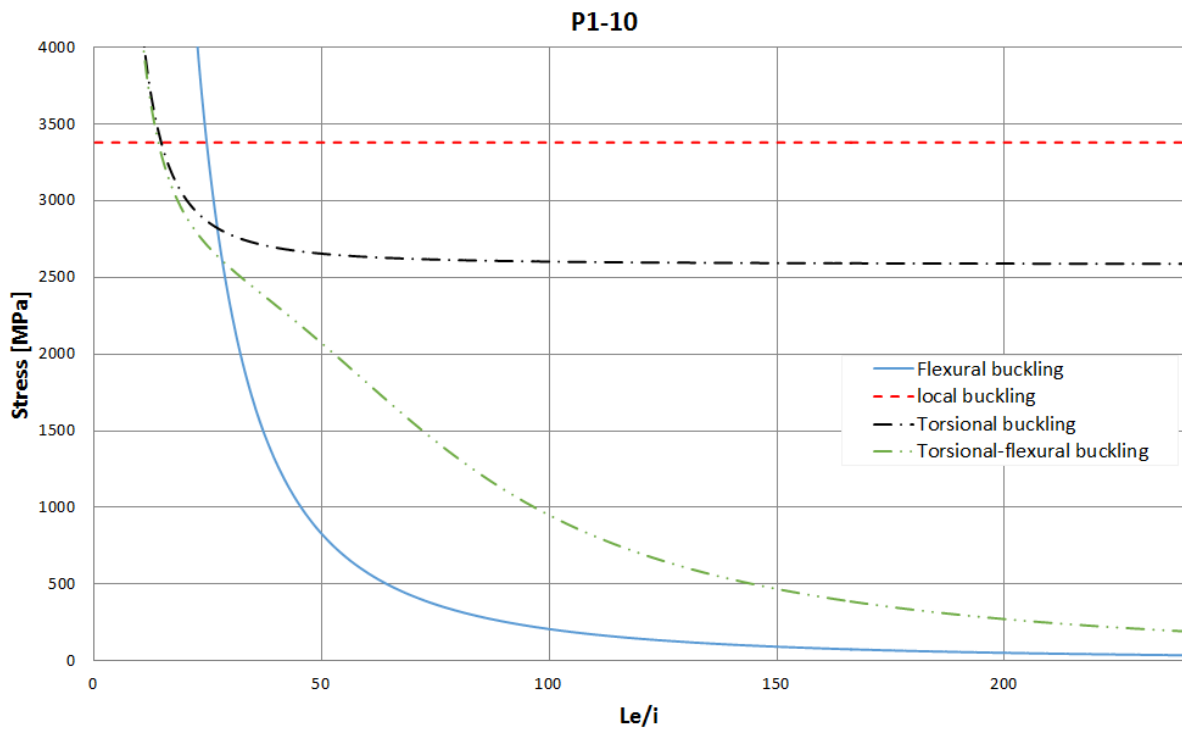


Figure 17.3: Elastic critical load assessment. Cross-section P1-10.

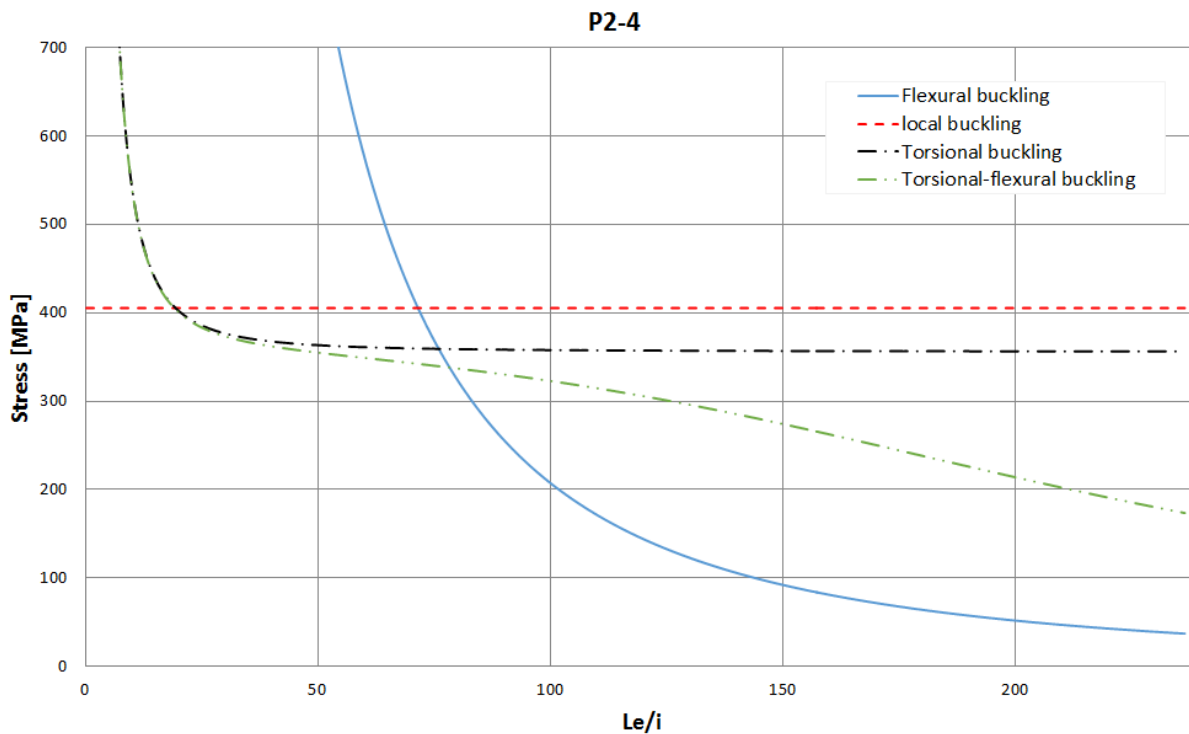


Figure 17.4: Elastic critical load assessment. Cross-section P2-4.

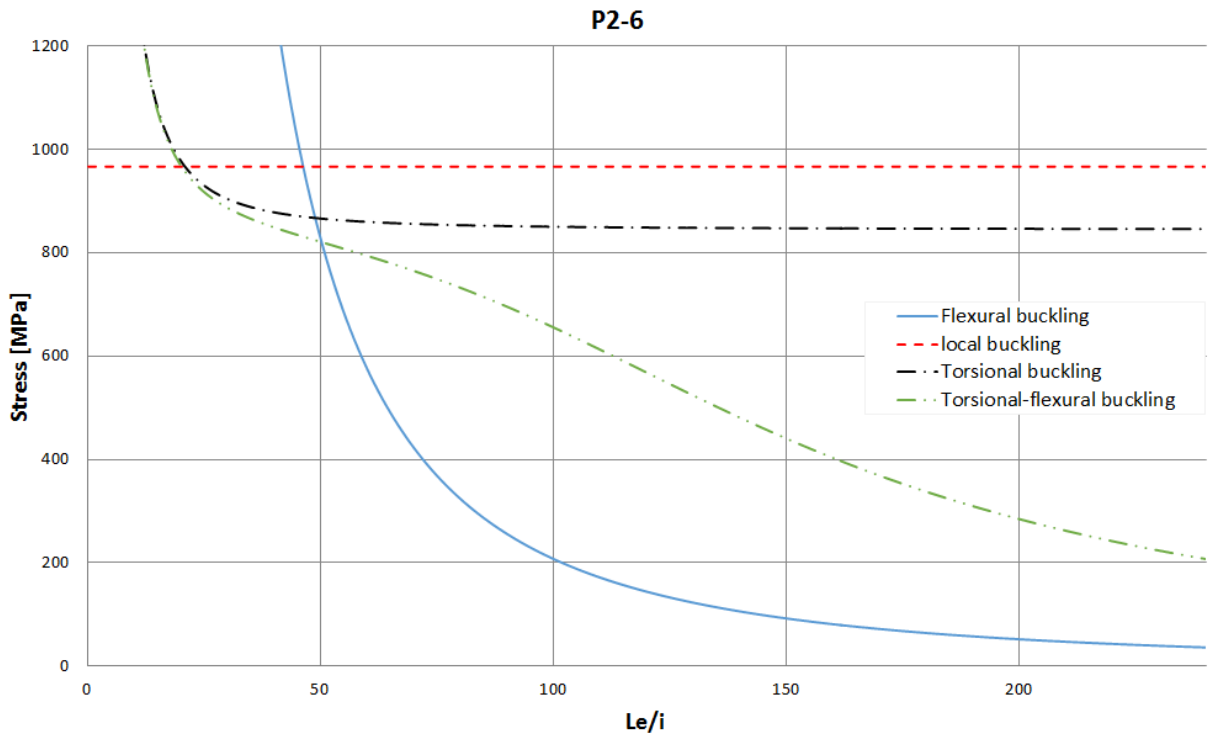


Figure 17.5: Elastic critical load assessment. Cross-section P2-6.

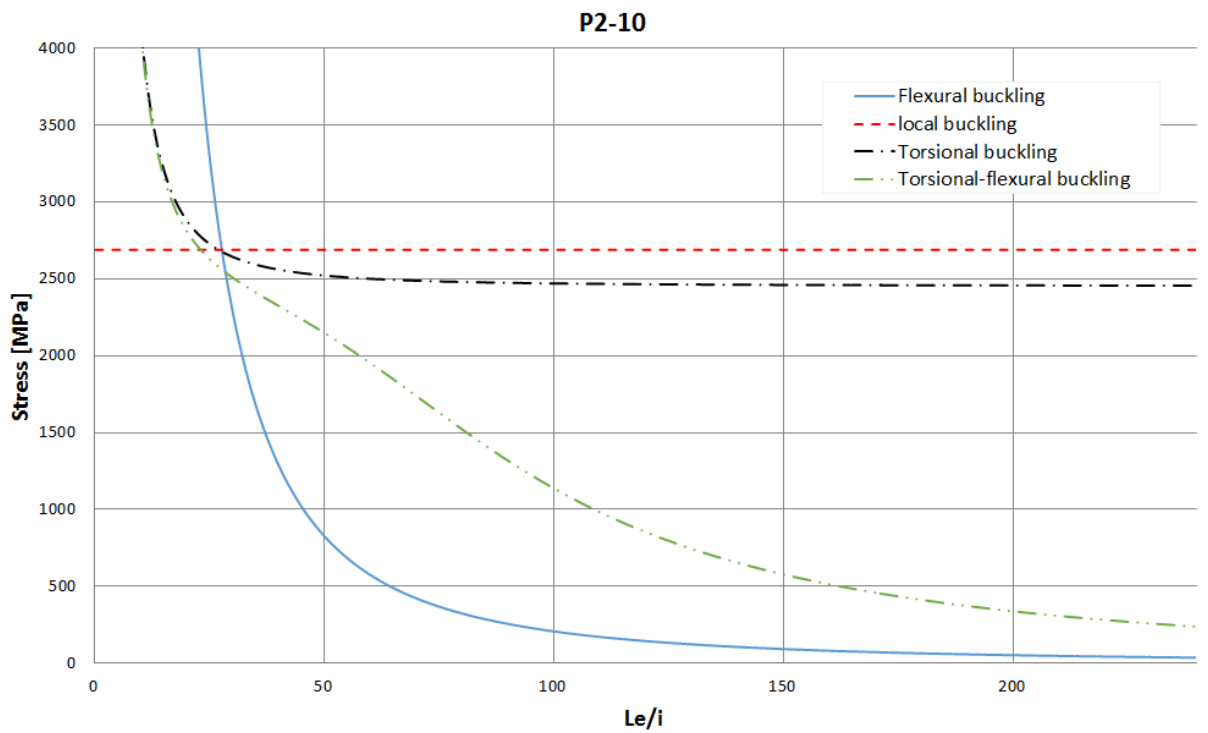


Figure 17.6: Elastic critical load assessment. Cross-section P2-10.

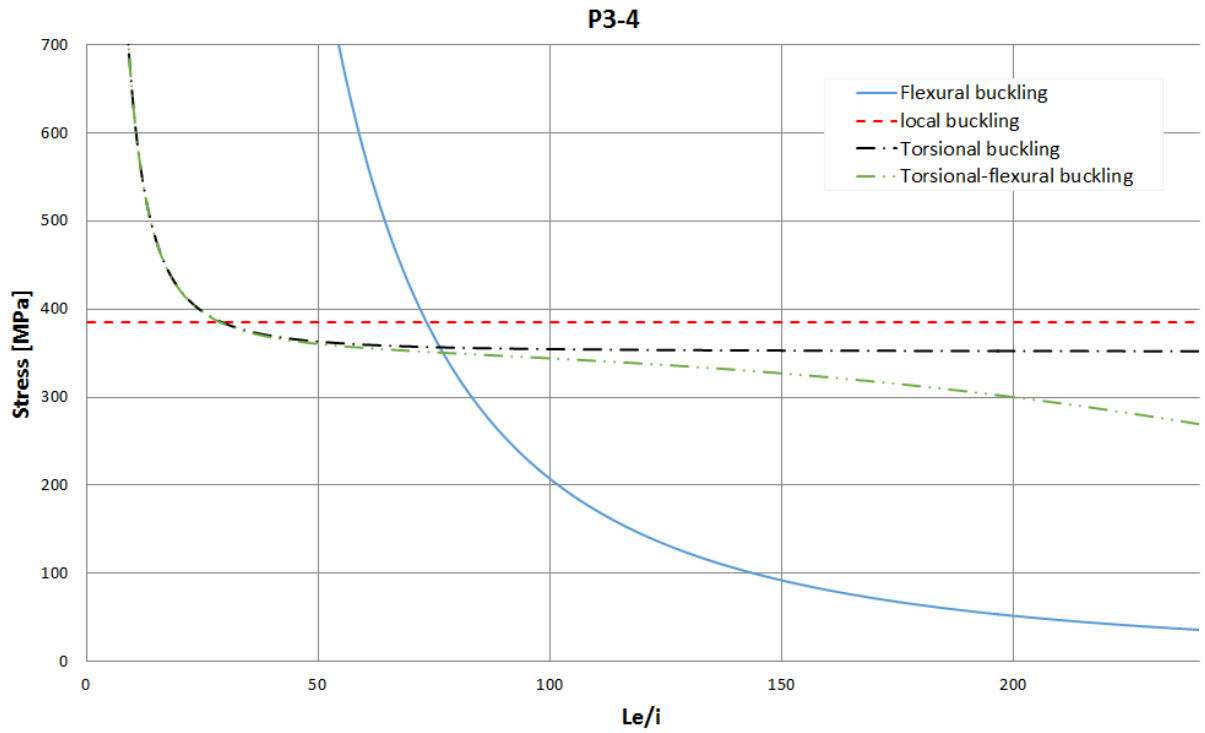


Figure 17.7: Elastic critical load assessment. Cross-section P3-4.

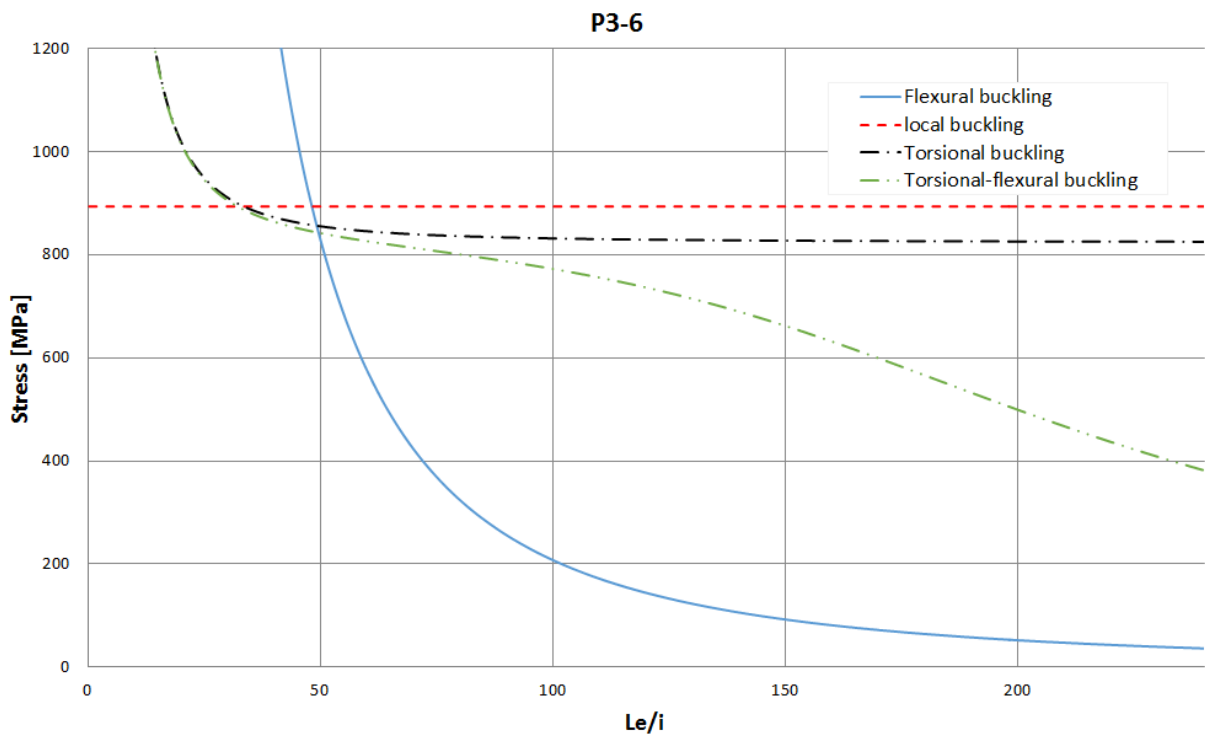


Figure 17.8: Elastic critical load assessment. Cross-section P3-6.

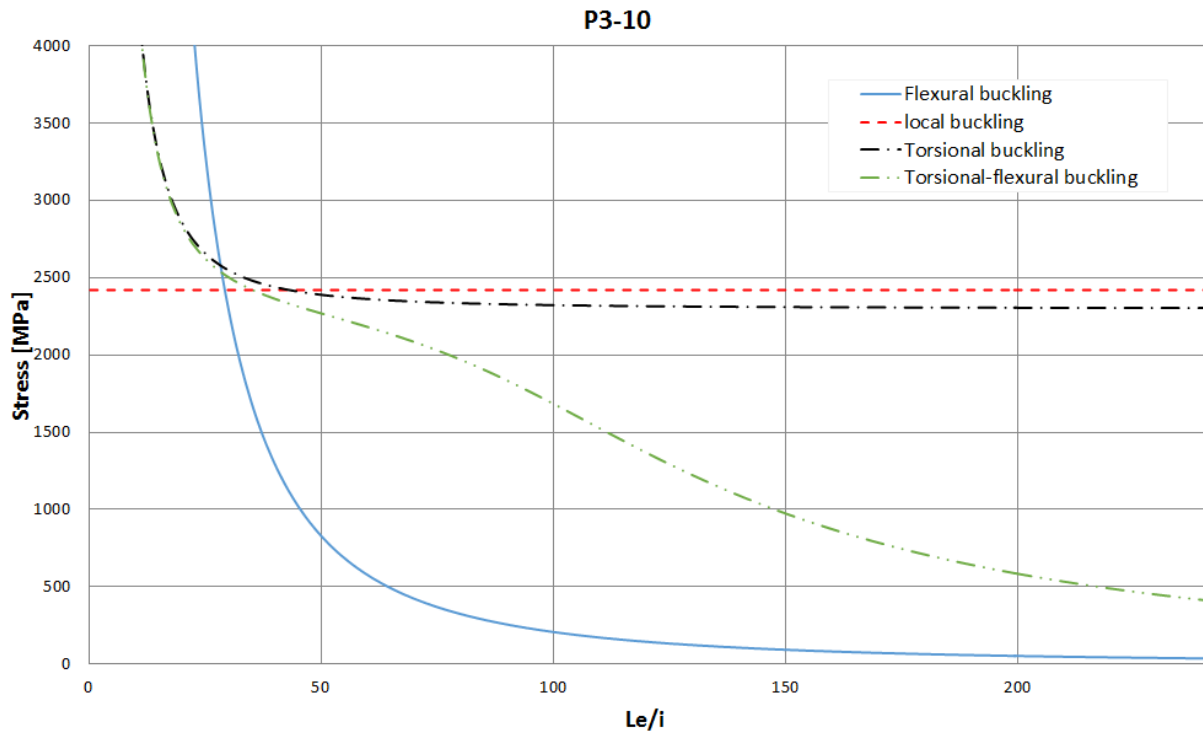


Figure 17.9: Elastic critical load assessment. Cross-section P3-10.

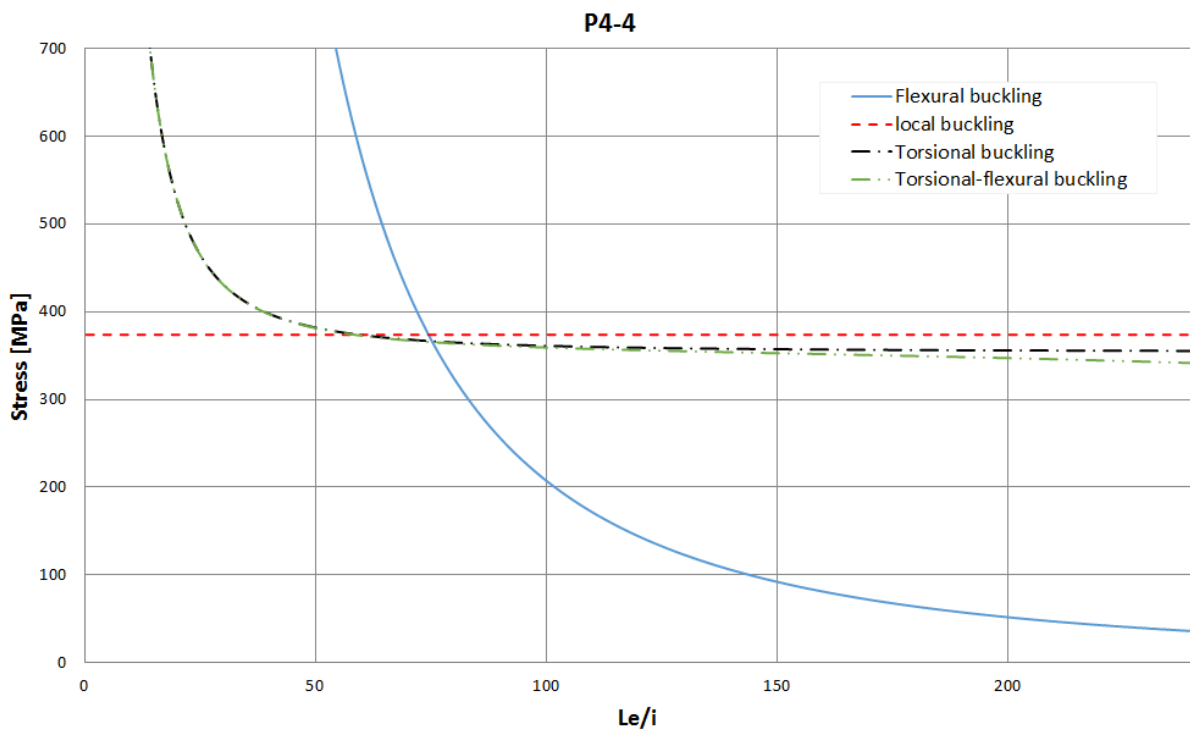


Figure 17.10: Elastic critical load assessment. Cross-section P4-4.

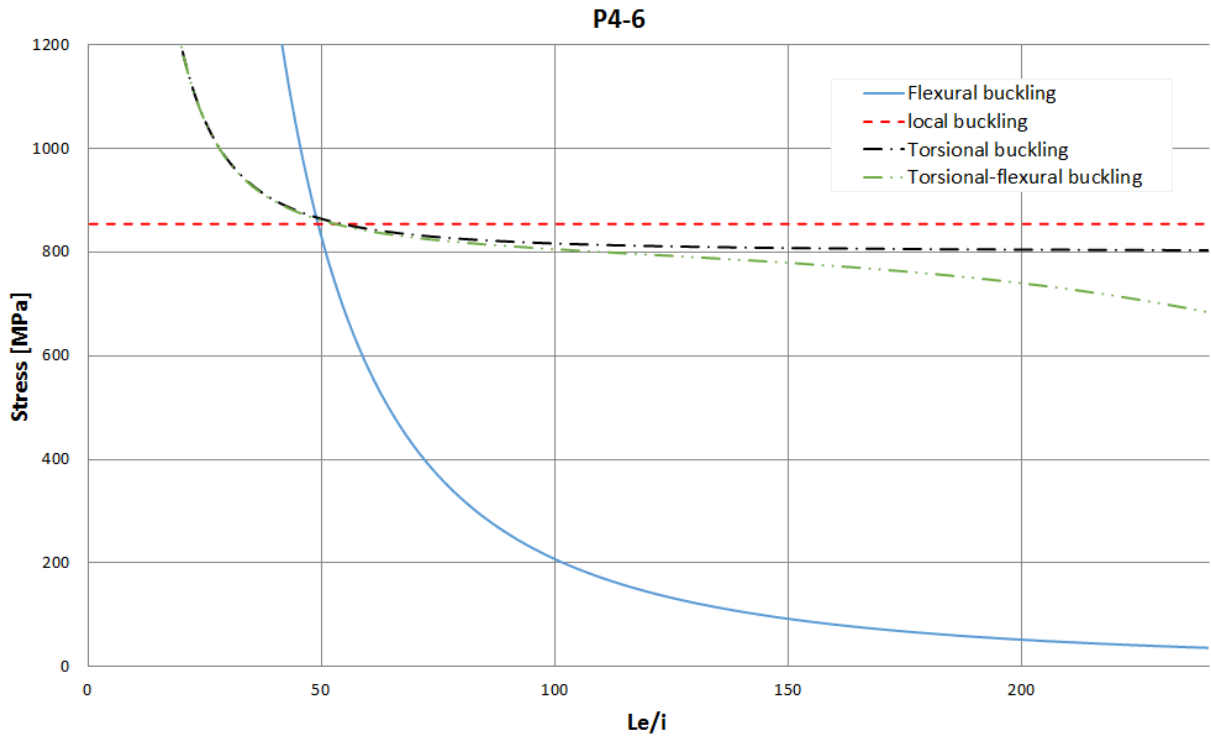


Figure 17.11: Elastic critical load assessment. Cross-section P4-6.

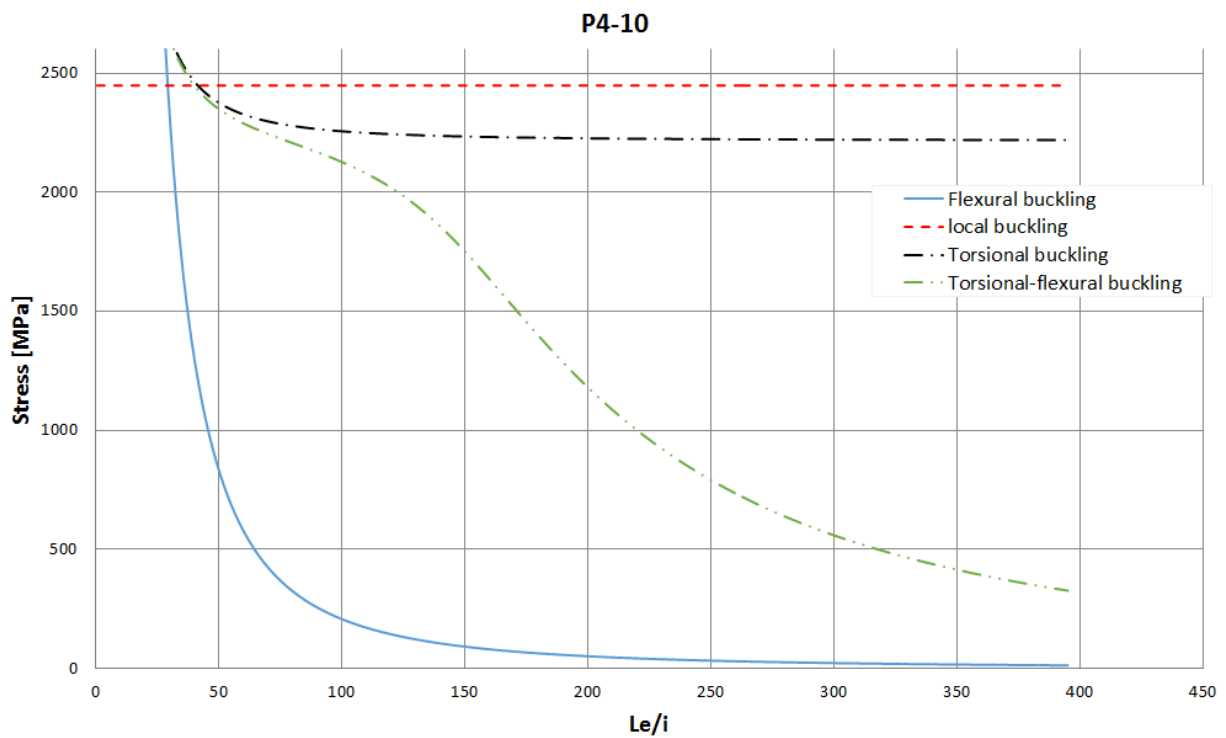


Figure 17.12: Elastic critical load assessment. Cross-section P4-10.

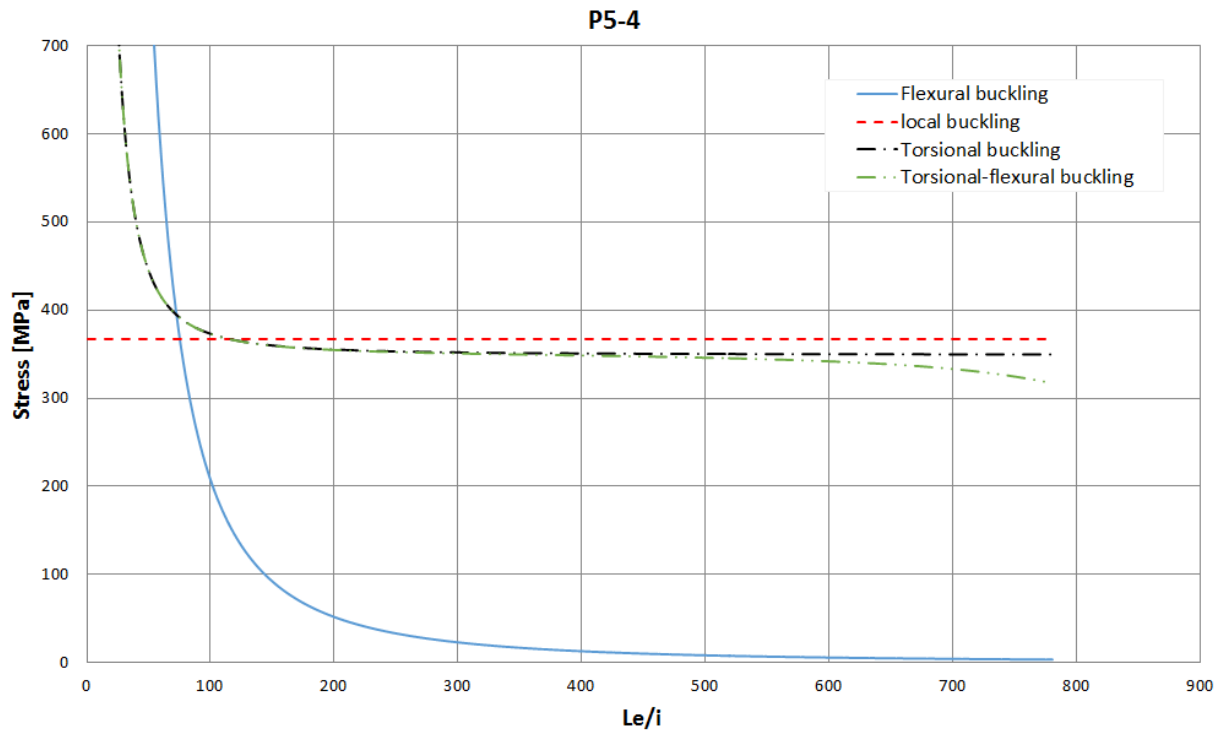


Figure 17.13: Elastic critical load assessment. Cross-section P5-4.

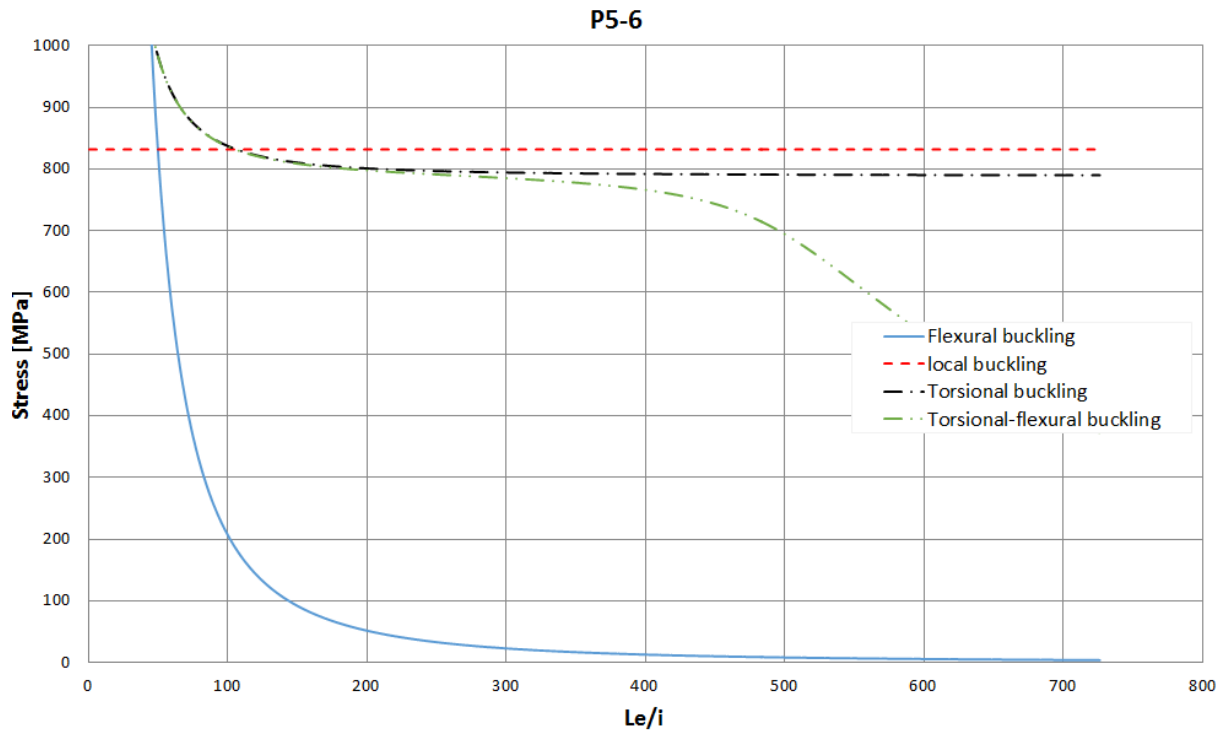


Figure 17.14: Elastic critical load assessment. Cross-section P5-6.

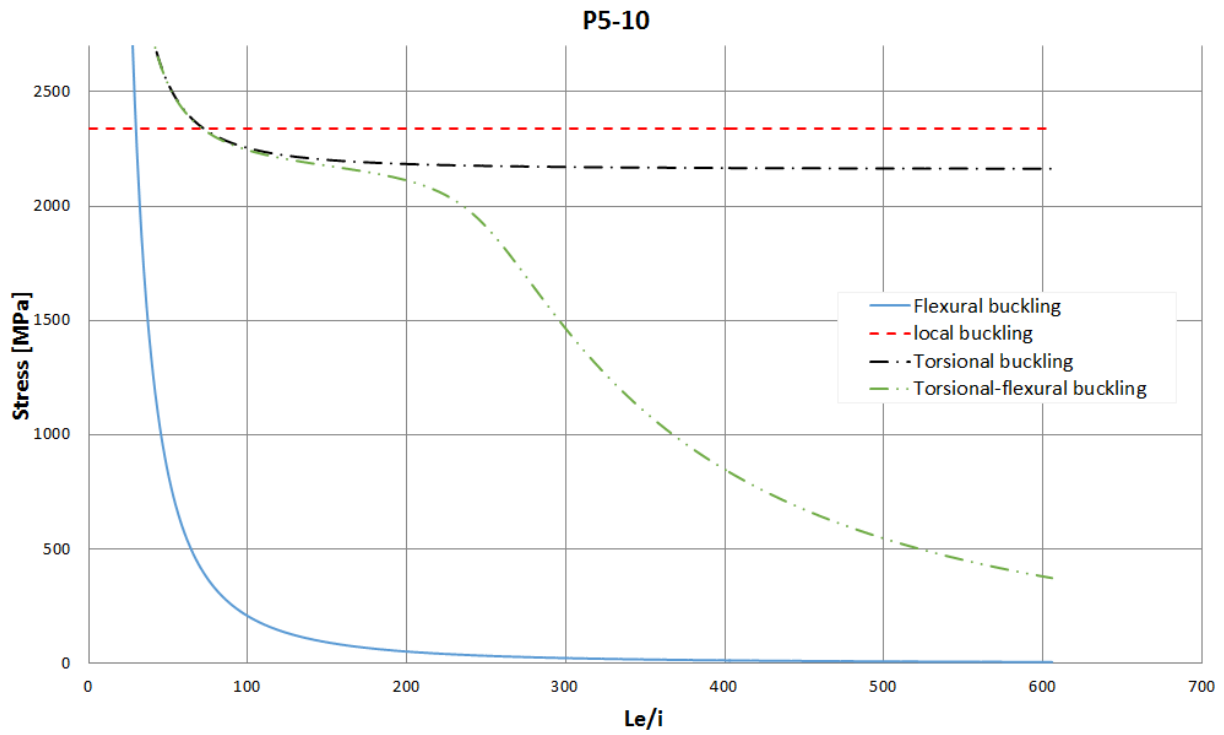


Figure 17.15: Elastic critical load assessment. Cross-section P5-10.

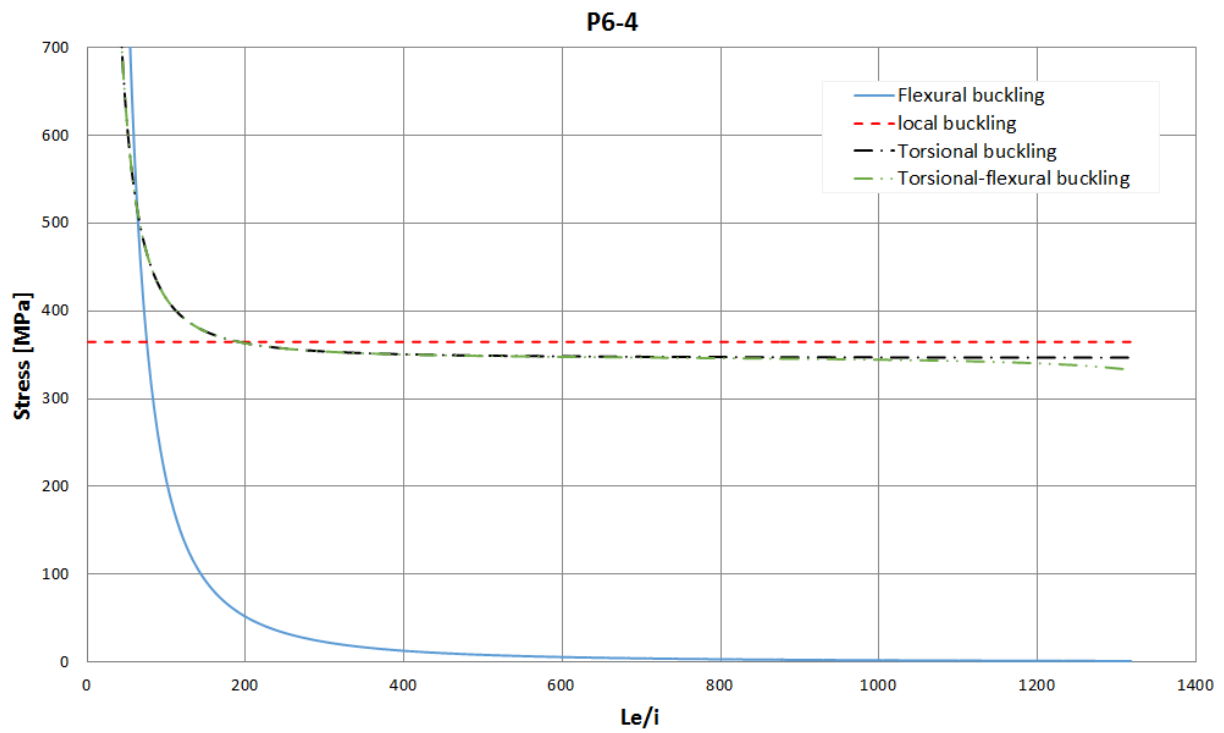


Figure 17.16: Elastic critical load assessment. Cross-section P6-4.

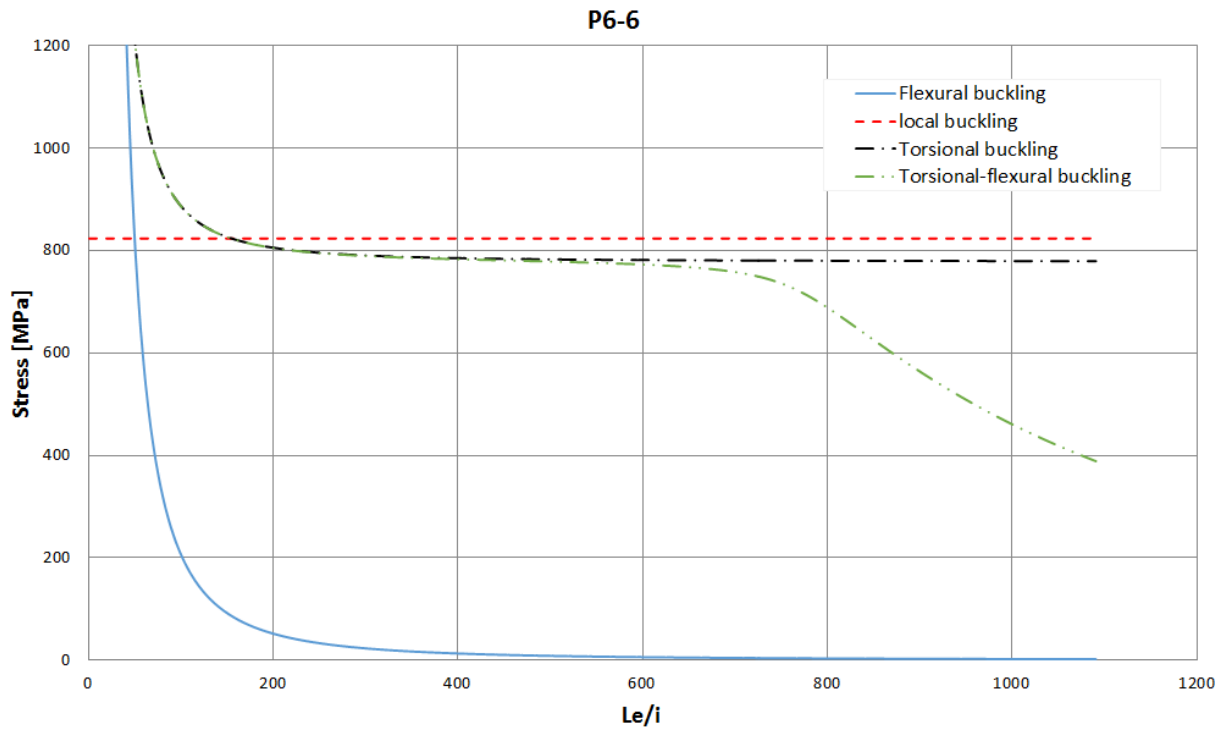


Figure 17.17: Elastic critical load assessment. Cross-section P6-6.

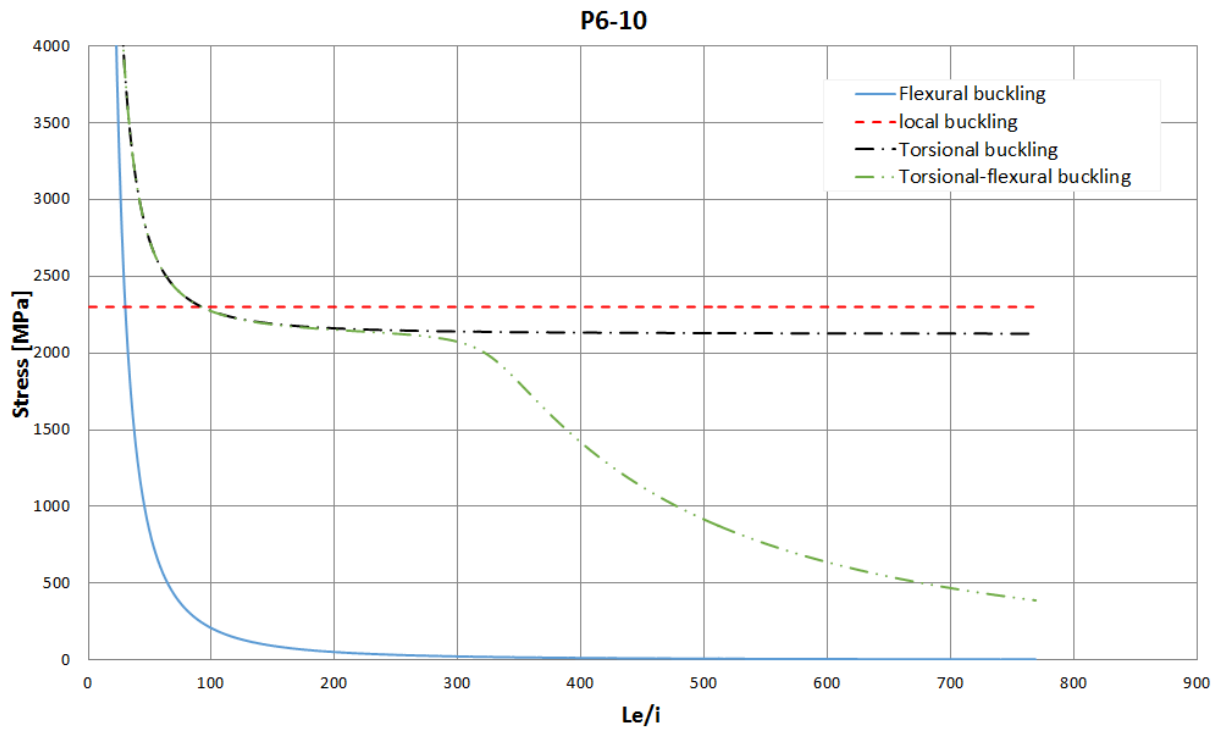


Figure 17.18: Elastic critical load assessment. Cross-section P6-10.

Buckling curves – Group P1

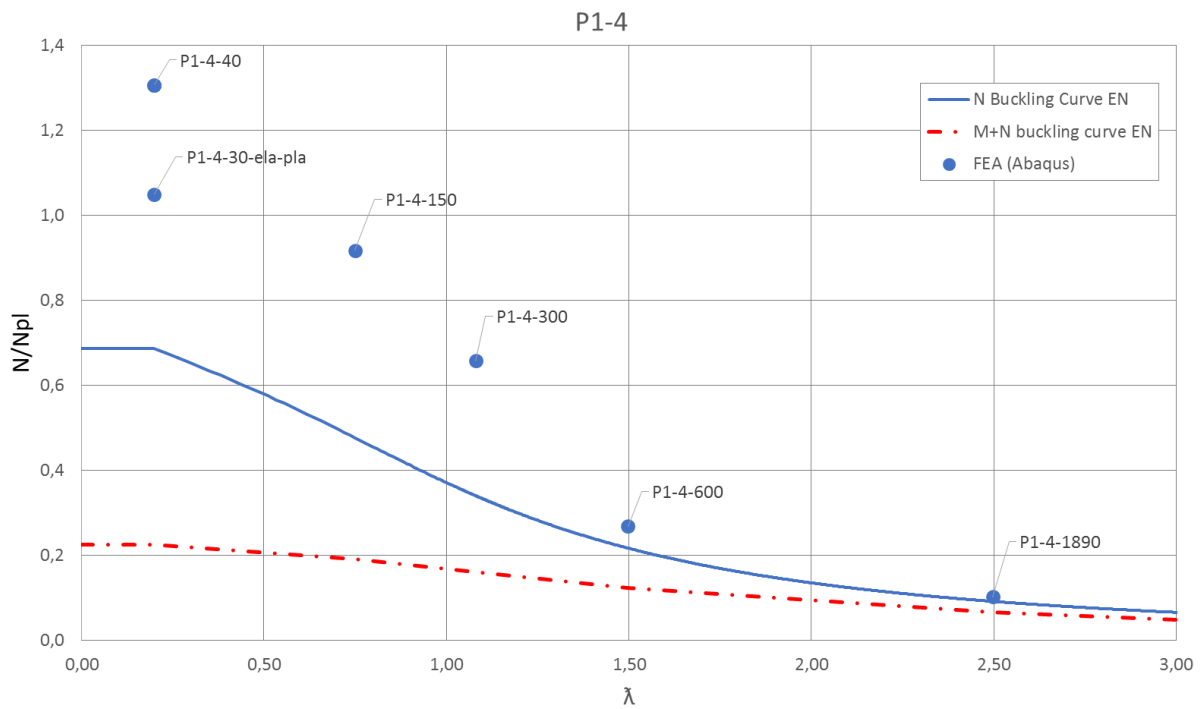


Figure 18.1: Buckling curves. Cross-section P1-4.

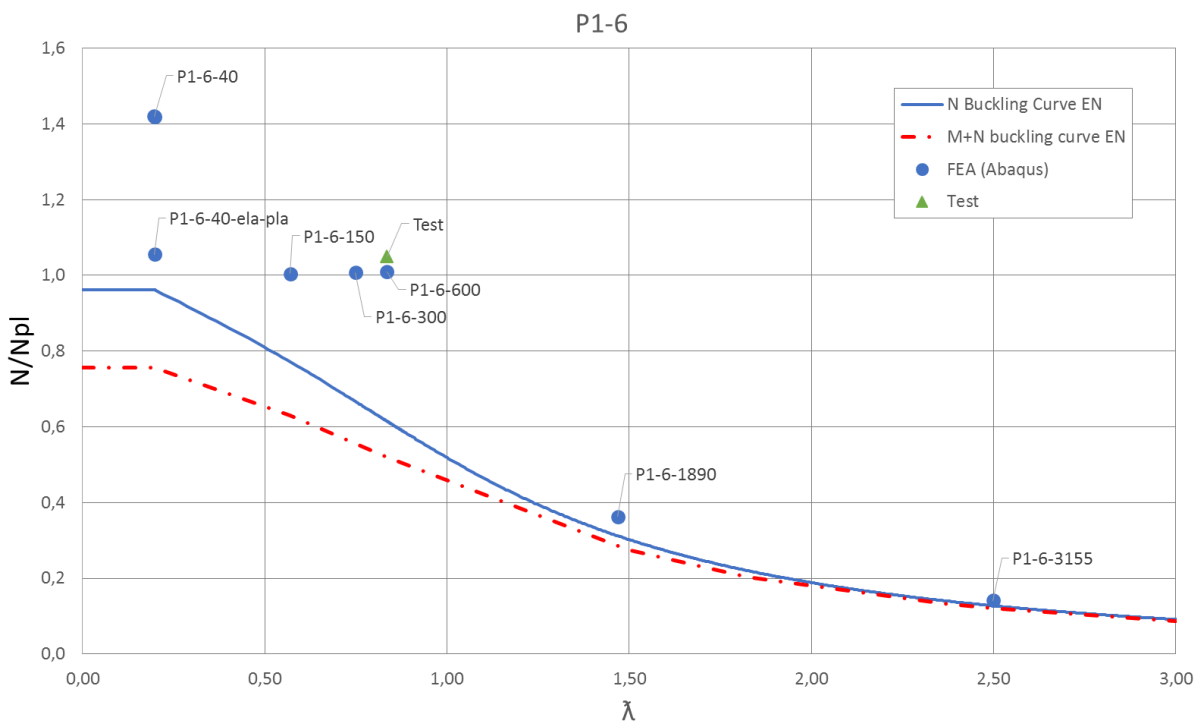


Figure 18.2: Buckling curves. Cross-section P1-6.

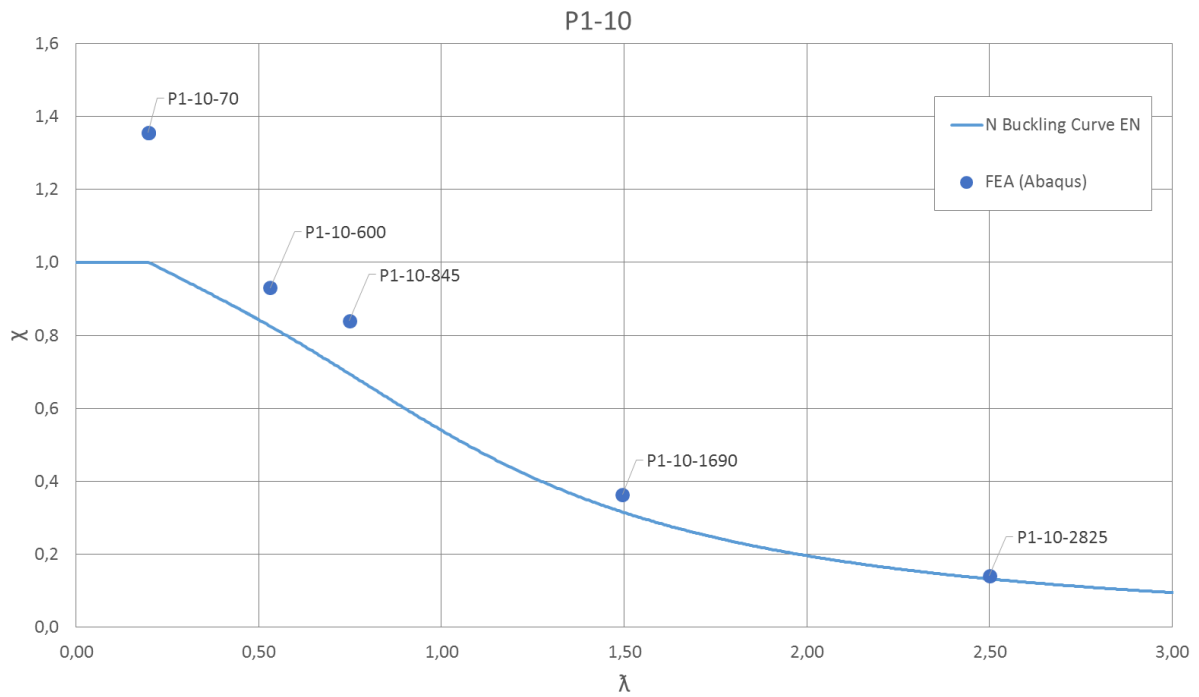


Figure 18.3: Buckling curves. Cross-section P1-10.

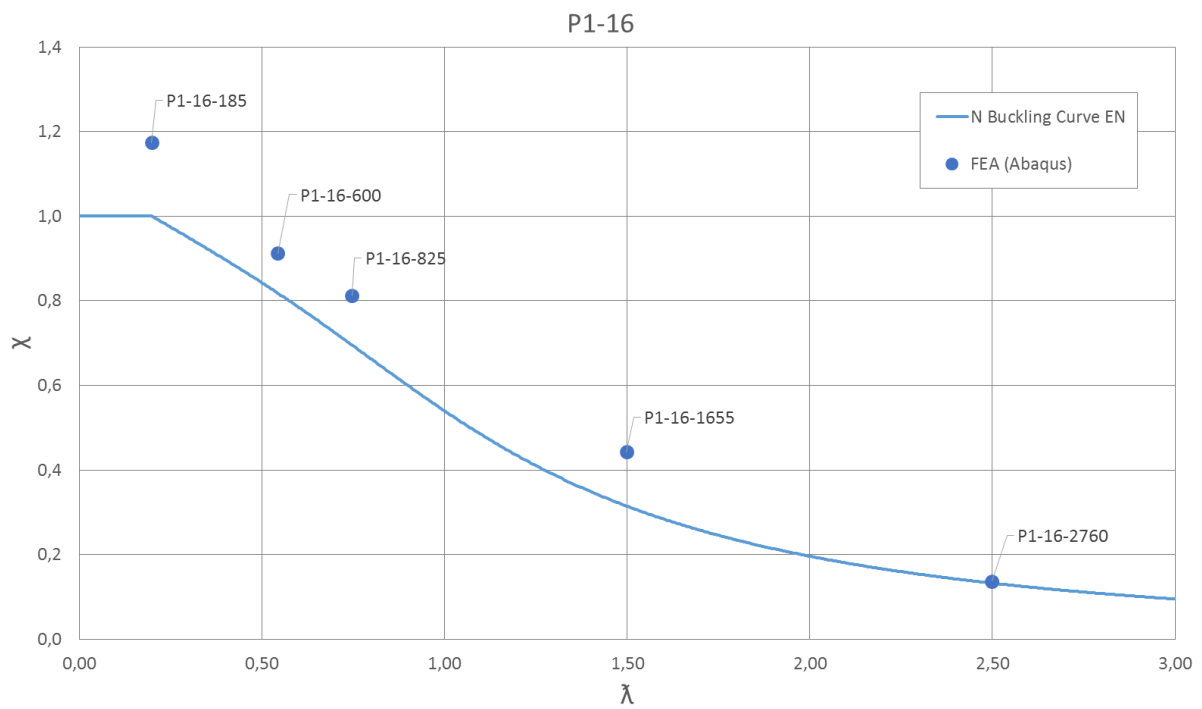


Figure 18.4: Buckling curves. Cross-section P1-16.

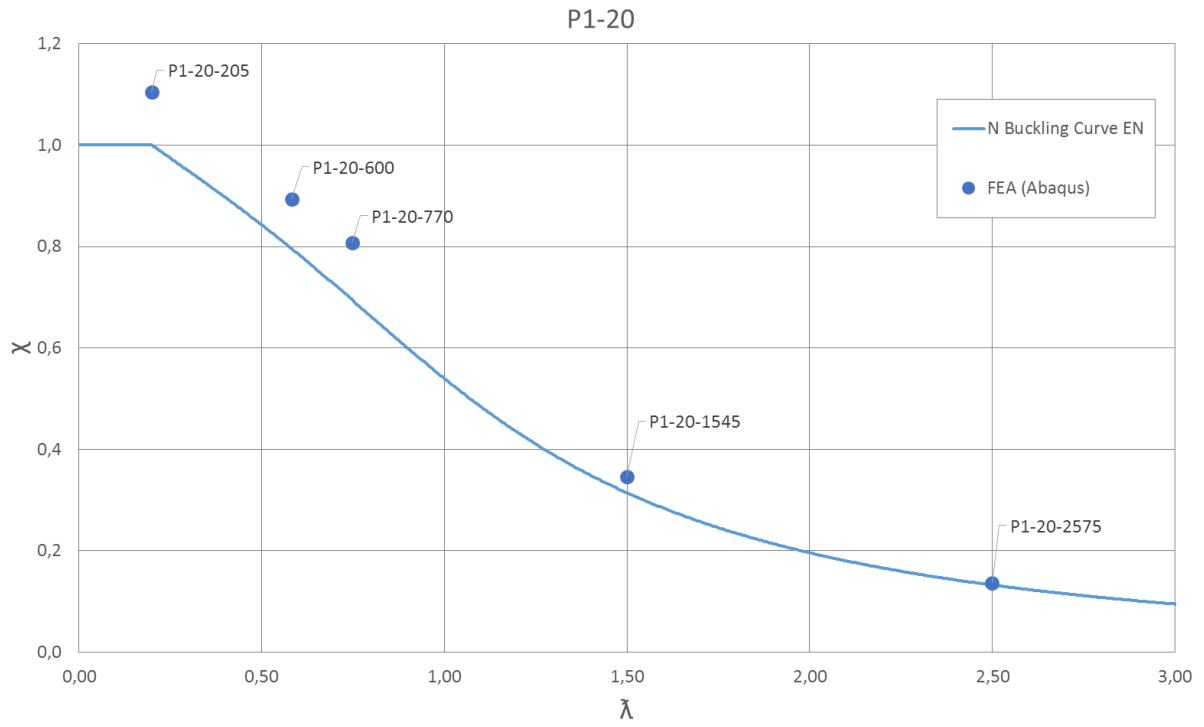


Figure 18.5: Buckling curves. Cross-section P1-20.

Buckling curves – Group P2

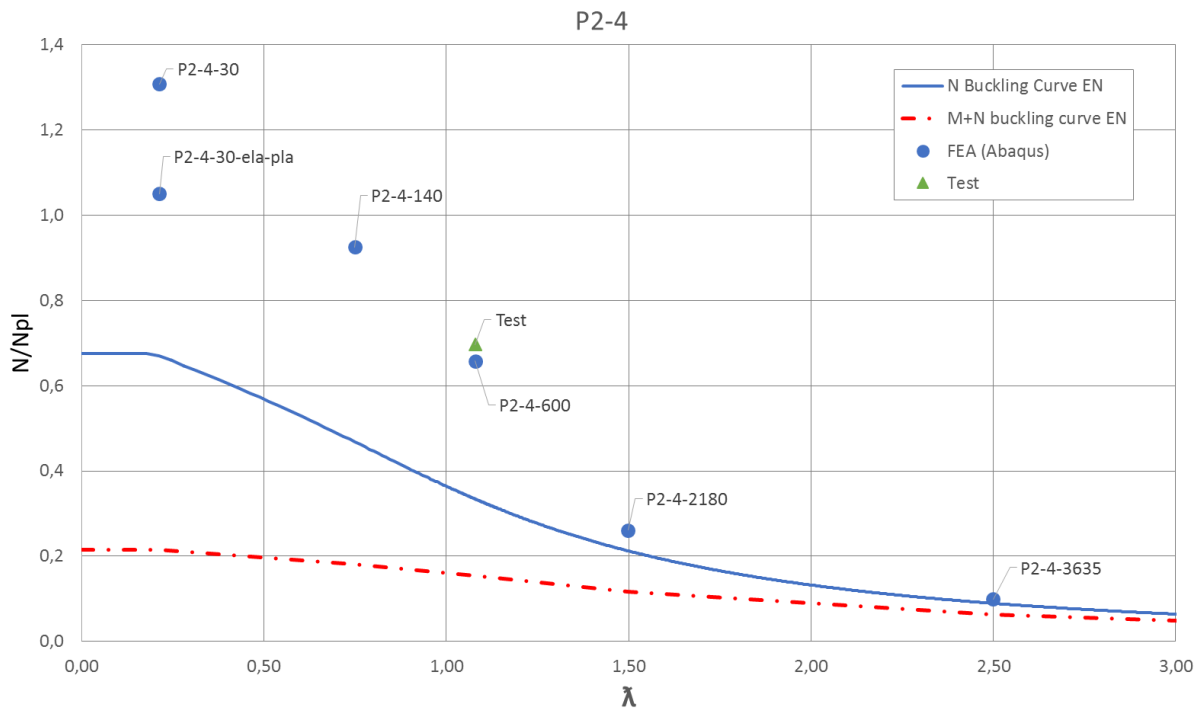


Figure 18.6: Buckling curves. Cross-section P2-4.

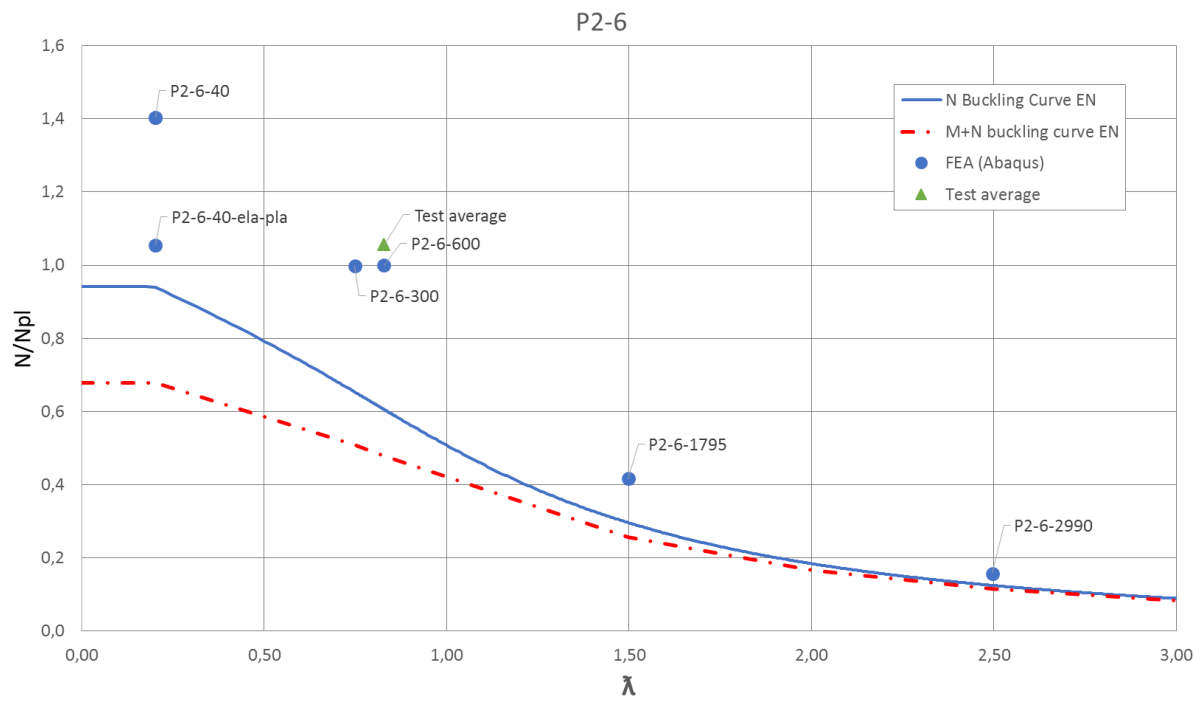


Figure 18.7: Buckling curves. Cross-section P2-6.

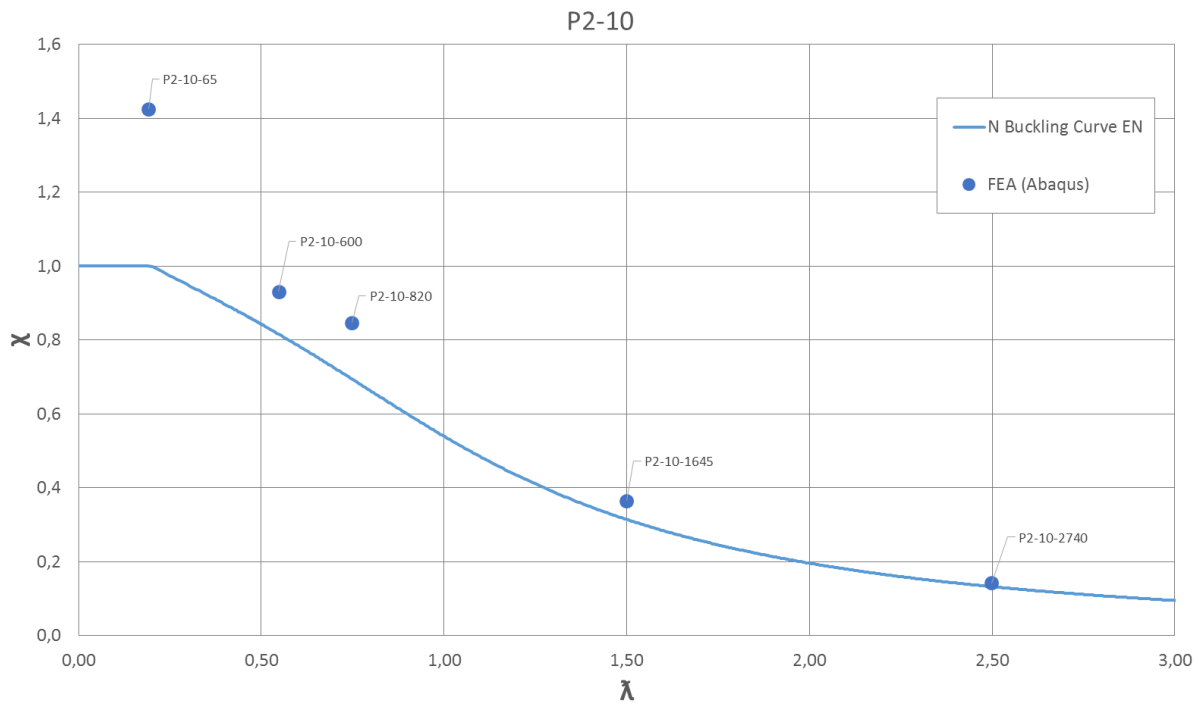


Figure 18.8: Buckling curves. Cross-section P2-10.

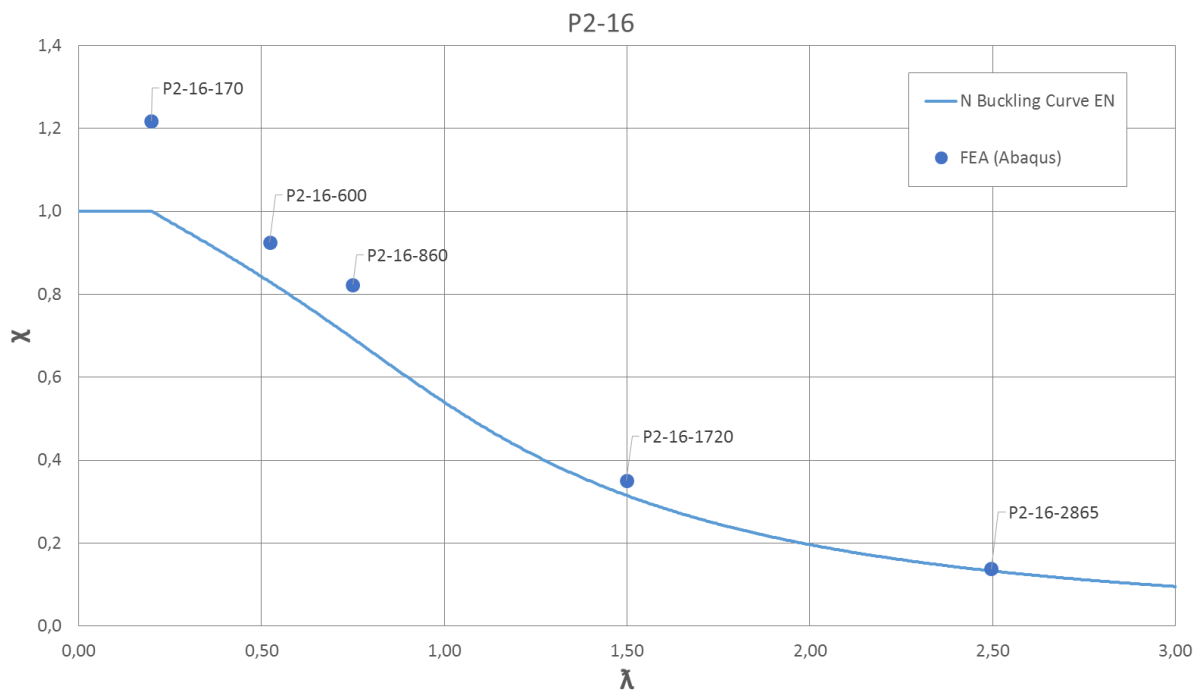


Figure 18.9: Buckling curves. Cross-section P2-16.

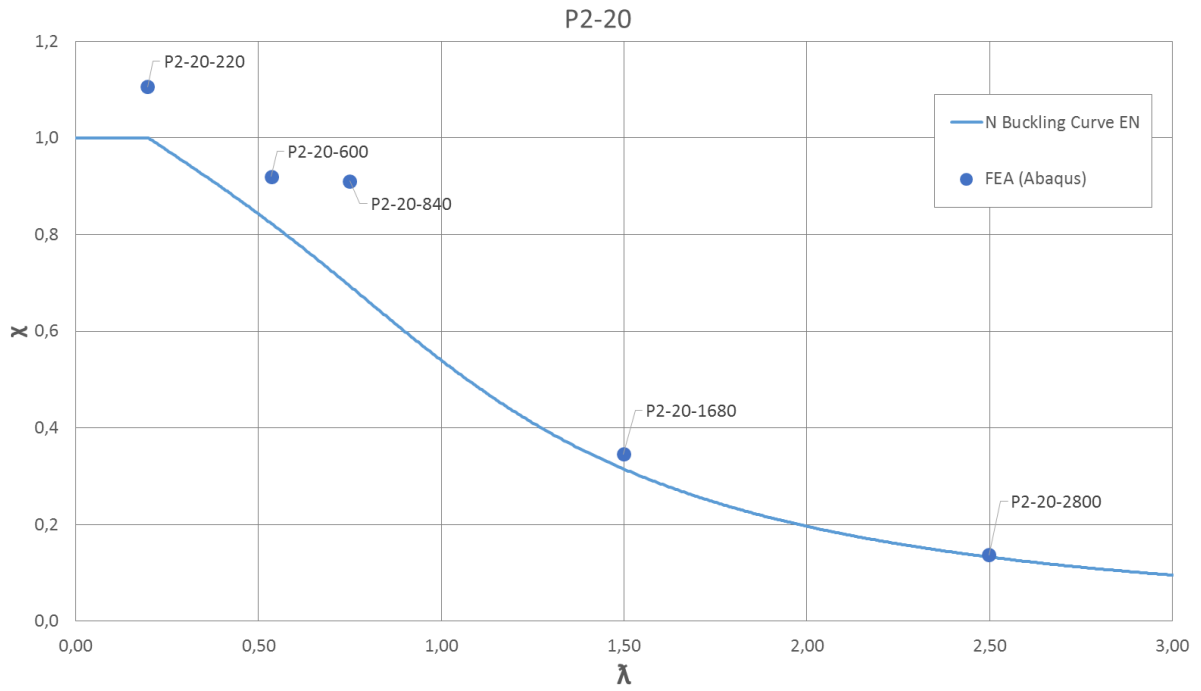


Figure 18.10: Buckling curves. Cross-section P2-20.

Buckling curves – Group P3

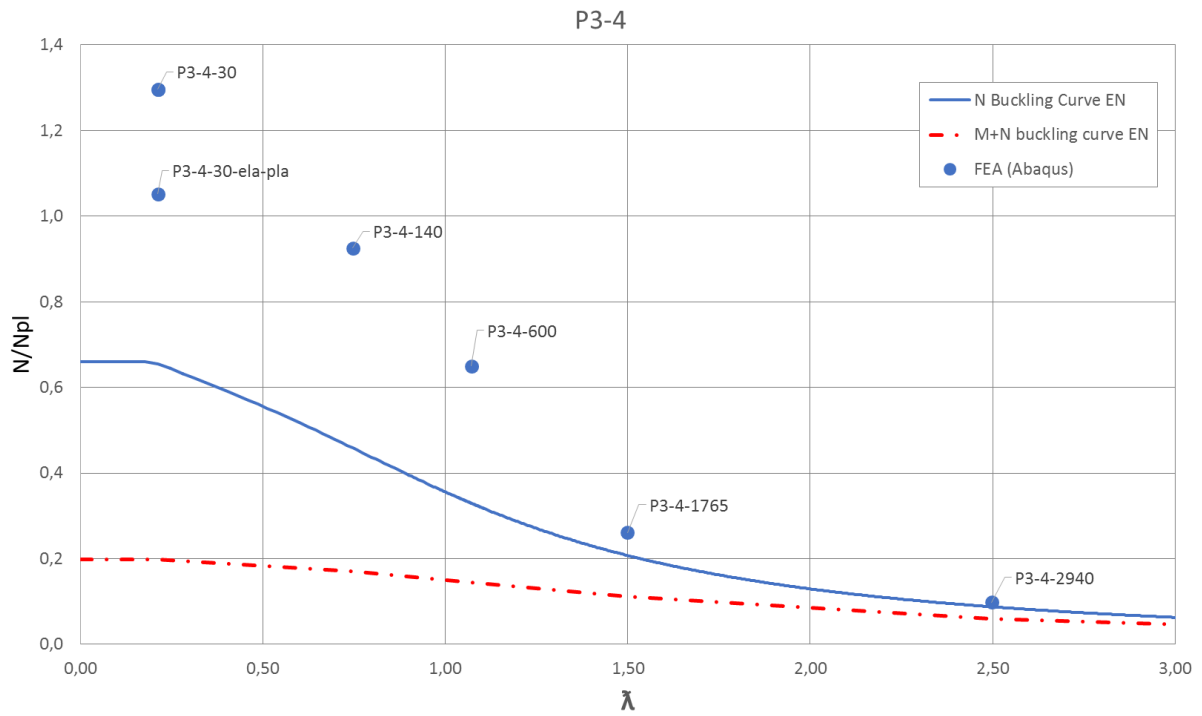


Figure 18.11: Buckling curves. Cross-section P3-4.

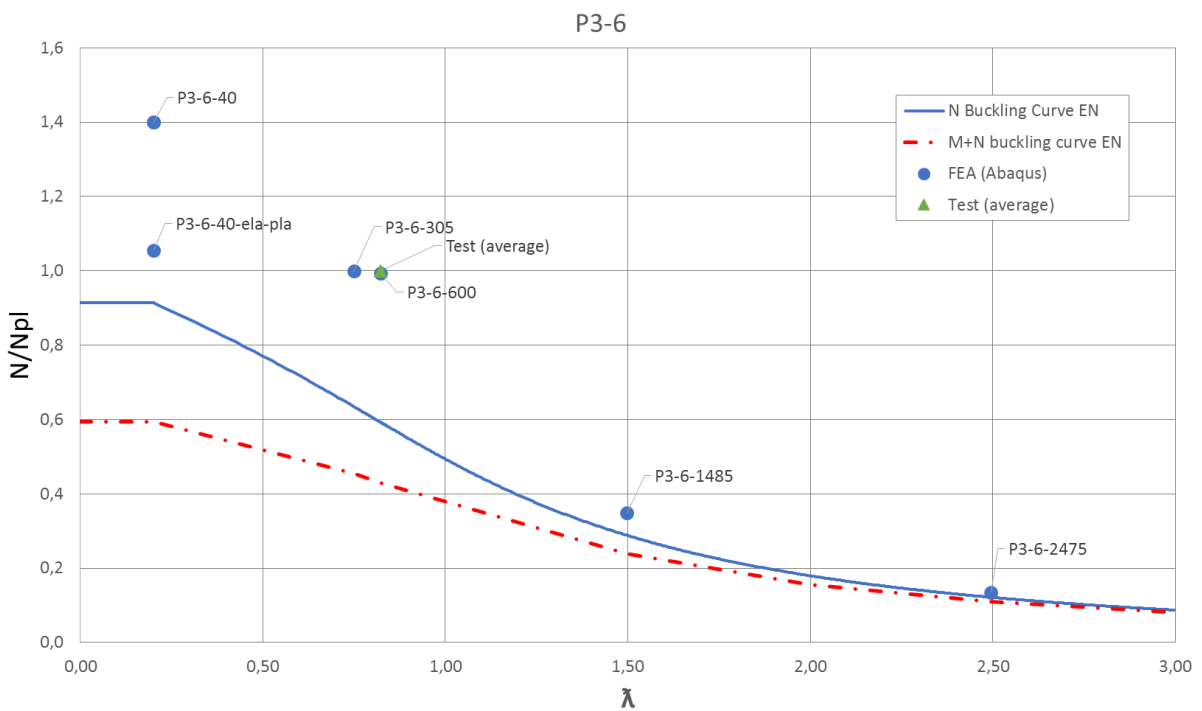


Figure 18.12: Buckling curves. Cross-section P3-6.

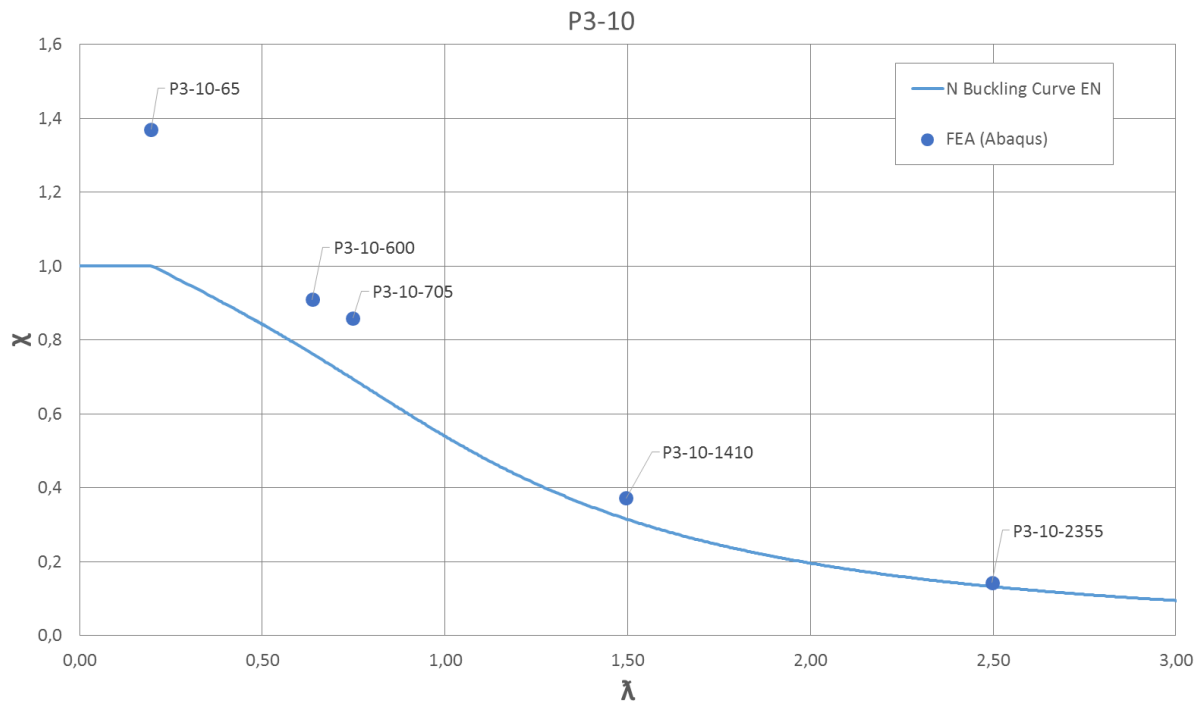


Figure 18.13: Buckling curves. Cross-section P3-10.

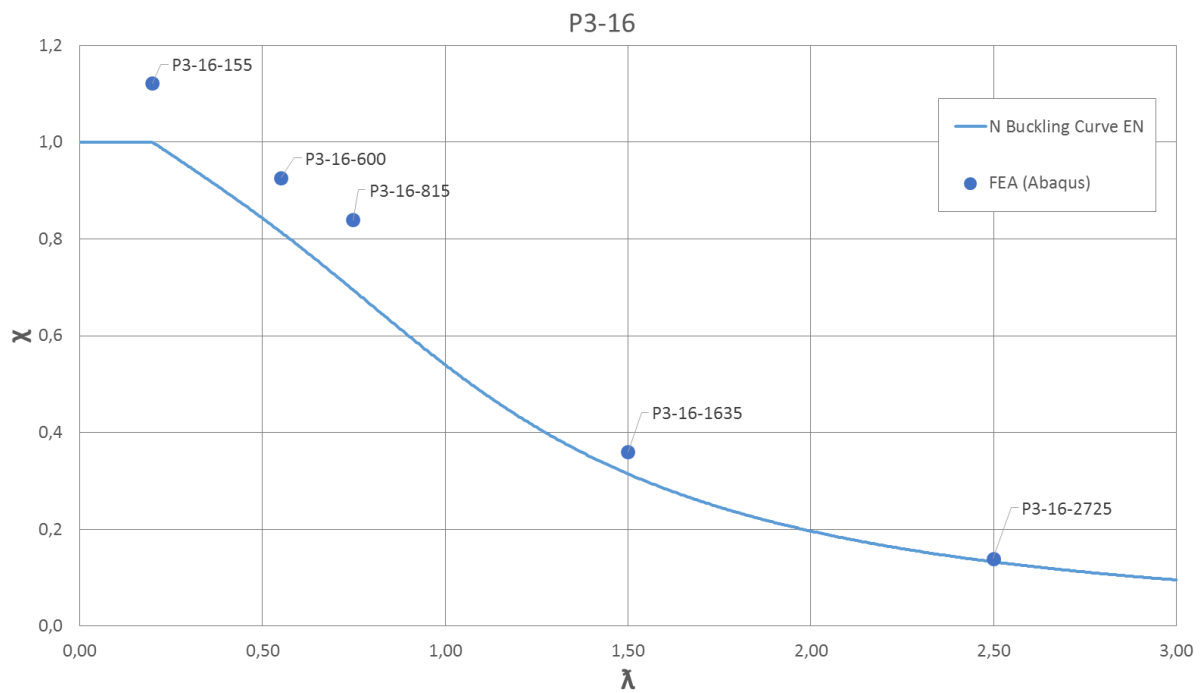


Figure 18.14: Buckling curves. Cross-section P3-16.

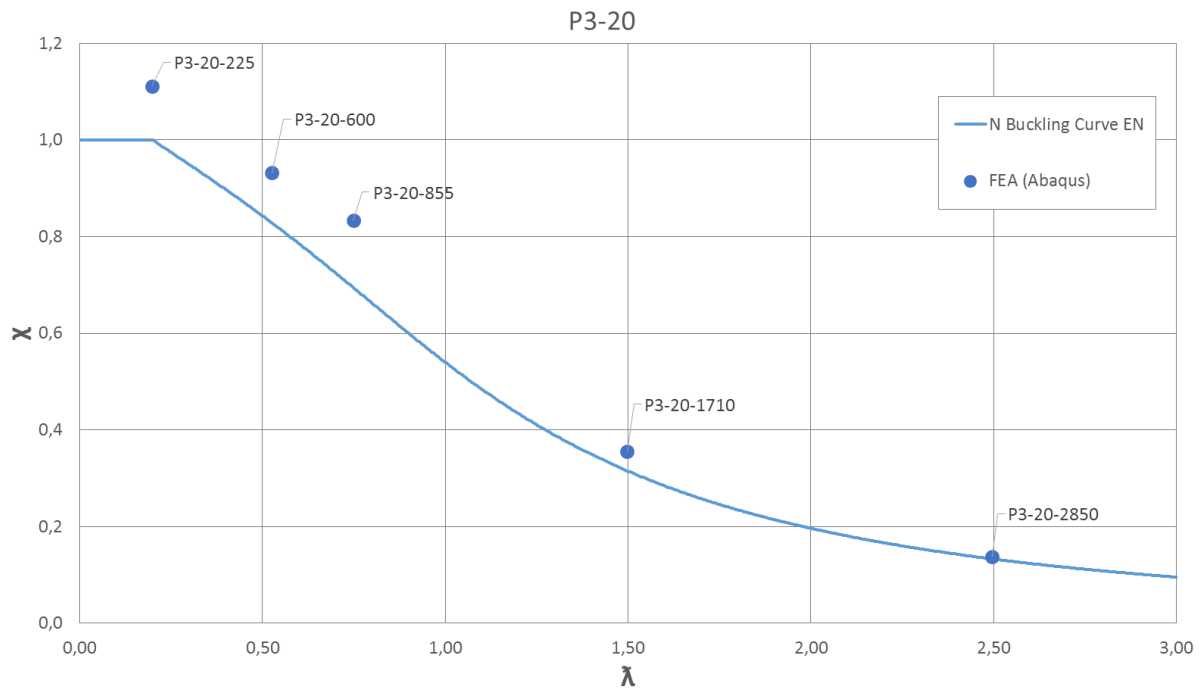


Figure 18.15: Buckling curves. Cross-section P3-20.

Buckling curves – Group P4

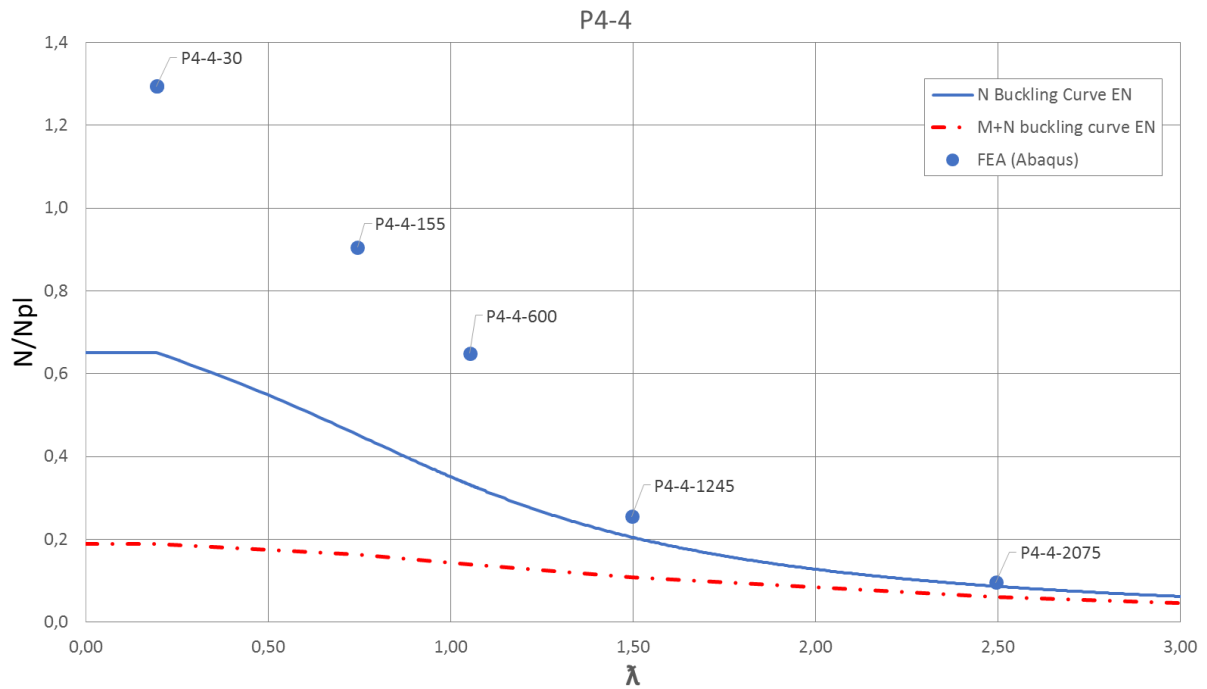


Figure 18.16: Buckling curves. Cross-section P4-4.

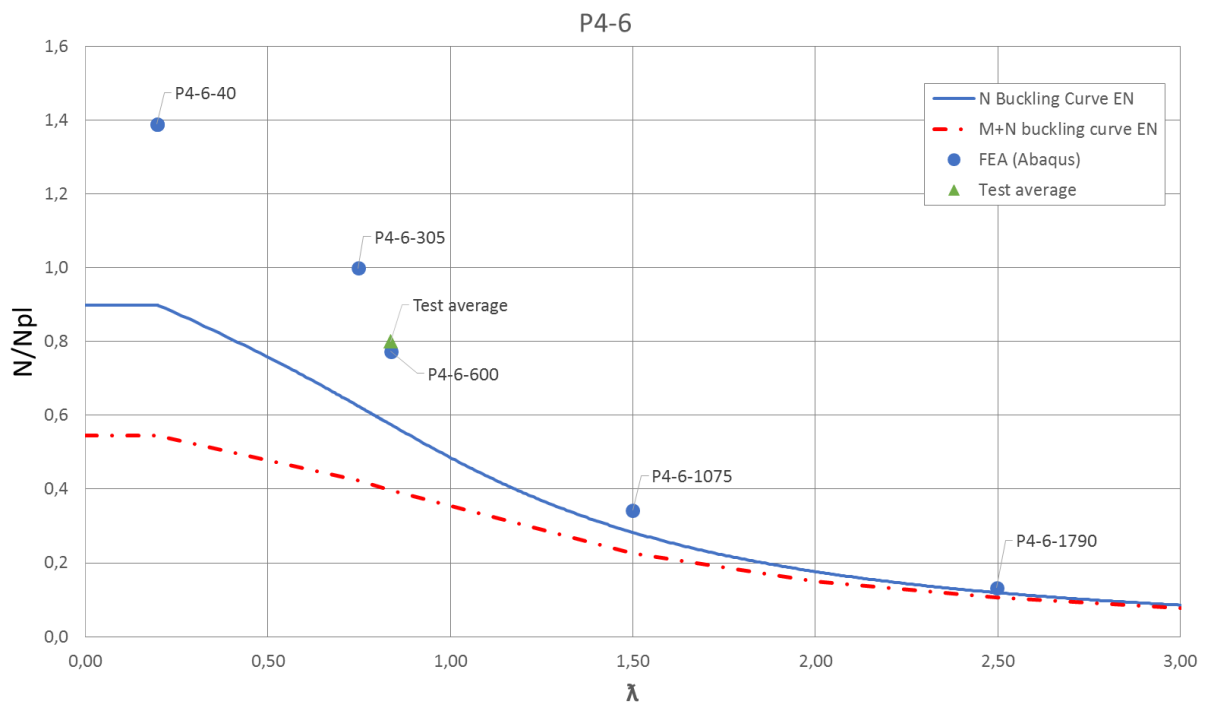


Figure 18.17: Buckling curves. Cross-section P4-6.

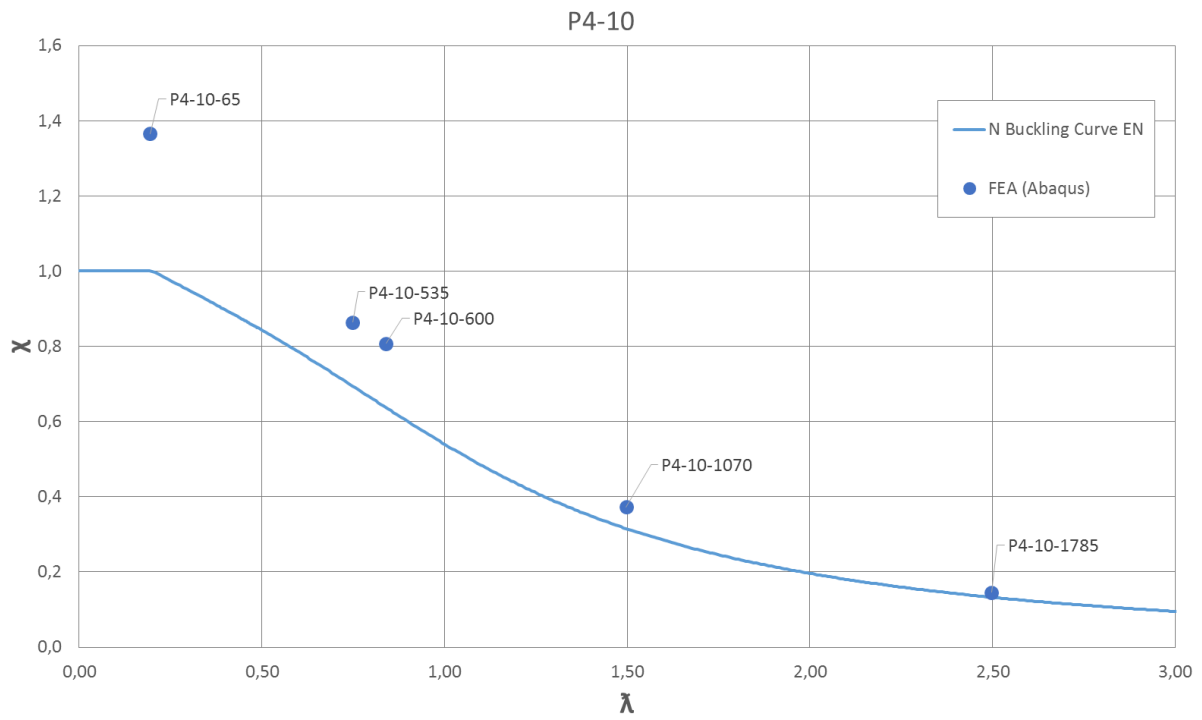


Figure 18.18: Buckling curves. Cross-section P4-10.

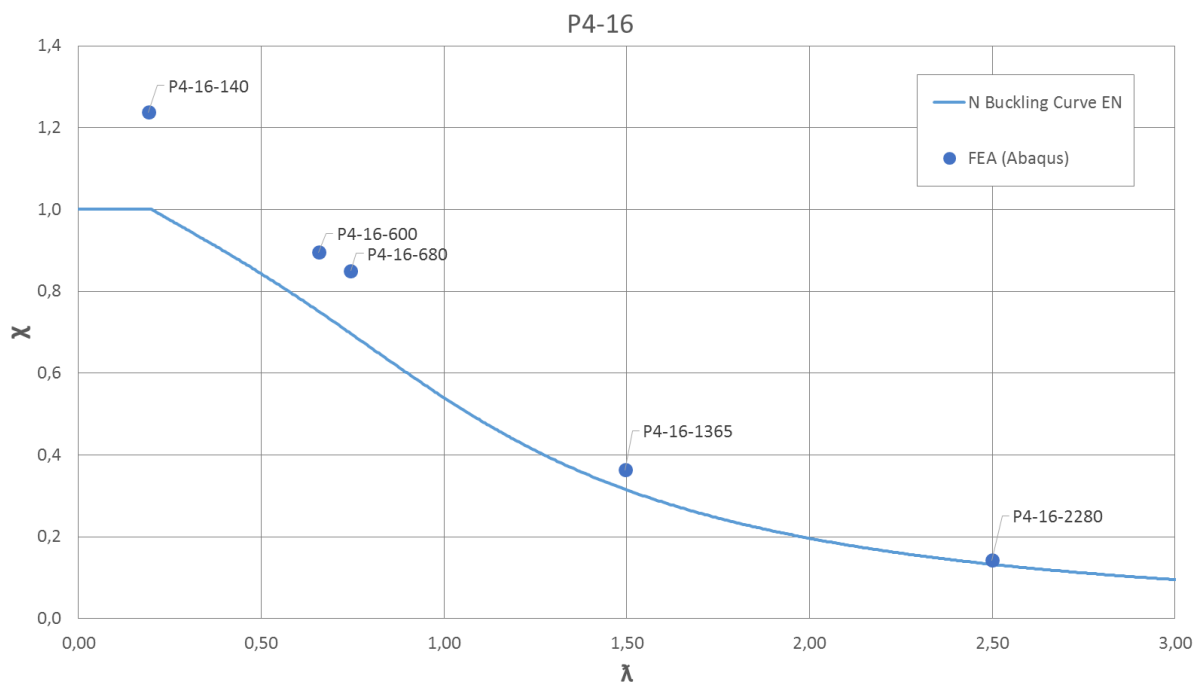


Figure 18.19: Buckling curves. Cross-section P4-16.

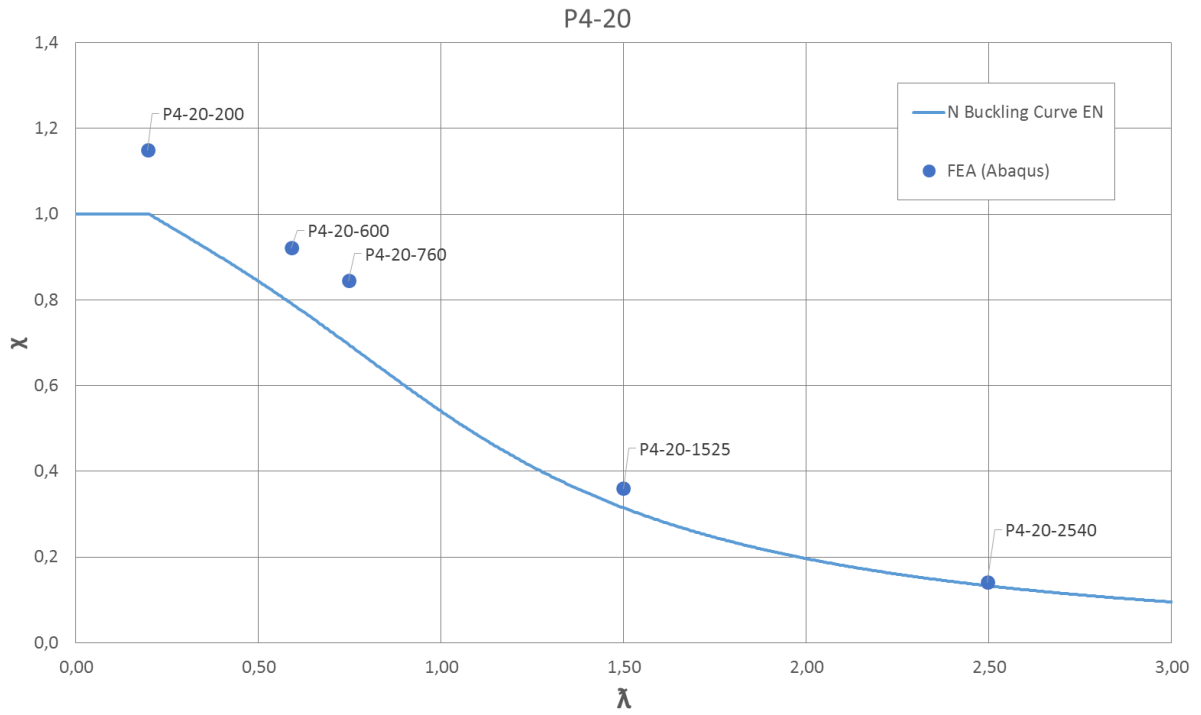


Figure 18.20: Buckling curves. Cross-section P4-20.

Buckling curves – Group P5

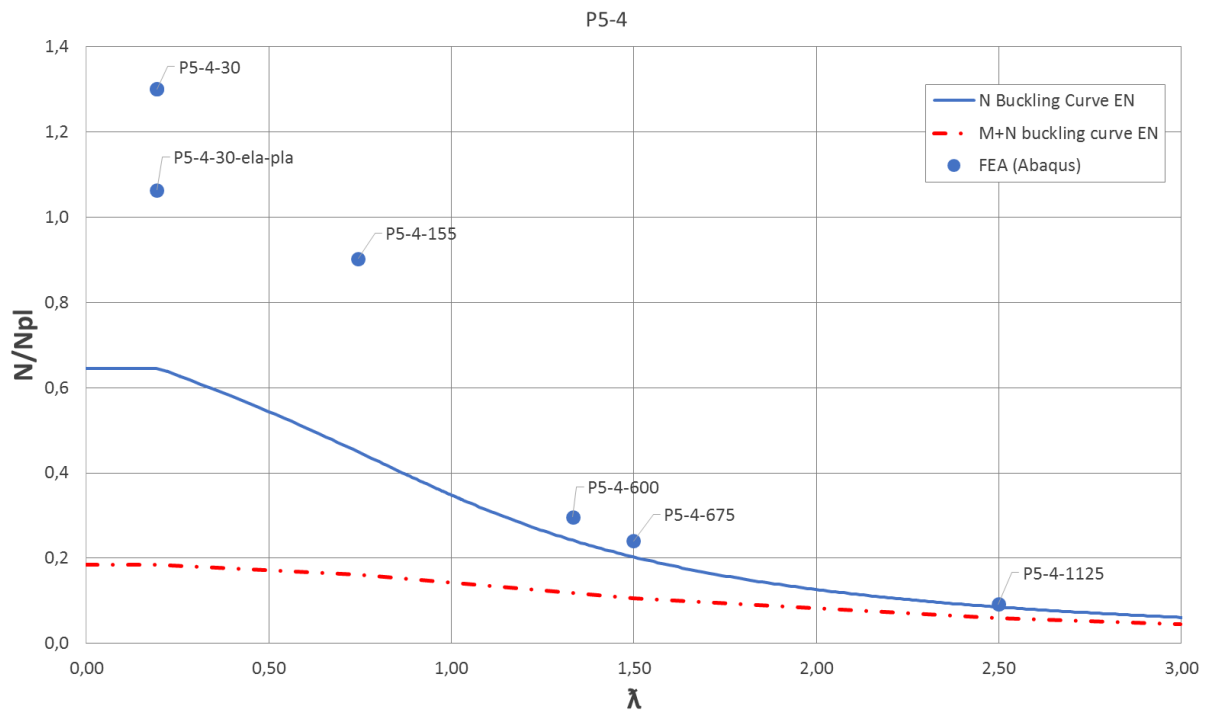


Figure 18.21: Buckling curves. Cross-section P5-4.

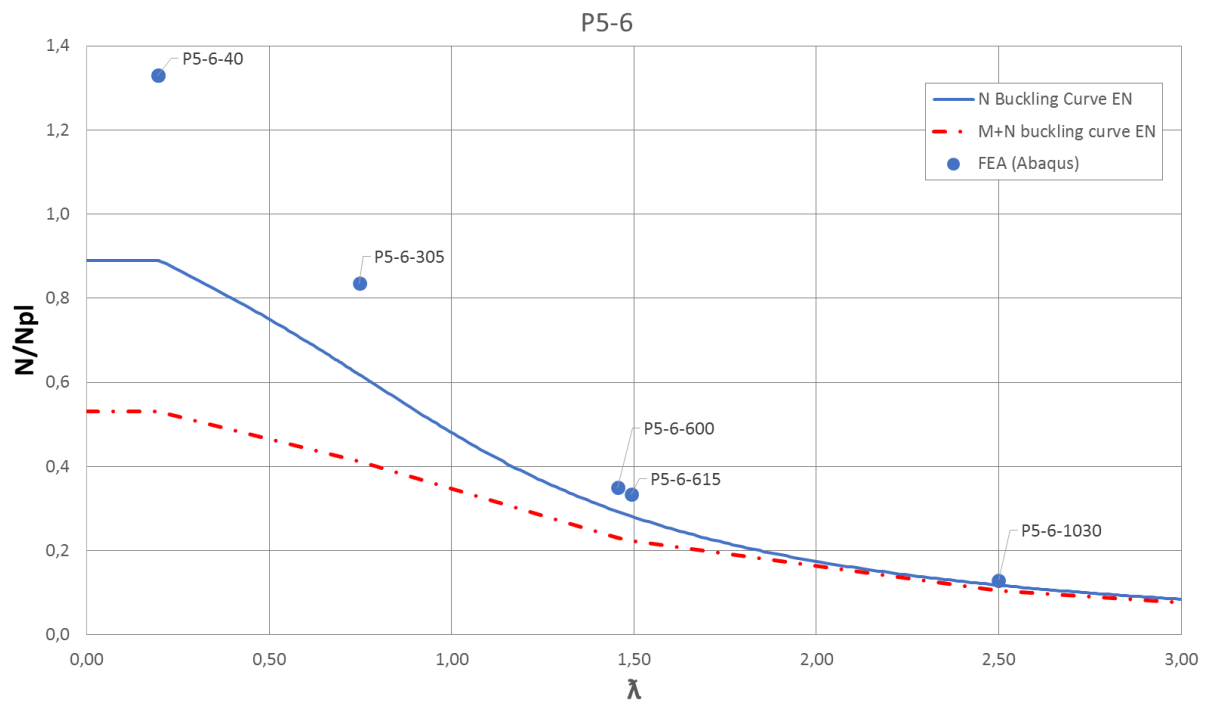


Figure 18.22: Buckling curves. Cross-section P5-6.

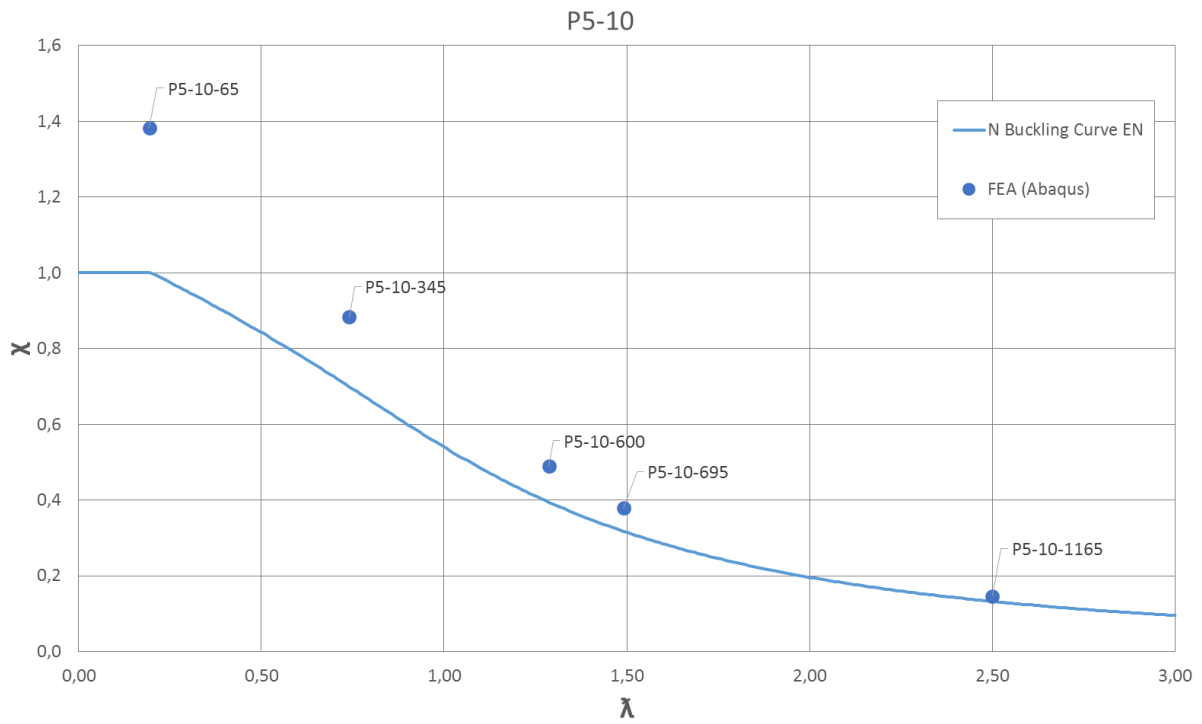


Figure 18.23: Buckling curves. Cross-section P5-10.

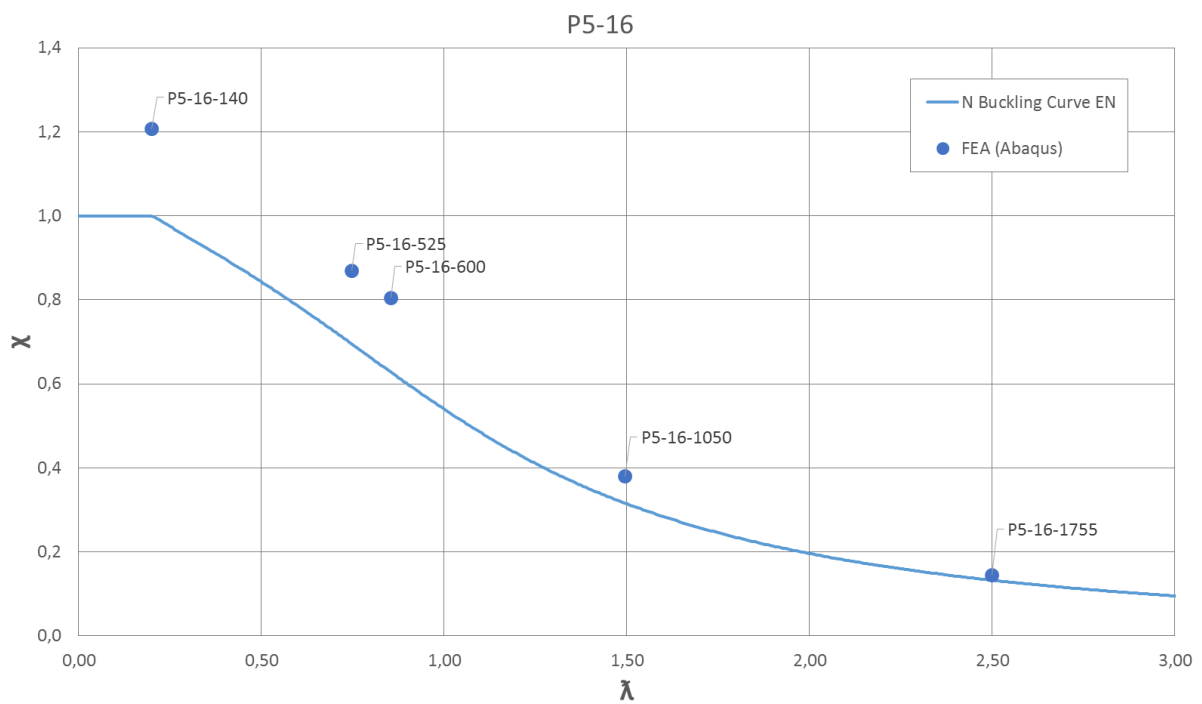


Figure 18.24: Buckling curves. Cross-section P5-16.

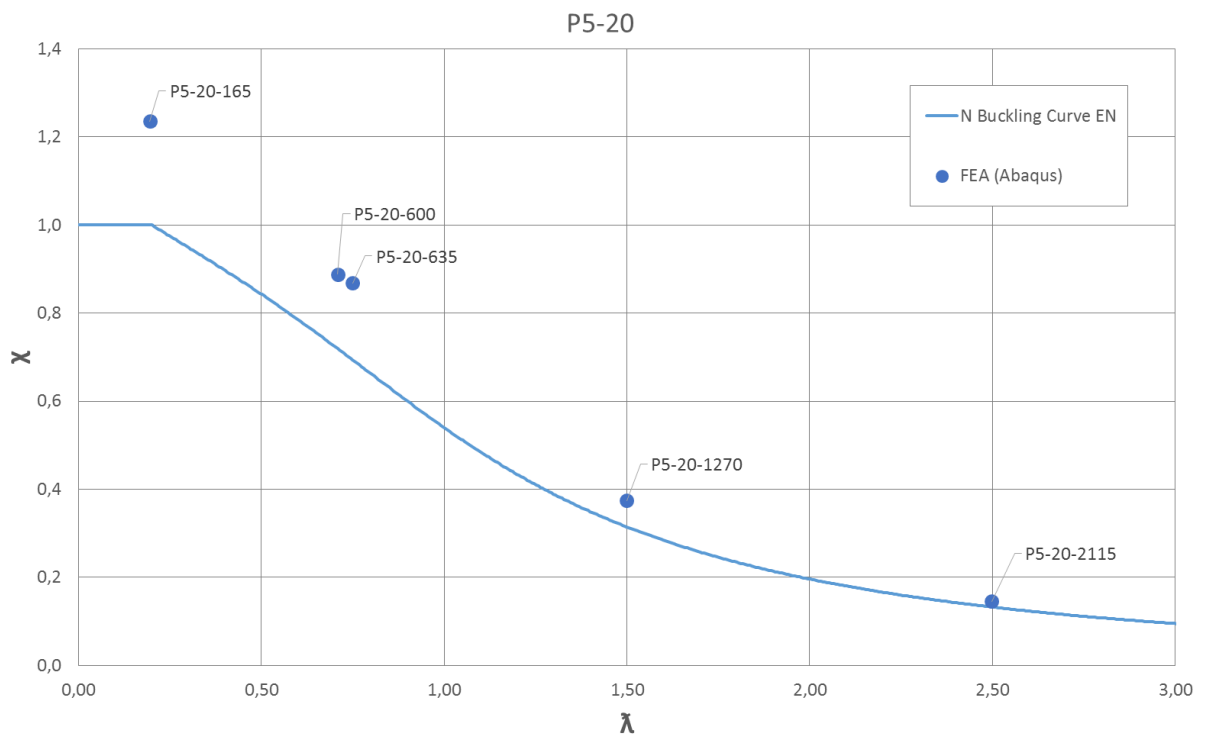


Figure 18.25: Buckling curves. Cross-section P5-20.

Buckling curves – Group P6

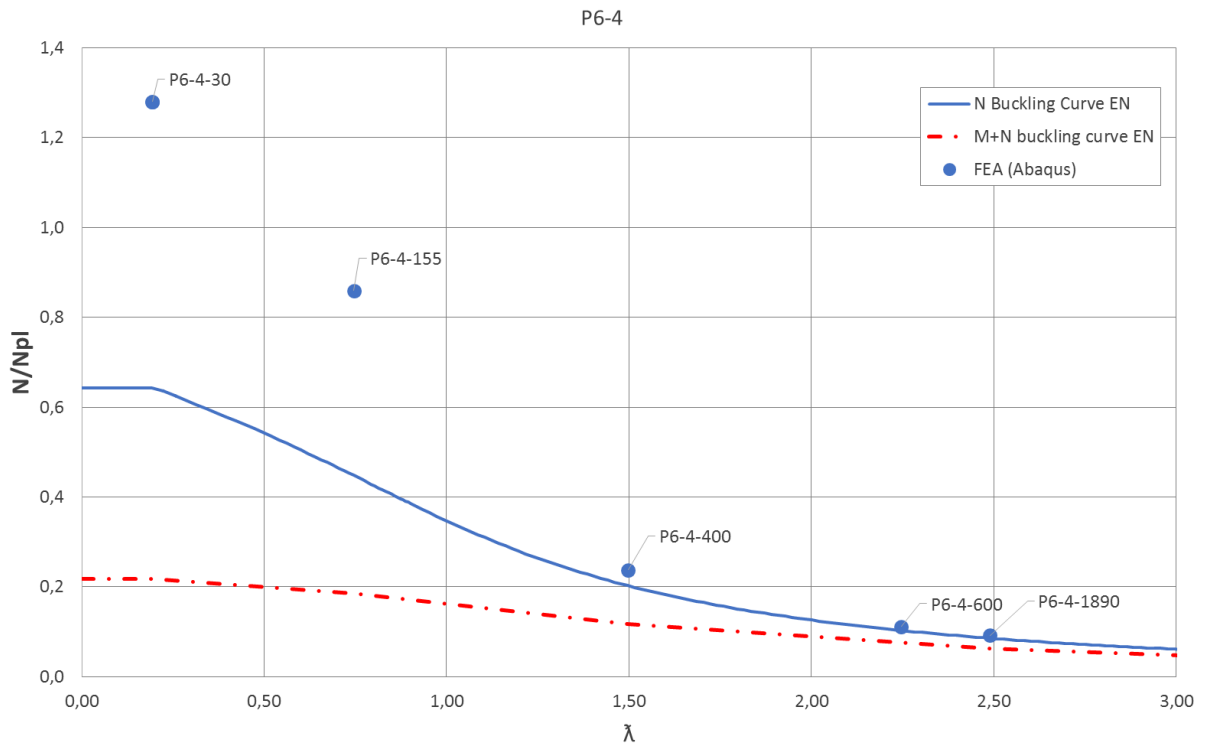


Figure 18.26: Buckling curves. Cross-section P6-4.

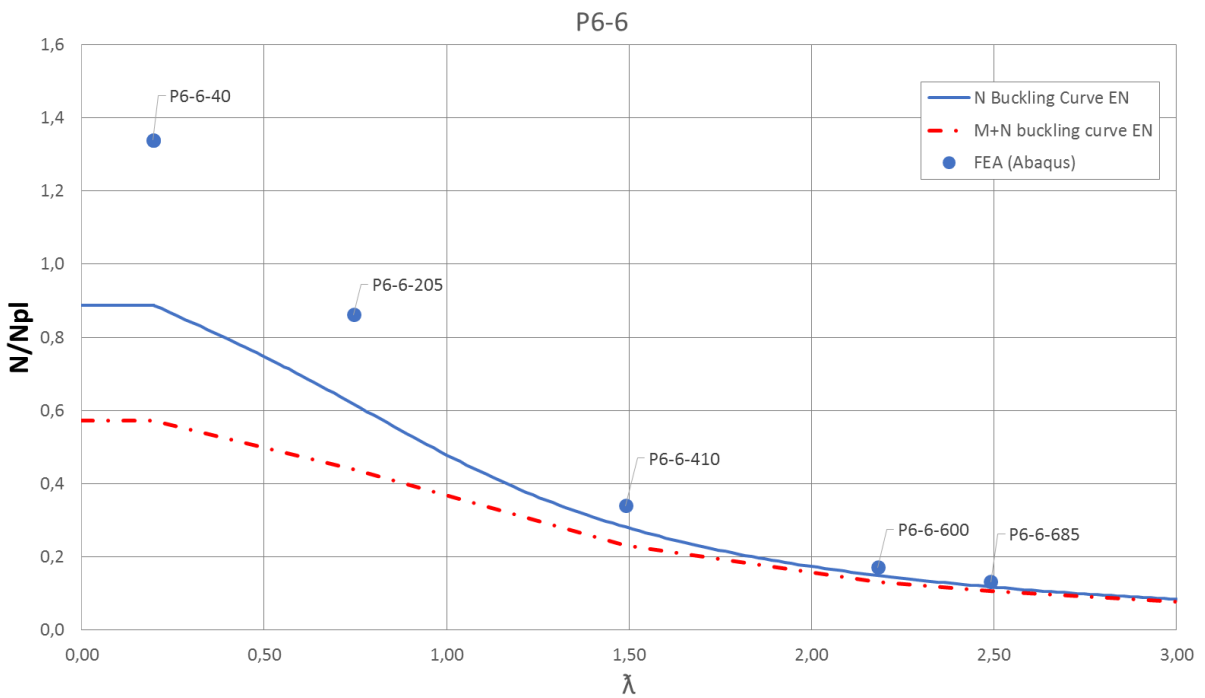


Figure 18.27: Buckling curves. Cross-section P6-6.

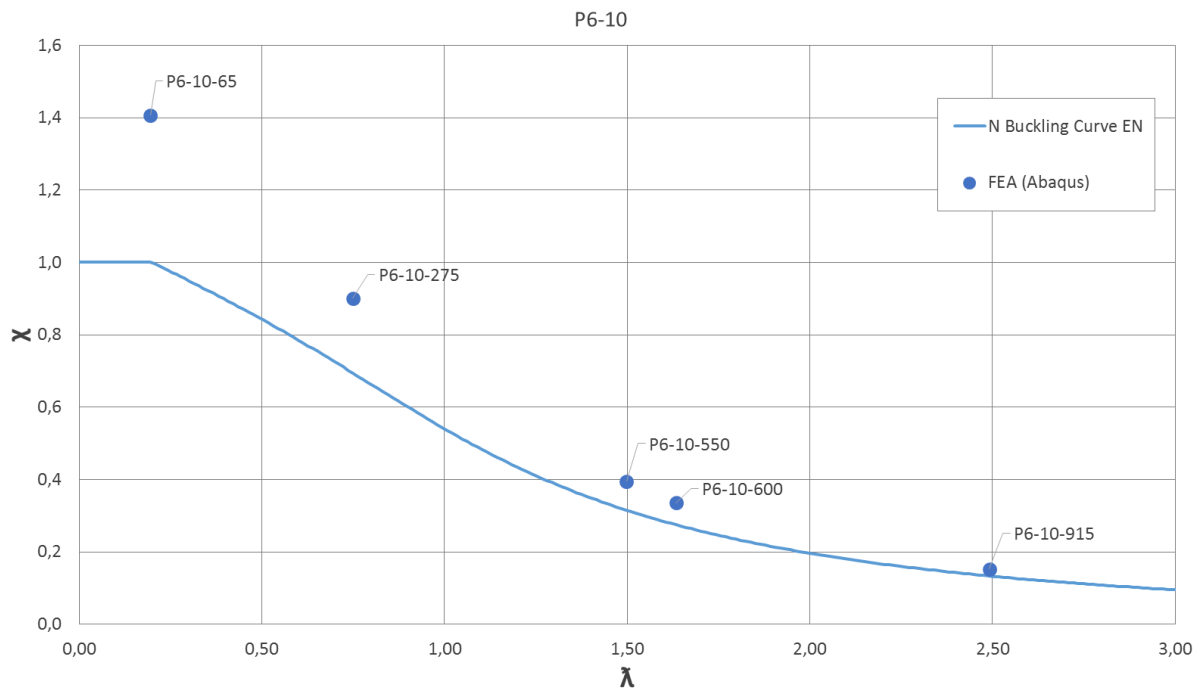


Figure 18.28: Buckling curves. Cross-section P6-10.

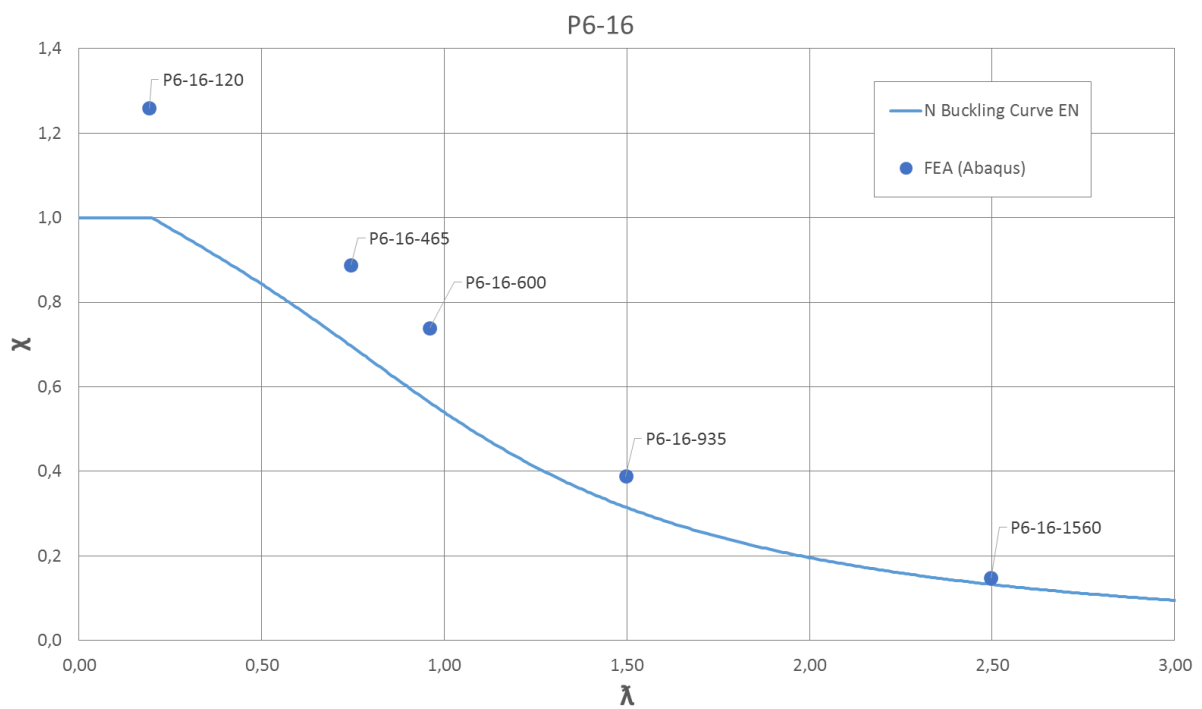


Figure 18.29: Buckling curves. Cross-section P6-16.

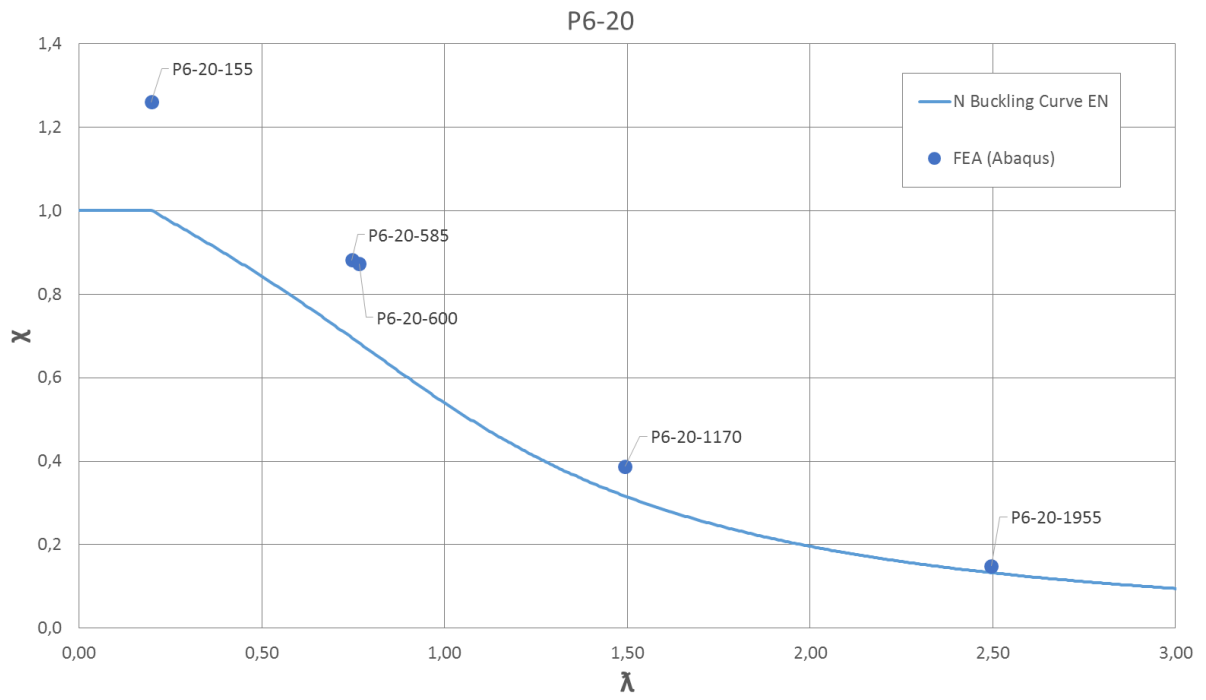


Figure 18.30: Buckling curves. Cross-section P6-20.

Load-displacement curves (test results)

P1-6

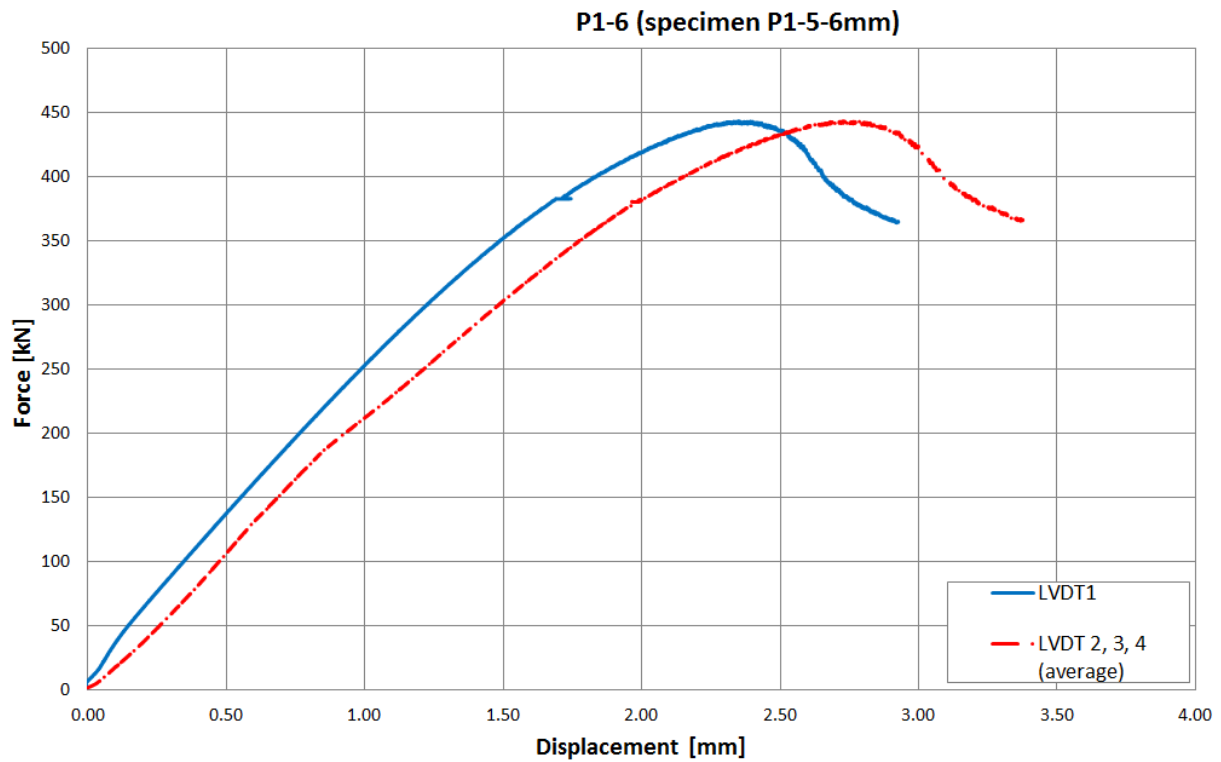


Figure 19.1: Force-displacement curves (test results). Specimen P1-5-6mm.

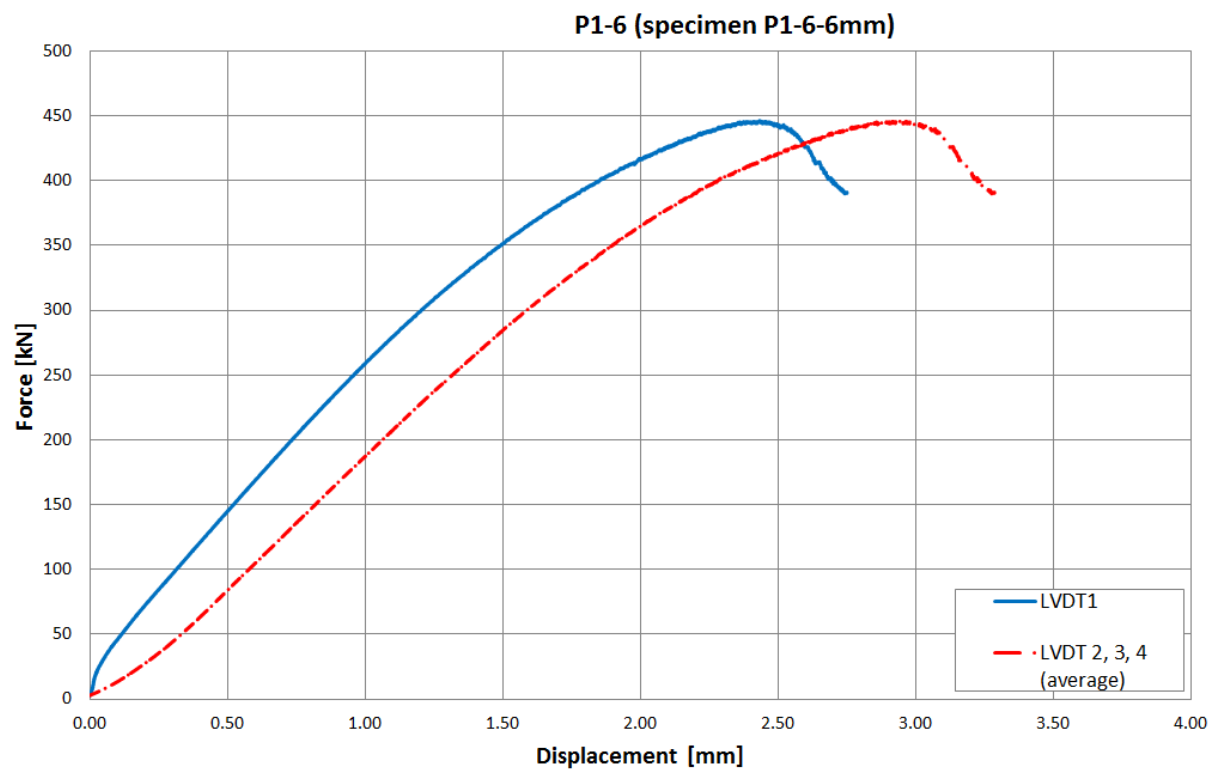


Figure 19.2: Force-displacement curves (test results). Specimen P1-6-6mm.

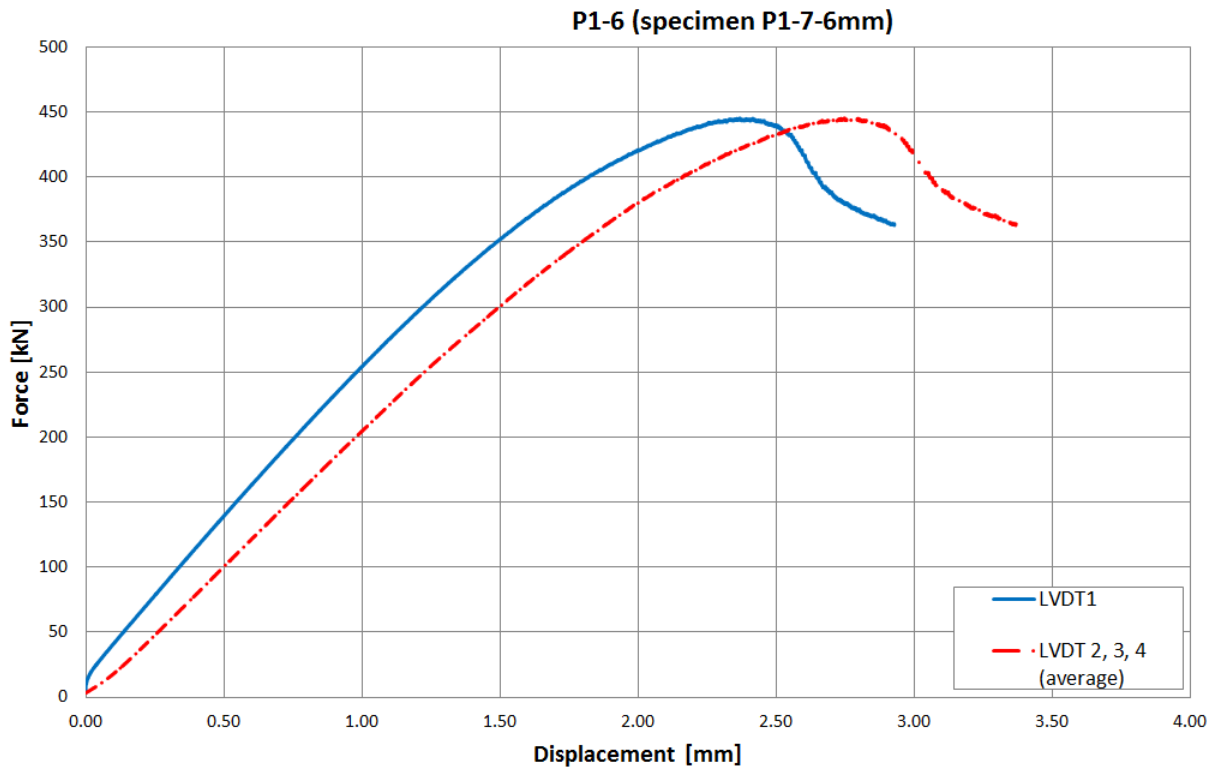


Figure 19.3: Force-displacement curves (test results). Specimen P1-7-6mm.

P2-4

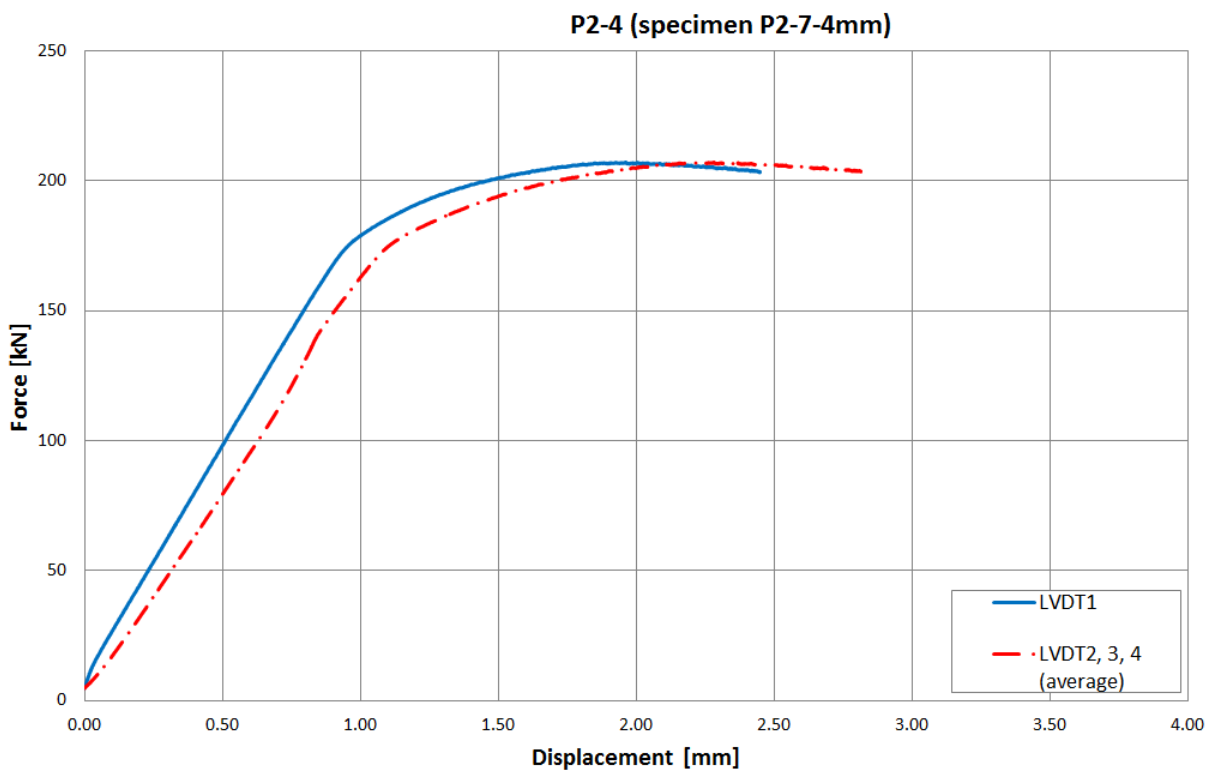


Figure 19.4: Force-displacement curves (test results). Specimen P2-7-4mm.

P2-6

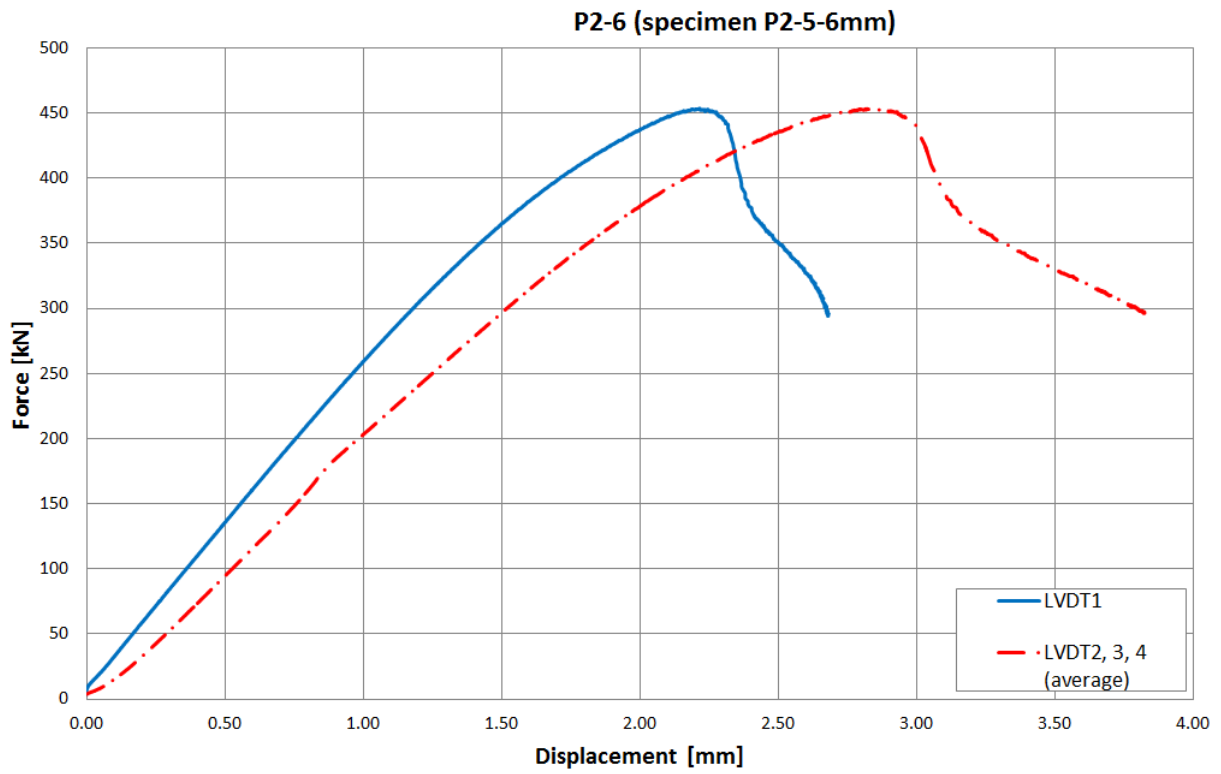


Figure 19.5: Force-displacement curves (test results). Specimen P2-5-6mm.

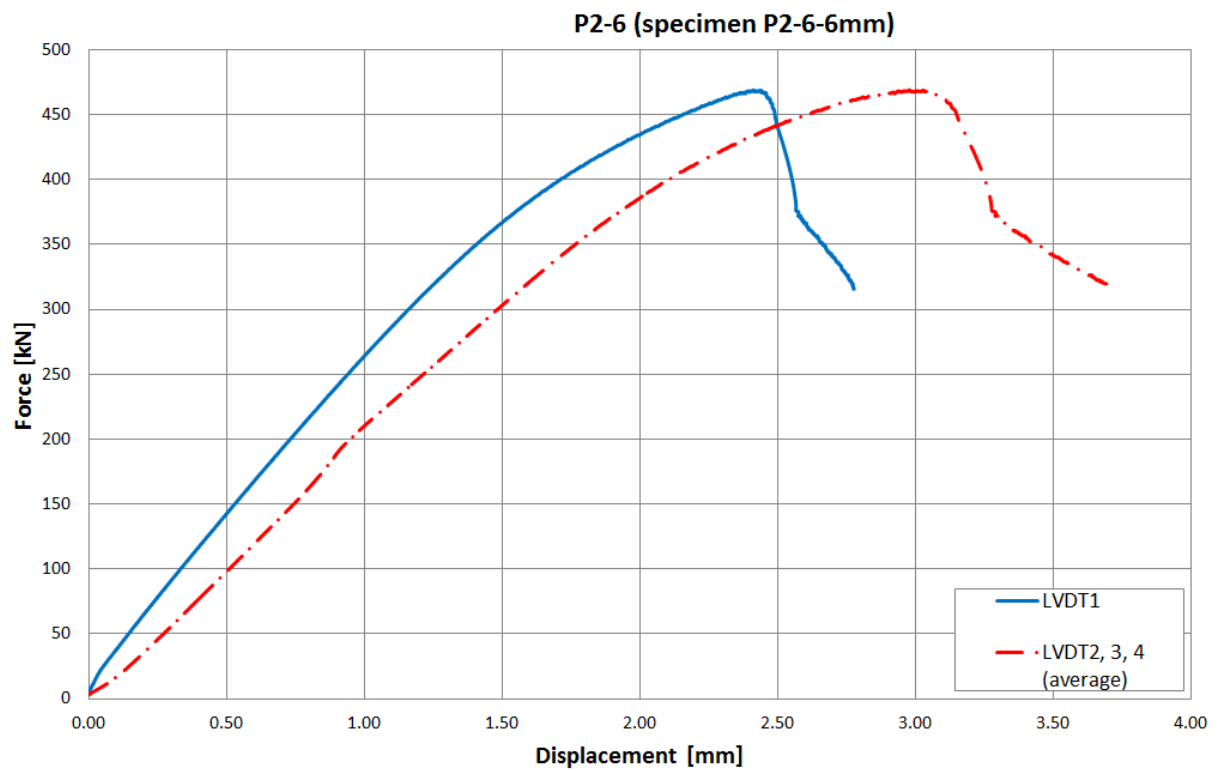


Figure 19.6: Force-displacement curves (test results). Specimen P2-6-6mm.

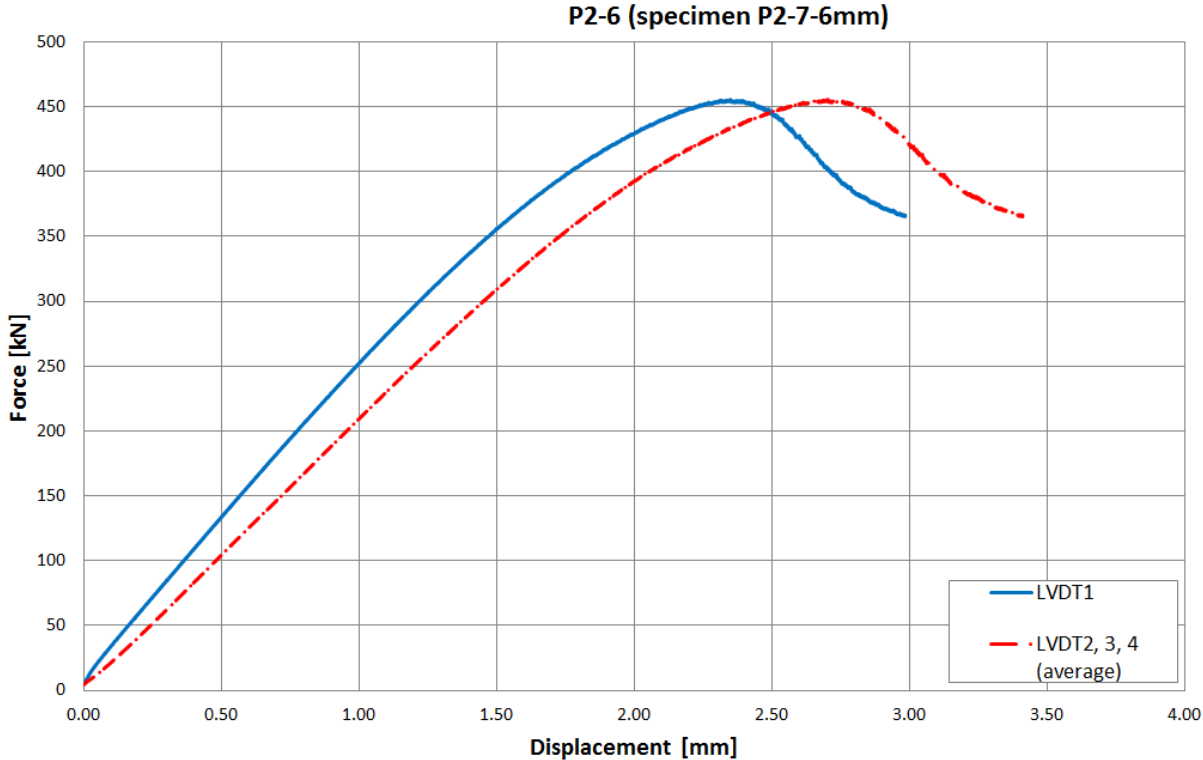


Figure 19.7: Force-displacement curves (test results). Specimen P2-7-6mm.

P3-6

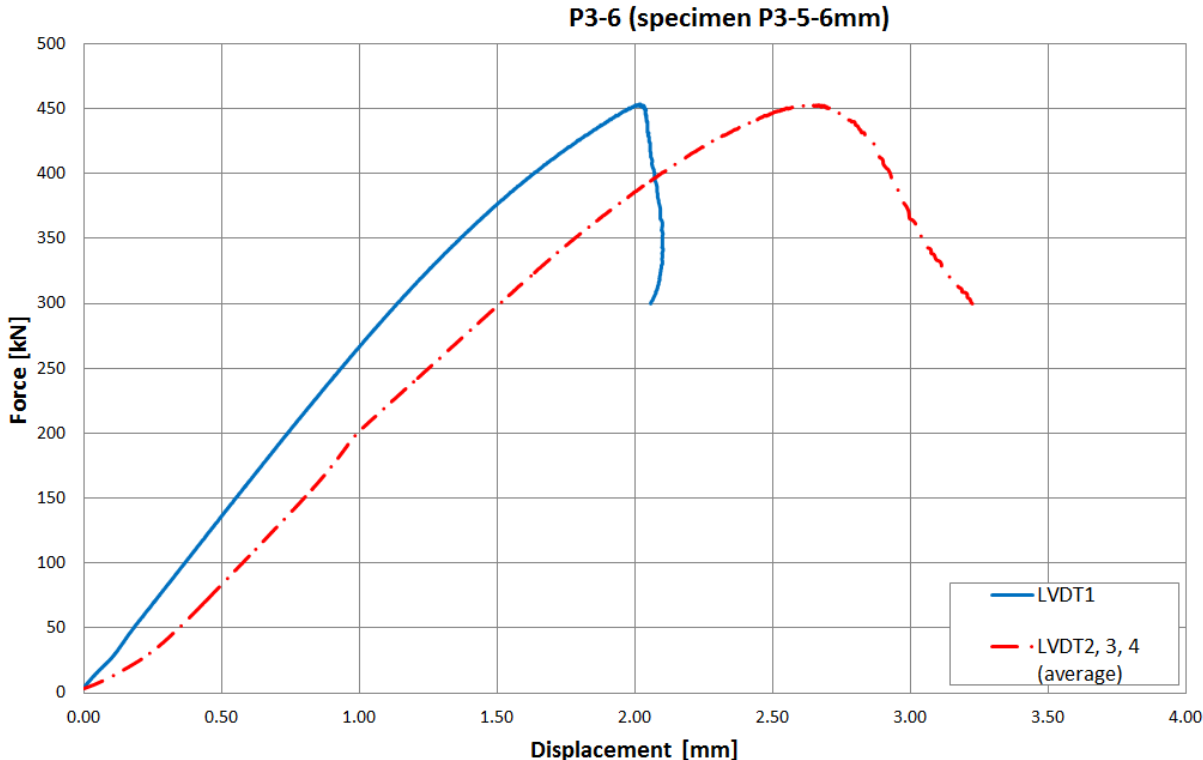


Figure 19.8: Force-displacement curves (test results). Specimen P3-5-6mm.

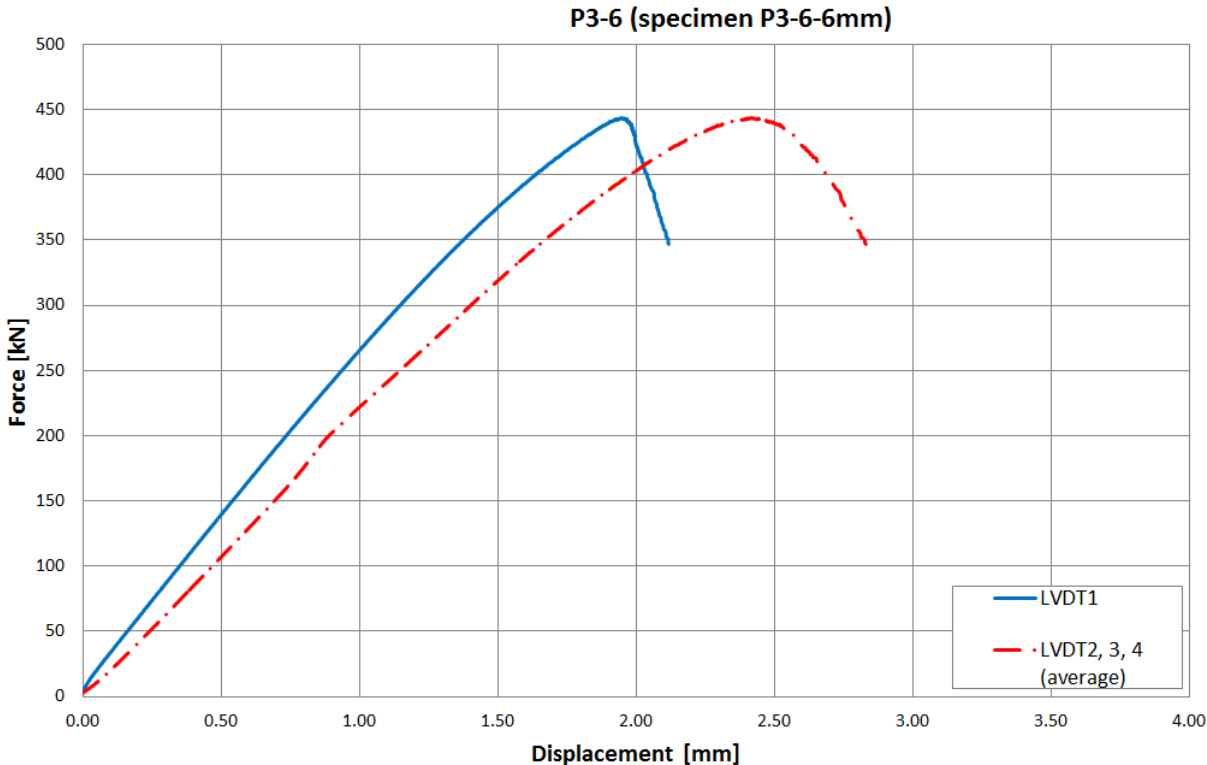


Figure 19.9: Force-displacement curves (test results). Specimen P3-6-6mm.

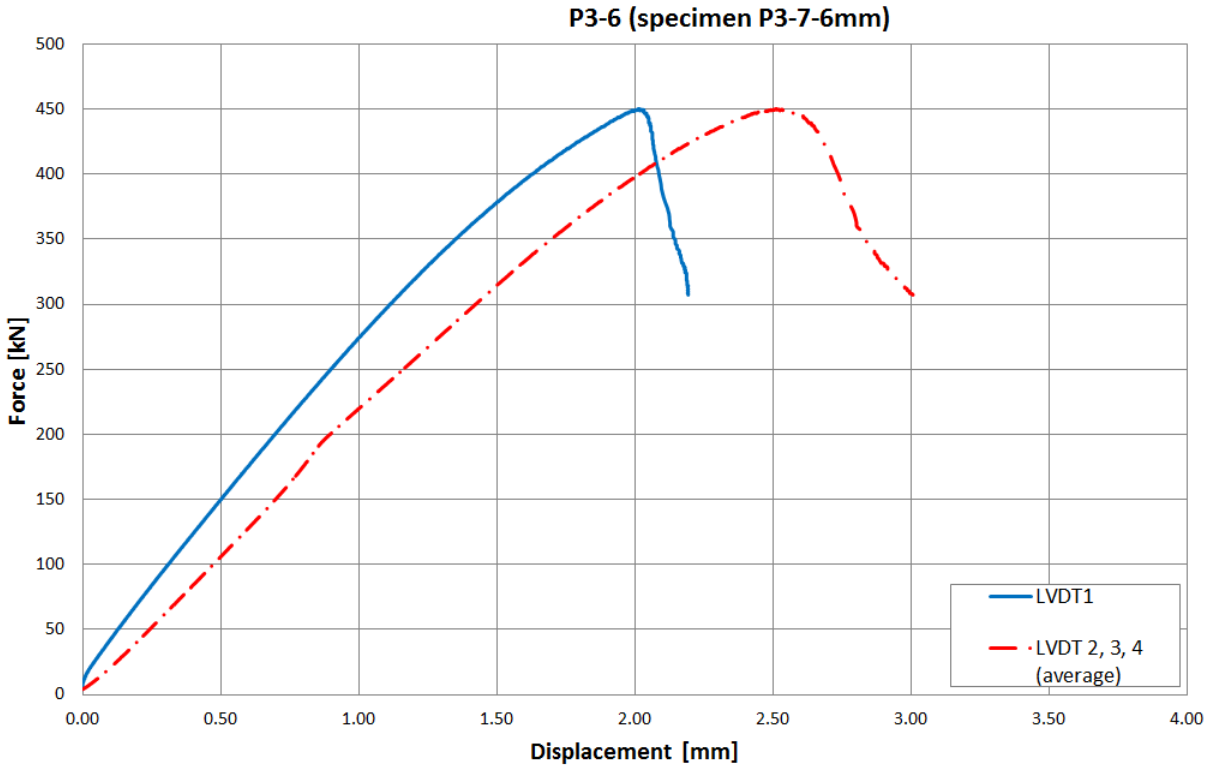


Figure 19.10: Force-displacement curves (test results). Specimen P3-7-6mm.

P4-6

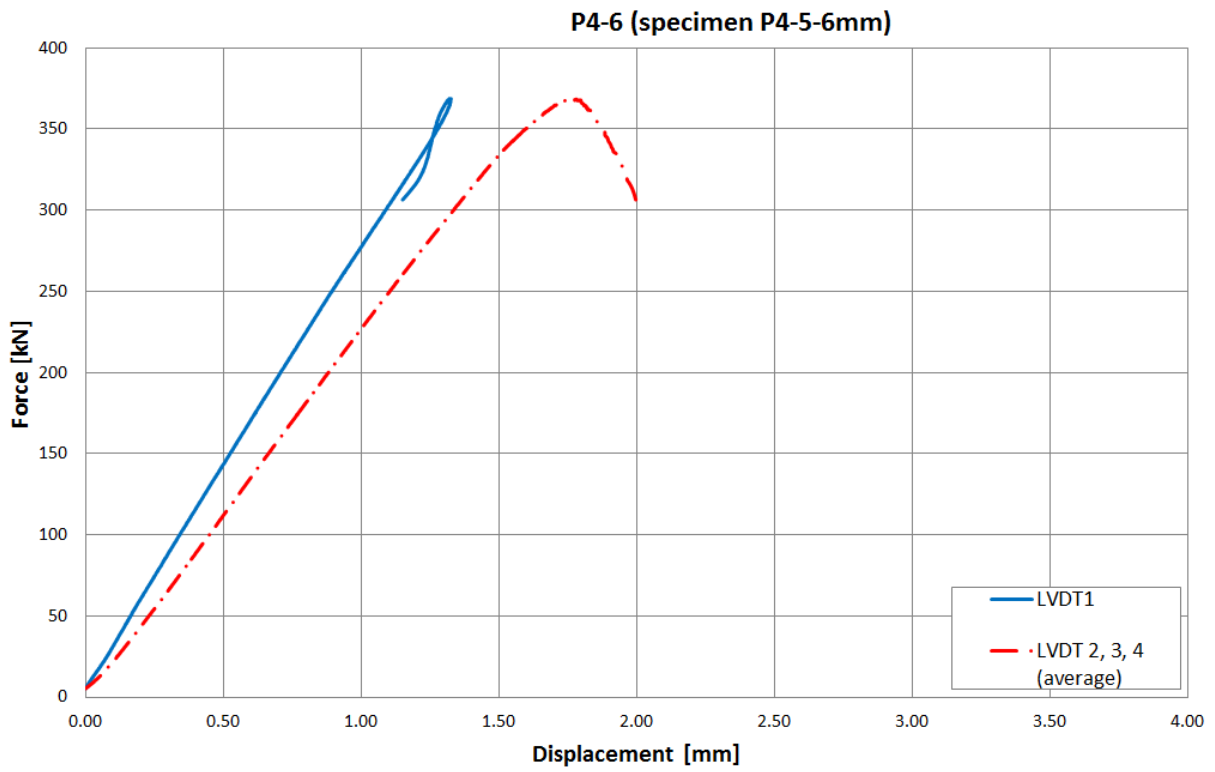


Figure 19.11: Force-displacement curves (test results). Specimen P4-5-6mm.

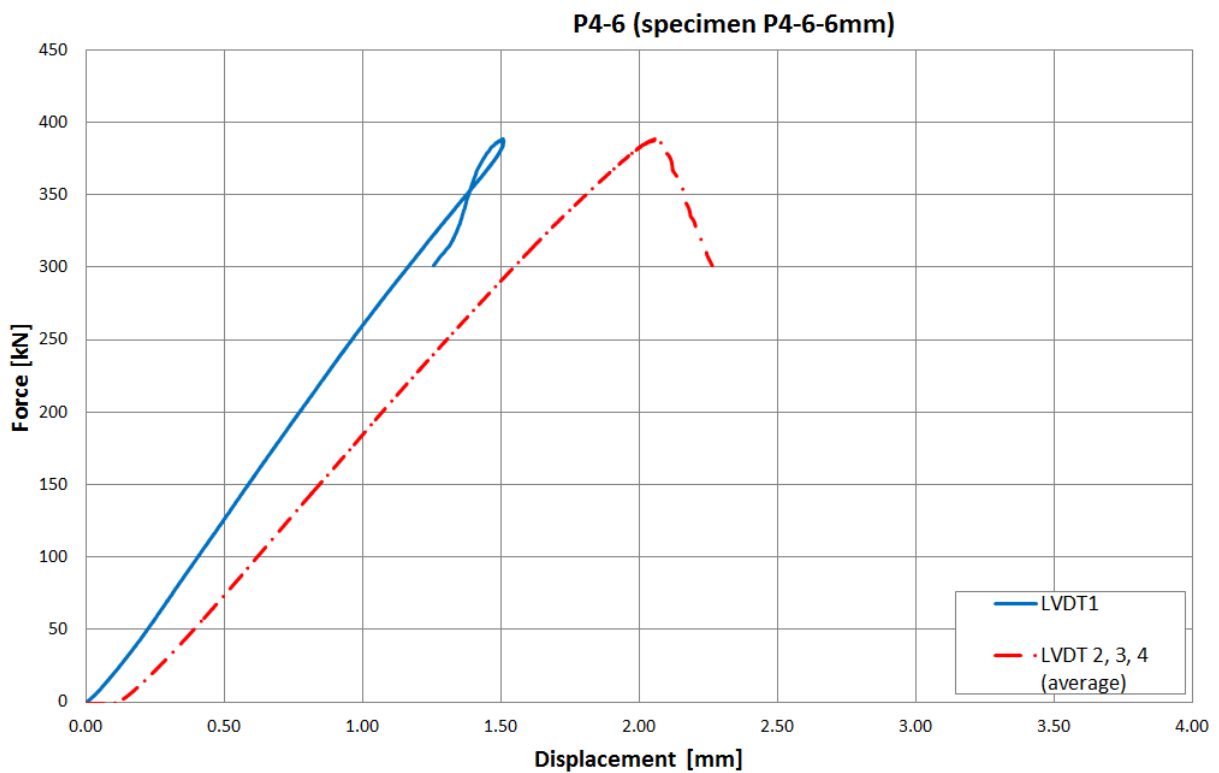


Figure 19.12: Force-displacement curves (test results). Specimen P4-6-6mm.

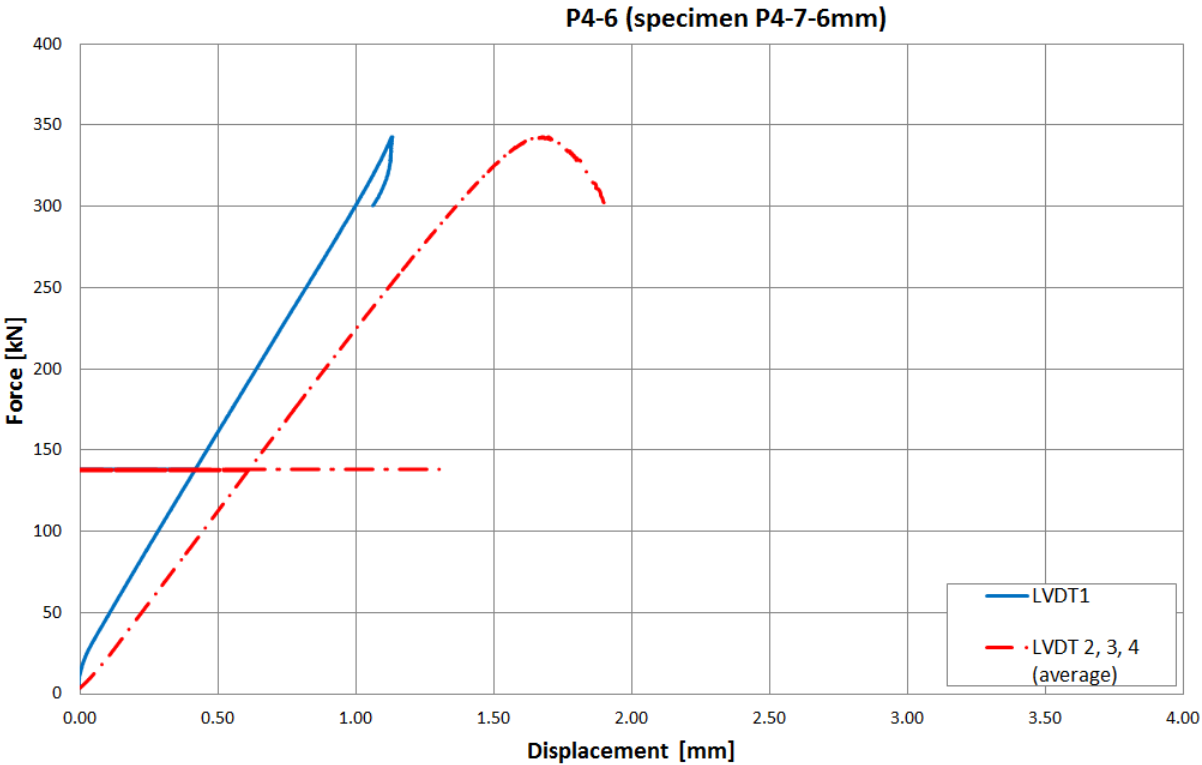


Figure 19.13: Force-displacement curves (test results). Specimen P4-7-6mm.

13 REFERENCES

1. Anis, A., Bjork, T., & Heinilla, S. (2012). Prediction of residual stresses in cold. *Journal of Advanced Science and Engineering Research Vol 2*, 1-13.
2. Beg, D., Kuhlmann, U., Davaine, L., & Braun, B. (2012). *Design of Plated Structures - Eurocode 3: Design of Steel Structures, Part 1-5 – Design of Plated Structures (First Edition)*. Berlin: Ernst & Sohn.
3. Bulson, P. S. (1969). *The Stability of Flat Plates*. New York: Elsevier.
4. Corp., D. S. (2013). *Abaqus Standard User`s Manual*.
5. Dinis, P. B., & Camotim, D. (2011). Buckling, post-buckling and strength of equal-leg angle and cruciform columns: Similarities and differences. *Proc., 6th European Conf. on Steel and Composite Structures (EUROSTEEL)* (stránky 105-110). Brussels (Belgium): European Convention for Constructional Steelwork (ECCS).
6. Dinis, P. B., Camotim, D., & Silvestre, N. (2010). On the local and global buckling behaviour of angle, T-section and cruciform thin-walled columns and beams. *Thin-Walled Struct.* 48(10–11), 786-797.
7. Dinis, P. B., Camotim, D., & Silvestre, N. (2010). Post-buckling behavior and strength of angle columns. *Proc., Int. Colloquium on Stability and Ductility of Steel Structures (SDSS)* (stránky 1141-1150). Rio de Janeiro: E. Batista, P. Vellasco, and L. Lima, eds., Federal Univ. of Rio de Janeiro and State Univ. of Rio de Janeiro.
8. Dinis, P. B., Camotim, D., & Silvestre, N. (2012). Buckling, postbuckling, strength and design of angle columns. *Proc., USB Key Drive Structural Stability Research Council Annual Stability Conf.,.* Rolla: Structural Stability Research Council.
9. Dinis, P. B., Camotim, D., & Silvestre, N. (2012). On the mechanics of thin-walled angle column instability. *J. Thin-Walled Struct.,* 52, 80-89.
10. Dubina, D., Ungureanu, V., & Landolfo, R. (2013). *Design of Cold-formed Steel Structures: Eurocode 3: Design of Steel Structures. Part 1-3 - Design of Cold-formed Steel Structures, First Edition*. Weinheim, Germany: Wiley-VCH Verlag GmbH & Co. KGaA.
11. Ellobody, E., & Young, B. (2005). Behavior of cold-formed steel plain angle columns. *J. Struct. Eng.,* 131(3), 457-466.
12. Galambos, T. V. (1998). *Guide to Stability Design Criteria for Metal Structures (5th edition)*. New York: John Wiley and Sons.
13. *Handbook - Swedish Regulations for Steel Structures, BSK 99*. (2003).
14. Chodraui, G. M., Shifferaw, Y., Malite, M., & Schafer, B. W. (2006). Cold-formed steel angles under axial compression. *Proc., 18th Int. Specialty Conf. on Cold-Formed Steel*

- Structures* (stránky 285–300). Rolla, MO: R. LaBoube and W.-W. Yu, eds., Univ. of Missouri-Rolla.
15. Karren, K. (1967). *K. Corner properties of cold-formed steel shapes*. J Strcut Div (ASCE) 93:401-32.
 16. King, C. (2006). Design of Mono-symmetric and Asymmetric Sections in Compression using BS 5950-1:2000. *New Steel Construction magazine, vol.14, No6*.
 17. Mesacasa, J. (2013). Mode interaction in thin-walled equal-leg angle columns. *Thin-WalledStructures*.
 18. Moen, C., & Schafer, B. (16. 2 2006). Načteno z www.ce.jhu.edu/:
http://www.ce.jhu.edu/bschafer/dsm_holes/Progress%20Report%201%20CDM%20Rev%204.doc
 19. Naranayan, R. (1982). *Axially Compressed Structures. Stability and Strength*. Barking, Essex, England: Applied Science Publishers,.
 20. Narayanan, R., Kalyanaraman, V., Santhakumar, A., S.Seetharaman, Kumar, S. S., Jayachandran, S. A., & Senthil, R. (1999, August). *Steel-insdag.org*. Retrieved from Teaching Materials - Contents: http://www.steel-insdag.org/TM_Content.asp
 21. Nemetschek. (2013). *Nemetschek Scia Academic Software*. Načteno z Nemetschek SCIA: <http://nemetschek-scia.com/en/nemetschek-scia-academic-software>
 22. Popovic, D., Hancock, G. J., & Rasmussen, K. J. (1999). Axial compression tests of cold-formed angles. *J. Struct. Eng.*, 127 (6), 600-607.
 23. Popovic, D., Hancock, G. J., & Rasmussen, K. J. (2001). Compression tests on cold-formed angles loaded parallel with a leg. *J. Struct. Eng.*, 127 (6), 600-607.
 24. Quach W.M., J. T. (2. May 2006). *sciencedirect.com*. Načteno z <http://www.sciencedirect.com/science/article/pii/S0141029606001039#>
 25. Rasmussen, K. J. (2003). *Design of angle columns with locally unstable legs*. Sydney (Australia): Department of Civil Engineering, University of Sydney (Research Rep. No. R830).
 26. Rasmussen, K. J. (2005). Design of angle columns with locally unstable legs. *J. Struct. Eng.*, 131(10), 1553–1560.
 27. Rasmussen, K. J. (2006). Design of slender angle section beam-columns by the direct strength method. *J. Struct. Eng.*, 132(2), 204–211.
 28. Rasmussen, K. J., & Young, B. (1999). Shift of effective centroid of channel columns. *Journal of Structural Engineering*, 524-531.
 29. Ruukki. (4. October 2013). *Ruukki.com*. Načteno z Structural steels: <http://www.ruukki.com/Products-and-solutions/Steel-products/Hot-rolled-steels/Structural-steels>

30. Sedlacek, P. D.-I., & Müller, D.-I. C. (n.d.). *cbmm.com.br*. Retrieved from http://www.cbmm.com.br/portug/sources/techlib/science_techno/table_content/sub_4/images/pdfs/047.pdf
31. Shi, G., Liu, Z., & Chung, K. F. (2009). Numerical study on the local buckling of 420MPa steel equal angle columns under axial compression. *Proc., 6th Int. Conf. on Advances in Steel Structures (ICASS), Vol. 1, S. L. Chan, ed.* (stránky 387–394). Hong Kong: The Hong Kong Institute of Steel Construction.
32. Silvestre, N., Dinis, P., & Camotim, D. (2013). Developments on the Design of Cold-Formed Steel Angles. *J. Struct. Eng. 139, SPECIAL ISSUE: Cold-Formed Steel Structures*, 680–694.
33. Simoes da Silva, L., Simoes, R., & Gervasio, H. (2010). *Design of Steel structures*. ECCS - European Convention for Constructional Steelwork.
34. Standardization, E. C. (2005). *EN 1993: Design of steel structures - Part 1-1: General rules and rules for buildings*. Brussels.
35. Standardization, E. C. (2006). *Eurocode 3 - Design of steel structures - Part 1-3: General rules*. Brussels.
36. Standardization, E. C. (2006). *Eurocode 3 - Design of steel structures - Part 1-5: Plated*. Brussels.
37. Standardization, E. C. (2007). *Eurocode 3 - Design of steel structures - Part 1-12: Additional*. Brussels.
38. Timoshenko, S., & Gere, J. M. (1963). *Theory of Elastic Stability*. New York: McGraw Hill Kogakusha Ltd.
39. Young, B. (2004). Tests and design of fixed-ended cold-formed steel plain angle columns. *J. Struct. Eng., 130(12)*, 1931–1940.
40. Young, B., & Rasmussen, K. J. (1998). Tests of fixed-ended plain channel columns. *Journal of Structural Engineering*, 131–139.